

Engineering of a Thermostable PETase by Directed Evolution

A thesis submitted to the University of Manchester for the degree of
Doctor of Philosophy in the Faculty of Biology, Medicine & Health

2021

Elizabeth L. Bell

School of Biological Sciences

Table of Contents

Table of Contents.....	2
Abbreviations.....	7
ABSTRACT: Engineering a Thermostable PETase by Directed Evolution.....	10
Declaration and Copyright Statement.....	12
Acknowledgements.....	13
CHAPTER 1: Introduction.....	14
1.1 Plastics - An Overview.....	14
1.2 Reasons for Plastic Accumulation.....	18
1.3 Detrimental Effects of Mismanaged Plastic Waste.....	20
1.4 Current Challenges and Mechanisms for Plastic Release Mitigation.....	22
1.5 Developing a Circular Plastics Economy.....	23
1.6 Biodegradation: The Process of Natural Polymeric Deconstruction.....	25
1.7 Using Nature as Inspiration - Biodegradation for the Depolymerisation of Plastics.....	26
1.8 Promiscuous PET-Deconstructing Enzymes.....	27
1.9 Commercially Useful PETases.....	29
1.10 <i>IsPETase</i> - A Natural PET Depolymerase.....	30
1.11 How Do PETases Breakdown Plastics?.....	32
1.12 Interesting Structural Features of <i>IsPETase</i>	35
1.13 Attempts to Improve <i>IsPETase</i> Functionality.....	38
1.14 Complementary Approaches to Improving Plastic Deconstruction by PETases.....	42
1.15 Can Directed Evolution Provide a Gateway to Better Plastic Degrading Enzymes?.....	43
1.16 References.....	44
CHAPTER 2 : Introduction to Directed Evolution.....	52
2.1 Foreword.....	52
2.2 Acknowledgements.....	52
2.3 Introduction.....	52
2.4 Library Generation.....	54
2.5 Library Evaluation – Screening Techniques.....	55
2.6 Library Evaluation – Selection Techniques.....	58
2.7 Optimising and Enhancing Natural Enzymes.....	59
2.8 Mechanistic Promiscuity as a Gateway to New Functions.....	63

2.9 Directed Evolution of Computationally Designed Enzymes	64
2.10 Designing New Reactivities by Combining DE and Genetic Code Expansion	67
2.11 References	70
CHAPTER 3: Aims.....	76
CHAPTER 4: Directed Evolution of an Efficient and Thermostable PETase.....	77
4.1 Foreword	77
4.2 Acknowledgements.....	77
4.3 Abstract	77
4.4 Introduction	78
4.5 Results	80
4.6 Discussion.....	88
4.7 References	89
CHAPTER 5: Deconstruction of PET-Based Materials and a Bio-Derived Plastic by a Thermostable PETase	92
5.1 Foreword	92
5.2 Acknowledgements.....	92
5.3 Abstract	92
5.4 Introduction.....	93
5.5 Results.....	95
5.6 Discussion	99
5.7 References	100
CHAPTER 6: Introduction to Genetic Code Expansion	102
6.1 Foreword.....	102
6.2 Acknowledgements.....	102
6.3 Biocatalysts with Non-Canonical Amino Acids	103
6.3 References	107
CHAPTER 7: Capturing an <i>Is</i>PETase Acyl-Enzyme Intermediate Using Genetic Code Expansion	108
7.1 Foreword	108
7.2 Acknowledgements.....	108
7.3 Abstract	108
7.4 Introduction.....	109
7.5 Results.....	112
7.6 Discussion	115

7.7 References	116
CHAPTER 8: Conclusions and Outlook.....	117
CHAPTER 9: Experimental	120
9.1 Foreword.....	120
<i>9.2 Supporting Information for Chapter 4: Directed Evolution of an Efficient and Thermostable PETase.....</i>	<i>120</i>
<i>9.2.1 Methods</i>	<i>120</i>
9.2.1.1 Materials.....	120
9.2.1.2 Gene Construction.....	120
9.2.1.3 Library Construction	121
9.2.1.4 Semi-Preparative Protein Production for Library Screening.....	121
9.2.1.5 Preparative Protein Production for Time-Course Assays.....	122
9.2.1.6 Library Screening Using Amorphous PET Film (amoPET).....	122
9.2.1.7 Time-Resolved PET Depolymerisation Assays Using Crystalline PET Powder.....	123
9.2.1.8 Chromatographic Analysis	123
9.2.1.9 Melting Temperature Assessment	124
9.2.1.10 Chemical Synthesis of Reaction Substrates and Standards.....	124
9.2.1.11 Structure Determination of HotPETase	124
9.2.1.12 References	125
<i>9.2.2 Extended Data.....</i>	<i>126</i>
9.2.2.1 Extended Data, Figure 1.	126
9.2.2.2 Extended Data, Figure 2.....	126
9.2.2.3 Extended Data, Figure 3.	127
9.2.2.4 Extended Data, Figure 4.....	131
9.2.2.5 Extended Data, Figure 5.....	131
9.2.2.6 Extended Data, Figure 6.....	132
9.2.2.7 Extended Data, Figure 7.....	133
9.2.2.8 Extended Data, Figure 8.	133
9.2.2.9 Extended Data, Figure 9.....	134
9.2.2.10 Extended Data, Figure 10.....	134
9.2.2.11 Extended Data, Figure 11.....	135
9.2.2.12 Extended Data, Figure 12.....	135
9.2.2.13 Extended Data, Figure 13.....	136
9.2.2.14 Extended Data, Figure 14.....	136
9.2.2.15 Extended Data, Figure 15.	137

9.2.2.16 Extended Data, Figure 16.....	137
9.2.2.17 NMR Spectra.....	138
9.2.2.18 References.....	139
9.2.3 Supplementary Information.....	140
9.2.3.1 Supplementary Information, Figure 1.....	140
9.2.3.2 Supplementary Information, Table 1.....	142
9.2.3.3 Supplementary Information, Table 2.....	142
9.2.3.4 Supplementary Information, Figure 2.....	150
9.2.3.5 Supplementary Information, Figure 3.....	150
9.2.3.6 Supplementary Information, Table 3.....	151
9.3 Supporting Information for Chapter 5: Deconstruction of PET-Based Materials and a Bio-Derived Plastic by a Thermostable PETase.....	152
9.3.1 Methods.....	152
9.3.1.1 Materials.....	152
9.3.1.2 Preparation of PET Materials for Assays.....	152
9.3.1.3 Protein Production.....	152
9.3.1.4 Solid Substrate Depolymerisation Assays.....	153
9.3.1.5 PETG and PEF Subunit Hydrolysis Assays.....	153
9.3.1.6 Chromatographic PET Depolymerisation Analysis.....	153
9.3.1.7 Chromatographic PETG and PETG Subunit Hydrolysis Analysis.....	154
9.3.1.8 Chromatographic PEF and PEF Subunit Hydrolysis Analysis.....	154
9.3.1.9 Chemical Synthesis of Reaction Substrates.....	155
9.3.1.10 Characterisation of PET-based Substrates.....	155
9.3.1.11 Chemical Synthesis of PETG and PEF subunits.....	155
9.3.2 Extended Data.....	156
9.3.2.1 Extended Data, Figure 1.....	156
9.3.2.2 Extended Data, Figure 2.....	156
9.3.2.3 Extended Data, Table 1.....	157
9.3.2.4 Extended Data, Figure 3.....	157
9.3.2.5 Extended Data, Figure 4.....	158
9.3.2.6 Extended Data, Figure 5.....	159
9.3.3 Supplementary Information.....	160
9.3.3.1 Supplementary Information, Table 1.....	160
9.3.3.2 Supplementary Information, Figure 1.....	160
9.3.3.3 Supplementary Information, Figure 2.....	161

9.4 Supporting Information for Chapter 7: Capturing an IsPETase Acyl-Enzyme Intermediate Using Genetic Code Expansion	162
9.4.1 <i>Methods</i>	162
9.4.1.1 <i>Materials</i>	162
9.4.1.2 <i>Gene Construction</i>	162
9.4.1.3 <i>Protein Production</i>	162
9.4.1.4 <i>Acyl-Enzyme Intermediate Capture Assays</i>	163
9.4.1.5 <i>Mass Spectrometry</i>	163
9.4.1.6 <i>Chemical Synthesis of Photocaged 2,3-Diaminopropionic Acid (p-DAP)</i>	164
9.4.1.7 <i>References</i>	169
9.4.2 <i>Extended Data</i>	170
9.4.2.1 <i>Extended Data, Table 1</i>	170
9.4.2.2 <i>Extended Data, Figure 1</i>	171
9.4.3 <i>Supplementary Information</i>	172
9.4.3.1 <i>Supplementary Information, Table 1</i>	172
9.4.3.2 <i>Supplementary Information, Figure 1</i>	172
9.4.3.3 <i>Supplementary Information, Figure 2</i>	173
9.4.3.4 <i>NMR Spectra</i>	173

Word Count: 34,315

Abbreviations

2YT	yeast extract and tryptone broth
aaRS	aminoacyl-tRNA synthetase
ABH	α/β hydrolase
AIM	autoinduction media
amoPET	amorphous poly(ethylene terephthalate) film
avg. mw.	average molecular weight
BCDT	bis(2-cyclohexylenedimethylene) terephthalate
BHET	bis(2-hydroxyethyl) terephthalate
BHEF	bis(2-hydroxyethyl) furanoate
bgPET	bottle grade poly(ethylene terephthalate) pellets
CBM	carbohydrate binding module
cryPET	semi-crystalline poly(ethylene terephthalate) powder
DAP	2,3-diaminopropionic acid
DE	directed evolution
DMAP	4-dimethylaminopyridine
DMSO	dimethyl sulfoxide
DNA	deoxyribonucleic acid
dNTP	deoxynucleotide triphosphate
DSB	disulphide bond
DSF	differential scanning fluorimetry
<i>E. coli</i>	<i>Escherichia coli</i>
e.e.	enantiomeric excess
EG	ethylene glycol
FACS	fluorescence activated cell sorting
FCA	2,5-furandicarboxylic acid
<i>HiC</i>	cutinase from <i>Humicola insolens</i>
HPLC	high pressure liquid chromatography
HotPETase	variant of <i>IsPETase</i> engineered by directed evolution
HotPETase ^{LR}	HotPETase with $\beta 7$ - $\alpha 5$ loop reverted to wildtype
<i>I. sakaiensis</i>	<i>Ideonella sakaiensis</i>
<i>IsPETase</i>	PETase from <i>I. sakaiensis</i>
<i>IsPETase</i> ^{TS}	engineered thermostable variant of <i>IsPETase</i>

IsPETase ^{TS} -DAP	DAP modified IsPETase ^{TS}
IsPETase ^{TS} -p-DAP	photocaged DAP modified IsPETase ^{TS}
IsPETase ^{WT}	wildtype form of IsPETase
IsMHETase	MHETase from <i>Idonella sakaiensis</i>
IRED	imine reductase
UPLC	ultrahigh pressure liquid chromatography
KRED	ketoreductase
LB	lysogeny broth
LCC	leaf-branch compost cutinase
LCC ^{ICCG}	engineered leaf-branch compost cutinase
LPMO	lytic polysaccharide monooxygenase
MAO	monoamine oxidase
MCDT	mono-2-cyclohexylenedimethylene terephthalate
Me-His	N _δ -methylhistidine
MHET	mono-2-hydroxyethyl terephthalate
MHETase	MHET-degrading enzyme
MHEF	mono-2-hydroxyethyl furanoate
MS	mass spectroscopy
ncAA	non-canonical amino acid
NMR	nuclear magnetic resonance
NQ	not qualified
OD	optical density
P450	P450 monooxygenase
PCR	polymerase chain reaction
p-DAP	photocaged 2,3-diaminopropionic acid
PDB	protein data bank
PE	polyethylene
PEF	poly(ethylene furanoate)
PET	poly(ethylene terephthalate)
PETase	PET-degrading enzyme
PETG	poly(ethylene glycol-co-1,4-cyclohexanedimethanol terephthalate)
RFP	red fluorescent protein
rpm	rotations per minute
r.t.	room temperature

s.d.	standard deviation
SDS-PAGE	sodium dodecyl sulphate-polyacrylamide gel electrophoresis
<i>T. fusca</i>	<i>Thermobifida fusca</i>
<i>TfCut</i>	cutinase from <i>T. fusca</i>
T_m	melting temperature
T_g	glass transition temperature
TPA	terephthalic acid
tRNA	transfer ribonucleic acid
UV	ultraviolet
WT	wildtype

ABSTRACT

Engineering of a Thermostable PETase by Directed Evolution

A thesis submitted to The University of Manchester for the degree of Doctor of Philosophy in the Faculty of Biology, Medicine & Health, School of Biological Sciences, 2021

Elizabeth L. Bell

Plastics are exceptionally useful materials. With a wide range of beneficial characteristics and capabilities, plastics have been instrumental in the progression of modern society by underpinning the development of new technologies across a spectrum of industries from food packaging to medicine. Yet many of the attributes that make these materials such a valuable commodity lends them to becoming a serious environmental threat. It has become impossible to ignore the duplicitous nature of anthropogenic polymers and the failure of current recycling methodologies to curb the ever-increasing plastic pollution problem. Biocatalytic depolymerisation has the potential to overcome some of the challenges faced by conventional recycling strategies, such as mechanical or chemical methods, but the absence of industry-ready enzymes has hindered wide-scale adoption of this technology. Indeed, for biological recycling to become a viable methodology, biocatalysts must be able to withstand tough plastic processing conditions and function competitively, both practically and economically, as compared to alternative methods. The research presented in this thesis describes a method to rapidly optimise plastic degrading enzymes to enhance their commercial applicability, detailing the design and deployment of a high-throughput directed evolution platform to engineer the poly(ethylene terephthalate) (PET) deconstructing enzyme from *Ideonella sakaiensis* (*IsPETase*). The resulting biocatalyst, HotPETase, has superior characteristics to its parent protein: it has the ability to function at elevated temperatures close to the glass transition temperature of PET (60-70°C) and to depolymerise a range of PET-containing materials, including highly crystalline PET, PET composites and PET copolymers, that would be present in realistic post-consumer waste streams. Structural characterisation of HotPETase sheds light on the features installed during directed evolution that augment stability and catalytic performance. To further understand the structural basis and catalytic mechanism of polymer deconstruction by *IsPETase* and its engineered variants, a method to trap and characterise a close analogue of

a key catalytic intermediate is also presented, taking advantage of genetic code expansion technologies. It is anticipated that the engineering strategies described within, along with the enhanced characteristics and broad substrate scope of HotPETase, in conjunction with an elevated understanding of the mechanism of enzymatic PET deconstruction, will contribute to the future development of a suite of complementary, industrially-viable, plastic-deconstructing enzymes.

The research carried out during this PhD is presented as a series of manuscripts that are either published, or planned for submission at peer-reviewed journals. The research has been presented in this manner as the majority of the candidate's research has been published or is at a suitable stage for the preparation of draft manuscripts. Furthermore, the review article, book chapter and prepared research manuscripts lend themselves to a clear narrative and their preparation has taken equal time and consideration to that of a traditional thesis.

The contents are organised as followed:

Chapter 1: An introduction to plastics and the potential for their enzymatic deconstruction.

Chapter 2: A book chapter containing an introduction to the field of directed evolution and its uses. (*Bell, E.L. et al, Modern Developments in Biocatalysis, (2022)*)

Chapter 3: Aims of the PhD project.

Chapter 4: A research article describing the directed evolution of an efficient and thermostable PETase. (*Bell, E.L. et al Directed Evolution of an Efficient and Thermostable PET Depolymerase. ChemRxiv. Cambridge: Cambridge Open Engage (2021)*)

Chapter 5: A research article describing the use of an engineered PETase to deconstruct PET-containing materials and a bio-based PET derivative.

Chapter 6: A review article discussing the use of genetic code expansion for biocatalysis. (*Bell, E. L. et al. Biocatalysis. Nature Reviews Methods Primers 1, 46 (2021)*)

Chapter 7: A research article describing the underpinning work to allow the capture of an intermediate in the catalytic cycle of IsPETase.

Chapter 8: Conclusions of the thesis and future outlook.

Chapter 9: Supporting information for the presented research articles including materials and methods.

Declaration and Copyright Statement

No portion of the work referred to in the thesis has been submitted in support of an application for another degree or qualification of this or any other university or other institute of learning.

- i. The author of this thesis (including any appendices and/or schedules to this thesis) owns certain copyright or related rights in it (the “Copyright”) and s/he has given The University of Manchester certain rights to use such Copyright, including for administrative purposes.
- ii. Copies of this thesis, either in full or in extracts and whether in hard or electronic copy, may be made only in accordance with the Copyright, Designs and Patents Act 1988 (as amended) and regulations issued under it or, where appropriate, in accordance with licensing agreements which the University has from time to time. This page must form part of any such copies made.
- iii. The ownership of certain Copyright, patents, designs, trademarks and other intellectual property (the “Intellectual Property”) and any reproductions of copyright works in the thesis, for example graphs and tables (“Reproductions”), which may be described in this thesis, may not be owned by the author and may be owned by third parties. Such Intellectual Property and Reproductions cannot and must not be made available for use without the prior written permission of the owner(s) of the relevant Intellectual Property and/or Reproductions.
- iv. Further information on the conditions under which disclosure, publication and commercialisation of this thesis, the Copyright and any Intellectual Property and/or Reproductions described in it may take place is available in the University IP Policy (see <http://documents.manchester.ac.uk/DocuInfo.aspx?DocID=24420>), in any relevant Thesis restriction declarations deposited in the University Library, The University Library’s regulations (see <http://www.library.manchester.ac.uk/about/regulations/>) and in The University’s policy on Presentation of Theses.

Acknowledgements

Firstly, I would like to thank my Supervisor Professor Anthony Green for welcoming me into his lab and giving me the opportunity to work on a project to solve a problem I am very passionate about. I have gained an immeasurable number of skills both in and out of the laboratory, working under his attentive intellectual and practical guidance. I would also like to thank my Co-Supervisor Dr Philip Day for his support, the MRC for their generous funding, and Buddi for their funding and continued encouragement even when the project moved in a different direction.

I would like to acknowledge all of the colleagues I have had the pleasure of working with. I have immensely enjoyed being part of the busy and vibrant Green Group, with special mentions to Amy Crossley, Dr Ashleigh Burke and Dr Rebecca Crawshaw for their help and support to make it through the sometimes-gruelling process of directed evolution, to Dr Mary Ortmayer for her bright and cheerful chatter, and to Ross Smithson for his uncomplaining help and support in taking seemingly endless assay time points. I would also like to say thank you to Dr Jo Saddler and Dr Andy Currin for helping me settle into the MIB when I first arrived, and navigate the bumpy first year of my PhD, and to my DTP buddy Lottie Criscuolo for always offering sage advice. I'm immensely grateful to Amy, Ashleigh, Mary and Flo for proof-reading my thesis.

Finally, I would like to thank my family and friends, especially my Mum for her unwavering confidence in me (I think Dad would be proud), my Nana (who will be greatly missed) and Grandad for their unconditional support, Alex for his unparalleled patience and for kindly sharing his Excel powers, and Winnie, Müsli and Gizmo, who has kept me company during the entirety of writing this thesis. Without their understanding and encouragement over the last four years, it would have been impossible for me to complete this PhD.

CHAPTER 1

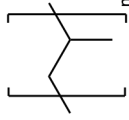
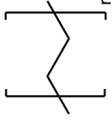
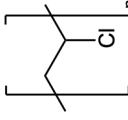
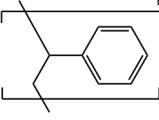
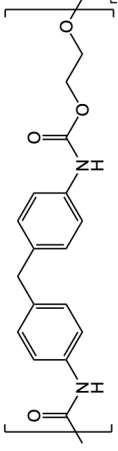
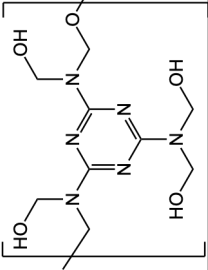
Introduction

Plastics have played a prominent role in the development of modern society. The versatility of plastics, coupled with their low-cost, has enabled them to be adapted for a multitude of applications: they have become a commodity that seems almost irreplaceable. Unfortunately, the properties that make plastics appealing, such as their inertness and durability, means that they become a particularly harmful pollutant if disposed of improperly. It is now widely recognized that the accumulation of plastics in the environment poses a serious global pollution threat, especially in marine ecosystems. There is therefore urgent need to incentivise repurposing this waste, by designing an economically viable plastics processing system that creates output products of value to society. To meet these requirements, existing technologies need to be improved, or alternative methods developed to treat and recycle plastic waste, in order to prevent an environmental catastrophe.

1.1 Plastics - An Overview

Plastics are synthetic polymers: large (10-500 kDa), man-made macromolecules comprising repeating units known as monomers.¹ These polymers are created by a process of polymerisation, whereby monomers are chemically bonded together to form a three-dimensional network of high-molecular weight chains.^{2,3} By cleverly combining monomers with different functional groups, plastics with a wide range of chemical, thermal and mechanical properties can be produced (Table 1). Due to the incredible versatility of plastics and their capacity for use in a plethora of applications, it is unsurprising that plastic production yields huge economic and societal benefits.⁴ There is a wide variety of plastics available, which can be grouped and classified in numerous ways.² Plastics can be made of identical repeating monomeric units, known as homopolymers, or concatenated from multiple different subunits, known as copolymers. They can form linear chains or have branching substituents, and often contain additional additives to improve their characteristics. The amalgamation of these physical and chemical properties dictates a polymer's response to heating: thermosets are irreversibly hardened when heated, as complex covalent crosslinks form between the polymer chains, making them very strong and perfect for high temperature applications.⁵ Conversely, thermoplastics melt when heated and harden when cooled.⁶⁻⁸

Table 1. Examples of commonly used plastic polymers.

Name	Monomers	Polymer	Classification	Example Uses
Polypropylene (PP)	Propylene		Homopolymer, Thermoplastic, C-C backbone	Buckets, crates, piping ⁷
Polyethylene (PE)	Ethylene		Homopolymer, Thermoplastic, C-C backbone	Packaging applications, e.g. supermarket shopping bags, plastic films, shampoo bottles ⁸
Polyvinylchloride (PVC)	Vinyl Chloride		Homopolymer, Thermoplastic, C-C backbone	Utilised by the construction industry ²
Polystyrene (PS)	Styrene		Homopolymer, Thermoplastic, C-C backbone	Disposable packaging material, insulation ²
Polyurethane (PUR)	Triisocyanate Polyol		Copolymer, Thermoset, C-X-backbone	Building insulation foams, adhesives, sealants ²
Melamine	Melamine Formaldehyde		Copolymer, Thermoset, C-X-backbone	Tableware, kitchen surfaces ⁶

Thermoplastics, can also be described by the degree of order within the polymer, known as its crystallinity (Fig. 1). As the plastic cools following heating, sections of the polymer may fold to form areas of highly ordered, aligned chains, known as crystalline regions. The less ordered areas are known as amorphous regions. The degree of crystallinity depends upon a range of factors, such as monomer chemical composition and production techniques.¹¹ Controlling the levels of crystallinity within a plastic can drastically alter the characteristics of the polymer produced. For example, highly crystalline plastic resins are more resistant to chemical attack, whilst lower crystallinity leads to a more flexible polymer which is prone to changes in physical characteristics at elevated temperatures. This is because the amorphous regions of the plastic demonstrate a property known as glass transition.¹² At a certain temperature, known as the glass transition temperature (T_g), the amorphous regions of the polymer convert from hard and brittle to rubbery and soft. Consequently, polymers of identical chemical composition can display widely varying properties depending on their degree of crystallinity and the temperatures they are subjected to.

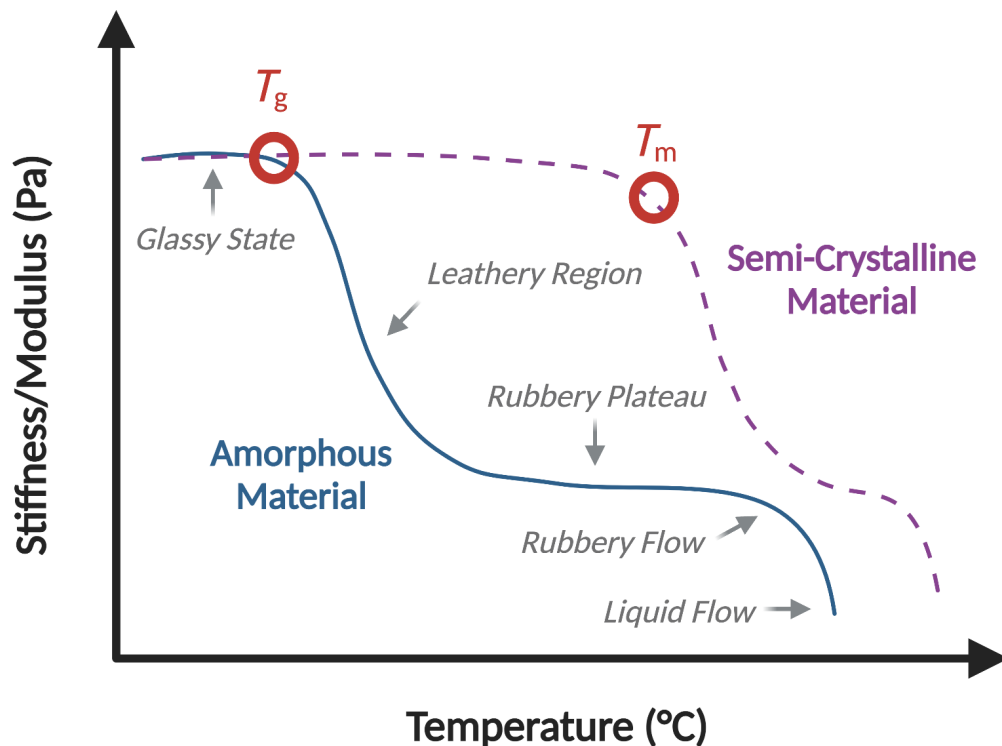


Figure 1. Melting and softening behaviour of semi-crystalline and amorphous materials. As materials are heated, they pass through several states changing from a solid glassy state to a more liquid flowing state.¹² As amorphous materials (blue solid line) move above their glass transition temperature (T_g) they begin to soften, quickly losing their strength, whilst semi-crystalline materials (purple dashed line) maintain their mechanical properties until the melting temperature of the material is reached (T_m).

In terms of their chemistry, plastics can be broadly split into two main groups, those with a C-C-containing backbone and those with a C-X-containing backbone, where X = O or N.⁹ The backbone composition of polymers affects both their stability and their potential for depolymerisation. In general, sp^3 hybridised, C-C-linked polymers, such as polyethylene (PE), polystyrene (PS) and polypropylene (PP), are highly resilient, as the C-C bonds are challenging to cleave. Hence, depolymerisation of these types of plastics typically requires a non-catalytic, thermal process. In contrast, C-O- and C-N-linked polymers, for example poly(ethylene terephthalate) (PET), polyamide (PA) and polyurethane (PU), are more labile: depolymerisation of their heteroatom backbones exhibits a much lower reaction barrier as compared to C-C-linked polymers. For these plastics, depolymerisation can be catalysed by nucleophilic attack of carbonyl groups. Due to their differing properties and usages, both C-C- and C-X-linked plastics are manufactured on an enormous scale, with derivatives of PE and PET being the most abundantly produced C-C- and C-X-containing backbone plastics respectively (Fig. 2).¹⁰

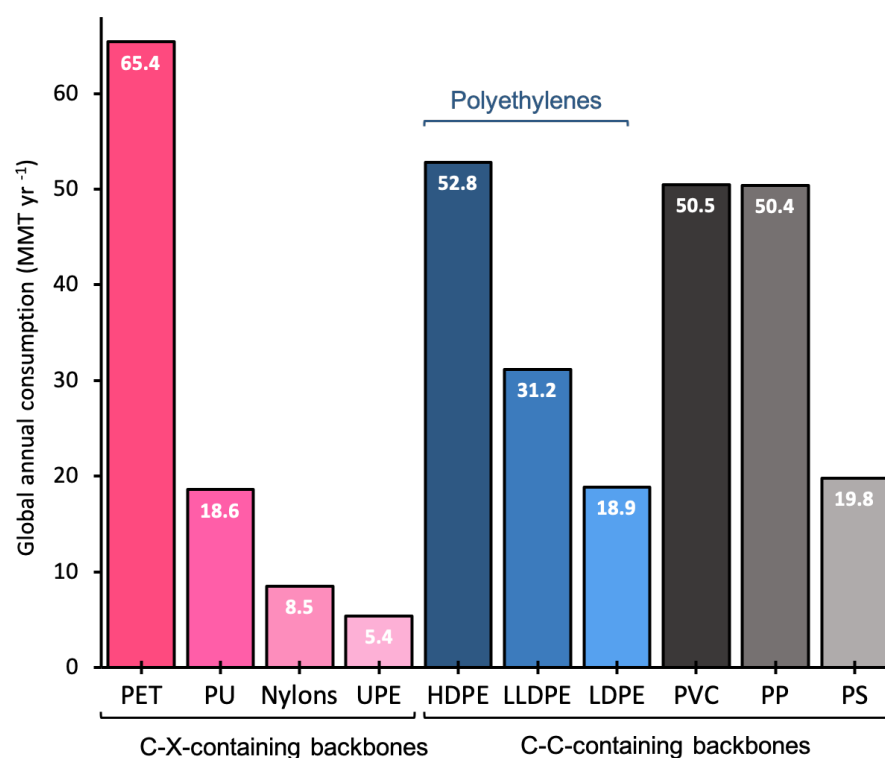


Figure 2. Annual global market size of the most popular plastics. Bar chart showing the average global consumption of the four most prevalent synthetic polymers containing either C-X- (pinks) or C-C-linked backbones (blues and greys), measured in millions of metric tonnes per year (MMT yr⁻¹).¹⁰ For the C-X-linked group, PET is the most in demand, followed by PU, nylons and unsaturated polyesters (UPE). For the C-C-linked group, PE is the most popular (blues), split into high density PE (HDPE), low density PE (LDPE) and linear LDPE (LLDPE), followed by PVC, PP and PS.

PET, the most in-demand C-X-linked polymer, has garnered particular notoriety with the public due to its use in the bottling and single-use plastic industries.¹³ PET is a copolymer, and can be manufactured from the crude oil-derived intermediates terephthalic acid (TPA) and ethylene glycol (EG) (Fig. 3). These monomers are joined in a polycondensation reaction and depending on the reaction conditions and TPA isomer used, polymers with a range of crystallinities can be formed.¹⁴ Alternatively, PET can be produced via a transesterification reaction of dimethyl terephthalate (DMT) and excess EG. PET is desirable for a vast range of applications from textiles to food packaging,¹⁵ and due to its excellent physical and chemical properties it has become one of the most extensively used plastics.¹⁶ PET is both strong and durable, yet easily mouldable and transparent with low gas permeability.¹⁷ Indeed, it has become an integral part of modern-day society with PET production capacity reaching 33 million tons per year in 2017.¹⁸ Typically, textile fibres account for around 60% of global PET manufacture,¹⁹ and packaging for approximately 30%: an estimated 580 billion plastic bottles were manufactured in 2021 alone.²⁰

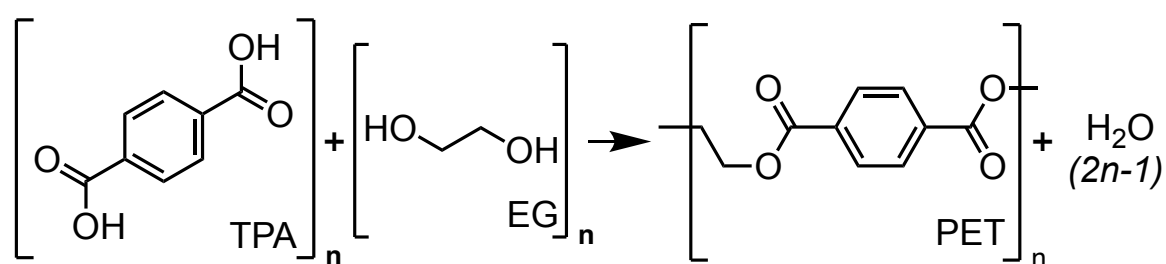


Figure 3. PET can be produced in polycondensation reactions of TPA and EG monomers.

1.2 Reasons for Plastic Accumulation

As plastics are long-lived and persistent materials, it seems intuitive that plastic items would be used for long periods of time prior to their disposal. Somewhat paradoxically, this is not the case. On average, plastics are only used for around five years before they are discarded, whilst the majority of plastic packaging is often disposed of within the same year it was made.²¹ Indeed, the prodigious global production and consumption of plastics has led to a deluge of polymer waste to be disposed of.²² Of the 8.3 billion tons of plastics that were produced as of 2015, it is estimated that over 75% has ended up as plastic rubbish.²¹ The fate of a large proportion of this waste plastic is the natural environment, with the problem set to increase in severity, with a predicted 239 million tons of mismanaged plastic waste predicted to be produced per year by 2040 (Fig. 4).²³ The problem is so extensive that the

presence of plastics in sedimentary ground strata has been suggested as a marker for the Anthropocene - an era where humans have begun to dominate fundamental earth geological processes.^{24,25}

Ineffective plastic management is of great concern, as once this plastic debris has entered environmental systems it is very difficult to reclaim. Plastics have been described as poorly reversible pollutants: pollutants for which emissions are not easily curtailed and which have a long environmental residency time.²⁶ Due to their chemical durability and impermeability, if plastics are left in the environment, they are prone to fragmentation rather than degradation. Over protracted periods of time, abiotic mechanisms such as solar UV radiation, abrasive action and thermal degradation instigate polymer chain scission and surface deterioration which lead to plastic embrittlement.²⁷⁻²⁹ Eventually, this leads to the plastic surface becoming increasingly fragile, with further stresses leading to microscopic flakes detaching from the polymer surface. These pieces of plastic, that are <5 mm in diameter, are known as microplastics.^{27,30} Invisible to the naked eye, microplastics are mobile terrestrially, aquatically and atmospherically; they are one of the most pervasive modern pollutants.³¹

For all practical purposes, plastic disintegration to microplastics is where the environmental polymeric degradation process ceases, as further breakdown is incredibly slow.³² In fact, it is not currently known exactly how long plastics would take to naturally breakdown in the environment.³³ Plastics certainly prevail submerged in the marine environment for decades,³⁴ but may endure for hundreds of years if present on the ocean surface,³⁰ or even millennia in the deep sea where low temperatures and lack of photodecomposition prohibit further breakdown.³⁵ All in all, this means that it is highly likely that all of the plastics that have ever been made, apart from those that were incinerated, are still present on Earth in some form today.³⁶ As plastics encompass a wide range of chemical compositions, morphologies and properties, environmental residence times will be quite diverse. Hence, even current calculations may not capture the true impact of this heterogenous class of polymers.

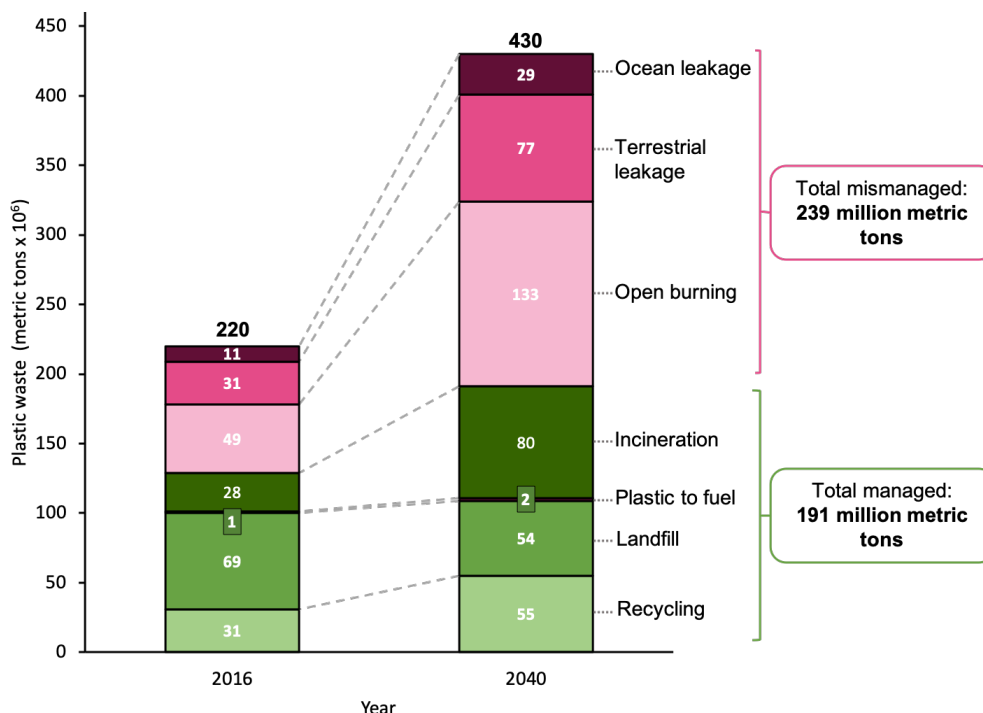


Figure 4. Growth in plastic waste following a business-as-usual scenario. If current trends continue, the amount of plastic waste (microplastics and macroplastics) will grow from 220 million metric tons to 430 million metric tons by 2040.²³ This will cause a concurrent rise in mismanaged plastic waste (pinks) which will enter the natural environment in some form. Open burning can have a large negative effect on human health due to the toxic emissions produced, so this increase is of particular concern. There are various methods to prevent environmental dispersal of plastic waste (green), but under a business-as-usual scenario their growth will not be rapid enough to mitigate the predicted rise in plastic waste.

1.3 Detrimental Effects of Mismanaged Plastic Waste

As the vast majority of common plastics do not biodegrade, they accumulate in the natural environment rather than decompose (Fig. 5).³⁵ This is of particular concern in the oceans: it is estimated that 11% of plastic waste produced in 2016 entered aquatic systems.³⁷ Plastic debris has been found from the poles to deep ocean basins, with huge masses of floating waste accumulating in ocean gyres. Where it accumulates it can have disastrous impacts on local ecosystems. Over 900 species of marine megafauna including seabirds, mammals and all species of sea turtle have been documented to have ingested or become entangled in plastics.³⁸ The ingestion of microplastics by organisms can cause changes in feeding rates, growth and reproduction, with the problem compounded across trophic levels as the microplastics and associated adsorbed toxins bioaccumulate up the food chain.²⁶ Humans are also directly affected by this phenomenon, as microplastics, alongside their heavy metal contaminants, have been found in the gills of sea bass, a common human food source.³⁹

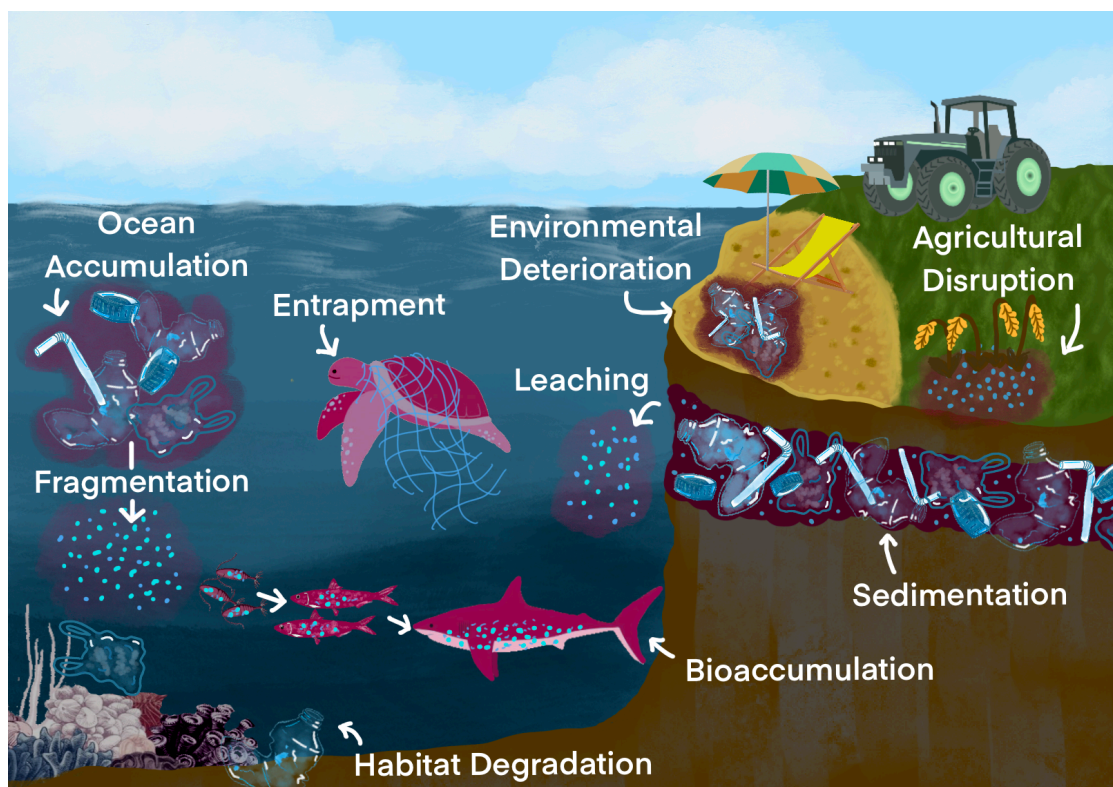


Figure 5. Effects of plastic waste accumulation. Once plastic has entered the environment it can have a broad range of negative environmental impacts. Macroplastics can accumulate in the oceans where they can entrap large organisms and can cause the deterioration of habitats. On land, they can cause the deterioration of human environments and sediment in the soil. Plastics can then break down into microplastics, which can leach into the terrestrial environment causing disruption to agriculture, or leach into the oceans. Ocean microplastics can be ingested by organisms and bioaccumulate up the food chain with increasing detrimental effect.

Not only do plastics affect aquatic systems, but they can also impact the terrestrial environment. Plastic particle accumulation can affect soil biodiversity⁴⁰ and seed germination,⁴¹ with negative impacts on soil fertility due to the long-term accumulation of toxic polymer additives.²⁶ Indeed, microplastic presence is so comprehensive, they have even permeated the atmosphere. For example, it has been demonstrated that microplastics are found in the snow falling in the supposedly pristine Arctic.⁴² Plastic pollution can also affect human economies: marine polymer pollution is believed to cost society up to \$2.5 trillion a year, due to its negative effects on ecosystem services, fishing and tourism industries.⁴³

The tide of plastic pollution shows no signs of stopping. Consumers continue to demand convenient, resilient, cheap and lightweight materials, with a recent spike in the need for

single-use plastics, such as medical gloves, masks and packaging, associated with the ongoing COVID-19 pandemic.⁴⁴ Promisingly, most governments and the public now acknowledge that plastic pollution is a serious economic, public health and environmental issue,⁴⁵ with it being a key topic in the upcoming 2022 United Nations Environmental Assembly.⁴⁶ Plastics have been both a blessing and a hidden curse, instrumental in promoting and enhancing technology that has shaped modern civilisation, whilst leaving us with a mountain of refuse to be dealt with.

1.4 Current Challenges and Mechanisms for Plastic Release Mitigation

Stemming the flow of plastic waste into the environment is an imposing task. A seemingly obvious strategy for pollution mitigation would be to disincentivise the use of single-use plastics (SUPs).⁴⁷ This would both reduce the potential amount of plastic that would enter natural systems, alongside reducing the demand for crude oil-derived virgin plastic, whose manufacture has additional associated environmental costs.⁴³ Although successful for plastic microbeads and bags,⁴⁸ it is not as easy to ban all SUPs as they have facilitated huge advances in the medical and food transportation industries.⁴⁹ Indeed, substituting plastics for other materials can have hidden penalties, negatively impacting health and socioeconomic factors, alongside increasing greenhouse gas emissions.⁵⁰ It is also difficult to easily coordinate the re-use of plastics to match the scale of plastic production. The expansion of reuse schemes quickly becomes logistically unfeasible, as there needs to be a network of collection points and there are large costs associated with transporting the waste for refilling.⁵¹ For a plastic release mitigation strategy to be useful, it is important to do a full techno-economic, life cycle and socio-economic analysis of the processes involved, to make sure such nuanced negative effects are not missed.⁵²

To add to these challenges, post-consumer waste is a complicated mix of multiple polymers with distinct chemical properties that would require different strategies for their recovery. The normal destination for these types of challenging waste streams is storage or destruction, by landfill or incineration.⁵¹ However, these are not suitable solutions for plastics. Landfill conditions increase plastic disintegration, which thence pollutes soils and watercourses as microplastic leachate,^{53,54} whilst poorly managed incineration, leads to large greenhouse gas emissions and toxic chemical release.⁵⁵ Furthermore, unlike glass and cardboard, it is immensely difficult to simply recycle most streams of post-consumer plastic

waste, as the different composites and mixtures of polymers must be sorted prior to processing,⁹ which often costs more than simply remaking plastics from virgin materials.⁵⁶

When plastics can be sorted effectively there a number of different mechanisms by which single-polymer waste streams can then be recycled. Mechanical recycling uses physical methods to break the bonds of higher molecular weight polymers into smaller chains which can then be re-extruded.⁵⁷ However, the resulting polymer has inferior mechanical properties as compared to the original plastic, and often needs mixing with virgin plastic to create a desirable end-product.⁵⁸ Furthermore, materials produced by this method often cannot be used for certain applications, and this cycle can only be performed a finite number of times. Chemical dissolution methods have been suggested as strategies to mitigate the deterioration of polymer characteristics post-recycling, however, limitations on solvent availability and energy considerations hamper their scalability.⁴⁹ Given these difficulties, it is unsurprising that less than 1% of plastics are currently being recycled more than once.²¹

An effective end-of-life plan for plastics therefore needs to overcome the current challenges faced by polymer waste disposal. It needs to be a future-proof, long term solution where plastic debris no longer causes environmental harm. Energetic, environmental and economic considerations all need to be considered, alongside reducing the need for new 'virgin' plastic, lessening the associated environmental impacts of its production.⁵⁹ To do this we will need new, innovative technologies, using currently available plastic waste reduction methods only 10% of annual plastic waste emissions could be prevented from entering the environment by 2030,³⁷ alongside detailed techno- and socio-economic assessments of the full life-cycle of any novel methodologies.⁵²

1.5 Developing a Circular Plastics Economy

The gold standard of recycling processes would be a closed-loop system, whereby polymers and their by-products are never released into the environment (Fig. 6).⁶⁰ This is the aim of a circular plastic economy, whereby the economic value and utility of plastics are constantly maintained within a system, hence, anthropogenic polymers never become waste material.⁶¹ However, the circularisation of a polymer life cycle is not without its challenges. It is thermodynamically complex, as no process is 100% efficient, and can be economically problematic if methods of recycling are costly.⁴⁹

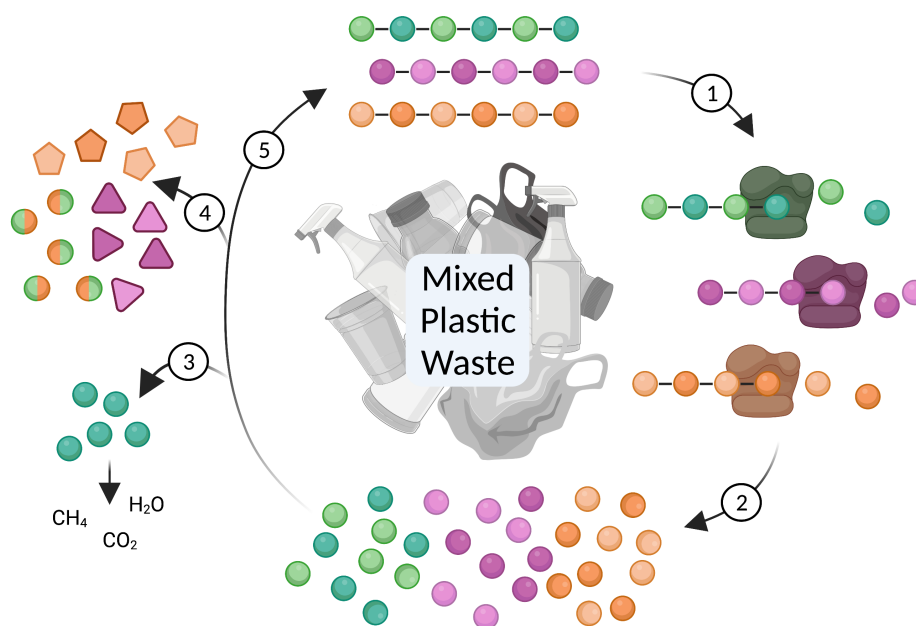


Figure 6. A circular plastics economy. (1) Different polymers present in plastic waste could be selectively deconstructed by specialised polymer-specific catalysts.⁶⁰ (2) The site-specific cleavage of polymer bonds leads to the release of monomers. (3) Some monomers, for example from specifically designed naturally biodegradable plastics, may be released into the environment where they can break down without causing damage. (4) Some monomers may be combined in new ways or synthesised into value-added compounds such as surfactants. (5) Remaining monomers will act as feedstocks for repolymerisation.

The ideal scenario would be where plastics can be broken down into their constituent monomers, in an environmentally sensitive way, with the resulting chemicals conscripted for new polymer synthesis, or used as building blocks for other high value chemical feedstocks.⁶² Chemical recycling goes some way towards meeting the requirements of a circular system. Via pyrolysis or chemical methods, polymer-derived moieties are salvaged and reused for remanufacturing of plastics or as precursors for other chemicals.⁶⁰ Unfortunately, these processes are very polymer specific, and can be severely disrupted by the compositional heterogeneity and presence of common plastic additives in even single-polymer waste streams.⁵¹ Furthermore, chemical recycling processes also often require huge initial thermal energy inputs to carry out the depolymerisation process, with additional greenhouse gas emissions associated with refining the products to give disappointingly low yields of high value products.⁴⁹ Thus, innovative technologies are required which can not only cope with complex mixed post-consumer waste streams, but also maximise and retain the economic worth of the recycled material, whilst keeping the greenhouse gas production and energy intensities of monomer recovery and refinement below those of primary plastic production.

1.6 Biodegradation: The Process of Natural Polymeric Deconstruction

Waste polymers are not a new problem, for instance, for naturally occurring polymeric materials, such as proteins, carbohydrates and DNA, the process of decomposition is delegated to a host of organisms and microorganisms. Fungi, bacteria and algae are all employed as natural recyclers in the process of biodegradation: the organismal scission of polymers via microbially-secreted catalytic agents into their bioavailable component monomers.⁶³ These monomers are converted into new biomass and metabolic by-products, hence, preventing their environmental accumulation.⁶⁴

Catalytic biodegradation agents are often enzymes. A good example is the synergistic suite of biocatalysts which breakdown the highly chemically recalcitrant lignocellulose, one of the most abundant biopolymers on earth.⁶⁵ Each enzyme class plays a different role: glycosidic bonds are randomly hydrolysed by endo-active cellulases, whilst exo-active cellulases processively hydrolyse cellobiose from polymer chain termini, which is further cleaved into glucose by β -glucosidases.⁶⁶ These hydrolytic enzymes act in a concerted manner to convert the insoluble lignocellulose into soluble glucose monomers. In contrast to the hydrolytic polysaccharide monooxygenases (LPMOs), a family of metalloenzymes,^{65,67} operate slightly differently. Via a mechanism involving molecular oxygen and an electron donor, LMPO-catalysed lignocellulose breakdown leads to oxidation of carbons in β -1,4-glycosidic bonds in hard-to-degrade, crystalline regions of the polymer. Without the synergistic action of these specialised biocatalysts, lignocellulose, composed of a complex network of tightly packed polymeric chains, would be rendered unresponsive to chemical and biological deconstruction.⁶⁸

Although nature is exceptionally efficient at breaking down natural polymers such as cellulose, unfortunately, nature's intrinsic clean up mechanism cannot currently cope with anthropogenic polymeric plastics. Plastics are highly recalcitrant to biological break down.⁶⁹ The presence of large numbers of hydrophobic subunits renders them insoluble in water, and hence sparingly bioavailable for microbial assimilation, whilst additionally hampering the adsorption of any potential depolymerising enzyme.⁷⁰ Plastics also tend to contain high-molecular weight chains, with complete items often having low surface area to volume ratios, restricting any microbial attack to a process of surface erosion.⁷¹ Considering the different types of polymer chemistries, the C-C-linked backbones of the polyolefin plastics are likely to be the most resistant to biodegradation, due to their chemical inertness.⁹ The

biocatalytic deconstruction of C-X-linked polymers may be more realistic as C-O and C-N bonds are amenable to hydrolysis. Despite this, challenges are still apparent. For example, with regards to PET, repeating aromatic terephthalate moieties in its polyester backbone result in limited chain mobility, rendering PET particularly stubborn to break down.⁷²⁻⁷⁴ However, even if C-X-linked polymer biocatalytic deconstruction can be envisioned, as plastic is an anthropogenic polymer that has only recently been introduced into the biosphere, there are few microbes biochemically equipped to facilitate its deconstruction.⁷⁵ There has not yet been sufficient time for evolutionary adaptation and optimisation of enzymes and metabolic pathways needed for efficient plastic bioremediation.^{76,77}

1.7 Using Nature as Inspiration - Biodegradation for the Depolymerisation of Plastics

Despite the challenges posed by biological plastic depolymerisation, enzymatic plastic deconstruction is still an appealing solution, due to the intrinsic properties of biocatalysts.⁹ Able to function at ambient temperatures and under environmentally benign conditions, enzymes could in principle deconstruct certain plastics with minimal negative environmental consequences. Enzymes are also highly substrate specific, with the potential to target and degrade a single plastic from within a complex mixed waste stream. This draws parallels with the deconstruction of natural materials: wood is composed of the biopolymers lignin, hemicellulose and cellulose, with each component being degraded by different substrate-specific enzymes. Using this as inspiration, the biocatalytic deconstruction of a complete plastic bottle, for example, could be imagined, with the PET bottle, PP lid and PE wrapper being individually targeted by specialised enzymes. The specificity of biocatalysts extends to the deconstruction output, with enzymes being able to produce a homogenous chemical product of choice, depending on the precise enzyme used. Furthermore, biocatalysts have the potential to be combined in cascades to sequentially depolymerise and convert the resulting product into higher-value chemicals.⁷⁸ This is a realistic proposition due to the significant advances and interest in synthetic biology over the past decade, with large efforts being put into the development of competent microbes for industrial enzymatic cascade processes.⁷⁹ With the potential for minimal reaction by-products coupled with their inherent renewability, enzymes could offer an ideal green route to a circular plastic recycling system.

1.8 Promiscuous PET-Deconstructing Enzymes

For the biological deconstruction of plastics to be effective, we first need to discover enzymes with plastic-degrading capabilities. As PET is one of the most abundant anthropogenic polyesters, it has garnered much scientific interest as a potential start point for designing and creating a model circular waste management system. Original studies looked at wild-type enzymes with promiscuous PET deconstruction activities (PETases),⁸⁰⁻⁸⁷ whilst more modern-day approaches use genome-mining or bioprospecting to search for enzymes that potentially have the right catalytic machinery to degrade plastics (Table 2).^{77,88,89} Although it is unclear exactly how many enzymes might have a secondary plastic deconstruction function,⁹⁰ it is estimated that there could be over 800 potential PETases across both the terrestrial and marine prokaryotic and fungal kingdoms.⁷⁷

Individual enzyme performances are highly reliant on the PET plastic substrate, substrate pre-treatment and reaction conditions used, hence, due to the absence of standardized protocols, ranking potential polymer deconstructing biocatalysts using available data is very difficult. As catalytic plastic degradation is an interfacial reaction with a solid substrate, usual methods of reporting enzyme kinetic parameters, for example k_{cat} and K_M , do not directly apply, making comparisons even more challenging.⁹¹ These difficulties are also faced in the study of biopolymer deconstruction: the enzymatic depolymerisation of lignocellulose to produce biofuels is similarly complicated, with kinetic modelling of the involved biocatalysts proving particularly complex.⁹² Promisingly, methods to obtain more realistic kinetic parameters for PETases are beginning to emerge.⁹³ For instance, inverse Michaelis-Menten models, where reactions are arranged so that the enzyme being studied is far in excess of the substrate, were successfully used to more accurately compare the performances of two PETase mutants.⁹⁴

Table 2. Examples of notable promiscuous PET-degrading enzymes. Reaction conditions and substrates vary widely between the different PETases studied. Percentage crystallinity of reaction substrates is recorded in brackets. NQ signifies where a value was not quoted in the study.

Organism	Enzyme	Substrate	Activity
<i>Fusarium solani</i>	FsC, cutinase	Low crystallinity PET (3%)	5% weight loss of PET, reaction at 50°C for 96 hrs ⁸⁰
<i>Humicola insolens</i>	HiC, cutinase	Bottle-grade PET, high crystallinity (NQ%)	0.52% weight loss of PET, at 37°C, reaction for 28 days ⁸⁰
<i>Candida antarctica</i>	CALB, lipase	Low crystallinity PET (7%)	97% weight loss of PET, reaction at 70°C for 96 hrs ⁸¹
<i>Thermobifida fusca</i>	TfCut1	Low crystallinity PET film (NQ%)	5% weight loss of PET, reaction at 50°C for 96 hrs ⁸⁰
KW3	TfCut2	Low crystallinity PET film (NQ%)	<11% weight loss of PET, reaction at 55°C for 48 hrs ⁸²
<i>Thermobifida fusca</i>	TfH	Bottle grade PET, high crystallinity (10%)	<12% weight loss of PET, reaction at 55°C for 48 hrs ⁸²
<i>Saccharomonospora viridis</i> AHK190	Cut190	Low crystallinity PET film (NQ%)	50% weight loss of PET, reaction at 55°C for 3 weeks ⁸³
<i>Pseudomonas aestusnigri</i>	PE-H	Low crystallinity PET film (NQ%)	12% weight loss of PET, reaction at 63°C for 3 days ⁸⁴
<i>Bacillus subtilis</i>	BsEstB	3-PET (short chain PET homologue)	Less than 1% deconstruction of PET (calculated from MHET release), reaction at 30°C for 48 hrs ⁸⁷
<i>Thermobifida cellulosilytica</i>	Thc_Cut1	PET powder (NQ%)	~24% of 3-PET deconstructed (calculated from MHET and TPA released), reaction at 30°C for 30 hrs ⁸⁶
Unknown, found in leaf/branch compost	LCC ⁹⁵	Low crystallinity PET film (NQ%)	~23% of a PET powder deconstructed (calculated from MHET and TPA released), reaction at 50°C for 72 hrs ⁸⁵
			<5% weight loss, reaction at 50°C for 8 hrs ⁹⁶

Despite the challenges associated with quantifying an enzyme's plastic degrading activity, in general, promiscuous PETases have rudimentary abilities to convert solid plastic substrates into soluble products. With this in mind, there have been a number of attempts to improve the characteristics of these enzymes.⁹⁷⁻¹⁰⁰ A particularly popular strategy has been to promote enzyme stability to maximise polymer deconstruction by introducing disulphide bridges into putative calcium binding sites of the proteins.⁹⁸⁻¹⁰¹ This negates the need to supplement enzymes with metal ions, whilst retaining the architectural stability they provide. The most successful study of this kind combined insertion of a disulphide bridge alongside some additional mutations to create a four-point mutant of leaf/branch compost cutinase (LCC), LCC^{ICCG}.¹⁰⁰ LCC^{ICCG} can depolymerise 90% of a micronized plastic sample, at a reaction temperature of 72°C in around 9 hours, with an enzyme substrate loading of 3 mg protein per gram of PET. However, this impressive activity can only be reached by extensively pre-processing the PET to amorphize the material, a process that has both negative economic and environmental ramifications.¹⁰² It appears to be a general feature of promiscuous PET-deconstructing cutinases described to date, that they are poorly equipped to depolymerise more crystalline materials.¹⁰³⁻¹⁰⁵

1.9 Commercially Useful PETases

If an enzyme is to be used for industrial scale biocatalysis, it needs to be able to catalyse the bulk decomposition of commercially relevant plastic substrates. Easily enzymatically hydrolysable PET “tails” protruding from plastic fibre and films comprise less than 0.1% of PET materials commonly used for packaging.⁹⁸ Hence, any viable PETase will need to be able to access more than just the convenient loose ends. Unfortunately, commercial grade PET-based plastics possess high degrees of crystallinity (30-50%),¹⁰⁶ which, due to limited chain mobility, prohibits enzyme access.¹⁰⁷ However, we can promote enzyme attack by heating up the plastic to its glass transition temperature (T_g). Here, the amorphous regions of the plastic become more flexible, enabling biocatalyst-polymer chain binding and subsequent enhanced catalysis. The average T_g of commercial grade PET is around 70-80°C,¹⁰⁸ but this is lowered to around 60-70°C in aqueous solution due to increased motility and flexibility of polymer chains as water molecules diffuse between them.^{84,109} Successful plastic depolymerisers will therefore need to be thermostable to take advantage of this substrate accessibility enhancing process.

Finally, it is important that the enzyme can depolymerise plastics in a timely manner to make an attractive, cost-effective process. One limitation of promiscuous PET-degrading enzymes is that they have not evolved specifically for the breakdown of plastic, hence their catalytic ability is likely to be sub-par. A natural PET-depolymerising enzyme, however, could offer optimised catalytic machinery, with superior PET-degrading activities. As plastic is a fairly novel environmental substrate on evolutionary timescales, true PETases are very rare as they have not yet had time to differentiate from ancestral proteins and specialise in the decomposition of this recalcitrant material. However, the prospect of a bio-inspired plastic recycling route has recently been lent credence by the fortuitous discovery of a primitive true PET-hydrolysing enzyme from the *Ideonella sakaiensis* bacterium.⁹⁶ As plastics are synthetic, man-made polymers, it is quite remarkable that a genuine PET-degrading enzyme (PETase) is present in nature at all.

1.10 *Is*PETase - A Natural PET Depolymerase

Isolated from outside a bottle recycling factory in Osaka, Japan, the bacterial strain *I. sakaiensis* 201-F6 adheres to PET and uses it as its premier energy source.⁹⁶ In a two-stage process, first, a secreted enzyme, *Is*PETase, hydrolyses the PET polymer to release mono(2-hydroxyethyl) terephthalic acid (MHET) and terephthalic acid (TPA), with a small amount of bis(2-hydroxyethyl) terephthalate (BHET). In the second step, MHET is internalised and hydrolysed further by a second, synergistic enzyme, *Is*MHETase to produce ethylene glycol (EG) and TPA (Fig. 7).^{96,110} *Is*PETase is the only enzyme found to date that links PET degradation to catabolism in a single microbe: it uses the building blocks of plastic for metabolism.

There are a number of indicators that *Is*PETase has genuinely evolved for PET plastic hydrolysis. Firstly, it is a mesophile, operating at the ambient temperatures where its host organism resides. Indeed, when presented with amorphous PET film, it can reach between 6 and 120-fold higher degradation rates at 30°C than homologous promiscuous PETases such as the *T. fusca*, LCC and *F. solani* cutinases.⁹⁶ These wild-type homologous enzymes require additional heat inputs to reach comparable activities.¹¹¹ Secondly, as compared to other PET-hydrolyses, it has superior activity towards highly-crystalline bottle-grade PET,⁹⁶ which is more challenging to deconstruct and is more reflective of the grades of polymer which would be present in a recycling context.⁹⁴ In conjunction, *Is*PETase demonstrates

higher specificity for PET than other PET-depolymerising enzymes,⁹⁶ hinting that it could be of use for deployment in the degradation of PET in mixed plastic waste streams.

Although, the characteristics of *IsPETase* are promising, it is very rare for natural enzymes to be directly deployable as industrial catalysts. Wild-type *IsPETase* is no different as it suffers from several flaws. Firstly, as the availability of environmental plastic as a potential energy source is a relatively new phenomenon, *IsPETase* can be considered to be at the beginning of its evolutionary journey. In line with this, the activity of the purified enzyme is low: only 0.018 mg of MHET and TPA were produced after an 18 hr, 30°C incubation of *IsPETase* with a PET film disc, corresponding to only ~3% deconstruction of the polymer.⁹⁶ The protein is also extremely heat labile, exhibiting severely compromised activity when incubated at 40°C.¹¹² Indeed, the protein has a melting temperature (T_m) of only 48.8°C. The T_m of a protein is defined as the temperature at which the concentrations of folded and unfolded states of the protein are equal, and so is a measure of the thermostability of a protein. Hence, *IsPETase* would denature rendering it inactive at 70°C, meaning that it could not currently exploit the advantages of operating at the T_g of PET.

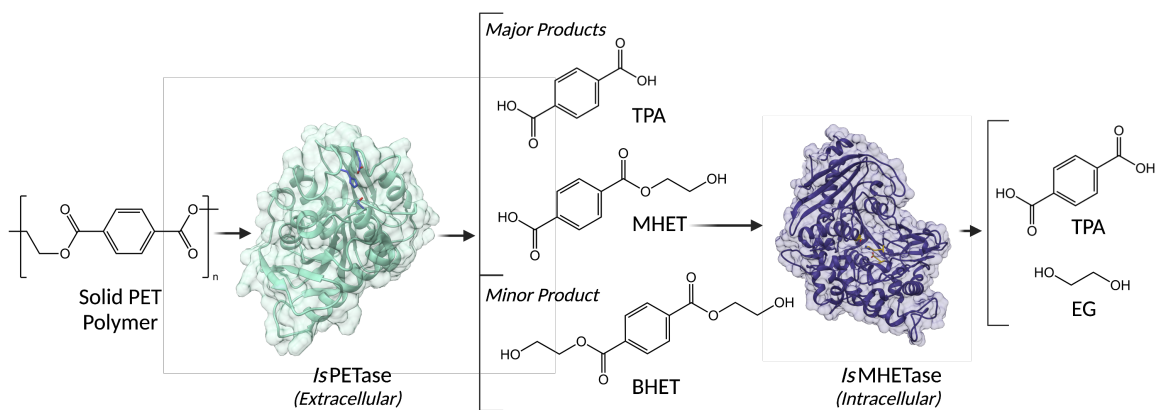


Figure 7. *IsPETase* catalyses the hydrolysis of solid PET plastic. *IsPETase* (PDB: 6EQE) is secreted by *I. sakaiensis*, where it acts directly on the polymer surface to release the soluble aromatic products MHET and TPA, with a small amount of BHET. BHET can be further broken down into MHET and TPA by *IsPETase*. MHET is subsequently internalised by the microorganism and hydrolysed by the enzyme *IsMHETase* (PDB: 6QGB) into TPA and EG, which can then be used for metabolism.

Despite this, a natural PETase with an active site specifically tailored for PET binding and hydrolysis is immensely promising for the development of a bio-based plastic recycling process. With this in mind, it is important to understand how this catalyst operates and what makes it special compared to other homologous enzymes, so that we can identify how to tailor the enzyme for large-scale application.

1.11 How Do PETases Breakdown Plastics?

Interestingly, sequencing and structural studies place enzymes from the cutinase and lipase family as ancestral parents of *IsPETase*: enzymes which were previously explored for their promiscuous PET-deconstructing activities.^{90,96,113} As a group, both promiscuous and true PETases, are ester bond breaking specialists from the serine α/β hydrolase (ABH) superfamily of enzymes,^{77,90} hydrolysing the ester bonds present in PET to release its constituent monomers. Serine ABHs are ubiquitous across all domains of life,¹¹⁴ partaking in ester and peptide bond hydrolysis,¹¹⁵ along with involvement in decarboxylation,¹¹⁶ heteroaromatic ring-deoxygenation,¹¹⁷ and carbon-carbon bond breaking reactions.¹¹⁸

One of the defining features of the serine ABHs is a conserved architecture consisting of a number of α -helical bundles, surrounding a core twisted β -sheet.¹¹⁹ Embedded in this structure is a triad of residues responsible for catalysis. *IsPETase* is no different, with the central region formed of nine β -sheets (β 1-9), surrounded by seven α -helices (α 1-7). It has a canonical catalytic triad consisting of Ser160, Asp206, and His237, along with a transition state stabilising oxyanion hole, comprising of backbone NH groups from amino acids Tyr87 and Met161 (Fig. 8).^{90,113,120} The purpose of the coordinated nucleophile-acid-base triad is to generate and prime the eponymous serine nucleophile to enable covalent catalysis.^{121,122} The carboxylate of the acidic aspartate polarises and accurately positions the histidine base to allow for effective activation of the catalytic serine.¹²³

Once activated, the Ser nucleophile is poised to hydrolyse the ester bonds present in PET, via a nucleophilic substitution reaction (Fig. 8). First the polymer binds, forming the enzyme-substrate complex. The Ser residue then attacks the carbonyl carbon (C=O) of the substrate, creating a covalent bond to form the first tetrahedral intermediate. The concomitant build-up of negative charge on the first substrate transition state is stabilised by the oxyanion hole. Proton donation by the His residue leads to the ejection of the first product, with the simultaneous formation of an acyl-enzyme intermediate.

A mechanistically similar deacetylation process then follows: this time a water molecule which is activated by the His base is used as the nucleophile. As before, the collapse of the tetrahedral intermediate leads to the ejection of the second product and the regeneration of the serine nucleophile.

Depending on where along the polymer chain a PETase binds, a number of hydrolysis products can be formed, from higher molecular weight chains to the smaller subunits of MHET, BHET and TPA. If cleavage occurs in the middle of a polymer chain it is known as endo-type chain scission, whilst if the end of a chain is targeted exo-type cleavage occurs, leading to the release of soluble depolymerisation products.¹⁰⁵ For *IsPETase* it has been suggested that a combination of these two processes occurs, ultimately leading to the formation of TPA and MHET as the dominant products.^{90,124} However, important questions on the mechanisms of polymer deconstruction remain, including whether *IsPETase* preferentially operates in an endo or exo-type fashion and whether the enzyme is processive, i.e. catalysing sequential hydrolytic reactions without releasing the polymer chain, or non-processive.⁹

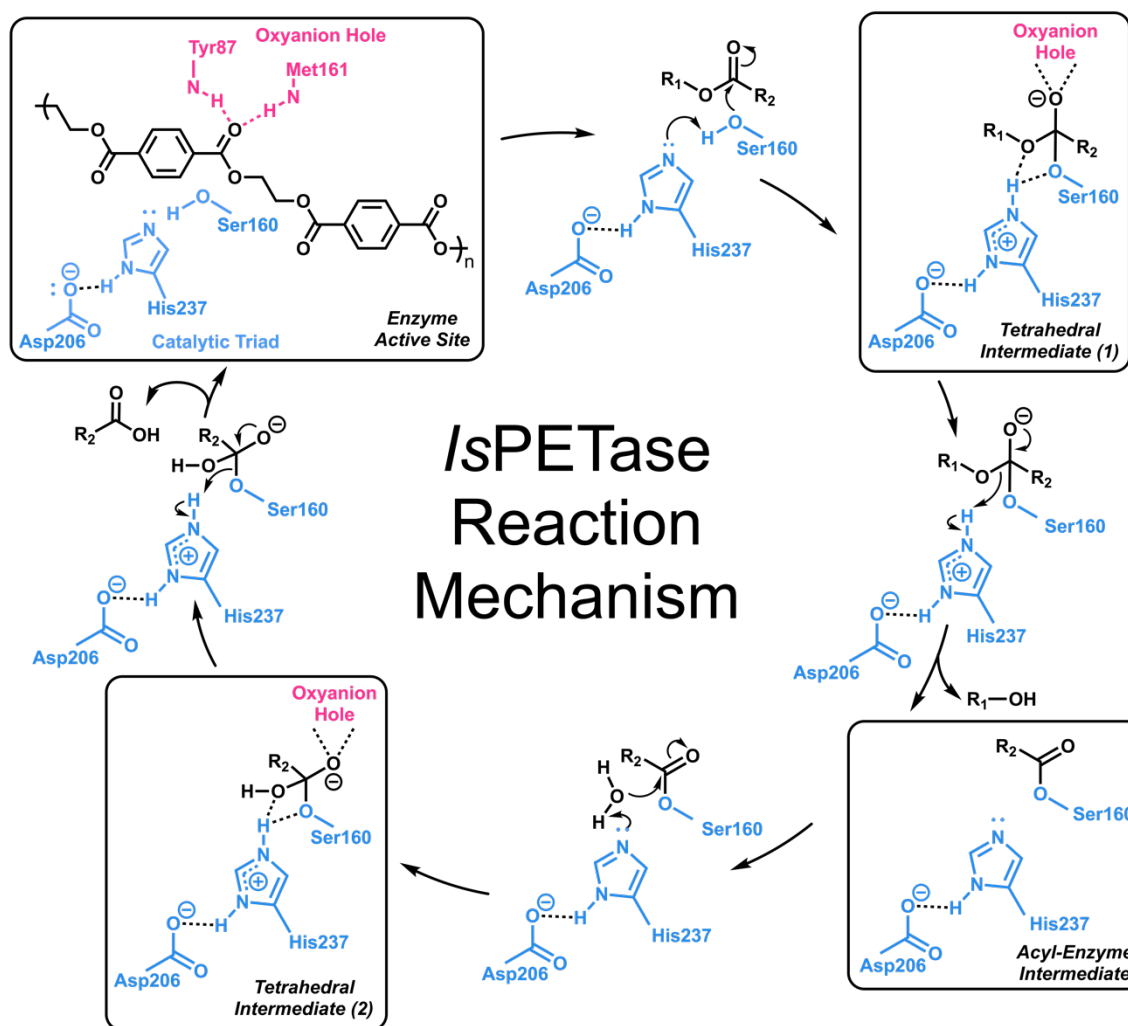


Figure 8. IsPETase reaction mechanism. IsPETase is a serine hydrolase which uses a canonical catalytic triad (blue), imbedded in the enzyme active site, for the hydrolysis of the ester bonds in PET. The reaction proceeds through a first tetrahedral intermediate, which is stabilised by an oxyanion hole (pink). This then collapses to give the covalently bound acyl-enzyme intermediate. Nucleophilic attack by a water molecule leads to the formation of a second tetrahedral intermediate, which again collapses to reform the active catalytic triad. R₁ and R₂ represent the rest of the PET polymer chain.

1.12 Interesting Structural Features of *IsPETase*

As the mechanism of action of PETases is well conserved, the superior PET-degrading activities of *IsPETase* compared to its homologues, must be down to other additional structural features. Sequence analysis has elucidated that PETase enzymes fall into three subgroups, type I, type IIa and type IIb.⁹⁰ *IsPETase* belongs to the type IIb category. This means that in addition to a conserved disulphide bridge across PETase homologues (Cys273-Cys289 in *IsPETase*), *IsPETase* has a second disulphide bond adjacent to the active site (Cys203-Cys239).^{113,120} Crystal structure analysis suggests this additional stabilising bonding interaction may allow for a longer, more mobile loop structure to exist in the *IsPETase*'s active site, without compromising its structural integrity (Fig. 9).¹²⁵ The increase in flexibility may help the enzyme to rapidly bind to the rigid polymer substrate and then release the resulting degradation products more effectively than other homologues.

Another interesting feature of the *IsPETase* is its exceptionally broad active site consisting of two subsites (subsite I and II) which form a hydrophobic L-shaped cleft, within which multiple PET moieties can sit (Fig. 10a).¹²⁰ This is up to three times wider than the active site pocket of its nearest structural homologue *T. fusca* cutinase. This is aided by the presence of a tryptophan, Trp159, situated in a generally conserved sequence known as the "lipase box" (Gly-x1-Ser-x2-Gly motif, where x1=Trp159 in the PETase). In other cutinases, phenylalanine or histidine usually occupies position x1; the presence of tryptophan in the *IsPETase* is purported to enlarge the active site-adjacent hydrophobic surface, aiding substrate binding.

A second tryptophan Trp185 is also of particular interest (Fig. 9, Fig. 10b).^{113,126} This residue also has the interesting property that it seems to be "wobbly" - having the ability to rotate, with different conformations seen in the ligand-free crystal structure. The wobbling is enabled by a serine residue, Ser214, which due to its small side chain, allows the tryptophan to move freely, as compared to the histidine present in the same position in homologues, which pins Trp185 to a single conformation. This movement is further aided by the unique isoleucine residue present at position 218 (Ile218), which again due to its small size reduces steric hindrance, allowing multiple Trp185 conformations.¹²⁷ The result of tryptophan wobbling is the introduction of a structural flexibility that aids the entry of bulky substrate polymers into the active site.¹²⁵ Trp185 is also purported to form π - π stacking interactions

with the benzene ring of an MHET moiety of the substrate, promoting the stabilisation of the PET polymer chain within the binding pocket.^{120,128}

Crystal structures and analysis can also give insights into the lack of thermal stability of *IsPETase* compared to related proteins, which tend to be more tolerant to high temperatures. Firstly, there are a number of highly flexible loop regions in the protein; although architecture flexibility is critical for catalysis, it can also render proteins thermally labile. The loop connecting the $\beta 6$ - $\beta 7$ region of *IsPETase* has been identified as particularly flexible in *IsPETase* compared to other more thermostable cutinases, with the $\beta 1$ - $\beta 2$ and $\beta 7$ - $\alpha 5$ connecting loop regions exhibiting similar flexible properties.^{112,128} Furthermore, an inherent structural instability has been found in the $\beta 6$ sheet, where a non-conserved proline residue, Pro181, disrupts the continuity of the sheet structure prohibiting hydrogen bonding between neighbouring main chains.¹¹² Together, these unique features begin to reveal why *IsPETase* is particularly heat sensitive.

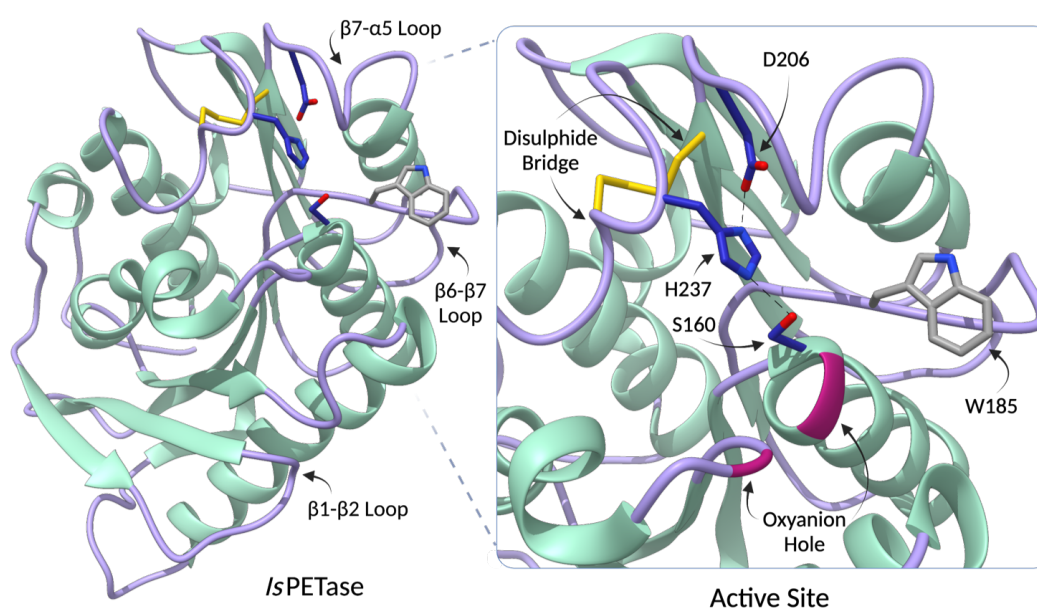


Figure 9. Crystal structure of *IsPETase*. Ribbon representation of *IsPETase* with important structural features annotated (PDB: 6EQE). The catalytic triad is represented by blue sticks, the active site adjacent disulphide bridge (C203-C239) by yellow sticks and the “wobbling tryptophan” (W185) by grey sticks. Residues forming the oxyanion hole are highlighted in pink (Y87, M161).

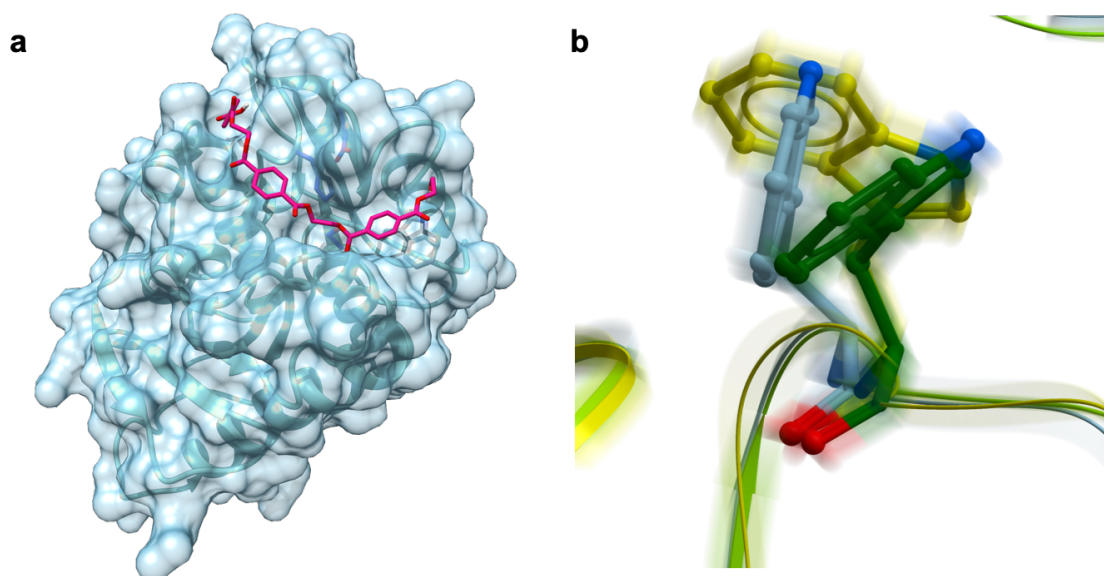


Figure 10. Important structural characteristics of *IsPETase*. (a) Surface representation of *IsPETase* (blue) with a PET surrogate, 2-hydroxyethyl-(monohydroxyethyl terephthalate)₃ (3PET) (pink) docked in the active site (PDB:6EQE). Docking was carried out using AutoDock Vina in Chimera. (b) Overlaid image of the three main possible configurations of W185. The protein backbone is represented as a ribbon, with the three wobbling tryptophan positions shown as green, yellow and blue sticks.

Often further insight into an enzyme's mechanism and stability can be found by studying a protein co-crystallised with its substrate. Unfortunately, for *IsPETase* this has proved challenging as PET is a large solid substrate. A small number of studies have bound smaller, soluble surrogate molecules, however, their lack of similarity to a polymer chain means the information they can provide is limited.^{90,113} Some larger molecules have been docked computationally, suggesting that up to four MHET moieties may be accommodated by the *IsPETase* active site across two subsites: subsite I where catalysis takes place, and subsite II, where additional substrate units are held.⁹⁰ However, this has been disputed as the rigidity of the polymer may preclude the PET chain adopting the angle it would need to fit the L-shaped active site cleft.¹²⁹ The lack of a realistic substrate bound-crystal structure, means that there are still some parts of the biological plastic-deconstructing mechanism that remain elusive.^{9,130}

1.13 Attempts to Improve *IsPETase* Functionality

Both the reactivity and the stability of the wild-type *IsPETase* (*IsPETase*^{WT}) are far from ideal: honing it into realistic industrial plastic deconstructing biocatalyst requires some human intervention. The enzyme needs an enhanced catalytic rate and an increased thermotolerance, ideally with a T_m above 70°C to allow it to degrade as much plastic as possible by operating at the T_g of PET. This is where protein engineering techniques can be leveraged. Protein engineering is an immensely powerful tool for fine-tuning enzymes by modulating characteristics of interest.

Almost all current reports of PETase engineering so far, have been carried out using a rational design process. Structural and mechanistic information is utilised to identify and mutate individual target amino acids to new residues thought to proffer preferable characteristics. Strategies vary by their intended effect. For instance, some studies aim to enhance catalytic ability by altering the enzyme's active site. Methods in this vein broadly fall into two categories: altering the shape of the active site to make it more receptive to accepting the bulky PET polymer,^{120,131} or encouraging active site cleft hydrophobicity to boost enzyme-substrate interaction (Table 3).^{90,132}

On the other hand, in order to augment the robustness of *IsPETase*, rational mutagenesis has also been used to mimic more thermostable homologues or to correct areas of protein instability.^{112,133-135} Residues for mutation have been selected either by directly analysing crystal structures,^{112,133} or by using multi-layer computational algorithms.^{134,135} These methods often focus on promoting stabilising interactions such as hydrogen bonds and salt bridges which can improve protein thermal tolerance.

With regards to the enhancement of *IsPETase*, two studies are particularly noteworthy. Firstly, a homology-based study by Son *et al.* who took inspiration from the more stable *TfCut2*.¹¹² They remodelled the flexible β 6- β 7 connecting loop of *IsPETase* to mimic the homologue, installing a hydrogen bond between two residues (S212E/D186H), to secure this region to the α 2 helix. This was then combined with a previously discovered rational mutation, R280A, thought to increase the size of the substrate binding cleft.⁹⁰ The resulting thermostable variant, *IsPETase* (S121E/D186H/R280A) (*IsPETase*^{TS}) had an 8°C greater T_m than *IsPETase*^{WT} and 14-fold higher activity at 40°C than the wildtype enzyme. This is an impressive improvement; however, the protein is still fairly heat intolerant.

Using a different approach Cui *et al.*, used computational methods to assemble a number of mutations to increase the thermostability of *IsPETase*.¹³⁴ Using a newly created protein design method termed greedy accumulated strategy for protein engineering or “GRAPE”, they computationally derived potential individual stabilising mutations based on a number of parameters including predicted folding energies and homology modelling calculations. The resulting 10-point mutant enzyme, DuraPETase (S214H/I168/W159H/ S188Q/R280A/A180I/G165A/Q119Y/L117F/T140D), was significantly more stable than the *IsPETase*^{WT} enzyme, with a T_m of 71°C. However, its optimum operating temperature of 50°C is still well below the T_g of PET.

Due to our incomplete understanding of protein sequence to function relationships,¹³⁶ rational mutagenesis of *IsPETase* can only improve its characteristics so far. The simultaneous engineering of both stability and catalytic activity in this way is particularly complex. Behind the seemingly positive PETase rational mutagenesis studies, are many examples of residue mutations and combinations which increased the thermostability of *IsPETase*, but curbed its PET-deconstructing ability.^{90,112,120,131-134} Engineering several characteristics at the same time presents a multi-factorial problem that rational mutagenesis can often struggle to solve.

There is undoubtedly scope for improving *IsPETase* further. One of the most powerful ways to engineer enzymes is directed evolution, but its use in conjunction with PETases has been precluded to date by the lack of a high-throughput screening strategy.¹³⁷ Directed evolution would require the assessment of the plastic degrading capabilities of thousands of protein variants; current assays cannot cope with this number. This is in part due to plastic deconstruction being carried out on a solid substrate, for which high-throughput assays and analyses are hard to design and implement. Currently, the only documented attempt to use directed evolution to enhance a plastic degrading enzyme is for the engineering of a poly- β -hydroxybutyrate (PHB) depolymerase from *Ralstonia pickettii* T1.¹³⁸ Unfortunately, none of the mutant proteins created had improved activity on the solid substrate, emphasising the obstacles that would need to be overcome in order to harness this technique for PETases.

Table 3. Mutations of *IsPETase* that have positively affected activity or thermostability, grouped by engineering strategy. All mutational positions based on *IsPETase* PDB ID code 6EQE. Exact screening conditions between examples vary, but increased activities quoted are all on a solid PET substrate.

Mutational Strategy	Mutations	Results	Reasoning	Reference
Replicate the active site of a homologous enzyme	S238F, W159H	Increased activity by 17% compared to WT at 30°C, increased activity towards more crystalline substrates	Allowed PET molecule to sit deeper within the active site cleft, increased π -stacking interactions between the enzyme and substrate	Austin <i>et al.</i> (2018) ¹¹⁴
Alter active site	R280A	Increased activity by 22% compared to WT at 30°C	Increased the space available in the active site, promoting substrate binding	Joo <i>et al.</i> (2018) ⁸⁵
Alter active site	W159H _____ S214H	Increased activity by 1.2-fold and 1-fold respectively, compared to WT at 30°C	Increased the space available in the active site, increased the hydrophobicity of binding pocket, promoting substrate binding	Liu <i>et al.</i> (2018) ¹²⁵
Alter active site	R90A _____ L117F _____ I208F	Increased activity by 40%, 110% and 150% respectively, compared to WT at 30°C	Removed hindrance to product release, increased the hydrophobicity of binding pocket, promoting substrate binding	Ma <i>et al.</i> (2018) ¹²⁶

Table 3. Continued.

Mutational Strategy	Mutations	Results	Reasoning	Reference
Replicate structural features of homologous enzyme	P181A S121E, D186H, R280A	Increased T_m by 0.5°C, reduced activity by 40%, compared to WT at 40°C Increased T_m by 8.8°C, increased activity by 14-fold, compared to WT at 40°C	Corrected disruption of $\beta 6$ sheet Created stabilising hydrogen bonds, increased space available in the active site	Son <i>et al.</i> (2019) ¹¹² Son <i>et al.</i> (2019) ¹¹²
Replicate the active site of a homologous enzyme	S121E, D186H, S242T, N246D	Increased T_m by 9.8°C, increased activity by 58-fold, compared to WT at 37°C	Increased the hydrophobicity of binding pocket, promoting substrate binding, formation of a salt bridge to aid stability	Son <i>et al.</i> (2020) ¹³³
Use computational methods based on protein homology to increase protein thermostability	S214H, I168, W159H, S188Q, R280A, A180I, G165A, Q119Y, L117F, T140D	Increased T_m by 22°C, enzyme active at 50°C and 60°C (WT inactive at these temperatures)	Introduced new stabilising electrostatic interactions, improved hydrophobic packing of the protein, increased hydrophobicity of binding pocket, promoting substrate binding	Cui <i>et al.</i> (2021) ¹³⁴
Used computational methods based on natural sequence evolution to increase thermostability and activity	W159H, F229Y	Increased T_m by 10.4°C, increased activity by 40-fold, compared to WT at 40°C	Undetermined, maybe increased hydrogen bonding interactions	Meng <i>et al.</i> (2021) ¹³⁵

1.14 Complementary Approaches to Improving Plastic Deconstruction by PETases

Alongside the mutational remodelling of the PETase itself, improvement in substrate turnover for plastic decomposition can be achieved by integrating additional techniques to promote polymer surface binding and catalysis. This can be as simple as supplementing PET hydrolysis reactions with chemical additives, such as anionic surfactants. Surfactants facilitate contact between the hydrophobic plastic surface and cationic *Is*PETase; their inclusion in PET depolymerisation reactions can increase the activity of the enzyme towards PET film by 120-fold at 30°C.¹³⁹ Altering electrostatic interactions between proteins can also enhance activities. For instance, glycosylation of LCC prevented temperature-induced protein aggregation, which was negatively affecting the enzyme's PET hydrolysing ability.¹⁴⁰

More inventive approaches draw insights from nature. Fungi have a suite of strategies for degrading the highly recalcitrant hydrophobic lignin and crystalline cellulose, which could be co-opted for plastic degradation.¹⁴¹ For example, fusion of proteins to fungal hydrophobins can increase plastic degradation by increasing the concentration of PETase at the polymer surface. These small, low molecular weight, amphipathic proteins are specialised to adsorb to hydrophobic surfaces,¹⁴² and have been shown to provide a 16-fold improvement in activity when fused to *Thc_Cut1*.¹⁴³ The fusion of other binding proteins such as carbohydrate binding modules (CBMs), also shows promise. Acting in nature to draw catalytic domains towards insoluble polymeric substrates such as cellulose, their fusion to PETases can increase activity.¹⁴⁴ CBMs with ever increasing PET affinity continue to be uncovered.¹⁴⁵

Taking bio-inspiration to the next level, plastic decomposition could be further facilitated by using multi-enzyme complexes. In nature, cellulose deconstruction is enhanced by tethering several synergistically active proteins together to form a cellulosome.¹⁴⁶ Spatially grouping biocatalysts in this way allows different functionalities to be directed to the same area of the polymer surface, with the option of shuttling degradation products through several alternative enzymes to increase polymer breakdown. In a similar pattern, PETases can be fused to catalytically active auxiliary proteins. One of the most successful demonstrations of this idea is the fusion of *Is*PETase to its naturally occurring PET-degrading partner, MHETase.¹⁴⁷ *Is*PETase:MHETase fusion proteins exhibit enhanced plastic decomposition abilities as compared to the free individual enzymes. It is conceivable that building even more complex multi-enzyme systems may offer even greater PET

hydrolysis abilities with additional complementary activities built in. Although judicious selection of enzymes will be needed to allow for effective synergistic activities, the development of competent PET-deconstructing cellulosomes could be very powerful.

1.15 Can Directed Evolution Provide a Gateway to Better Plastic Degrading Enzymes?

Enzymes have the potential to help address the plastic pollution problem by acting as rapid, selective, eco-friendly catalysts to deconstruct environmentally damaging anthropogenic polymers. They offer the opportunity to create a circular plastics economy, with the plausible capacity to deal with certain polymers in currently challenging mixed waste streams. The integration of effective biocatalytic plastic deconstruction strategies with improved methods for dealing with enzymatically intractable polymers, offers a promising route to better end-of-life plastic waste processing. The discovery of the natural depolymerising enzyme, *IsPETase*, hints at a system capable of rising to this challenge with regards to PET plastic. An industrially relevant biocatalyst, however, needs to have exceptional catalytic ability. In its wildtype form, *IsPETase* does not possess this capability, being unable to operate at the elevated temperatures which would facilitate rapid PET hydrolysis. Despite this, the theorised superior catalytic machinery present in the naturally evolved *IsPETase*, as compared to its homologues, could be harnessed if the protein was engineered to be more thermostable. Although numerous protein engineering strategies exist to enable this, they have been used with limited success; the most powerful technique, directed evolution, has not been applied to date, due to the lack of a suitable high-throughput screening platform. However, the development of directed evolution methodologies for PETases and other plastic deconstructing enzymes could provide a fertile platform for designing superior biocatalytic recycling strategies. The development and implementation of such a platform is the topic of this thesis.

1.16 References

1. Ebnesajjad, S. *Introduction to Plastics. Chemical Resistance of Engineering Thermoplastics* (William Andrew Publishing, 2016).
2. McKeen, L. W. & van der Zande, E. *Introduction to Plastics and Polymers. Permeability Properties of Plastics and Elastomers* 21–37 (2012).
3. Hench, L. L., Jones, J. R. & Institute of Materials, M. *Biomaterials, artificial organs and tissue engineering*. (CRC Press, 2005).
4. PlasticsEurope. *Plastics- the Facts 2019, An analysis of European plastics production, demand and waste data*. (2019).
5. Horie, K. *et al.* Definitions of terms relating to reactions of polymers and to functional polymeric materials (IUPAC Recommendations 2003): *Pure and Applied Chemistry* **76**, 889–906 (2004).
6. PlasticsEurope. *Plastics- the Facts 2018, An analysis of European plastics production, demand and waste data*. (2018).
7. Goodship, V. Plastic Recycling. *Science Progress* **90**, 245–268 (2007).
8. Shen, L. & Worrell, E. Handbook of Recycling, Chapter 13 - Plastic Recycling. in (eds. Worrell, E. & Reuter, M.) 179–190 (Elsevier, 2014).
9. Ellis, L. D. *et al.* Chemical and biological catalysis for plastics recycling and upcycling. *Nature Catalysis* **4**, 539–556 (2021).
10. Nicholson, S. R., Rorrer, N. A., Carpenter, A. C. & Beckham, G. T. Manufacturing energy and greenhouse gas emissions associated with plastics consumption. *Joule* **5**, 673–686 (2021).
11. Bashir, Z., Al-Aloush, I., Al-Raqibah, I. & Ibrahim, M. Evaluation of three methods for the measurement of crystallinity of PET resins, preforms, and bottles. *Polymer Engineering & Science* **40**, 2442–2455 (2000).
12. Shrivastava, A. Introduction to Plastics Engineering. in *Introduction to Plastics Engineering* (ed. Shrivastava, A.) 1–16 (William Andrew Publishing, 2018).
13. Wei, R. & Zimmermann, W. Biocatalysis as a green route for recycling the recalcitrant plastic polyethylene terephthalate. *Microbial Biotechnology* **10**, 1302–1307 (2017).
14. Awaja, F. & Pavel, D. Recycling of PET. *European Polymer Journal* **41**, 1453–1477 (2005).
15. Webb, H. *et al.* Plastic Degradation and Its Environmental Implications with Special Reference to Poly(ethylene terephthalate). *Polymers* **5**, 1–18 (2012).
16. Carr, C. M., Clarke, D. J. & Dobson, A. D. W. Microbial Polyethylene Terephthalate Hydrolases: Current and Future Perspectives. *Frontiers in Microbiology* **11**, 2825 (2020).
17. Caldicott, R. J. *The Basics of Stretch Blow Molding PET Containers*. (Plastics Engineering, 1999).
18. PlasticsInsight. Polyethylene Terephthalate (PET): Production, Price, Market and its Properties. <https://www.plasticsinsight.com/resin-intelligence/resin-prices/polyethylene-terephthalate/> (2017).
19. Park, S. H. & Kim, S. H. Poly (ethylene terephthalate) recycling for high value added textiles. *Fashion and Textiles* **1**, 1 (2014).
20. Garside, M. Global PET bottle production 2004-2021. <https://www.statista.com/statistics/723191/production-of-polyethylene-terephthalate-bottles-worldwide/> (2019).
21. Geyer, R., Jambeck, J. & Law, K. Production, use, and fate of all plastics ever made. *Science Advances* **3**, e1700782 (2017).

22. Gu, F., Guo, J., Zhang, W., Summers, P. A. & Hall, P. From waste plastics to industrial raw materials: A life cycle assessment of mechanical plastic recycling practice based on a real-world case study. *Science of The Total Environment* **601–602**, 1192–1207 (2017).
23. The Pew Charitable Trusts. *Breaking the Plastic Wave*. https://www.pewtrusts.org/-/media/assets/2020/10/breakingtheplasticwave_mainreport.pdf (2020).
24. Crutzen, P. J. Geology of mankind. *Nature* **415**, 23–23 (2002).
25. Zalasiewicz, J. *et al.* The geological cycle of plastics and their use as a stratigraphic indicator of the Anthropocene. *Anthropocene* **13**, 4–17 (2016).
26. MacLeod, M., Arp, H. P. H., Tekman, M. B. & Jahnke, A. The global threat from plastic pollution. *Science* **373**, (2021).
27. Andrady, A. L. Microplastics in the marine environment. *Marine Pollution Bulletin* **62**, 1596–1605 (2011).
28. Lucas, N. *et al.* Polymer biodegradation: Mechanisms and estimation techniques – A review. *Chemosphere* **73**, 429–442 (2008).
29. Sammon, C., Yarwood, J. & Everall, N. An FT-IR study of the effect of hydrolytic degradation on the structure of thin PET films. *Polymer Degradation and Stability* **67**, 149–158 (2000).
30. Gregory, M. R. & Andrady, A. L. Plastics in the Marine Environment. in *Plastics and the Environment* 379–401 (John Wiley & Sons, Inc., 2004).
31. Rochman, C. M. Microplastics research— from sink to source. *Science* **360**, 28–29 (2018).
32. Whitacre, D. M. *Reviews of Environmental Contamination and Toxicology*. (Springer , 2014).
33. Chamas, A. *et al.* Degradation Rates of Plastics in the Environment. *ACS Sustainable Chemistry & Engineering* **8**, 3494–3511 (2020).
34. Krause, S. *et al.* Persistence of plastic debris and its colonization by bacterial communities after two decades on the abyssal seafloor. *Scientific Reports* **10**, 9484 (2020).
35. Barnes, D. K. A., Galgani, F., Thompson, R. C. & Barlaz, M. Accumulation and fragmentation of plastic debris in global environments. *Philosophical Transactions of the Royal Society B: Biological Sciences* **364**, 1985–1998 (2009).
36. Thompson, R. *et al.* New directions in plastic debris. *Science (New York, N.Y.)* **310**, 1117 (2005).
37. Borrelle, S. *et al.* Predicted growth in plastic waste exceeds efforts to mitigate plastic pollution. *Science* **369**, (2020).
38. Kühn, S. & van Franeker, J. A. Quantitative overview of marine debris ingested by marine megafauna. *Marine Pollution Bulletin* **151**, 110858 (2020).
39. Barboza, L. G. A. *et al.* Microplastics cause neurotoxicity, oxidative damage and energy-related changes and interact with the bioaccumulation of mercury in the European seabass, *Dicentrarchus labrax* (Linnaeus, 1758). *Aquatic Toxicology* **195**, 49–57 (2018).
40. Song, Y. *et al.* Uptake and adverse effects of polyethylene terephthalate microplastics fibers on terrestrial snails (*Achatina fulica*) after soil exposure. *Environmental Pollution* **250**, 447–455 (2019).
41. Bosker, T., Bouwman, L. J., Brun, N. R., Behrens, P. & Vijver, M. G. Microplastics accumulate on pores in seed capsule and delay germination and root growth of the terrestrial vascular plant *Lepidium sativum*. *Chemosphere* **226**, 774–781 (2019).
42. Bergmann, M. *et al.* White and wonderful? Microplastics prevail in snow from the Alps to the Arctic. *Science Advances* **5**, eaax1157 (2019).

43. Beaumont, N. J. *et al.* Global ecological, social and economic impacts of marine plastic. *Marine Pollution Bulletin* **142**, 189–195 (2019).
44. Patrício Silva, A. L. *et al.* Increased plastic pollution due to COVID-19 pandemic: Challenges and recommendations. *Chemical Engineering Journal* **405**, 126683 (2021).
45. Catarino, A. I., Kramm, J., Völker, C., Henry, T. B. & Everaert, G. Risk posed by microplastics: Scientific evidence and public perception. *Current Opinion in Green and Sustainable Chemistry* **29**, 100467 (2021).
46. UNEA-5. Fifth session of the United Nations Environment Assembly. <https://www.unep.org/environmentassembly/unea5> (2022).
47. da Costa, J. P., Mouneyrac, C., Costa, M., Duarte, A. C. & Rocha-Santos, T. The Role of Legislation, Regulatory Initiatives and Guidelines on the Control of Plastic Pollution. *Frontiers in Environmental Science* **8**, 104 (2020).
48. Willis, K., Maureaud, C., Wilcox, C. & Hardesty, B. D. How successful are waste abatement campaigns and government policies at reducing plastic waste into the marine environment? *Marine Policy* **96**, 243–249 (2018).
49. Korley, L., Epps, T., Helms, B. & Ryan, A. Toward polymer upcycling—adding value and tackling circularity. *Science* **373**, 66–69 (2021).
50. Lord, R. *et al.* *Plastics and Sustainability: A Valuation of Environmental Benefits, Costs and Opportunities for Continuous Improvement*. (2016).
51. Hopewell, J., Dvorak, R. & Kosior, E. Plastics recycling: challenges and opportunities. *Philosophical transactions of the Royal Society of London. Series B, Biological sciences* **364**, 2115–26 (2009).
52. Singh, A. *et al.* Techno-economic, life-cycle, and socioeconomic impact analysis of enzymatic recycling of poly(ethylene terephthalate). *Joule* **5**, (2021).
53. Horton, A. A., Walton, A., Spurgeon, D. J., Lahive, E. & Svendsen, C. Microplastics in freshwater and terrestrial environments: Evaluating the current understanding to identify the knowledge gaps and future research priorities. *Science of The Total Environment* **586**, 127–141 (2017).
54. Alimi, O. S., Farnier Budarz, J., Hernandez, L. M. & Tufenkji, N. Microplastics and Nanoplastics in Aquatic Environments: Aggregation, Deposition, and Enhanced Contaminant Transport. *Environmental Science & Technology* **52**, 1704–1724 (2018).
55. Eriksson, O. & Finnveden, G. Plastic waste as a fuel - CO₂ -neutral or not? *Energy & Environmental Science* **2**, 907 (2009).
56. Miller, S. A. Five Misperceptions Surrounding the Environmental Impacts of Single-Use Plastic. *Environmental Science & Technology* **54**, 14143–14151 (2020).
57. Ragaert, K., Delva, L. & van Geem, K. Mechanical and chemical recycling of solid plastic waste. *Waste Management* **69**, 24–58 (2017).
58. Schyns, Z. O. G. & Shaver, M. P. Mechanical Recycling of Packaging Plastics: A Review. *Macromolecular Rapid Communications* **42**, 2000415 (2021).
59. Panda, A. K., Singh, R. K. & Mishra, D. K. Thermolysis of waste plastics to liquid fuel: A suitable method for plastic waste management and manufacture of value-added products—A world prospective. *Renewable and Sustainable Energy Reviews* **14**, 233–248 (2010).
60. Kakadellis, S. & Rosetto, G. Achieving a circular bioeconomy for plastics. *Science* **373**, 49–50 (2021).

61. Ellen MacArthur Foundation. *The New Plastics Economy: Rethinking the future of plastics & catalysing action*. <https://www.ellenmacarthurfoundation.org/publications/the-new-plastics-economy-rethinking-the-future-of-plastics-catalysing-action> (2017).
62. Sardon, H. & Dove, A. Plastics recycling with a difference. *Science* **360**, 380–381 (2018).
63. Göpferich, A. Mechanisms of polymer degradation and erosion. *Biomaterials* **17**, 103–114 (1996).
64. Leja, K. & Lewandowicz, G. Polymer Biodegradation and Biodegradable Polymers – a Review. *Polish Journal of Environmental Studies* **19**, 255–266 (2010).
65. Villares, A. *et al.* Lytic polysaccharide monoxygenases disrupt the cellulose fibers structure. *Scientific Reports* **7**, 40262 (2017).
66. Müller, G., Várnai, A., Johansen, K. S., Eijsink, V. G. H. & Horn, S. J. Harnessing the potential of LPMO-containing cellulase cocktails poses new demands on processing conditions. *Biotechnology for Biofuels* **8**, 187 (2015).
67. Vaaje-Kolstad, G. *et al.* An Oxidative Enzyme Boosting the Enzymatic Conversion of Recalcitrant Polysaccharides. *Science* **330**, 219–222 (2010).
68. Ruiz-Dueñas, F. J. & Martínez, Á. T. Microbial degradation of lignin: how a bulky recalcitrant polymer is efficiently recycled in nature and how we can take advantage of this. *Microbial Biotechnology* **2**, 164–177 (2009).
69. Vijaya, C. & Reddy, R. M. Impact of soil composting using municipal solid waste on biodegradation of plastics. *Indian Journal of Biotechnology* **7**, 235–239 (2008).
70. Wierckx, N. *et al.* Plastic Biodegradation: Challenges and Opportunities. in *Consequences of Microbial Interactions with Hydrocarbons, Oils, and Lipids: Biodegradation and Bioremediation* 1–29 (Springer International Publishing, 2018).
71. Mueller, R.-J. Biological degradation of synthetic polyesters—Enzymes as potential catalysts for polyester recycling. *Process Biochemistry* **41**, 2124–2128 (2006).
72. Araújo, R. *et al.* Tailoring cutinase activity towards polyethylene terephthalate and polyamide 6,6 fibers. *Journal of Biotechnology* **128**, 849–857 (2007).
73. Silva, C. *et al.* Engineered *Thermobifida fusca* cutinase with increased activity on polyester substrates. *Biotechnology Journal* **6**, 1230–1239 (2011).
74. Marten, E., Müller, R.-J. & Deckwer, W.-D. Studies on the enzymatic hydrolysis of polyesters. II. Aliphatic–aromatic copolyesters. *Polymer Degradation and Stability* **88**, 371–381 (2005).
75. Wei, R. & Zimmermann, W. Microbial enzymes for the recycling of recalcitrant petroleum-based plastics: how far are we? *Microbial biotechnology* **10**, 1308–1322 (2017).
76. Andrady, A. L. Assessment of Environmental Biodegradation of Synthetic Polymers. *Journal of Macromolecular Science, Part C: Polymer Reviews* **34**, 25–76 (1994).
77. Danso, D. *et al.* New Insights into the Function and Global Distribution of Polyethylene Terephthalate (PET)-Degrading Bacteria and Enzymes in Marine and Terrestrial Metagenomes. (2018).
78. Sadler, J. C. & Wallace, S. Microbial synthesis of vanillin from waste poly(ethylene terephthalate). *Green Chemistry* **23**, 4665–4672 (2021).
79. Voigt, C. A. Synthetic biology 2020–2030: six commercially-available products that are changing our world. *Nature Communications* **11**, 6379 (2020).
80. Ronkvist, M. A.° sa, Xie, W., Lu, W. & Gross, R. A. Cutinase-Catalyzed Hydrolysis of Poly(ethylene terephthalate). *Macromolecules* **42**, 5128–5138 (2009).

81. Carniel, A., Valoni, É., Nicomedes, J., Gomes, A. da C. & Castro, A. M. de. Lipase from *Candida antarctica* (CALB) and cutinase from *Humicola insolens* act synergistically for PET hydrolysis to terephthalic acid. *Process Biochemistry* **59**, 84–90 (2017).
82. Then, J. *et al.* Ca²⁺ and Mg²⁺ binding site engineering increases the degradation of polyethylene terephthalate films by polyester hydrolases from *Thermobifida fusca*. *Biotechnology Journal* **10**, 592–598 (2015).
83. Müller, R.-J., Schrader, H., Profe, J., Dresler, K. & Deckwer, W.-D. Enzymatic Degradation of Poly(ethylene terephthalate): Rapid Hydrolysis using a Hydrolase from *T. fusca*. *Macromolecular Rapid Communications* **26**, 1400–1405 (2005).
84. Kawai, F. *et al.* A novel Ca²⁺-activated, thermostabilized polyesterase capable of hydrolyzing polyethylene terephthalate from *Saccharomonospora viridis* AHK190. *Applied Microbiology and Biotechnology* **98**, 10053–10064 (2014).
85. Herrero Acero, E. *et al.* Enzymatic Surface Hydrolysis of PET: Effect of Structural Diversity on Kinetic Properties of Cutinases from *Thermobifida*. *Macromolecules* **44**, 4632–4640 (2011).
86. Ribitsch, D. *et al.* Hydrolysis of polyethylene terephthalate by *p*-nitrobenzylesterase from *Bacillus subtilis*. *Biotechnology Progress* **27**, 951–960 (2011).
87. Bollinger, A. *et al.* A Novel Polyester Hydrolase From the Marine Bacterium *Pseudomonas aestusnigri* – Structural and Functional Insights. *Frontiers in Microbiology* vol. II 114 (2020).
88. Almeida, E. L., Carrillo Rincón, A. F., Jackson, S. A. & Dobson, A. D. W. *In silico* Screening and Heterologous Expression of a Polyethylene Terephthalate Hydrolase (PETase)-Like Enzyme (SM14est) With Polycaprolactone (PCL)-Degrading Activity, From the Marine Sponge-Derived Strain *Streptomyces sp. SM14*. *Frontiers in Microbiology* **10**, 2187 (2019).
89. Pérez-García, P., Danso, D., Zhang, H., Chow, J. & Streit, W. R. Chapter Seven - Exploring the global metagenome for plastic-degrading enzymes. in *Methods in Enzymology* (eds. Weber, G., Bornscheuer, U. T. & Wei, R.) vol. 648 137–157 (Academic Press, 2021).
90. Joo, S. *et al.* Structural insight into molecular mechanism of poly(ethylene terephthalate) degradation. *Nature Communications* **9**, 382 (2018).
91. Kari, J., Andersen, M., Borch, K. & Westh, P. An Inverse Michaelis–Menten Approach for Interfacial Enzyme Kinetics. *ACS Catalysis* **7**, 4904–4914 (2017).
92. Olkiewicz, M., Tylkowski, B., Montornés, J. M., Garcia-Valls, R. & Gulaczyk, I. Modelling of enzyme kinetics: cellulose enzymatic hydrolysis case. *Physical Sciences Reviews* (2020).
93. Bååth, J. A., Borch, K., Jensen, K., Brask, J. & Westh, P. Comparative Biochemistry of Four Polyester (PET) Hydrolases. *ChemBioChem* **22**, 1627–1637 (2021).
94. Erickson, E. *et al.* Comparative performance of PETase as a function of reaction conditions, substrate properties, and product accumulation. *ChemSusChem* **n/a**, (2021).
95. Sulaiman, S. *et al.* Isolation of a novel cutinase homolog with polyethylene terephthalate-degrading activity from leaf-branch compost by using a metagenomic approach. *Applied and Environmental Microbiology* **78**, 1556–62 (2012).
96. Yoshida, S. *et al.* A bacterium that degrades and assimilates poly(ethylene terephthalate). *Science* **351**, 1196–9 (2016).
97. Wei, R. *et al.* Engineered bacterial polyester hydrolases efficiently degrade polyethylene terephthalate due to relieved product inhibition. *Biotechnology and Bioengineering* **113**, 1658–1665 (2016).

98. Oda, M. *et al.* Enzymatic hydrolysis of PET: functional roles of three Ca²⁺ ions bound to a cutinase-like enzyme, Cut190*, and its engineering for improved activity. *Applied Microbiology and Biotechnology* 1–11 (2018).
99. Then, J. *et al.* A disulfide bridge in the calcium binding site of a polyester hydrolase increases its thermal stability and activity against polyethylene terephthalate. *FEBS Open Bio* **6**, 425–432 (2016).
100. Tournier, V. *et al.* An engineered PET depolymerase to break down and recycle plastic bottles. *Nature* **580**, 216–219 (2020).
101. Zhong-Johnson, E., Voigt, C. & Sinskey, A. An absorbance method for analysis of enzymatic degradation kinetics of poly(ethylene terephthalate) films. *Scientific Reports* **11**, (2021).
102. Zimmermann, W. Biocatalytic recycling of polyethylene terephthalate plastic. *Philosophical Transactions of the Royal Society A: Mathematical, Physical and Engineering Sciences* **378**, 20190273 (2020).
103. Brueckner, T., Eberl, A., Heumann, S., Rabe, M. & Guebitz, G. M. Enzymatic and chemical hydrolysis of poly(ethylene terephthalate) fabrics. *Journal of Polymer Science Part A: Polymer Chemistry* **46**, 6435–6443 (2008).
104. Vertommen, M. A. M. E., Nierstrasz, V. A., Veer, M. van der & Warmoeskerken, M. M. C. G. Enzymatic surface modification of poly(ethylene terephthalate). *Journal of Biotechnology* **120**, 376–386 (2005).
105. Wei, R. *et al.* Biocatalytic Degradation Efficiency of Postconsumer Polyethylene Terephthalate Packaging Determined by Their Polymer Microstructures. *Advanced Science* **6**, (2019).
106. Kawai, F., Kawabata, T. & Oda, M. Current knowledge on enzymatic PET degradation and its possible application to waste stream management and other fields. *Applied Microbiology and Biotechnology* **103**, 4253–4268 (2019).
107. Mohanan, N., Montazer, Z., Sharma, P. K. & Levin, D. B. Microbial and Enzymatic Degradation of Synthetic Plastics. *Frontiers in Microbiology* **11**, 2837 (2020).
108. Jog, J. P. Crystallization of Polyethylene terephthalate. *Journal of Macromolecular Science, Part C* **35**, 531–553 (1995).
109. Kikkawa, Y., Fujita, M., Abe, H. & Doi, Y. Effect of Water on the Surface Molecular Mobility of Poly(lactide) Thin Films: An Atomic Force Microscopy Study. *Biomacromolecules* **5**, 1187–1193 (2004).
110. Palm, G. J. *et al.* Structure of the plastic-degrading *Ideonella sakaiensis* MHETase bound to a substrate. *Nature Communications* **10**, 1717 (2019).
111. Nikolaivits, E., Kanelli, M., Dimarogona, M. & Topakas, E. A Middle-Aged Enzyme Still in Its Prime: Recent Advances in the Field of Cutinases. *Catalysts* **8**, 612 (2018).
112. Son, H. F. *et al.* Rational Protein Engineering of Thermo-Stable PETase from *Ideonella sakaiensis* for Highly Efficient PET Degradation. *ACS Catalysis* **9**, 3519–3526 (2019).
113. Han, X. *et al.* Structural insight into catalytic mechanism of PET hydrolase. *Nature Communications* **8**, 2106 (2017).
114. Mindrebo, J. T., Nartey, C. M., Seto, Y., Burkart, M. D. & Noel, J. P. Unveiling the functional diversity of the alpha/beta hydrolase superfamily in the plant kingdom. *Current Opinion in Structural Biology* **41**, 233–246 (2016).
115. Botos, I. & Wlodawer, A. The expanding diversity of serine hydrolases. *Current Opinion in Structural Biology* **17**, 683–690 (2007).

116. Auldridge, M. E. *et al.* Emergent decarboxylase activity and attenuation of α/β -hydrolase activity during the evolution of methylketone biosynthesis in tomato. *The Plant Cell* **24**, 1596–607 (2012).
117. Steiner, R. A., Janssen, H. J., Roversi, P., Oakley, A. J. & Fetzner, S. Structural basis for cofactor-independent dioxygenation of *N*-heteroaromatic compounds at the α/β -hydrolase fold. *Proceedings of the National Academy of Sciences* **107**, 657–662 (2010).
118. Gruber, K., Gugganig, M., Wagner, U. G. & Kratky, C. Atomic Resolution Crystal Structure of Hydroxynitrile Lyase from *Hevea brasiliensis*. *Biological Chemistry* **380**, 993–1000 (1999).
119. Nardini, M. & Dijkstra, B. W. Alpha/beta hydrolase fold enzymes: the family keeps growing. *Current opinion in structural biology* **9**, 732–7 (1999).
120. Austin, H. P. *et al.* Characterization and engineering of a plastic-degrading aromatic polyesterase. *Proceedings of the National Academy of Sciences of the United States of America* **115**, E4350–E4357 (2018).
121. Berg, J. M., Tymoczko, J. L. & Stryer, L. *Biochemistry, Fifth Edition*. (W.H. Freeman, 2002).
122. Rajagopalan, S. *et al.* Design of activated serine-containing catalytic triads with atomic-level accuracy. *Nature Chemical Biology* **10**, 386–91 (2014).
123. Blow, D. M. The tortuous story of Asp-His-Ser: structural analysis of alpha-chymotrypsin. *Trends in Biochemical Sciences* **22**, 405–8 (1997).
124. Samak, N. A. *et al.* Recent advances in biocatalysts engineering for polyethylene terephthalate plastic waste green recycling. *Environment International* **145**, 106144 (2020).
125. Fecker, T. *et al.* Active Site Flexibility as a Hallmark for Efficient PET Degradation by *I. sakaiensis* PETase. *Biophysical Journal* **114**, 1302–1312 (2018).
126. Chen, C.-C., Han, X., Ko, T.-P., Liu, W. & Guo, R.-T. Structural studies reveal the molecular mechanism of PETase. *The FEBS Journal* **285**, 3717–3723 (2018).
127. Chen, C.-C. *et al.* General features to enhance enzymatic activity of poly(ethylene terephthalate) hydrolysis. *Nature Catalysis* **4**, 425–430 (2021).
128. da Costa, C. H. S. *et al.* Assessment of the PETase conformational changes induced by poly(ethylene terephthalate) binding. *Proteins: Structure, Function, and Bioinformatics* **89**, 1340–1352 (2021).
129. Wei, R. *et al.* Conformational fitting of a flexible oligomeric substrate does not explain the enzymatic PET degradation. *Nature Communications* **10**, 3–6 (2019).
130. Taniguchi, I. *et al.* Biodegradation of PET: Current Status and Application Aspects. *ACS Catalysis* **9**, 4089–4105 (2019).
131. Liu, B. *et al.* Protein Crystallography and Site-Direct Mutagenesis Analysis of the Poly(ethylene terephthalate) Hydrolase PETase from *Ideonella sakaiensis*. *ChemBioChem* **19**, 1471–1475 (2018).
132. Ma, Y. *et al.* Enhanced Poly(ethylene terephthalate) Hydrolase Activity by Protein Engineering. *Engineering* **4**, 888–893 (2018).
133. Son, H. F. *et al.* Structural bioinformatics-based protein engineering of thermo-stable PETase from *Ideonella sakaiensis*. *Enzyme and Microbial Technology* **141**, 109656 (2020).
134. Cui, Y. *et al.* Computational Redesign of a PETase for Plastic Biodegradation under Ambient Condition by the GRAPE Strategy. *ACS Catalysis* **11**, 1340–1350 (2021).
135. Meng, X. *et al.* Protein engineering of stable IsPETase for PET plastic degradation by Premuse. *International Journal of Biological Macromolecules* **180**, 667–676 (2021).

136. Packer, M. S. & Liu, D. R. Methods for the directed evolution of proteins. *Nature Reviews Genetics* **16**, 379–394 (2015).
137. Zhu, B., Wang, D. & Wei, N. Enzyme Discovery and Engineering for Sustainable Plastic Recycling. *Trends in Biotechnology* (2021).
138. Tan, L.-T., Hiraishi, T., Sudesh, K. & Maeda, M. Directed evolution of poly[(R)-3-hydroxybutyrate] depolymerase using cell surface display system: functional importance of asparagine at position 285. *Applied Microbiology and Biotechnology* **97**, 4859–4871 (2013).
139. Furukawa, M., Kawakami, N., Oda, K. & Miyamoto, K. Acceleration of Enzymatic Degradation of Poly(ethylene terephthalate) by Surface Coating with Anionic Surfactants. *ChemSusChem* **11**, 4018–4025 (2018).
140. Shirke, A. N. *et al.* Stabilizing Leaf and Branch Compost Cutinase (LCC) with Glycosylation: Mechanism and Effect on PET Hydrolysis. (2018).
141. Daly, P. *et al.* From lignocellulose to plastics: Knowledge transfer on the degradation approaches by fungi. *Biotechnology Advances* **50**, 107770 (2021).
142. Wösten, H. A. B. & de Vocht, M. L. Hydrophobins, the fungal coat unravelled. *Biochimica et Biophysica Acta (BBA) - Reviews on Biomembranes* **1469**, 79–86 (2000).
143. Ribitsch, D. *et al.* Enhanced Cutinase-Catalyzed Hydrolysis of Polyethylene Terephthalate by Covalent Fusion to Hydrophobins. *Applied and Environmental Microbiology* **81**, 3586–3592 (2015).
144. Ribitsch, D. *et al.* Fusion of Binding Domains to *Thermobifida cellulosilytica* Cutinase to Tune Sorption Characteristics and Enhancing PET Hydrolysis. *Biomacromolecules* **14**, 1769–1776 (2013).
145. Weber, J. *et al.* Interaction of carbohydrate-binding modules with poly(ethylene terephthalate). *Applied Microbiology and Biotechnology* **103**, 4801–4812 (2019).
146. Doi, R. H. & Kosugi, A. Cellulosomes: plant-cell-wall-degrading enzyme complexes. *Nature Reviews Microbiology* **2**, 541–551 (2004).
147. Knott, B. C. *et al.* Characterization and engineering of a two-enzyme system for plastics depolymerization. *Proceedings of the National Academy of Sciences* **117**, 25476 (2020).

CHAPTER 2

Introduction to Directed Evolution

Elizabeth L. Bell¹, Amy Crossley¹ & Anthony P. Green^{1}*

¹Manchester Institute of Biotechnology, 131 Princess Street, University of Manchester, Manchester, M1 7DN, UK.

2.1 Foreword

This chapter consists of an excerpt from a book chapter entitled “Modern Developments in Biocatalysis”, published in 2022, reviewing the process of directed evolution and its application. This excerpt, titled “Directed Evolution” serves as an introduction to laboratory evolution and current advancements in this field.

2.2 Acknowledgements

The excerpt presented in this chapter was a collaborative effort between the doctoral candidate and the following researchers: Amy Crossley and Anthony P. Green. The doctoral candidate wrote the sections 2.7 to 2.10, and co-edited the manuscript as a whole.

2.3 Introduction

Natural enzymes are typically sub-optimal for industrial applications without first undergoing optimisation. Unfortunately, due to our limited understanding of sequence structure-function relationships, rational optimisation of enzymes has proven challenging.¹ Instead, directed evolution (DE) has emerged as a powerful enzyme engineering strategy which mimics natural evolution on a substantially shortened timescale, allowing enzymes to be tailored towards industrial applications, to perform new functions and even catalyse reactions not observed in nature (Fig. 1).¹⁻³

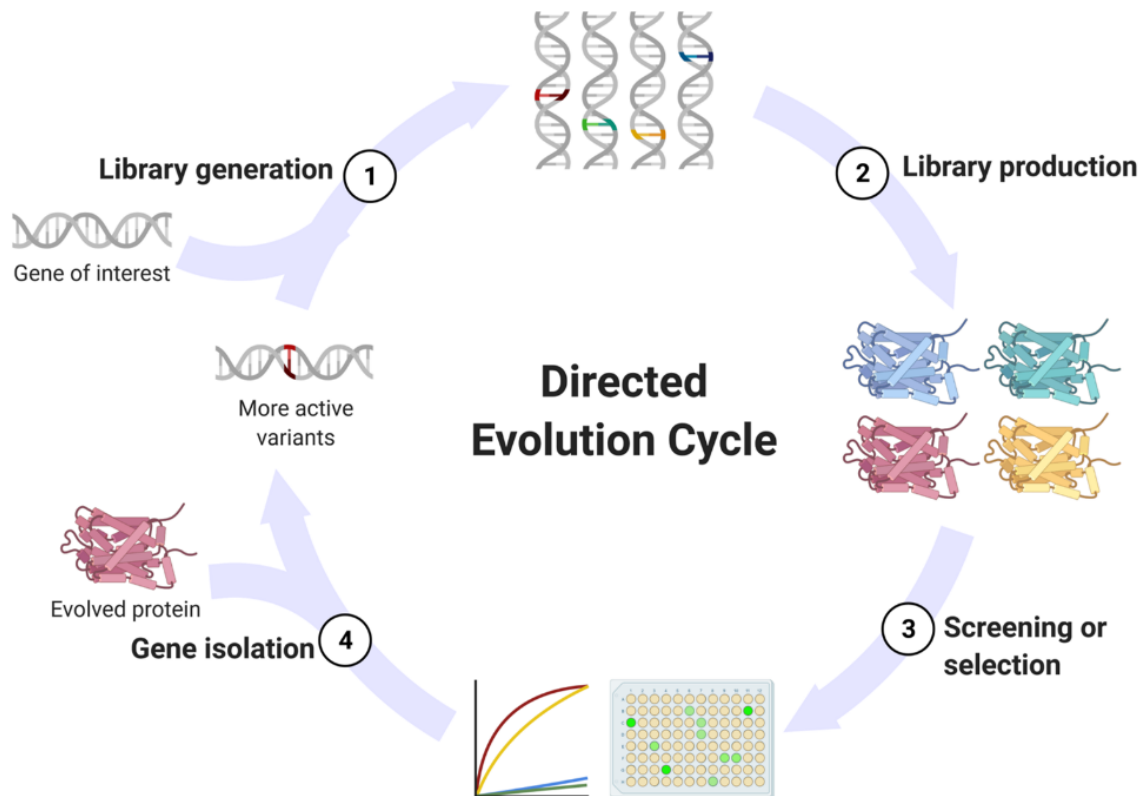


Figure 1. Directed evolution cycle. (1) First, libraries of variants are created by mutating the gene of interest. (2) The gene libraries are expressed to produce a library of proteins. (3) These proteins are then assessed for their activity either by screening for the function of interest or selection-based approaches. (4) The best protein variants are selected and the associated genes isolated. These new gene variants are then the substrate for the next round of evolution.

Enzymes can be optimised through iterative rounds of mutagenesis and high-throughput screening or selection to improve a range of properties such as catalytic efficiency and substrate specificity.³ To begin this cycle a suitable starting enzyme must be chosen, which typically exhibits detectable levels of activity towards the desired reaction.^{2,4} DNA libraries are then generated through mutagenesis and the corresponding genes are expressed and screened for library variants exhibiting improved properties.^{3,5} The best variants are isolated and used as the parent gene for subsequent rounds of evolution.⁵ To identify the genes encoding the most active variants, an effective directed evolution protocol requires a tight link between genotype and phenotype that must be maintained throughout.^{2,6}

2.4 Library Generation

There are two main strategies employed for library generation: random mutagenesis and focused mutagenesis. The method chosen is dictated by a number of factors including screening capacity and the availability of structural information.⁶ Random mutagenesis comprises an unbiased approach to incorporate mutations throughout the gene of interest.^{7,8} The most common way to undertake random mutagenesis is through the use of error-prone PCR, which utilises low-fidelity DNA polymerases to incorporate errors into the gene at a rate of around 10^{-4} - 10^{-3} errors per replicated base.⁷ As this method introduces diversity randomly throughout the gene, it requires no prior knowledge of structure-function relationships and can also lead to the discovery of beneficial mutations outside of the active site that cannot be predicted by current computational methods.^{2,5,7} Although this approach is useful in the absence of structural information, most library members have deleterious or neutral mutations meaning a large number of variants must be screened to obtain improvements to the desired property. The information gathered from this approach is typically used to identify areas of the gene amenable to mutagenesis. This allows the identification of 'hot-spots' to target for subsequent rounds of evolution.⁹

Focused (or targeted) mutagenesis is another approach for library generation which involves the introduction of mutations at targeted positions within the gene predicted to improve a desired property.^{7,10} Structural information and computational modelling can be used to guide the selection of amino acid residues which are then randomised through saturation mutagenesis. Degenerate codons such as NNK or NNS (N = C/T/G/A; S = C/G; K = G/T) are employed to encode all 20 amino acids using only 32 of the 64 possible codons thus reducing the number of library members to assess.²

Larger gains in activity can often be achieved by designing libraries where multiple residues are mutated simultaneously leading to the identification of synergistic mutations. Combinatorial active site testing (CASTing) is one such approach in which small libraries are created through simultaneous randomisation of two or three spatially close residues within the active site.¹¹ It is important to note however that library size increases exponentially with the number of residues randomised.² Therefore, there is a limitation on the number of residues that can be mutated at a time, dictated by the capacity of the selected screening method. Due to this, a number of strategies have been developed to reduce library sizes and thus screening effort by using a further reduced set of codons. For example, NDT

only encodes 12 amino acids while still representing a diverse array of amino acid properties, whilst the 22-codon trick uses a precise combination of primers containing degenerate bases to encode all 20 amino acids.^{3,9,12}

One further approach to library generation is DNA shuffling which mimics homologous recombination.¹³ This approach involves the shuffling of mutations between a number of homologous gene variants enabling synergistic mutations and thus improved variants to be identified. This method can be employed between rounds of directed evolution to shuffle beneficial mutations identified from screening to obtain the most active variant which is then used as a template for subsequent rounds of mutagenesis. The original method of DNA shuffling involved the fragmentation of the gene using DNase followed by reassembly in a PCR void of primers.⁷ Other shuffling strategies such as staggered extension process (StEP), which uses shortened elongation steps to generate new variants, and assembly PCR, which creates shuffled variants through the use of overlapping primers, have been developed.^{14,15} Typically, a combination of all the above-mentioned mutagenesis techniques are utilised during an evolution project to maximise the improvements obtained.

2.5 Library Evaluation – Screening Techniques

Library evaluation is typically the bottleneck in most directed evolution ventures. Protein sequence space is vast, and therefore a large number of library members need to be assessed to maximise the chances of identifying beneficial mutations. Consequently, the development of a robust and high-throughput strategy is key to a successful evolution endeavour. Common techniques to evaluate library members can be split into two methodologies: screening or selection. Screening strategies assess each library member for a measurable output that is linked to activity, whilst selection strategies couple enzyme activity to survival of the host organism (Fig. 2).¹⁶

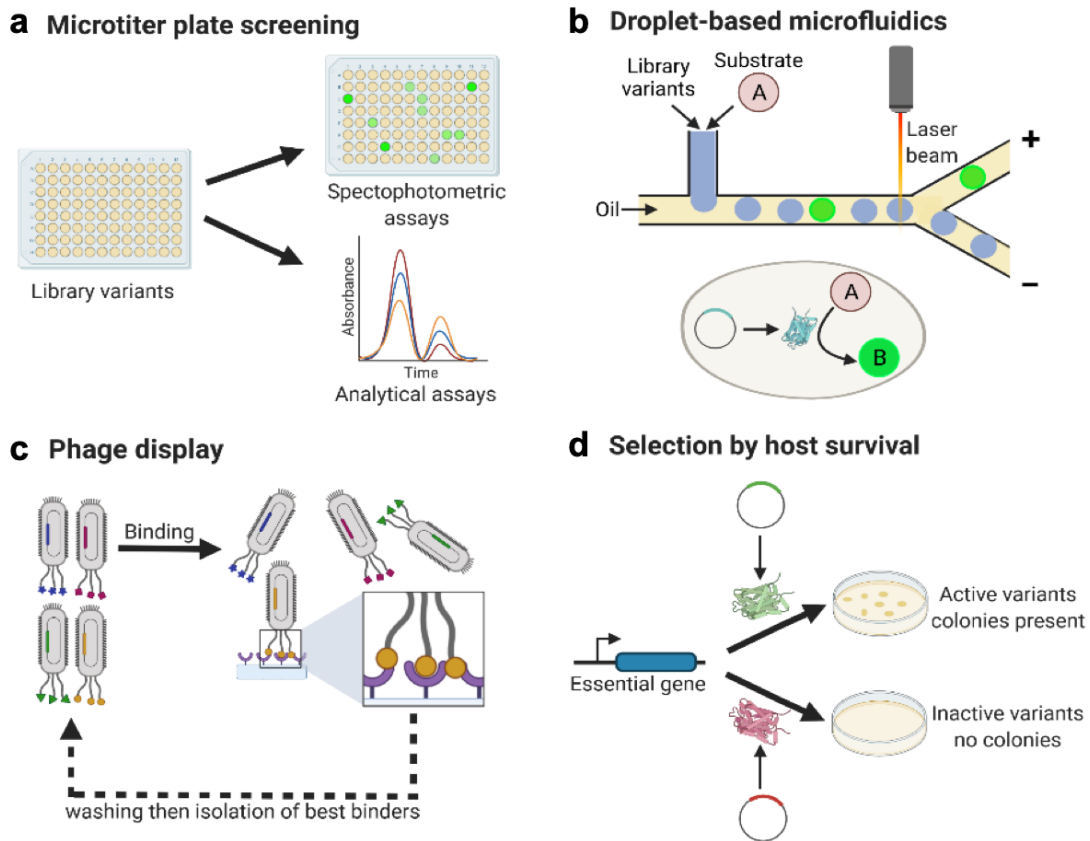


Figure 2. Examples of screening and selection techniques implemented in directed evolution. a) Microtiter plate screening. Library variants are picked into well plates and then screened for activity by either spectrophotometric or analytical assays such as HPLC or gas chromatography. b) Droplet-based microfluidics. A higher throughput screening method in which library members are encapsulated with reagents into water-oil droplets and sorted based on the production of a fluorescent product. c) Phage display. A selection assay for binding affinity. Library variants are expressed by phages and improved variants are selected through binding to a target molecule attached to an immobilised surface. d) Selection by host survival. Enzyme activity is linked to the transcription of an essential gene. Active variants lead to transcription; therefore, bacteria survive and colonies are present. Inactive variants lead to death of the bacteria and therefore, no colonies.

Microtiter plate screening is a commonly employed method for library evaluation in which single colonies of transformed libraries are arrayed into well plates, typically 96, for protein expression (Fig 2a).^{16,17} These are then screened for substrate consumption or product formation using a wide range of techniques including HPLC, gas chromatography or spectrophotometric analysis allowing a variety of properties and activities to be evaluated.^{2,7} If the enzyme reaction cannot be monitored using one of these methods, substrate surrogates can sometimes be utilised which are similar to the reaction substrate but couple enzyme activity to a detectable output.⁷ The throughput of this technique can also be

enhanced through its integration with automated workflows using robotic platforms to increase speed and accuracy.^{16,18}

Colony-based (solid-phase) screening offers an alternative method of evaluating library variants. Instead of picking single colonies into wells, libraries are screened directly on agar plates through the addition of reaction substrates either into the agar or on microporous membranes.¹⁹ Active variants are then identified through the formation of either coloured or fluorescent colonies allowing the efficient screening of large libraries. This method has been successfully implemented in numerous directed evolution endeavours, notably in the engineering of oxidases such as MAO-N.²⁰⁻²³ However, this approach requires catalytic function to be linked to the generation of a fluorescent or colorimetric output. In addition, this method provides only qualitative information, and further analysis is required to provide a quantitative comparison of promising variants.

Another high-throughput, yet quantitative, screening method is fluorescence activated cell sorting (FACS).^{2,7,24} This approach works by carrying out the enzyme reaction within a single host cell. Substrates diffuse into the cell and are catalysed to produce a fluorescent product that is detected. Cell sorting using flow cytometry then separates activate variants from inactive ones, dependant on the level of fluorescence measured.²⁴ However, this approach depends on the substrate of the reaction being able to diffuse into the cell, whilst the resulting fluorescent product is either retained within the cell or displayed on the cell surface.²⁵

To overcome this limitation *in vitro* compartmentalisation (IVC) and droplet-based microfluidics have been developed (Fig. 2b).^{26,27} Uniform droplets formed within water-oil emulsions are created that encapsulate a library variant and the reaction substrates, enabling enzyme activity to be reliably measured.^{7,25-27} Microfluidics can sort thousands of droplets per second giving a ultra-high throughput method of library screening and has been implemented in a number of directed evolution projects.²⁷⁻²⁹ Nevertheless, microfluidics, IVC and FACS screening methods are limited in their utility due to the requirement of enzyme activity being coupled to fluorescence. The recent development of mass activated droplet sorting (MADS) and Raman activated droplet sorting (RADS) however, highlights the ongoing research to improve the versatility of these high-throughput screening methods.³⁰⁻³³

2.6 Library Evaluation – Selection Techniques

Selection strategies offer another method for the assessment of enzyme libraries in which the desired activity is linked to survival of the gene offering an ultra-high-throughput approach. Selection methods can be separated into two main strategies: selection based on affinity and selection based on host survival.^{16,34}

Phage display is one such selection approach based on binding affinity (Fig. 2c). Each library sequence is inserted within a gene that encodes a phage coat protein so that the encoding enzyme is expressed onto the surface of the bacteriophage.^{35,36} Library members that possess desirable affinity are selected through binding to a target molecule, for example a transition state analogue, attached to an immobilised surface and all non-binding members are washed away. Phage display and other affinity-based methods such as mRNA display and ribosome display have been highly effective for the creation of therapeutic antibodies and evolving binding affinity.^{37,38} However, these methods have only been used in a limited number of enzyme evolution projects due to the fact that binding affinity does not necessarily improve catalytic activity.^{7,16}

Selection approaches have also been developed that are based on host survival through the linkage of improved catalytic activity to host viability (Fig. 2d). One such method for this is the coupling of enzyme activity to the transcription of an essential gene such as an antibiotic resistance gene. Active enzyme variants enable the transcription of an antibiotic resistance gene thus, the cell survives and the variant is retained.¹⁶ For example, Shultz and co-workers utilised this method to evolve pyrrolysyl tRNA synthetases to genetically incorporate non-canonical amino acids (ncAAs) into proteins. This approach has led to the creation of many evolved pyrrolysyl tRNA synthetases that enable over 150 ncAAs to be genetically incorporated.^{39,40}

Selection based on host survival has been further utilised in continuous evolution platforms. Rounds of directed evolution are continuously cycled with little manual intervention, enabling more than 100 rounds of evolution to be completed each week.^{2,41} Phage-assisted continuous evolution (PACE) is one example of this methodology in which enzyme activity is coupled to the expression of a phage protein (pIII) which is essential to infectivity and thus bacteriophage replication.⁴² Enzyme variants are created through the use of a mutagenesis plasmid and only active variants survive to be continually evolved. This

approach was first successfully implemented in the evolution of a polymerase for the recognition of other promoters and has also been utilised to engineer a TEV protease to cleave a different target sequence.^{42,43} The work of Liu and co-workers expanded the capability of continuous evolution into yeast cells through the creation of their OrthoRep system.^{44,45} OrthoRep utilises an error-prone, orthogonal DNA polymerase to selectively mutate the gene of interest *in vivo*. When linked to a tuneable selection pressure this methodology has enabled continuous evolution projects that have yielded promiscuous *Tm*TrpB variants and evolved drug-resistant dihydrofolate reductases.⁴⁴⁻⁴⁶

Whether being implemented in a traditional directed evolution project or within a continuous evolution platform, only a few evolution projects have utilised selection based on survival. This is most likely due to the considerable time and effort required to implement and optimise this selection method. It can be extremely difficult or impossible to link the desired property to host survival. However, when this is achieved, this method of library selection enables the rapid evolution of efficient enzymes.

2.7 Optimising and Enhancing Natural Enzymes

The most common application of directed evolution is the enhancement of naturally occurring enzymes. Typically, the protein's key catalytic residues are preserved, meaning that the native and evolved enzymes will operate in a mechanistically similar fashion (Fig. 3a & b). Evolution of this kind is used extensively across industry, to either tailor a biocatalyst's physical properties to specific process requirements,^{47,48} or to finely-tune a protein's active site to alter substrate preferences or reaction selectivity.^{49,50}

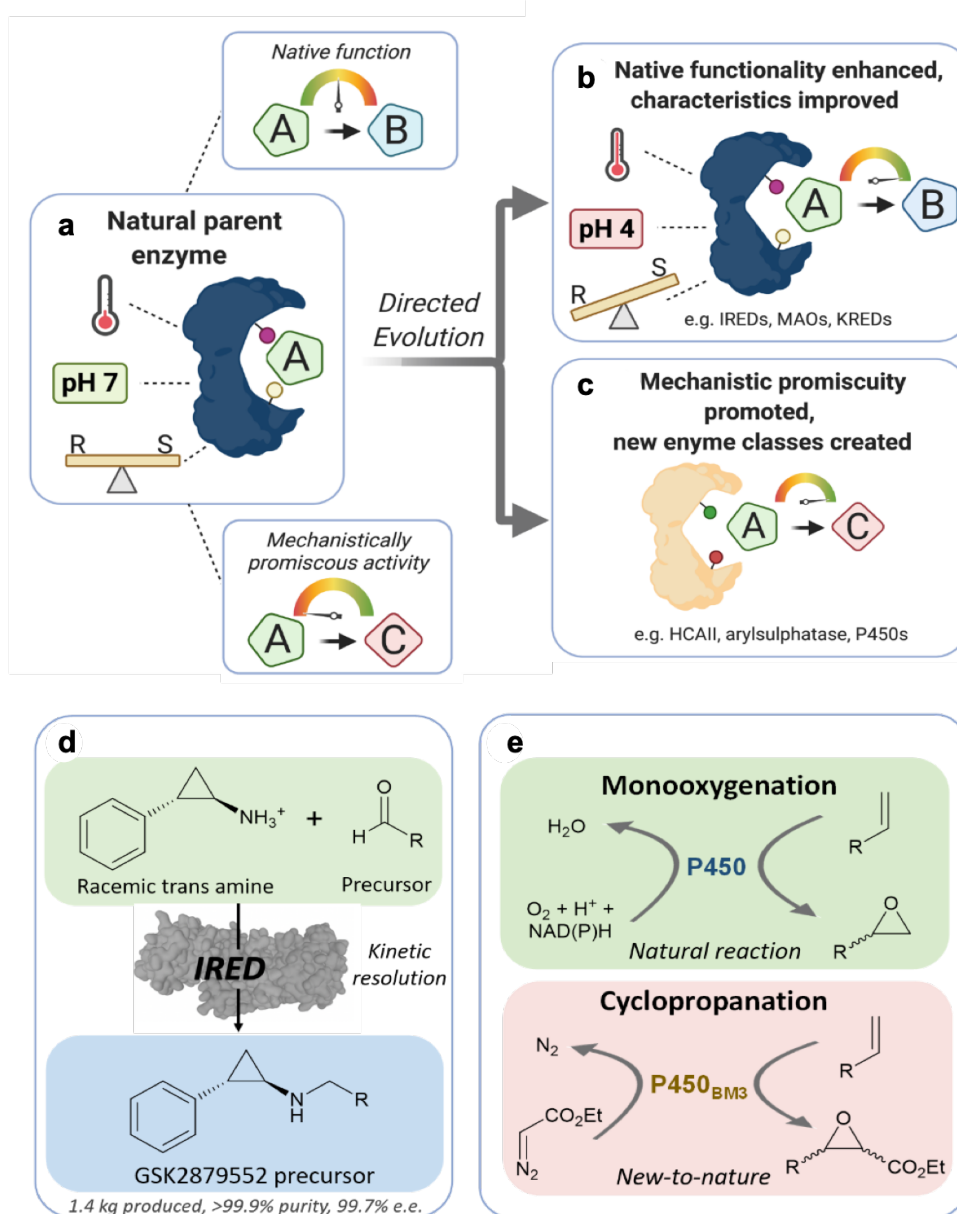


Figure 3. Directed evolution examples. a) Directed evolution can begin with a natural enzyme with a primary activity the same as or close to the reaction of interest (A→B). This enzyme may have characteristics which are undesirable or unsuitable for industrial application. b) Via directed evolution, the native functionality can be enhanced, with the original key catalytic residues and reaction mechanism conserved. Alongside this, key features for industrial process requirements may be improved, for instance, pH tolerance, thermostability and enantioselectivity. c) Alternatively, if an enzyme has a mechanistically promiscuous function (A→C), this can be promoted. This can also be accompanied by the tailoring of industrially relevant characteristics, and often results in the creation of new enzyme classes which can catalyse new-to-nature reactions. d) An example of the enhancement of an enzymes primary function by directed evolution is the engineering of an imine reductase (IRE D) to carry out asymmetric imine reduction under industrial conditions, to produce the leukaemia drug precursor, GSK2879552. e) The promiscuous activities of P450 enzymes have been promoted by directed evolution, converting them from monooxygenases into biocatalysts which can perform new-to-nature reactions such as cyclopropanation.

If an enzyme can be customised to meet the requirements demanded by large-scale manufacturing operations, it is of great interest for supporting or even supplanting traditional chemical syntheses.^{51,52} A key study is in the development of a natural ω -transaminase for the industrial production of the blockbuster antidiabetic drug, sitagliptin.⁵³ Although the original enzyme possessed the correct catalytic machinery to perform the reaction of interest, it had no activity towards the desired pro-sitagliptin reaction substrate. To obtain a functional enzyme, directed evolution was applied by using a substrate walking approach: starting from a truncated ketone analogue that the enzyme could bind, incremental changes were made to the substrate employed in each iteration of the evolution cycle, gradually making it more like the desired substrate, until the protein was able to accommodate the pro-sitagliptin ketone. The resulting engineered ω -transaminase was perfectly optimised for the necessary industrial conditions, withstanding a reaction temperature of 45°C for 24 hrs with high substrate loadings, alongside showing impressive solvent tolerance to both DMSO and acetone. The enzyme exhibited >99.9% e.e. converting 200 g L⁻¹ of pro-sitagliptin using 6 g L⁻¹ enzyme, with a 92% yield. The transaminase driven biocatalytic process outcompetes the original rhodium-catalysed route, with significant increases in productivity, whilst reducing the volume of waste products, cost of manufacture and elimination of the need for heavy metals.

Similar engineering processes have led to the creation of monoamine oxidases (MAOs) with dramatically expanded substrate scopes, including one enzyme tailored towards the stereoselective production of a key intermediate for the production of the Hepatitis C drug, telaprevir.^{54,55} The utility of engineered MAOs has been further exploited to enable the large-scale synthesis of a different Hepatitis C drug, Boceprevir. Evolution efforts lead to an enzyme that could asymmetrically oxidise a key amine intermediate, exhibiting a 150% increase in product yield compared to the original chemical process, with a concomitant reduction in waste products, water use and raw materials needed.⁵⁶ Furthermore, an impressive evolution effort by Codexis has exploited the keto-reductase (KRED) family of enzymes to produce a diverse panel of KREDs which can accept a plethora of substrates and function under numerous operating conditions, offering a highly useful selection of “plug-and-play” enzymes.⁵⁷

Laboratory evolution of an imine reductase for the direct synthesis of chiral amines, exemplifies how engineering of this type proceeds in practice. Schober *et al* were looking to create a realistic industrial catalyst for the large-scale production of leukaemia drug GSK2879552, through kinetic resolution of a racemic amine tranylcypromine sulphate precursor in a reductive amination process (Fig. 3d).⁵⁸ Chiral amine synthesis often requires complex multi-step procedures, that use toxic chemicals, and lead to high levels of by-products which can complicate product isolation.⁵⁹ Imine reductases offer a solution to this problem, having the unique ability to produce chiral amines via one of two routes: the majority of IREDs perform asymmetric imine reduction,⁵⁸ whilst a subset of this enzyme family (REDAmS) can catalyse intermolecular reductive amination.⁶⁰ Involving the stereoselective reduction of a C=N bond, biocatalysed asymmetric imine reduction is an attractive alternative to existing chemical chiral amine resolution methods.⁶¹ However, arguably the more valuable route to chiral amines is via reductive amination, where prochiral ketones are reduced to chiral amines directly in a single enzymatic step.⁶⁰ IREDs therefore offer an intriguing and convergent route to chiral amine synthesis.

The wild-type IRED (IR-46) chosen by Schober *et al*, although capable of promising reaction enantioselectivity, suffered from a number of key issues that precluded its direct commercial application: high enzyme/substrate loadings were necessary (450% wt/wt), alongside an inability to function at the acidic pH necessary to prevent product degradation. Three rounds of highly successful directed evolution, with increasingly stringent selection conditions, cumulated in the final B-point mutant IRED, M3. The evolution-guided mutation of both active site and distal residues proved important for the development of the robust M3 biocatalyst. Characterisation of the best enzyme variants created at the end of each evolutionary step, demonstrated a rapid gain in enzyme thermostability and pH tolerance, verifying the efficiency of the engineering programme employed. M3 was capable of generating an 84% yield of the desired product with 99% e.e. after only 4 hours. This impressive enzyme was now able to be used for kilogram-scale syntheses, with only 1.1% wt/wt lyophilized protein, operating at the necessary acidic pH. Hence, this example cleanly promotes the use of directed evolution as a swift route for the enhancement of an enzyme's inherent functionality, to prime it for commercial application.

2.8 Mechanistic Promiscuity as a Gateway to New Functions

An alternative route for the adaption of naturally occurring enzymes towards our needs, is the exploitation of proteins with low level promiscuous activities that can be coaxed to efficiently catalyse new reactions of chemical interest (Fig. 3c). In this manner, instead of focusing on the primary function of the enzyme, useful secondary side activities can be enhanced by directed evolution. This allows protein engineers to repurpose the diversity already present in the biological world to access reactions conceived and implemented in synthetic chemistry, but not necessarily familiar to natural enzymes.¹

The promotion of promiscuous activities has proven to be highly successful. For instance, directed evolution targeting the weak esterase activity of human carbonic anhydrase II, an enzyme whose primary physiological function is the reversible hydration of CO₂ towards 2-naphthyl acetate, led to the creation of a biocatalyst with a 40-fold increase in its ester hydrolysis activity.⁶² The gain in activity was ascribable, in the majority, to a mere two mutations. The importance of just a few key residues is reflected in other experiments of this kind: the 100,000-fold enhancement of the weak phenylphosphonate hydrolase activity of an arylsulfatase by directed evolution was attributed to two key active site mutations.⁶³ This approach has been further boosted by the advent of the ability to hunt through millions of protein variants for promiscuous activities using microfluidic platforms.⁶⁴ By “baiting” proteins with novel substrates, underlying, hidden activities can be revealed, unearthing a whole host of new potential start points for the acquisition of new biocatalytic functionality.

Some of the most famous examples of promiscuous activity enhancements come from the heme-containing family of enzymes. Catalysing a vast array of oxidation reactions, heme enzymes are prized for their biocatalytic potential, but can be compromised by low activities or stabilities. In early studies, the secondary peroxidase activity of a catalase from *Bacillus stearothermophilus* was enhanced via directed evolution,⁶⁵ whilst the enhancement of myoglobin’s promiscuous peroxidase⁶⁶⁻⁶⁸ or peroxygenase⁶⁹ activity has shown to be attainable via mutational studies; both these reactions have very different functions from the protein’s natural job as a reversible binder of dioxygen.

The most renown examples of the promotion of a heme enzyme’s secondary functions is the re-engineering of the active site of P450 enzymes to catalyse new-to-nature reactions, by the Arnold Lab.^{51,70} The Arnold Lab aimed to transcend the natural monooxygenation

mechanism of the P450s and develop enzymes that could promote non-biological carbene and nitrene transfers. These processes were expected to proceed through heme-carbenoid and nitrenoid intermediates, that are isoelectronic to the heme-oxene intermediates generated in natural heme catalysis. As an example, Coelho *et al*, looked to co-opt and engineer a P450 enzyme, to carry out the asymmetric cyclopropanation of styrenes (Fig. 3e). The generation of such highly strained cyclopropane motifs is intrinsic to the synthesis of many pharmaceuticals. Until this point the functionalisation of C=C and C-H bonds in this manner was only obtainable via a transition metal catalyst, and even then, the diversity of products formed was limited.

The wildtype *Bacillus megaterium* protein cytochrome P450 (P450_{BM3}) was chosen as the evolutionary start point, producing the desired product in low yield, but with promising stereoselectivity. From here, a panel of previously constructed mutant enzymes, derived from P450_{BM3}, were assessed and the enzyme refined further through targeted evolution of five active site residues to form a highly *cis*-selective cyclopropanation catalyst, P450_{BM3}-CIS. P450_{BM3}-CIS was highly diastereo- and enantioselective (92:8 *cis*:*trans*, 97% e.e._{*cis*}), with the enzyme catalysed cyclopropanations completed in 30 minutes. More in-depth analysis revealed that the installation of a serine (C400S) which axially coordinates the heme, shuts down the native monooxygenase activity, instead promoting the new chemistry.^{71,72} This initial work has spawned a new class of protein catalysts for a wide range of reactions: from N-H insertions,⁷³ aziridination⁷⁰ and sulfimidation⁷⁴ to borylation⁷⁵ and even Si-H insertion.⁷⁶ Enhancing the accessory functions of natural enzymes by directed evolution to deliver new-to-nature chemistries in an expanding and exciting area.

2.9 Directed Evolution of Computationally Designed Enzymes

Often, we would like to design biocatalysts for reactions that originate from the synthetic chemistry arena, but for which the necessary catalytic machinery does not exist within nature's repertoire of proteins. In these cases, how can we begin a directed evolution campaign when there is no parent protein to start with? This is where computational protein design comes to the fore, offering the prospect of producing artificial enzymes that can carry out new-to-nature processes from scratch, with desirable design features built in from the start (Fig. 4a).⁷⁷

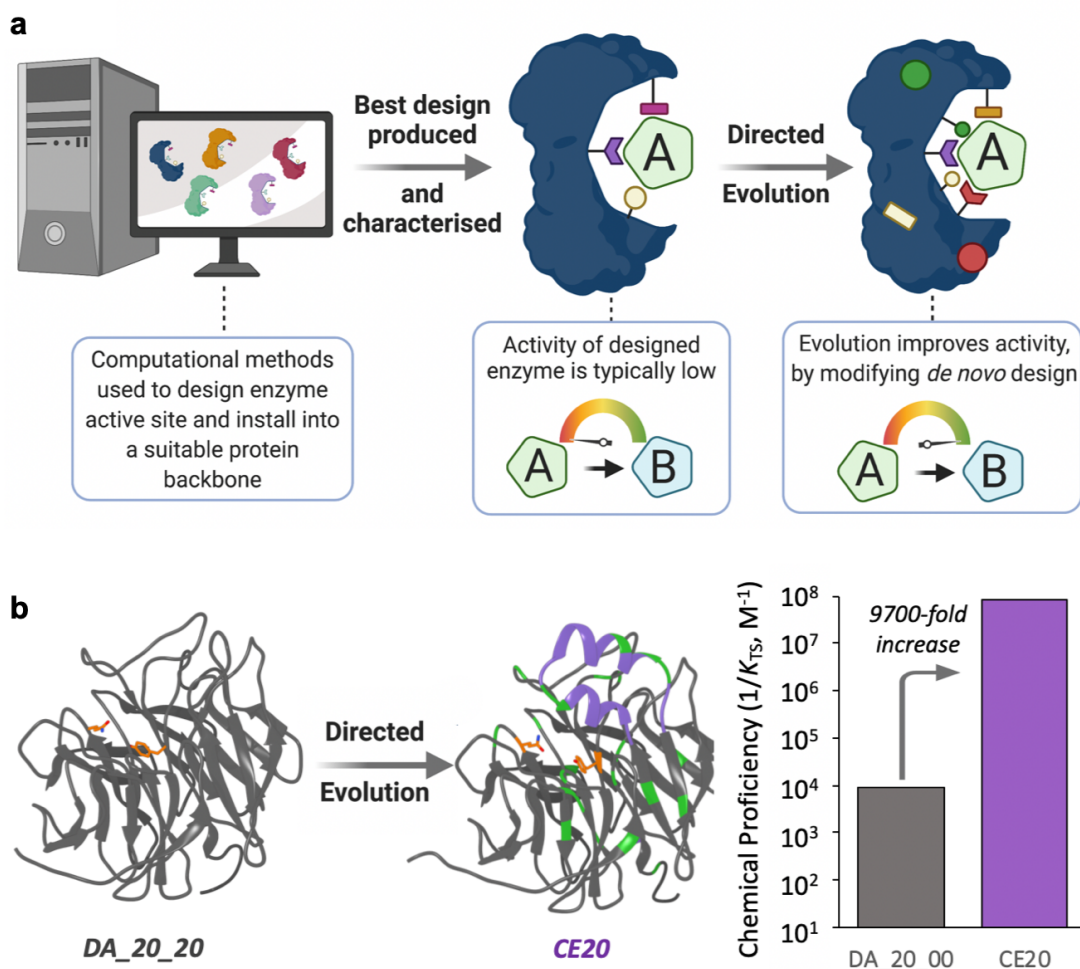


Figure 4. Directed evolution and computational protein design. a) When natural enzymes are unsuitable for the reaction of interest, parent proteins for directed evolution can be created via computational design. These *de novo* enzymes have a designed active site, modelled to form the desired enzyme-substrate complex, but often have very low activities. Directed evolution can improve the reactivity of the artificial protein, for example, by introducing mutations that remodel the active site, or changing residues that promote stability or substrate binding. These mutations were not predicted by the original computational design process. b) An artificially designed Diels-Alderase (DA_20_00, grey), containing a catalytic dyad composed of glutamine and tyrosine (orange), was subjected to multiple rounds of directed evolution, alongside crowd-sourced computational modeling. This led to the installation of 20 mutations (green) and a novel lid domain (purple) to give an improved biocatalyst (CE20) with a catalytic proficiency ($1/K_{TS} = [k_{cat}/(K_{diene} \cdot K_{dienophile})]/k_{uncat}$) over 9000-fold higher than that of the original computationally designed enzyme.

De novo protein design uses computational algorithms to generate idealized models of minimal active sites, known as theozymes, which are then built into suitable protein scaffolds *in silico*. Promising designs are subsequently produced in the laboratory and characterised.⁷⁷ The beauty of these artificial designs is that they are not constrained by natural design principles and eschew odd motifs fixed by neutral genetic drift in natural proteins. However, due to the lack of a complete understanding of enzyme structure-function relationships, initial protein designs often exhibit low activities, many orders of magnitude below those of natural enzymes.^{78,79}

Directed evolution can again offer a compelling route to enzymatic enhancement. Indeed, substantial activity gains can be achieved by high-throughput DE of *de novo* designed proteins. As a further benefit, an understanding of how molecular changes installed by evolution have improved the enzyme's function can be used to guide the next generation of computational protein design methods. Demonstrating the efficacy of this approach, computationally designed enzymes for Kemp elimination - a well-known benchmark reaction for *de novo* design efforts - have been subjected to directed evolution.^{78,80,81} Directed evolution led to dramatic changes in the enzyme architecture, initiating extensive active site remodelling, alongside the introduction of new catalytic residues which were not predicted by the computational design process. However, more nuanced mutational alterations were also important, proving pivotal in crafting the original inactive design into a fully functional Kemp eliminase.⁵⁰

Another striking example of this process is the generation of an enzyme for the bimolecular Diels-Alder reaction, developed through a combination of artificial enzyme design, targeted mutagenesis and *in silico* optimisation,⁷⁹ alongside laboratory evolution⁸² and even citizen science⁸³ (Fig. 4b). Comprising of the creation of two new C-C bonds and up to four new stereocentres, the intermolecular Diels-Alder reaction is mainstay of organic synthesis.^{84,85} This type of intramolecular cycloaddition reaction is notably absent from the catalytic repertoire present in natural enzymes.

Of the 84 enzyme designs originally created for the Diels-Alder reaction, only one, DA_20_00 was suitable for further exploration.⁷⁹ Rationally guided mutagenesis of the protein's active site gave rise to DA_20_10 which had a 100-fold improvement in activity over the parent enzyme but was only stable for around 30 turnovers. Human creativity

provided the next innovation for this protein: the citizen science game platform Foldit, asked players to functionally remodel the protein's structure.⁸³ This resulted in the addition of a 24-residue helix-turn-helix motif to form a lid domain to the parent protein, that helped to orientate and position the reaction substrates (known as protein CE6). The combination of this novel structural feature with directed evolution, resulted in enzyme CE20, a biocatalyst that could complete over 770 turnovers without destabilisation, with a chemical proficiency around 9,700 times greater than that of DA_20_00, the original computational design.⁸²

CE20 is significantly more proficient than any other biocatalyst available for the Diels-Alder reaction.⁸⁶⁻⁸⁹ Mutations introduced via evolution were varied but essential for catalytic proficiency: some clustered around the appended lid element, whilst others were instrumental in sculpting the substrate binding pocket without disturbing the core packing of the protein.⁸² Although still far from perfect: CE20 exhibits a turnover of merely 10 substrate molecules per hour, four to five magnitudes lower than that of natural enzymes with average activities,⁹⁰ *de novo* protein design and subsequent evolution provides us with key insights into the underlying fundamentals of protein folding and biochemistry.^{77,81} The hope is that this nascent area of research will eventually allow us to generate proteins-to-order from physical principles alone, whilst also enabling us to enhance our knowledge of how proteins function in the natural world.

Looking to the future, a number of computational advances will aid in sating the desire for enzymes-on-demand. Machine learning algorithms,⁹¹ quantum mechanical methods,⁵⁰ deep learning,^{92,93} and other data-driven methods will allow the creation and effective combination of superlative directed evolution strategies with enhanced designed artificial enzymes, offering a versatile avenue to new functions.

2.10 Designing New Reactivities by Combining DE and Genetic Code Expansion

Synthetic chemists have developed a wealth of catalytic transformations not found in nature. This broad reaction scope is facilitated by the availability of diverse functional groups which are able to mediate catalysis through a variety of activation modes. In contrast, enzymes are built from a limited amino acid alphabet. The restrictive range of canonical biomolecular building blocks limits the diversity of catalytic mechanisms that can be constructed within an enzyme's active site. However, modern methods to enable the site-

specific installation of alternative amino acids, known as non-canonical amino acids (ncAAs), offer a gateway to access new reactivities.^{94,95} NcAAs have a much broader architectural and functional scope than those provided by nature, offering the opportunity to amplify the mechanistic repertoire of enzymes.^{96,97}

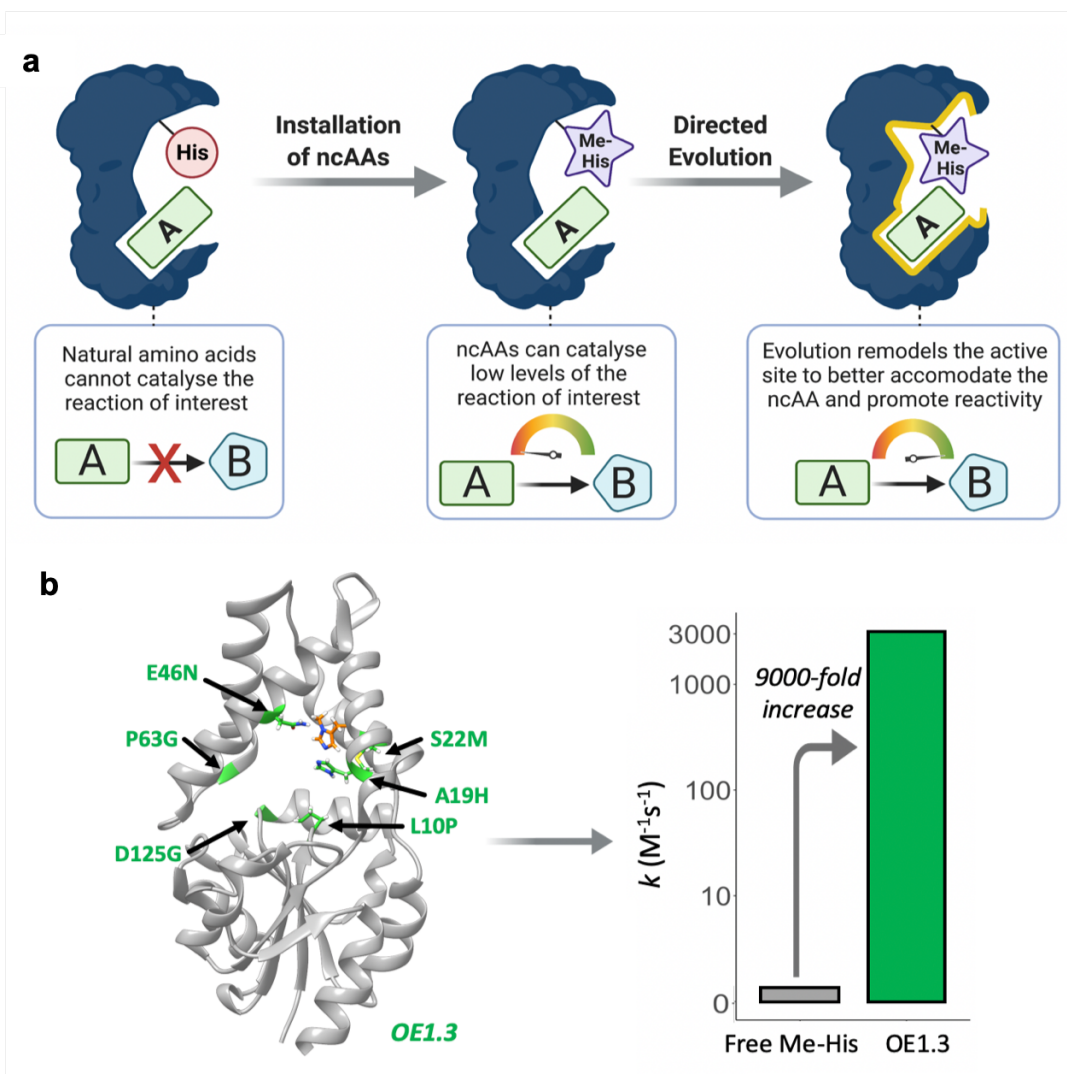


Figure 5. Directed Evolution and genetic code expansion. **a)** Sometimes we want to catalyse a reaction for which natural amino acids do not have the necessary reactivity. In this case we can install a non-canonical amino acid (ncAA), which has the correct catalytic features to promote the reaction of interest. However, as enzyme active sites are not designed to host ncAAs often the enzyme's catalytic ability is low. Hence, directed evolution is applied to remodel the active site to promote the reactivity of the ncAA with the substrate of interest. **b)** The computationally designed protein OEI was subjected to directed evolution to improve its esterase ability. The ribbon representation of the resulting OE1.3 enzyme (grey) highlights the mutations installed through evolution (green) alongside the ncAA, Me-His residue (ball-and-stick model, orange) which was essential to its catalytic activity. The optimized OE1.3's ester hydrolysis activity was accelerated by >9000-fold compared with the free ncAA (Me-His) in solution.

To date only a handful of enzymes that contain non-canonical functional components have been developed. Akin to the challenges faced by computationally designed enzymes, the catalytic activities of initial ncAA-containing enzymes are typically modest. Fortunately, directed evolution workflows have been adjusted to accommodate the necessary expanded genetic alphabet and readily applied to enhance functionality.^{68,98} In this way, a protein scaffold host can be carefully sculpted to support and accelerate catalysis by these non-canonical elements (Fig. 5a).

The amalgamation of genetic code expansion and directed evolution is nicely showcased by the development of an artificial hydrolase by installing the ncAA, N₈-methylhistidine (Me-His) as a catalytic nucleophile into the designed protein BH32 (Fig. 5b).⁹⁶ Methylation of the histidine residue proved essential for catalytic function as it led to the generation of a readily hydrolysable acyl-enzyme intermediate, in contrast to the unreactive intermediates formed in designed hydrolases equipped with canonical nucleophiles.⁹⁸⁻¹⁰¹

OEL, like other initial enzyme designs employing ncAA catalytic residues, exhibited modest starting activity. However, via iterative rounds of combinatorial active-site-mutagenesis, error prone PCR and beneficial diversity shuffling, directed evolution gave rise to the six-point mutant, OEL.3. OEL.3 was 15 times more effective than the starting parent protein and is 9000-fold more efficient than free Me-His in promoting ester hydrolysis. X-ray crystallography revealed that activity gains were due to a combination of factors, including the reduction of conformational flexibility of the Me-His residue, the creation of a network of functionally important polar interactions and an expansion of the active-site pocket. Three further mutations installed through additional rounds of evolution revealed the enantioselective OEL.4 variant, with an 8-fold higher activity towards the (*R*)-enantiomer compared to the (*S*)-enantiomer of a chiral fluorescein derived substrate. This study neatly demonstrates that the “bottom-up” generation of efficient and selective biocatalysts with non-canonical catalytic mechanisms is entirely plausible, with directed evolution offering an effective and practical means of optimizing catalytic function. A detailed understanding of the molecular features that emerge during evolution to support catalysis by the non-canonical functional group will facilitate the design of highly efficient and functionally diverse biocatalysts in the future.

2.11 References

1. Arnold, F. H. Directed Evolution: Bringing New Chemistry to Life. *Angewandte Chemie International Edition* **57**, 4143–4148 (2018).
2. Zeymer, C. & Hilvert, D. Directed Evolution of Protein Catalysts. *Annual Review of Biochemistry* **87**, 131–57 (2018).
3. Bornscheuer, U. T. *et al.* Engineering the third wave of biocatalysis. *Nature* **485**, 185–194 (2012).
4. Tracewell, C. A. & Arnold, F. H. Directed enzyme evolution: climbing fitness peaks one amino acid at a time. *Current Opinion in Chemical Biology* **13**, 3–9 (2009).
5. Cobb, R. E., Chao, R. & Zhao, H. Directed Evolution: Past, Present and Future. *AIChE journal. American Institute of Chemical Engineers* **59**, 1432–1440 (2013).
6. Bell, E. L. *et al.* Biocatalysis. *Nature Reviews Methods Primers* **1**, 46 (2021).
7. Packer, M. S. & Liu, D. R. Methods for the directed evolution of proteins. *Nature Reviews Genetics* **16**, 379–394 (2015).
8. Cadwell, R. & Joyce, G. Mutagenic PCR. *PCR Methods Appl.* **3**, 136–140 (1994).
9. Kille, S. *et al.* Reducing codon redundancy and screening effort of combinatorial protein libraries created by saturation mutagenesis. *ACS Synthetic Biology* **2**, 83–92 (2013).
10. Wells, J. A., Vasser, M. & Powers, D. B. Cassette mutagenesis: an efficient method for generation of multiple mutations at defined sites. *Gene* **34**, 315–323 (1985).
11. Reetz, M. T., Bocola, M., Carballeira, J. D., Zha, D. & Vogel, A. Expanding the range of substrate acceptance of enzymes: Combinatorial Active-Site Saturation Test. *Angewandte Chemie International Edition* **44**, 4192–4196 (2005).
12. Reetz, M. T., Kahakeaw, D. & Lohmer, R. Addressing the numbers problem in directed evolution. *ChemBioChem* **9**, 1797–1804 (2008).
13. Stemmer, W. P. C. Rapid evolution of a protein in vitro by DNA shuffling. *Nature* **370**, 389 (1994).
14. Zhao, H., Giver, L., Shao, Z., Affholter, J. A. & Arnold, F. H. Molecular evolution by staggered extension process (StEP) *in vitro* recombination. *Nature Biotechnology* **16**, 258–261 (1998).
15. Zha, D., Eipper, A. & Reetz, M. T. Assembly of Designed Oligonucleotides as an Efficient Method for Gene Recombination: A New Tool in Directed Evolution. *ChemBioChem* **4**, 34–39 (2003).
16. Xiao, H., Bao, Z. & Zhao, H. High Throughput Screening and Selection Methods for Directed Enzyme Evolution. *Industrial & engineering chemistry research* **54**, 4011–4020 (2015).
17. Turner, N. J. Directed evolution of enzymes for applied biocatalysis. *Trends in Biotechnology* **21**, 474–478 (2003).
18. Watt, A. P., Morrison, D., Locker, K. L. & Evans, D. C. Higher Throughput Bioanalysis by Automation of a Protein Precipitation Assay Using a 96-Well Format with Detection by LC–MS/MS. *Analytical Chemistry* **72**, 979–984 (2000).
19. Weiß, M. S., Bornscheuer, U. T. & Höhne, M. Solid-Phase Agar Plate Assay for Screening Amine Transaminases. in *Protein Engineering: Methods and Protocols* (eds. Bornscheuer, U. T. & Höhne, M.) 283–296 (Springer New York, 2018).
20. Alexeeva, M., Enright, A., Dawson, M. J., Mahmoudian, M. & Turner, N. J. Deracemization of α -Methylbenzylamine Using an Enzyme Obtained by *In Vitro* Evolution. *Angewandte Chemie International Edition* **41**, 3177–3180 (2002).

21. Green, A. P., Turner, N. J. & O'Reilly, E. Chiral amine synthesis using ω -transaminases: An amine donor that displaces equilibria and enables high-throughput screening. *Angewandte Chemie - International Edition* **53**, 10714–10717 (2014).
22. Weiß, M. S., Pavlidis, I. v, Vickers, C., Höhne, M. & Bornscheuer, U. T. Glycine oxidase based high-throughput solid-phase assay for substrate profiling and directed evolution of (R)- and (S)-selective amine transaminases. *Analytical Chemistry* **86**, 11847–11853 (2014).
23. Rowles, I., Malone, K. J., Etchells, L. L., Willies, S. C. & Turner, N. J. Directed Evolution of the Enzyme Monoamine Oxidase (MAO-N): Highly Efficient Chemo-enzymatic Deracemisation of the Alkaloid (\pm)-Crispine A. *ChemCatChem* **4**, 1259–1261 (2012).
24. Yang, G. & Withers, S. G. Ultrahigh-throughput FACS-based screening for directed enzyme evolution. *ChemBioChem* **10**, 2704–2715 (2009).
25. Chiu, F. W. Y. & Stavrakis, S. High-throughput droplet-based microfluidics for directed evolution of enzymes. *Electrophoresis* **40**, 2860–2872 (2019).
26. Griffiths, A. D. & Tawfik, D. S. Miniaturising the laboratory in emulsion droplets. *Trends Biotechnol* **24**, 395–402 (2006).
27. Agresti, J. J. *et al.* Ultrahigh-throughput screening in drop-based microfluidics for directed evolution. *Proceedings of the National Academy of Sciences of the United States of America* **107**, 4004–4009 (2010).
28. Debon, A. *et al.* Ultrahigh-throughput screening enables efficient single-round oxidase remodelling. *Nature Catalysis* **2**, 740–747 (2019).
29. Obexer, R. *et al.* Emergence of a catalytic tetrad during evolution of a highly active artificial aldolase. *Nature Chemistry* **9**, 50–56 (2017).
30. Holland-Moritz, D. A. *et al.* Mass Activated Droplet Sorting (MADS) Enables High-Throughput Screening of Enzymatic Reactions at Nanoliter Scale. *Angewandte Chemie International Edition* **59**, 4470–4477 (2020).
31. Diefenbach, X. W. *et al.* Enabling Biocatalysis by High-Throughput Protein Engineering Using Droplet Microfluidics Coupled to Mass Spectrometry. *ACS omega* **3**, 1498–1508 (2018).
32. Wang, X. *et al.* Raman-Activated Droplet Sorting (RADS) for Label-Free High-Throughput Screening of Microalgal Single-Cells. *Analytical Chemistry* **89**, 12569–12577 (2017).
33. McIlvenna, D. *et al.* Continuous cell sorting in a flow based on single cell resonance Raman spectra. *Lab on a Chip* **16**, 1420–1429 (2016).
34. Acevedo-Rocha, C. G., Agudo, R. & Reetz, M. T. Directed evolution of stereoselective enzymes based on genetic selection as opposed to screening systems. *Journal of Biotechnology* **191**, 3–10 (2014).
35. Smith, G. P. Filamentous Fusion Phage: Novel Expression Vectors That Display Cloned Antigens on the Virion Surface. *Science* **228**, 1315–1317 (1985).
36. Fernandez-Gacio, A., Uguen, M. & Fastrez, J. Phage display as a tool for the directed evolution of enzymes. *Trends in Biotechnology* **21**, 408–414 (2003).
37. Zahnd, C., Amstutz, P. & Plückthun, A. Ribosome display: selecting and evolving proteins *in vitro* that specifically bind to a target. *Nature Methods* **4**, 269–279 (2007).
38. Keefe, A. D. Protein Selection Using mRNA Display. *Current Protocols in Molecular Biology* **53**, 24.5.1–24.5.34 (2001).
39. Wang, L. & Schultz, P. G. A general approach for the generation of orthogonal tRNAs. *Chemistry and Biology* **8**, 883–890 (2001).

40. Wan, W., Tharp, J. M. & Liu, W. R. Pyrrolysyl-tRNA synthetase: An ordinary enzyme but an outstanding genetic code expansion tool. *Biochimica et Biophysica Acta - Proteins and Proteomics* vol. 1844 1059–1070 (2014).
41. Morrison, M. S., Podracky, C. J. & Liu, D. R. The developing toolkit of continuous directed evolution. *Nature Chemical Biology* **16**, 610–619 (2020).
42. Esvelt, K. M., Carlson, J. C. & Liu, D. R. A system for the continuous directed evolution of biomolecules. *Nature* **472**, 499–503 (2011).
43. Packer, M. S., Rees, H. A. & Liu, D. R. Phage-assisted continuous evolution of proteases with altered substrate specificity. *Nature Communications* **8**, 956 (2017).
44. Ravikumar, A., Arrieta, A. & Liu, C. C. An orthogonal DNA replication system in yeast. *Nature Chemical Biology* **10**, 175 (2014).
45. Zhong, Z. *et al.* Automated Continuous Evolution of Proteins *in Vivo*. *ACS Synthetic Biology* **9**, 1270–1276 (2020).
46. Rix, G. *et al.* Scalable continuous evolution for the generation of diverse enzyme variants encompassing promiscuous activities. *Nature Communications* **11**, 5644 (2020).
47. Moore, J. C. & Arnold, F. H. Directed evolution of a para-nitrobenzyl esterase for aqueous-organic solvents. *Nature Biotechnology* **14**, 458–467 (1996).
48. Garcia-Ruiz, E., Gonzalez-Perez, D., Ruiz-Dueñas, F. J., Martínez, A. T. & Alcalde, M. Directed evolution of a temperature-, peroxide- and alkaline pH-tolerant versatile peroxidase. *Biochemical Journal* **441**, 487–498 (2011).
49. Reetz, M. T. Changing the Enantioselectivity of Enzymes by Directed Evolution. in *Methods in Enzymology* vol. 388 238–256 (Academic Press, 2004).
50. Otten, R. *et al.* How directed evolution reshapes the energy landscape in an enzyme to boost catalysis. *Science* **370**, 1442–1446 (2020).
51. Coelho, P. S., Brustad, E. M., Kannan, A. & Arnold, F. H. Olefin Cyclopropanation via Carbene Transfer Catalyzed by Engineered Cytochrome P450 Enzymes. *Science* **339**, 307–310 (2013).
52. Hammer, S. C., Knight, A. M. & Arnold, F. H. Design and evolution of enzymes for non-natural chemistry. *Current Opinion in Green and Sustainable Chemistry* **7**, 23–30 (2017).
53. Savile, C. K. *et al.* Biocatalytic asymmetric synthesis of chiral amines from ketones applied to sitagliptin manufacture. *Science* **329**, 305–309 (2010).
54. Köhler, V. *et al.* Enantioselective Biocatalytic Oxidative Desymmetrization of Substituted Pyrrolidines. *Angewandte Chemie International Edition* **49**, 2182–2184 (2010).
55. Green, A. P. & Turner, N. J. Biocatalytic retrosynthesis: Redesigning synthetic routes to high-value chemicals. *Perspectives in Science* **9**, 42–48 (2016).
56. Li, T. *et al.* Efficient, Chemoenzymatic Process for Manufacture of the Boceprevir Bicyclic [3.1.0] Proline Intermediate Based on Amine Oxidase-Catalyzed Desymmetrization. *Journal of the American Chemical Society* **134**, 6467–6472 (2012).
57. Micklitsch, C., Duan, D. & Borra-Garske, M. KREDs: Toward Green, Cost-Effective, and Efficient Chiral Alcohol Generation. in *Industrial Enzyme Applications* 351–383 (John Wiley & Sons, Ltd, 2019).
58. Schober, M. *et al.* Chiral synthesis of LSD1 inhibitor GSK2879552 enabled by directed evolution of an imine reductase. *Nature Catalysis* **2**, 909–915 (2019).
59. Patil, M. D., Grogan, G., Bommarius, A. & Yun, H. Oxidoreductase-Catalyzed Synthesis of Chiral Amines. *ACS Catalysis* **8**, 10985–11015 (2018).

60. Sharma, M. *et al.* A Mechanism for Reductive Amination Catalyzed by Fungal Reductive Aminases. *ACS Catalysis* **8**, 11534–11541 (2018).
61. Hussain, S. *et al.* An (R)-Imine Reductase Biocatalyst for the Asymmetric Reduction of Cyclic Imines. *ChemCatChem* **7**, 579–583 (2015).
62. Gould, S. McQ. & Tawfik, D. S. Directed Evolution of the Promiscuous Esterase Activity of Carbonic Anhydrase II. *Biochemistry* **44**, 5444–5452 (2005).
63. Miton, C. M. *et al.* Evolutionary repurposing of a sulfatase: A new Michaelis complex leads to efficient transition state charge offset. *Proceedings of the National Academy of Sciences* **115**, E7293 (2018).
64. Colin, P. Y. *et al.* Ultrahigh-throughput discovery of promiscuous enzymes by picodroplet functional metagenomics. *Nature Communications* **6**, 1–12 (2015).
65. Trakulnaleamsai, S., Yomo, T., Yoshikawa, M., Aihara, S. & Urabe, I. Experimental sketch of landscapes in protein sequence space. *Journal of Fermentation and Bioengineering* **79**, 107–118 (1995).
66. Wan, L., Twitchett, M. B., Eltis, L. D., Mauk, A. G. & Smith, M. *In vitro* evolution of horse heart myoglobin to increase peroxidase activity. *Proceedings of the National Academy of Sciences* **95**, 12825 (1998).
67. Matsuura, T. *et al.* Nonadditivity of mutational effects on the properties of catalase I and its application to efficient directed evolution. *Protein Engineering, Design and Selection* **11**, 789–795 (1998).
68. Pott, M. *et al.* A Noncanonical Proximal Heme Ligand Affords an Efficient Peroxidase in a Globin Fold. *Journal of the American Chemical Society* **140**, 1535–1543 (2018).
69. Ozaki, S., Yang, H.-J., Matsui, T., Goto, Y. & Watanabe, Y. Asymmetric oxidation catalyzed by myoglobin mutants. *Tetrahedron: Asymmetry* **10**, 183–192 (1999).
70. Farwell, C. C., Zhang, R. K., McIntosh, J. A., Hyster, T. K. & Arnold, F. H. Enantioselective Enzyme-Catalyzed Aziridination Enabled by Active-Site Evolution of a Cytochrome P450. *ACS Central Science* **1**, 89–93 (2015).
71. Wang, Z. J. *et al.* Improved Cyclopropanation Activity of Histidine-Ligated Cytochrome P450 Enables the Enantioselective Formal Synthesis of Levomilnacipran. *Angewandte Chemie International Edition* **53**, 6810–6813 (2014).
72. Coelho, P. S. *et al.* A serine-substituted P450 catalyzes highly efficient carbene transfer to olefins *in vivo*. *Nature Chemical Biology* **9**, 485–487 (2013).
73. Wang, Z. J., Peck, N. E., Renata, H. & Arnold, F. H. Cytochrome P450-catalyzed insertion of carbenoids into N–H bonds. *Chemical Science* **5**, 598–601 (2014).
74. Farwell, C. C., McIntosh, J. A., Hyster, T. K., Wang, Z. J. & Arnold, F. H. Enantioselective Imidation of Sulfides via Enzyme-Catalyzed Intermolecular Nitrogen-Atom Transfer. *Journal of the American Chemical Society* **136**, 8766–8771 (2014).
75. Kan, S. B. J., Huang, X., Gumulya, Y., Chen, K. & Arnold, F. H. Genetically programmed chiral organoborane synthesis. *Nature* **552**, 132–136 (2017).
76. Kan, S. B. J., Lewis, R. D., Chen, K. & Arnold, F. H. Directed evolution of cytochrome c for carbon-silicon bond formation: Bringing silicon to life. *Science (New York, N.Y.)* **354**, 1048–1051 (2016).
77. Huang, P.-S., Boyken, S. E. & Baker, D. The coming of age of *de novo* protein design. *Nature* **537**, 320 (2016).
78. Röthlisberger, D. *et al.* Kemp elimination catalysts by computational enzyme design. *Nature* **453**, 190 (2008).

79. Siegel, J. B. *et al.* Computational Design of an Enzyme Catalyst for a Stereoselective Bimolecular Diels-Alder Reaction. *Science* **329**, 309–313 (2010).
80. Khersonsky, O. *et al.* Evolutionary Optimization of Computationally Designed Enzymes: Kemp Eliminases of the KE07 Series. *Journal of Molecular Biology* **396**, 1025–1042 (2010).
81. Blomberg, R. *et al.* Precision is essential for efficient catalysis in an evolved Kemp eliminase. *Nature* **503**, 418–421 (2013).
82. Preiswerk, N. *et al.* Impact of scaffold rigidity on the design and evolution of an artificial Diels-Alderase. *Proceedings of the National Academy of Sciences* **111**, 8013 (2014).
83. Eiben, C. B. *et al.* Increased Diels-Alderase activity through backbone remodeling guided by Foldit players. *Nature Biotechnology* **30**, 190–192 (2012).
84. Serafimov, J. M., Gillingham, D., Kuster, S. & Hilvert, D. The Putative Diels-Alderase Macrophomate Synthase is an Efficient Aldolase. *Journal of the American Chemical Society* **130**, 7798–7799 (2008).
85. Ose, T. *et al.* Insight into a natural Diels-Alder reaction from the structure of macrophomate synthase. *Nature* **422**, 185–189 (2003).
86. Gouverneur, V. E. *et al.* Control of the exo and endo Pathways of the Diels-Alder Reaction by Antibody Catalysis. *Science* **262**, 204–208 (1993).
87. Reetz, M. T. Artificial Metalloenzymes as Catalysts in Stereoselective Diels-Alder Reactions. *The Chemical Record* **12**, 391–406 (2012).
88. Yli-Kauhala, J. T. *et al.* Anti-Metallocene Antibodies: A New Approach to Enantioselective Catalysis of the Diels-Alder Reaction. *Journal of the American Chemical Society* **117**, 7041–7047 (1995).
89. Kim, H. J., Ruzsyczky, M. W., Choi, S., Liu, Y. & Liu, H. Enzyme-catalysed [4+2] cycloaddition is a key step in the biosynthesis of spinosyn A. *Nature* **473**, 109–112 (2011).
90. Bar-Even, A. *et al.* The moderately efficient enzyme: Evolutionary and physicochemical trends shaping enzyme parameters. *Biochemistry* **50**, 4402–4410 (2011).
91. Fox, R. J. *et al.* Improving catalytic function by ProSAR-driven enzyme evolution. *Nature Biotechnology* **25**, 338 (2007).
92. Russ, W. P. *et al.* An evolution-based model for designing chorismate mutase enzymes. *Science* **369**, 440 (2020).
93. Norn, C. *et al.* Protein sequence design by conformational landscape optimization. *Proceedings of the National Academy of Sciences* **118**, e2017228118 (2021).
94. Liu, C. C. & Schultz, P. G. Adding New Chemistries to the Genetic Code. *Annual Review of Biochemistry* **79**, 413–444 (2010).
95. Chin, J. W. Expanding and Reprogramming the Genetic Code of Cells and Animals. *Annual Review of Biochemistry* **83**, 379–408 (2014).
96. Burke, A. J. *et al.* Design and evolution of an enzyme with a non-canonical organocatalytic mechanism. *Nature* **570**, 219–223 (2019).
97. Drienovská, I., Mayer, C., Dulson, C. & Roelfes, G. A designer enzyme for hydrazone and oxime formation featuring an unnatural catalytic aniline residue. *Nature Chemistry* **10**, 946–952 (2018).
98. Bolon, D. N. & Mayo, S. L. Enzyme-like proteins by computational design. *Proceedings of the National Academy of Sciences of the United States of America* **98**, 14274–14279 (2001).
99. Richter, F. *et al.* Computational Design of Catalytic Dyads and Oxyanion Holes for Ester Hydrolysis. *Journal of the American Chemical Society* **134**, 16197–16206 (2012).

100. Moroz, Y. S. *et al.* New Tricks for Old Proteins: Single Mutations in a Nonenzymatic Protein Give Rise to Various Enzymatic Activities. *Journal of the American Chemical Society* **137**, 14905–14911 (2015).
101. Burton, A. J., Thomson, A. R., Dawson, W. M., Brady, R. L. & Woolfson, D. N. Installing hydrolytic activity into a completely *de novo* protein framework. *Nature Chemistry* **8**, 837 (2016).

CHAPTER 3

Aims

This project aims to develop an automated, high-throughput, enzymatic PET depolymerisation screening platform to underpin the directed evolution of *IsPETase*. The primary objective is to create and characterise an improved biocatalyst, with enhanced PET-degrading activities, thermotolerance and stability, that is unaffected by product inhibition and can operate at the glass transition temperature of the plastic. The second objective is to challenge the evolved PETase with a range of commercially-relevant substrates to explore its ability to act upon realistic post-consumer waste streams. Finally, the basis for elucidating a more complete understanding of the catalytic mechanism of *IsPETase* and evolved variants will be explored, taking advantage of state-of-the-art genetic code expansion methodologies to capture a reaction cycle intermediate.

The specific aims of this project are as follows:

1. Design an integrated, high-throughput, enzymatic PET plastic deconstruction screening platform to underpin the directed evolution study.
2. Subject *IsPETase* to iterative rounds of laboratory evolution, applying selection pressures for increased activity, thermostability and ability to degrade crystalline forms of PET material.
3. Perform biochemical and structural characterisation of the most highly evolved *IsPETase* variant and compare to the engineered cutinase homologue, LCC^{ICCG}.
4. Optimise PET deconstruction reaction conditions to achieve the maximum conversion of PET into soluble products over 24 hours.
5. Explore the capacity of the evolved *IsPETase* to depolymerise materials reminiscent of those found in mixed plastic waste streams and real-world packaging materials, including highly crystalline PET, a PET composite and copolymer, alongside a new biopolymer, poly(ethylene furanoate) (PEF).
6. Demonstrate the feasibility of capturing acyl-enzyme intermediates of *IsPETase* to allow future structural characterisation of a key catalytic cycle intermediate analogue.

CHAPTER 4

Directed Evolution of an Efficient and Thermostable PETase

Elizabeth L. Bell¹, Ross Smithson¹, Jake Foster¹, Florence Hardy¹, Colin Levy¹ & Anthony Green^{1*}

¹Manchester Institute of Biotechnology, 131 Princess Street, University of Manchester, Manchester, M1 7DN, UK.

4.1 Foreword

This chapter consists of a research article published on the ChemRxiv (January 2022), and describes the design of a high-throughput directed evolution platform for the deconstruction of PET and its application to *Is*PETase to create a more active and thermostable biocatalyst.

4.2 Acknowledgements

The research presented in this chapter was a collaborative effort between the doctoral candidate and the following researchers: Ross Smithson, Jake Foster, Florence Hardy, Colin Levy and Anthony P. Green. The doctoral candidate carried out molecular biology, assay development, directed evolution, protein production, purification, biochemical characterisation, reaction optimisation, data analysis and presentation. Ross Smithson and Jake Foster helped to take samples for time-resolved assays. Ross Smithson carried out the substrate synthesis of the MHET standard. Florence Hardy and Colin Levy interpreted and analysed structural data. We thank Mark Dunstan for assistance in automating the directed evolution workflow. The doctoral candidate and Anthony P. Green wrote the manuscript.

4.3 Abstract

The recent discovery of a hydrolytic enzyme, *Is*PETase, that can deconstruct poly(ethylene) terephthalate (PET), has sparked great interest in biocatalytic depolymerisations as a means of recycling plastics. Realisation of commercial utility will require the development of robust engineered enzymes that meet the demands of industrial processes. Although rationally engineered variants of PETases have been described, enzymes that have been experimentally optimised via directed evolution - the go-to method for engineering industrially useful biocatalysts - have not yet been developed, likely due to an absence of high-throughput

screening protocols that report on catalytic deconstruction of insoluble plastics. Here, we report the development and implementation of an automated, high-throughput directed evolution platform for the development of polymer degrading enzymes. Evaluation of over 13,000 *IsPETase* variants, applying catalytic activity at elevated temperatures as a primary selection pressure, afforded the *HotPETase* variant, containing 21 mutations, that can operate at the glass transition temperature of PET (60-70°C), and deconstructs semi-crystalline PET more rapidly than previously reported *PETases*. Structural characterisation of *HotPETase* reveals several interesting features that have emerged during evolution to improve thermotolerance and catalytic performance, including better packing of the central β -sheet region and formation of a new π -stacking interaction which restrains Trp185 to a single conformer. Our study demonstrates that powerful laboratory evolution protocols can be adapted to allow engineering of plastic degrading enzymes. By adapting the selection pressures, we anticipate that our platform will allow the development of enzymes specifically tailored to meet industrial needs, thus contributing to a versatile biocatalytic plastic waste recycling strategy.

4.4 Introduction

Fossil-fuel derived plastics have become an essential commodity in modern society. The versatility and low production costs of these man-made polymers means that they are produced on an enormous and ever-growing scale, with an estimated 360 million tonnes of plastic being manufactured each year.¹ Unfortunately, the properties that make plastics appealing, such as their inertness and durability, mean that they become especially problematic pollutants if disposed of incorrectly. It is now widely recognized that the accumulation of plastics in the environment poses a serious global pollution threat, with marine ecosystems being particularly at risk.² There is therefore urgent need for new technologies to treat and recycle plastic waste, in order to prevent an environmental catastrophe.

Poly(ethylene terephthalate) (PET) is amongst the most abundantly produced synthetic polymers. Demand for this material has grown substantially due to a heightened global appetite for convenient single-use containers,^{3,4} with an estimated 1 million PET bottles being produced every minute.⁵ Although mechanical recycling methods are available for PET, recycling rates remain low due to difficulties in sorting mixed post-consumer waste streams,⁶ and declining polymer properties after repeated processing cycles.⁷ In light of

these challenges, chemical recycling, involving catalysed hydrolysis and depolymerisation,^{8,9} has garnered interest as a means of circularising the PET life-cycle. Unfortunately, chemical recycling methods are often energy intensive, can require large volumes of organic solvents and produce low-quality mixtures of products that are difficult to separate, especially when attempting to recycle mixed plastic waste.¹⁰

In recent years, biological catalysis has emerged as a potentially attractive alternative to more traditional plastic recycling strategies.¹¹ Enzymes are the most proficient and selective catalysts known and can accelerate chemical processes with unrivalled specificities. In principle, composite materials could be selectively degraded by enzymes without need for manual sorting,¹² and the resulting deconstruction products tailored and fed into additional enzymatic cascades to create higher value chemical feedstocks and products,¹³ all carried out under low cost, low carbon, environmentally benign reaction conditions.¹⁰ For enzymatic PET recycling to be feasible, suitable biocatalysts must first be discovered and then engineered to tailor their properties for target applications. Unfortunately, while microorganisms are extremely well-equipped to deconstruct biological polymers such as proteins, DNA and carbohydrates, they are generally not well-adapted to achieve efficient depolymerisation of anthropogenic polymers.¹⁴ Nevertheless, some cutinases have been shown to have promiscuous PET degradation abilities.¹⁵⁻¹⁸ Unfortunately, these enzymes typically display poor activity towards PET materials with crystallinities similar to those commonly found in post-consumer waste. To function effectively, even engineered cutinases require the extensive pre-processing of PET substrates to amorphize the material,¹⁹ a process which compromises the economics and environmental sustainability of biocatalytic plastic recycling approaches.¹²

The recent serendipitous discovery of an organism, *Ideonella sakaiensis*, with the ability to use PET as a carbon source,²⁰ revealed a naturally-evolved, PET-hydrolysing enzyme (*IsPETase*^{WT}), that has an enhanced ability to depolymerise more crystalline forms of PET.^{20,21} There are interesting structural differences between *IsPETase* and homologous cutinases, which are thought to be linked to this improved activity,²¹ including a conformationally flexible Trp185 that has been proposed to aid polymer binding.^{22,23} The unique catalytic properties of *IsPETase* make it an attractive candidate as a biocatalyst for PET recycling. Unfortunately, the wildtype enzyme suffers from low thermostability,²⁰ meaning that biotransformations must be run at ambient temperatures far below the glass

transition temperatures of PET ($T_g \sim 70^\circ\text{C}$), which compromises the speed of polymer deconstruction.^{24,25}

In an effort to address these limitations, modest improvements in PETase stability have been achieved using a variety of rational engineering approaches.^{21,26-29} In contrast, experimental optimisation of *IsPETase* using directed evolution, which typically offers a more comprehensive approach to enzyme engineering,^{30,31} has not been described, likely due to the lack suitable protocols for monitoring the deconstruction of insoluble plastics with sufficient throughput.¹¹ Here we establish an automated, high-throughput directed evolution platform for engineering plastic deconstructing enzymes, which is showcased through engineering a thermostable variant of *IsPETase* which can operate at the glass transition temperature of PET.

4.5 Results

We selected a rationally designed ‘thermostable’ variant of *IsPETase* containing three mutations, S121E, D186H, R280A (*IsPETase*^{TS}, $T_m = 56.8^\circ\text{C}$),²⁶ as a starting point for engineering. Consistent with previous reports, *IsPETase*^{TS} displays superior PET degradation activity compared to the wild-type enzyme at 40°C , however, this activity decreases dramatically at more elevated temperatures (Extended Data, Fig. 1).

Our first objective was to develop a high-throughput screening workflow to underpin the directed evolution study. To this end, individual enzyme variants were evaluated as crude cell lysates arrayed in 96-well plates, using amorphous PET film (amoPET, sourced from Goodfellow) as the reaction substrate. The amoPET substrate allowed us to prepare uniform 6 mm diameter discs that could be easily placed into individual wells to allow fair comparison of variant activity (Fig. 1). Interestingly, we found that the addition of our standard chemical cell lysis reagents, lysozyme and polymyxin B, resulted in the production of a lysate with substantially reduced activity (Extended Data, Fig. 2), hence, we developed a method for 96-well plate cell lysis using the commercial reagent, BugBuster. The accumulation of mono(2-hydroxyethyl) terephthalic acid (MHET) and terephthalic acid (TPA) in the reaction supernatant was monitored by UPLC, as these are the known major products of *IsPETase*-initiated PET hydrolysis.^{20,32} Using the UPLC method developed here, MHET and TPA produced by a single degradation reaction can be analysed in under two

minutes (Extended Data, Fig. 2). Using our integrated, automated in-house system over 2000 enzyme variants can be assessed for plastic deconstruction activity in around two days.

The evolutionary strategy comprised of sequential rounds of saturation mutagenesis, using degenerate NNK codons to individually randomise between 24-30 residue positions per cycle. These residues were targeted for mutation based on a number of considerations, including previous reports of their involvement in substrate binding or thermostability, their identification by online protein stability-enhancing tools, or by visual inspection of the protein crystal structure (Extended Data, Fig. 3). Beneficial diversity found during each round was then combined by DNA shuffling. Between rounds 2-3, an additional disulphide bridge (N233C, S282C) was rationally generated in the protein, following reports that the inclusion of this structural feature increased protein stability in homologous, promiscuous PET-degrading cutinases.^{19,33}

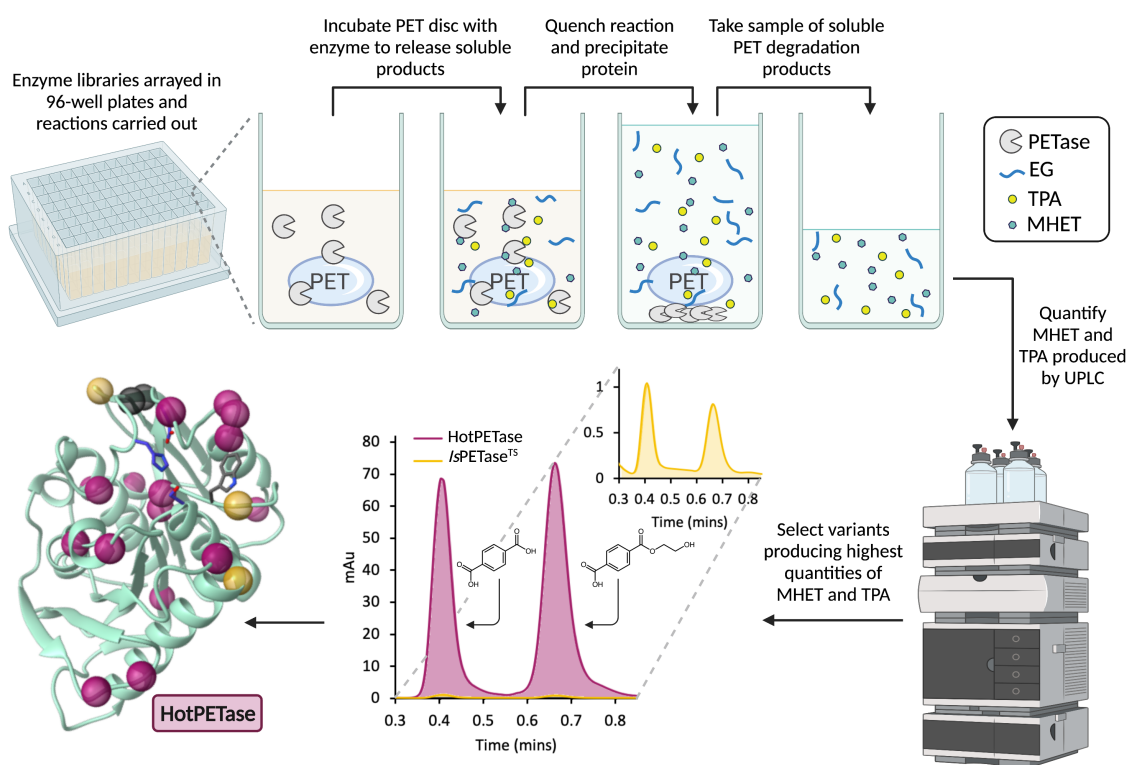


Figure 1. Workflow for the directed evolution of a PETase. Depiction of the laboratory evolution workflow for a single well in a 96-well plate. The example UPLC trace demonstrates a 5 hr PET degradation reaction (semi-crystalline PET powder, 4 mg mL^{-1}) using the best variant following evolution, HotPETase ($0.04 \text{ } \mu\text{M}$, pink), at 70°C as compared to the starting protein *IsPETase*^{TS} ($0.04 \text{ } \mu\text{M}$, yellow). The crystal structure shows the 21 amino acid positions mutated from *IsPETase*^{WT}: three positions mutated in the starting protein *IsPETase*^{TS} (yellow spheres), 16 installed through evolution (pink spheres) and a rationally installed disulphide bridge (black spheres). The catalytic triad and W185 are shown as blue sticks and grey sticks, respectively.

To simultaneously improve both thermostability and activity, the evolutionary pressures applied were gradually increased across rounds by raising both the reaction temperature and extending the reaction time. For rounds 1-4, the primary focus was on improved catalysis at elevated temperatures. Once a satisfactory level of thermostability was achieved, we then added an additional selection pressure of activity on more crystalline material. To this end, the top 3% of clones identified in rounds 5-6 were screened as purified enzymes against a commercially available semi-crystalline PET powder (cryPET, 36.4 % crystallinity, sourced from Goodfellow) that is more reminiscent of material dominant in post-consumer waste streams.³⁴

The most thermostable and active variant to emerge following six rounds of evolution, HotPETase, contains 21 mutations compared to *IsPETase*^{WT}: three from the starting protein template *IsPETase*^{TS}, two from rational insertion of a disulphide bridge and a further 16 found via directed evolution (Fig. 1). HotPETase has a melting temperature of 82.5°C, the highest T_m recorded to date of an *IsPETase* derivative. This elevated thermostability means that the enzyme can be incubated at 80°C for 90 minutes with minimal loss in activity (Extended Data, Fig. 4). Variants along the evolutionary trajectory were then compared based on their melting temperatures (T_m) and their activity in cryPET deconstruction assays performed at 60°C (Extended Data, Fig. 5). As shown in Figure 2a, evolution led to progressive improvements in these two parameters. Whilst both *IsPETase*^{WT} and *IsPETase*^{TS} have minimal activity at 60°C, HotPETase operates well under these conditions.

We next determined the activity of HotPETase across a range of temperatures by monitoring the release of MHET and TPA over time (Fig. 2b). For comparison, analogous experiments were performed using the starting template, *IsPETase*^{TS} and the engineered thermostable cutinase LCC^{ICCG}.¹⁹ Comparisons of the enzymes were carried out under the optimised buffer conditions for each individual protein, using cryPET powder as the substrate (Extended Data, Fig. 6). At 40°C, slightly improved initial reaction rates are achieved by HotPETase versus *IsPETase*^{TS} (Fig. 2b), demonstrating that the evolution of thermostability has not compromised activity at ambient temperatures. While the activity of *IsPETase*^{TS} is severely compromised at higher temperatures, the rate of PET-hydrolysis by HotPETase is significantly improved by operating at temperatures approaching the reported T_g of PET in aqueous solutions (ca. 60-65°C).¹⁷ At 65°C, each mole of HotPETase releases 2.7×10^4 moles of monomer product in one hour, a time-course over which reaction progression is linear.

At the same temperature, LCC^{ICCG} produces 5.7×10^3 moles of monomer product in the same time frame, highlighting the superior catalytic activity of the engineered *IsPETase*. Interestingly, for both HotPETase and LCC^{ICCG}, the reaction rates are slightly reduced at 70°C versus 65°C.

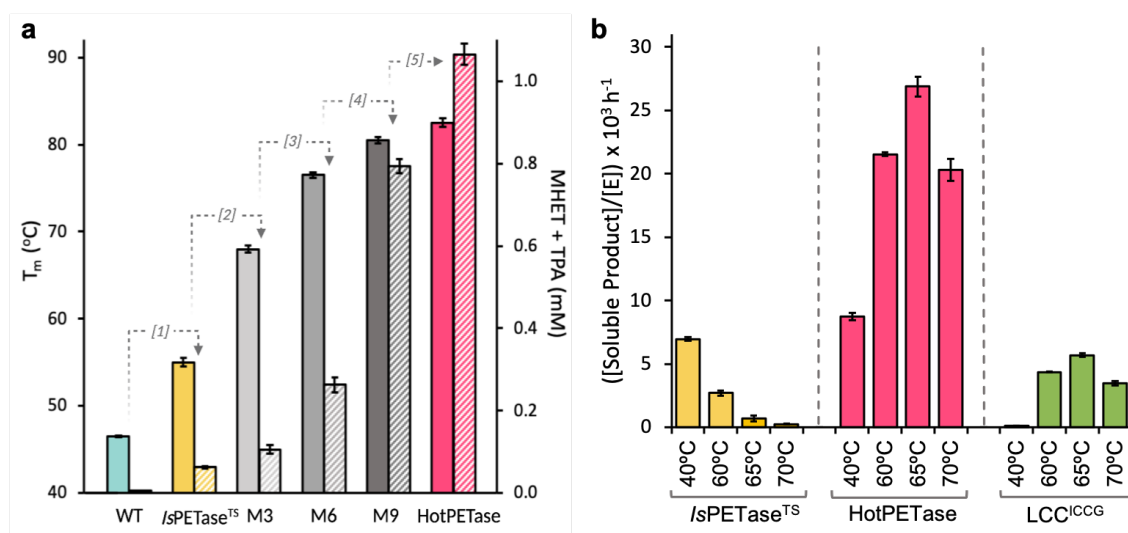


Figure 2. Directed evolution of *IsPETase*^{TS} has afforded a more thermostable and active catalyst.

(a) Bar chart demonstrating a snapshot of protein variants along the evolutionary trajectory from *IsPETase*^{WT} to HotPETase. Protein variants are on the x-axis; the mutations added to each variant compared to the previous variant are as follows: [1] = S121E, D186H, R280A, [2] = P181V, S207R, S214Y, [3] = Q119K, S213E, N233C, S282C, [4] = R90T, Q182M, N212K, R224L, [5] = S58A, S61V, K95N, M154G, N241C, K252M, T270Q. Solid coloured bars represent the T_m of each variant (left y-axis). Hashed bars represent amount of MHET and TPA produced by each enzyme variant ($0.04 \mu\text{M}$) over the course of 24 hrs, in a reaction at 60°C with cryPET (4 mg mL^{-1}) as the substrate. Reaction buffer contained no BugBuster. Reactions were carried out in duplicate; error bars represent the s.d. of the replicates. (b) Bar chart showing enzyme turnovers per hour (total MHET and TPA concentration/enzyme concentration (E)) after 1 hr, in a reaction with cryPET (4 mg mL^{-1}) at different temperatures with either *IsPETase*^{TS} ($0.04 \mu\text{M}$, yellow), HotPETase ($0.04 \mu\text{M}$, pink) or LCC^{ICCG} ($0.04 \mu\text{M}$, green) as the biocatalyst. Enzymes were assayed at their reported optimal pHs, as detailed in the Methods. Reactions were carried out in triplicate; error bars represent the s.d. of the replicates.

Comparison of reactions with HotPETase and *IsPETase*^{TS} at 40°C show that evolution has afforded a more robust catalyst (Fig. 3a, Extended Data, Fig.7). For *IsPETase*^{TS}, soluble product formation essentially ceases after 8 hrs. In contrast, for reactions with HotPETase, monomeric products continue to accumulate for >48 hrs. Consistent with previous studies,²⁸ the reaction profile is non-linear with faster initial phase for ca. 8 hrs, followed by a slower phase from 8-48 hrs. Similar, but more pronounced, non-linear reaction profiles are observed at elevated temperatures (from 60°C -70°C) (Extended Data, Fig. 8). The time course of reactions with HotPETase at 60°C demonstrate that product accumulation continues to rise rapidly for the first of 5 hrs of reaction (1.73 mM of MHET + TPA), but then slows substantially after this time to afford 1.85 mM of product after 48 hrs (Fig. 3b).

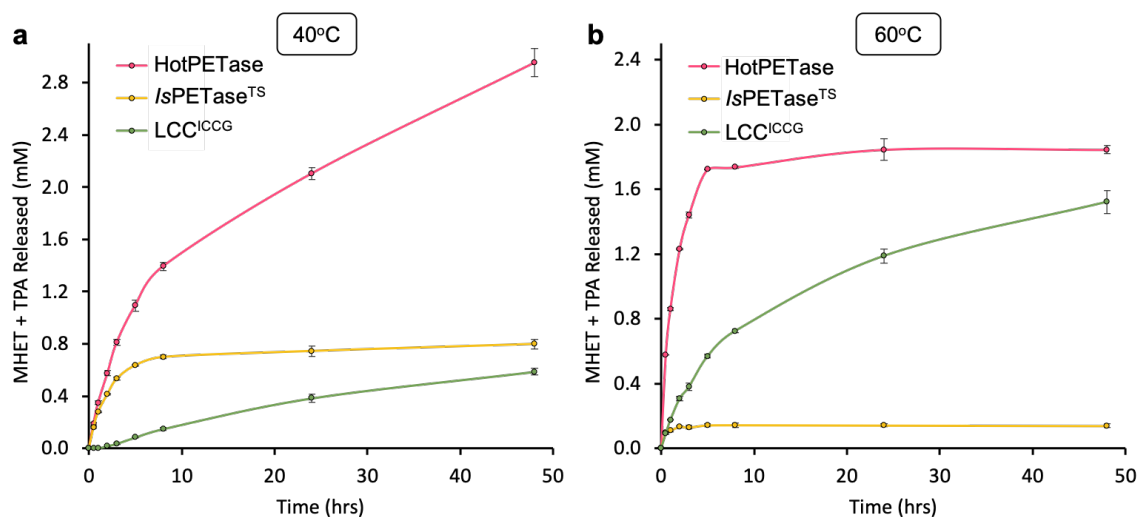


Figure 3. Comparison *IsPETase*^{TS}, HotPETase and LCC^{ICCG}. (a) 48-hr time-course reactions, with either HotPETase (0.04 μ M, pink), *IsPETase*^{TS} (0.04 μ M, yellow), or LCC^{ICCG} (0.04 μ M, green) showing total released MHET and TPA in reactions at 40°C, with cryPET (4 mg mL⁻¹) as the substrate. Reactions were carried out in triplicate; error bars represent the s.d. of the replicate measurements. (b) 48-hr time-course reactions, with either HotPETase (0.04 μ M, pink), *IsPETase*^{TS} (0.04 μ M, yellow) or LCC^{ICCG} (0.04 μ M, green), showing total released MHET and TPA in reactions at 60°C, with cryPET (4 mg mL⁻¹) as the substrate. Enzymes were assayed at their reported optimal pHs, as detailed in the Methods. Reactions were carried out in triplicate; error bars represent the s.d. of the replicate measurements.

Product accumulation over time is also non-linear for LCC^{ICCG}, with 0.57 and 1.50 mM of monomers produced over 5 and 48 hrs, respectively at 60°C. Addition of fresh HotPETase after 24 hrs, leads to similar product accumulation versus time trends as observed at the outset of the reaction (Extended Data, Fig. 9). In contrast, addition of fresh PET substrate does not give rise to any additional soluble products. These observations suggest that reactions stall due to a catalyst deactivation process, not as a result of inhibition by soluble released products or exhaustion of available plastic substrate. It is interesting to note that during evolution *IsPETase* libraries were analysed over time-frames ranging from three to seven hours, meaning that limited selection pressure was applied to catalyst longevity at elevated temperatures. We anticipate that adapting selection pressures during future rounds of evolution will lead to improved variants capable of operating efficiently at elevated temperatures for more extended periods.

To improve the extent of PET depolymerisation achievable with HotPETase, we next optimised several reaction parameters including pH, reaction buffer and enzyme loading (Extended Data, Fig. 10-12). Reaction conversions were found to be optimal using Glycine-OH buffer (pH9.7) in the presence of 4% BugBuster and an enzyme concentration of 0.5 μ M. Under these conditions, using cryPET as the substrate (20 mg), 6.07 mM of soluble monomer products (MHET:TPA ratio of 1:0.29) were formed within 5 hrs, corresponding to degree of depolymerisation of 31% (Extended Data, Fig. 13). The presence of BugBuster, a reagent used for cell lysis during evolution, was found to give a modest 11 % improvement in soluble product release, likely due to the presence of surfactants (Extended Data, Fig. 10b).^{35,36} The ability to run reactions at elevated enzyme concentrations is aided by the high-level cytosolic expression of soluble HotPETase (\sim 110 mg L⁻¹), in contrast to LCC^{ICCG} which must be produced in the periplasm resulting in a reduction in expression efficiency (\sim 20 mg L⁻¹) (Extended Data, Fig. 14a). In addition, for practical applications where purification is undesirable, it is interesting to note that HotPETase mediated PET deconstruction reactions can be conducted in cell lysate, where similar reaction profiles to those demonstrated with pure proteins are witnessed (Extended Data, Fig. 14b).

To gain insights into the origins of thermostability and improved activity at elevated temperatures of HotPETase, the crystal structure of the enzyme was solved and refined to a resolution of 2.2 Å for comparison to the starting variant *IsPETase*^{TS}. The structures of HotPETase and *IsPETase*^{TS} superimpose well, with a root-mean-square-deviation of 1.18 Å (Fig. 4a). In HotPETase, the disulphide bridge between the newly introduced Cys233 and Cys282 pair is formed as intended, with an S-S interatomic distance of 2.03 Å (Fig. 4b). The P181V mutation results in an additional hydrogen bond between Val181 and Leu199 leading to better packing of the central β-sheet region compared to *IsPETase*^{TS}, and is more reminiscent of thermostable cutinases (Fig. 4c). Analyses of the surface charge distributions of HotPETase and *IsPETase*^{TS} reveals substantial changes in the polymer binding cleft to reduce positive charge in the evolved enzyme (Fig. 4d). Further computational analysis and structural studies with bound substrate analogues is needed to correlate the observed changes in surface electrostatics to polymer positioning and binding affinity. Interestingly the ‘wobbling’ tryptophan, Trp185, a feature which is thought to aid substrate binding and catalysis in the wildtype enzyme,^{22,37} is present as a single well-defined conformer in the HotPETase structure. Extensive remodelling of the loop region connecting β7-α5, including introduction of a bulky Tyr214, leads to a new π-stacking interaction with Trp185 that restricts its conformational freedom (Fig. 4e). To explore the functional significance of the altered environment around Trp185, mutated residues installed in the β7-α5 connecting loop were reverted back to their wildtype amino acids (HotPETase^{LR} (K212N, E213S, Y214S, C215N)). These modifications led to a substantial 7.5°C reduction in T_m and compromised catalytic performance at elevated temperatures (Extended Data, Fig. 15). Interestingly, catalytic activity at low temperatures is minimally affected, suggesting that in the heavily engineered HotPETase, the fixed conformation of Trp185 is not detrimental to catalysis. Combined these results suggest that a flexible Trp185 is not a necessity for efficient PET deconstruction.

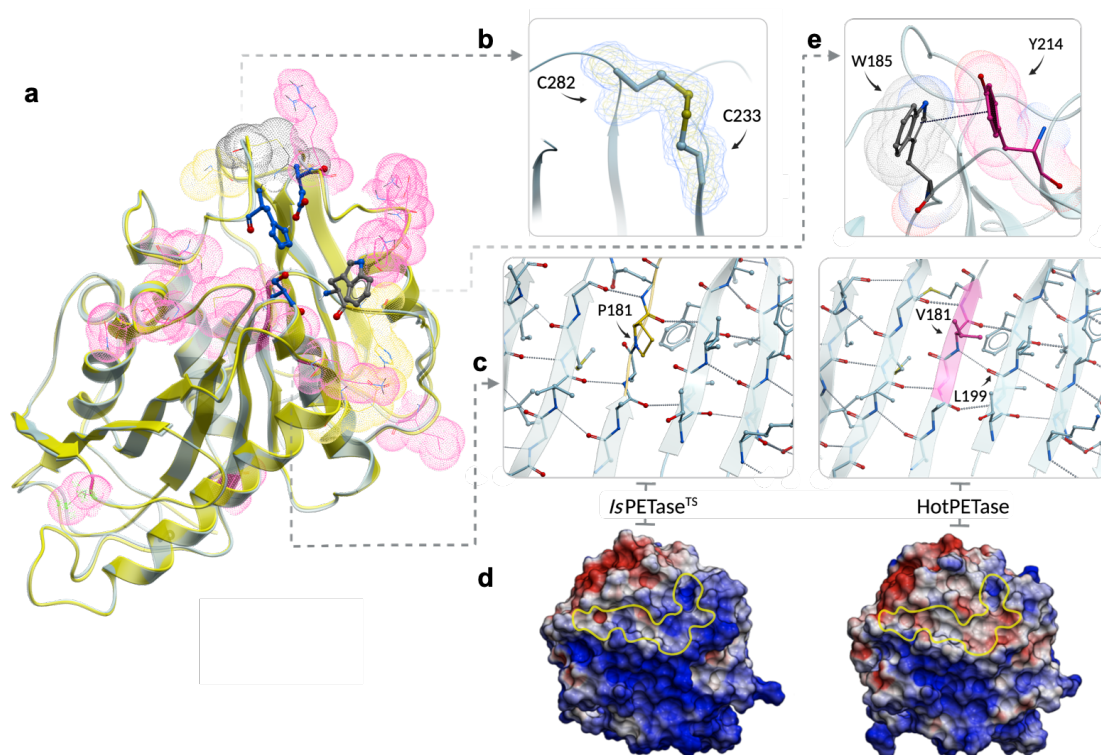


Figure 4. Comparison of crystal structures and features of HotPETase and *IsPETase*^{TS}. (a) A global superposition of *IsPETase*^{TS} (yellow) and HotPETase (light blue). Mutations in *IsPETase*^{TS} compared to *IsPETase*^{WT} are highlighted with yellow spheres. Mutations installed by directed evolution are highlighted with pink spheres. The rationally inserted disulphide bridge is highlighted with black spheres. The catalytic triad and W185 are represented as blue and grey sticks, respectively. (b) The disulphide bridge is correctly formed between C233 and C282 in HotPETase. Electron density is 2Fo-Fc contoured at 1 sigma (blue) and 2 sigma (yellow). (c) The conversion of P181 in *IsPETase*^{TS} (highlighted yellow) to V181 in HotPETase (highlighted pink) results in extension of β -sheet 6, and the formation of an additional hydrogen bond (dashed lines) to L199. (d) Electrostatic surface representation of *IsPETase*^{TS} and HotPETase. Blue and red represent positive and negative charge, respectively. The approximate polymer substrate binding cleft is indicated by a yellow line. (e) In HotPETase, the wobbling tryptophan (W185, grey sticks), forms a π -stacking interaction (dashed line) with the installed Y214 (pink sticks).

4.6 Discussion

Directed evolution has proven to be the most versatile and comprehensive strategy for engineering industrial biocatalysts. Somewhat surprisingly, despite great interest in enzymatic plastic deconstruction, PETase engineering efforts to date have focused on structure guided design using computational methods. The notable absence of PETases engineered via laboratory evolution likely reflects the challenges of developing suitable high-throughput, quantitative methods for analysing the catalytic deconstruction of insoluble polymers. Here, we have developed an automated directed evolution platform for engineering plastic deconstructing enzymes, and showcase its utility through the development of an evolved thermostable PETase (HotPETase, $T_m=82.5^\circ\text{C}$) that can operate at the glass transition temperature of PET and depolymerises semi-crystalline PET more rapidly than previously reported PETases. Structural characterisation of HotPETase highlights formation of a new disulphide bridge and improved packing of the central β -sheet region which likely aid thermostability, alongside the presence of a single well-defined conformer of Trp185, indicating that flexibility of this tryptophan is not a prerequisite for effective catalysis. To maximise the utility of our platform moving forward, it will be important to interface our evolution methods with alternative strategies for augmenting biocatalyst function, including computationally guided engineering,³⁸ introduction of polymer binding domains,³⁹ and the development of multi-enzyme complexes.⁴⁰ Likewise, combining and optimising biocatalytic deconstructions with enzymatic monomer upcycling methods will be an important avenue for exploration.^{13,41}

In the future, we anticipate that by adapting the selection pressures of our directed evolution workflows, we will be able to engineer a suite of useful biocatalysts with complementary functions and improved activities under process-relevant conditions. For example, we can extend catalyst lifetimes by increasing reaction times, optimise biocatalysts to act upon alternative plastic substrates, or enhance enzyme specificities in order that they operate on single polymer components from mixed plastic waste streams. In doing so, our laboratory evolution platform will contribute to a realistic solution to the problems associated with recovering value from mixed plastic waste streams, improving the feasibility of a commercially relevant biocatalytic recycling strategy.

4.7 References

1. PlasticsEurope. *Plastics- the Facts 2019, An analysis of European plastics production, demand and waste data*. (2019).
2. Borrelle, S. *et al.* Predicted growth in plastic waste exceeds efforts to mitigate plastic pollution. *Science* **369**, (2020).
3. Geyer, R., Jambeck, J. & Law, K. Production, use, and fate of all plastics ever made. *Science Advances* **3**, e1700782 (2017).
4. Jambeck, J. R. *et al.* Plastic waste inputs from land into the ocean. *Science* **347**, 768–771 (2015).
5. Laville, S. & Taylor, M. A million bottles a minute: world’s plastic binge ‘as dangerous as climate change’. *The Guardian* **28**, (2017).
6. Ellen MacArthur Foundation. *The New Plastics Economy: Rethinking the future of plastics & catalysing action*. <https://www.ellenmacarthurfoundation.org/publications/the-new-plastics-economy-rethinking-the-future-of-plastics-catalysing-action> (2017).
7. Rahimi, A. & García, J. M. Chemical recycling of waste plastics for new materials production. *Nature Reviews Chemistry* **1**, 0046 (2017).
8. Jehanno, C. *et al.* Organocatalysed depolymerisation of PET in a fully sustainable cycle using thermally stable protic ionic salt. *Green Chemistry* **20**, 1205–1212 (2018).
9. Karayannidis, G., Chatziavgoustis, A. P. & Achilias, D. Poly(ethylene terephthalate) recycling and recovery of pure terephthalic acid by alkaline hydrolysis. *Advances in Polymer Technology* **21**, 250–259 (2002).
10. Korley, L., Epps, T., Helms, B. & Ryan, A. Toward polymer upcycling—adding value and tackling circularity. *Science* **373**, 66–69 (2021).
11. Zhu, B., Wang, D. & Wei, N. Enzyme Discovery and Engineering for Sustainable Plastic Recycling. *Trends in Biotechnology* (2021).
12. Zimmermann, W. Biocatalytic recycling of polyethylene terephthalate plastic. *Philosophical Transactions of the Royal Society A: Mathematical, Physical and Engineering Sciences* **378**, 20190273 (2020).
13. Sadler, J. C. & Wallace, S. Microbial synthesis of vanillin from waste poly(ethylene terephthalate). *Green Chemistry* **23**, 4665–4672 (2021).
14. Andrady, A. L. Assessment of Environmental Biodegradation of Synthetic Polymers. *Journal of Macromolecular Science, Part C* **34**, 25–76 (1994).
15. Herrero Acero, E. *et al.* Enzymatic Surface Hydrolysis of PET: Effect of Structural Diversity on Kinetic Properties of Cutinases from *Thermobifida*. *Macromolecules* **44**, 4632–4640 (2011).
16. Sulaiman, S. *et al.* Isolation of a novel cutinase homolog with polyethylene terephthalate-degrading activity from leaf-branch compost by using a metagenomic approach. *Applied and Environmental Microbiology* **78**, 1556–62 (2012).
17. Kawai, F. *et al.* A novel Ca²⁺-activated, thermostabilized polyesterase capable of hydrolyzing polyethylene terephthalate from *Saccharomonospora viridis* AHK190. *Applied Microbiology and Biotechnology* **98**, 10053–10064 (2014).
18. Ribitsch, D. *et al.* Hydrolysis of polyethylene terephthalate by *p*-nitrobenzylesterase from *Bacillus subtilis*. *Biotechnology Progress* **27**, 951–960 (2011).
19. Tournier, V. *et al.* An engineered PET depolymerase to break down and recycle plastic bottles. *Nature* **580**, 216–219 (2020).

20. Yoshida, S. *et al.* A bacterium that degrades and assimilates poly(ethylene terephthalate). *Science* **351**, 1196–9 (2016).
21. Austin, H. P. *et al.* Characterization and engineering of a plastic-degrading aromatic polyesterase. *Proceedings of the National Academy of Sciences of the United States of America* **115**, E4350–E4357 (2018).
22. Han, X. *et al.* Structural insight into catalytic mechanism of PET hydrolase. *Nature Communications* **8**, 2106 (2017).
23. Joo, S. *et al.* Structural insight into molecular mechanism of poly(ethylene terephthalate) degradation. *Nature Communications* **9**, 382 (2018).
24. Ronkvist, M. A.° sa, Xie, W., Lu, W. & Gross, R. A. Cutinase-Catalyzed Hydrolysis of Poly(ethylene terephthalate). *Macromolecules* **42**, 5128–5138 (2009).
25. Wei, R. & Zimmermann, W. Biocatalysis as a green route for recycling the recalcitrant plastic polyethylene terephthalate. *Microbial Biotechnology* **10**, 1302–1307 (2017).
26. Son, H. F. *et al.* Rational Protein Engineering of Thermo-Stable PETase from *Ideonella sakaiensis* for Highly Efficient PET Degradation. *ACS Catalysis* **9**, 3519–3526 (2019).
27. Son, H. F. *et al.* Structural bioinformatics-based protein engineering of thermo-stable PETase from *Ideonella sakaiensis*. *Enzyme and Microbial Technology* **141**, 109656 (2020).
28. Cui, Y. *et al.* Computational Redesign of a PETase for Plastic Biodegradation under Ambient Condition by the GRAPE Strategy. *ACS Catalysis* **11**, 1340–1350 (2021).
29. Ma, Y. *et al.* Enhanced Poly(ethylene terephthalate) Hydrolase Activity by Protein Engineering. *Engineering* **4**, 888–893 (2018).
30. Arnold, F. H. Directed Evolution: Bringing New Chemistry to Life. *Angewandte Chemie International Edition* **57**, 4143–4148 (2018).
31. Zeymer, C. & Hilvert, D. Directed Evolution of Protein Catalysts. *Annual Review of Biochemistry* **87**, 131–57 (2018).
32. Zhong-Johnson, E., Voigt, C. & Sinskey, A. An absorbance method for analysis of enzymatic degradation kinetics of poly(ethylene terephthalate) films. *Scientific Reports* **11**, (2021).
33. Then, J. *et al.* A disulfide bridge in the calcium binding site of a polyester hydrolase increases its thermal stability and activity against polyethylene terephthalate. *FEBS Open Bio* **6**, 425–432 (2016).
34. Ügdüler, S. *et al.* Towards closed-loop recycling of multilayer and coloured PET plastic waste by alkaline hydrolysis. *Green Chemistry* **22**, 5376–5394 (2020).
35. Furukawa, M., Kawakami, N., Oda, K. & Miyamoto, K. Acceleration of Enzymatic Degradation of Poly(ethylene terephthalate) by Surface Coating with Anionic Surfactants. *ChemSusChem* **11**, 4018–4025 (2018).
36. Furukawa, M., Kawakami, N., Tomizawa, A. & Miyamoto, K. Efficient Degradation of Poly(ethylene terephthalate) with *Thermobifida fusca* Cutinase Exhibiting Improved Catalytic Activity Generated using Mutagenesis and Additive-based Approaches. *Scientific Reports* **9**, 1–9 (2019).
37. Chen, C.-C. *et al.* General features to enhance enzymatic activity of poly(ethylene terephthalate) hydrolysis. *Nature Catalysis* **4**, 425–430 (2021).
38. Huang, P.-S., Boyken, S. E. & Baker, D. The coming of age of *de novo* protein design. *Nature* **537**, 320 (2016).
39. Dai, L. *et al.* Enhancing PET hydrolytic enzyme activity by fusion of the cellulose-binding domain of cellobiohydrolase I from *Trichoderma reesei*. *Journal of Biotechnology* **334**, 47–50 (2021).

40. Knott, B. C. *et al.* Characterization and engineering of a two-enzyme system for plastics depolymerization. *Proceedings of the National Academy of Sciences* **117**, 25476 (2020).
41. Rorrer, N. A. *et al.* Combining Reclaimed PET with Bio-based Monomers Enables Plastics Upcycling. *Joule* **3**, 1006–1027 (2019).

CHAPTER 5

Deconstruction of PET-Based Materials and a Bio-Derived Plastic by a Thermostable PETase

Elizabeth L. Bell¹, Ross Smithson¹, Jake Foster¹, Siobhan Kilbride², Michael P. Shaver² & Anthony P. Green^{1}*

¹*Manchester Institute of Biotechnology, 131 Princess Street, University of Manchester, Manchester, M1 7DN, UK.*

²*Department of Materials, The University of Manchester, Manchester, M1 7DN, UK.*

5.1 Foreword

This chapter consists of a research article investigating the ability of the evolved biocatalyst, HotPETase, to depolymerise a range of PET-based plastic materials reminiscent of those found in a post-consumer waste stream, alongside a new bio-derived plastic PEF and the copolymer PETG, which is being increasingly used due to its applications in 3D printing.

5.2 Acknowledgements

The research presented in this chapter was a collaborative effort between the doctoral candidate and the following researchers: Ross Smithson, Jake Foster, Siobhan Kilbride, Michael P. Shaver and Anthony P. Green. The doctoral candidate carried out molecular biology, assay development, protein production, purification, reaction optimisation, time-resolved assays for all PET containing substrates, all data analysis and presentation. Ross Smithson prepared time-resolved assays for PEF and PETG substrates, aided by Jake Foster, and carried out all chemical syntheses. Siobhan Kilbride and Michael P. Shaver carried out physical analysis of the polymer materials. The doctoral candidate and Anthony P. Green wrote the manuscript.

5.3 Abstract

We have recently engineered an efficient and thermostable version of IsPETase, HotPETase. Here, we show that HotPETase is able to effectively deconstruct PET with a range of morphologies, including those of high crystallinity, reminiscent of plastics found in post-consumer waste streams. We also demonstrate that HotPETase is capable of degrading a PET composite-film, used as a packaging material. Additionally, we show that HotPETase

can depolymerise the PET co-polymer poly(ethylene glycol-co-1,4-cyclohexanedimethanol terephthalate) (PETG), widely used for 3D printing, and the bioderived plastic poly(ethylene furanoate) (PEF). The major monomeric products derived from these biotransformations are also characterised. Our study indicates that HotPETase is a broadly applicable biocatalyst that can serve as a versatile template for further engineering to meet specific industrial demands

5.4 Introduction

The rapid accumulation of plastic waste in the natural environment has led to an urgent search for strategies to ameliorate its adverse impacts.^{1,2} To this end, enzyme-driven biocatalytic depolymerisation has emerged as a potentially sustainable solution for recycling plastics, stemming their environmental leakage and diminishing the need for virgin, fossil-fuel derived polymers. The biocatalytic treatment of post-consumer plastic waste is appealing, as enzymes are exceptionally potent catalysts capable of accelerating chemical transformations with high efficiencies and substrate specificities, in an environmentally-friendly manner. In addition, perhaps the most attractive feature of enzymatic polymer deconstruction, is the potential to selectively degrade specific components from mixed plastic waste streams to give high purity monomeric products which can be used for repolymerisation³ or upcycled into value added-compounds,⁴ although this has not been readily tested (Fig. 1). Selective polymer deconstruction is of particular interest as traditional recycling methods require the costly and difficult sorting of heterogenous, mixed plastic waste streams, whose complexity can be further increased by the presence of both petroleum and bio-derived feedstocks.⁵

In contrast to the promiscuous cutinases, the naturally-evolved PET hydrolase, *IsPETase*,¹¹ is capable of deconstructing more crystalline PET, potentially meaning it is a more attractive start point for the development of a relevant biocatalyst.¹² However, *IsPETase*'s compromised thermostability and low activity means that in its wildtype form, it is unsuitable for industrial application. Hence, multiple strategies have been employed to try to improve the characteristics of *IsPETase*, ranging from computationally-guided¹³ and rational engineering attempts,¹⁴⁻¹⁶ to enzyme-fusion studies, where *IsPETase* has been linked to its natural synergistic partner MHETase¹⁷ or to PET-binding domains.¹⁸

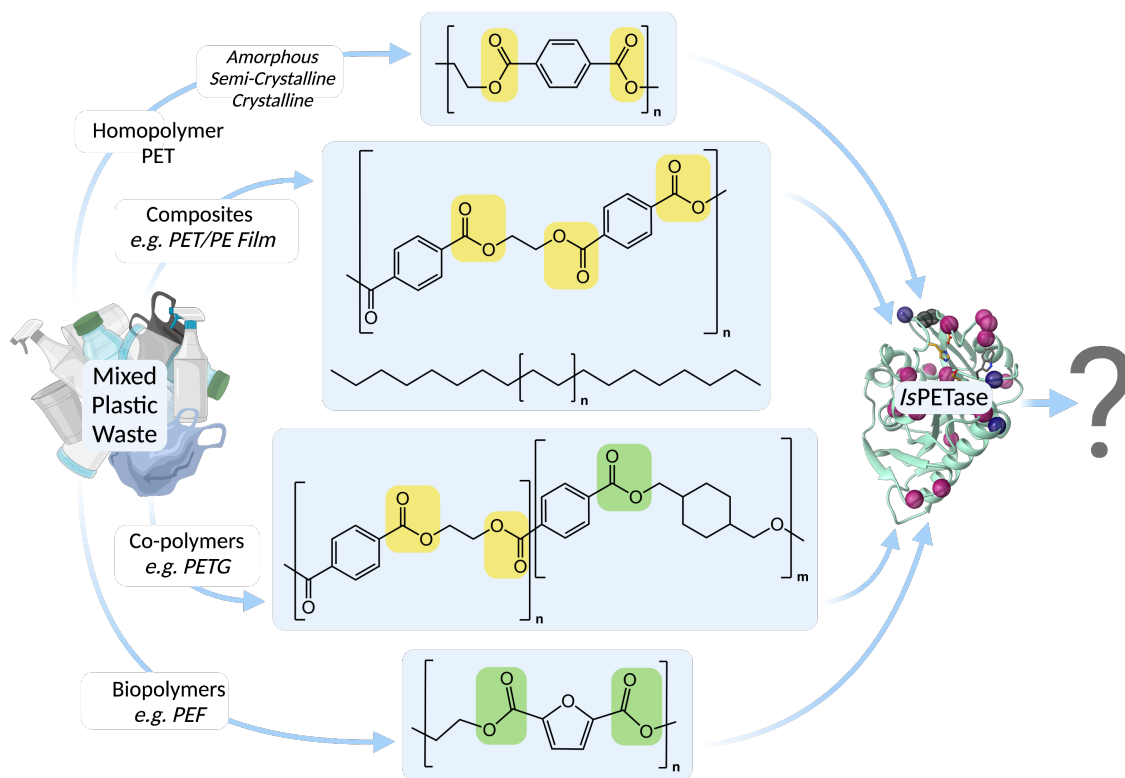


Figure 1. Plastic waste is a complex mixture of polymer morphologies which could be selectively degraded by enzymes such as *IsPETase*. For mixed waste streams, PET with varying crystallinities, PET composites and co-polymers, alongside structurally similar bio-derived plastics, may be present (blue boxes). Materials containing ester-bonded groups analogous to those found in PET (highlighted yellow), should be readily hydrolysable by PET-degrading enzymes such as *IsPETase*; for materials containing alternative ester-bonded motifs (highlighted green), it is not clear how proficient enzymatic hydrolysis will be and what the reaction output products are.

Adding to this effort, we recently engineered a more thermostable and active *IsPETase* variant, *HotPETase*, by a process of laboratory evolution, underpinned by the development of a high-throughput PET deconstruction analysis platform. Here, we demonstrate that *HotPETase* is a broadly useful biocatalyst, with the ability to operate on a diverse range of relevant PET polyester substrates, including highly-crystalline plastics commonly used for bottle production.¹⁹ The enzyme can operate across a range of PET morphologies including a composite PET/polyethylene (PE) packaging lid and a common PET co-polymer, poly(ethylene glycol-co-1,4-cyclohexanedimethanol terephthalate) (PETG), that is becoming increasingly popular due to its use in 3D printing.²⁰ Finally, we demonstrate the activity of *HotPETase* towards poly(ethylene furanoate) (PEF), a plastic made from bio-derived building blocks, that is tipped to be the successor to petroleum-based PET.^{21,22}

5.5 Results

We determined the activity of HotPETase on a range of PET materials by monitoring the release of the major products of *IsPETase*-mediated PET hydrolysis, mono-2-hydroxyethyl terephthalate (MHET) and terephthalic acid (TPA), in reactions at 60°C with 20 mg of the desired substrate. Full characterisations of the PET-based substrates used here are available in the Supplementary Information. As described previously, HotPETase can deconstruct a commercially available semi-crystalline PET powder (cryPET, 36.4% crystallinity, 300 micron), with the maximum level of product accumulation reached in around 5 hr, corresponding to the release of 1.71 mM of soluble monomers (Fig. 2a). We next sought to challenge HotPETase with commercially relevant, highly-crystalline, unprocessed, bottle-grade PET pellets (61% crystallinity). Product release is very low, with < 0.1 mM of soluble products being produced after 48 hrs, possibly due to high surface smoothness of the pellets prohibiting enzyme binding and the low pellet surface area to volume ratio (Extended Data, Fig 1.)

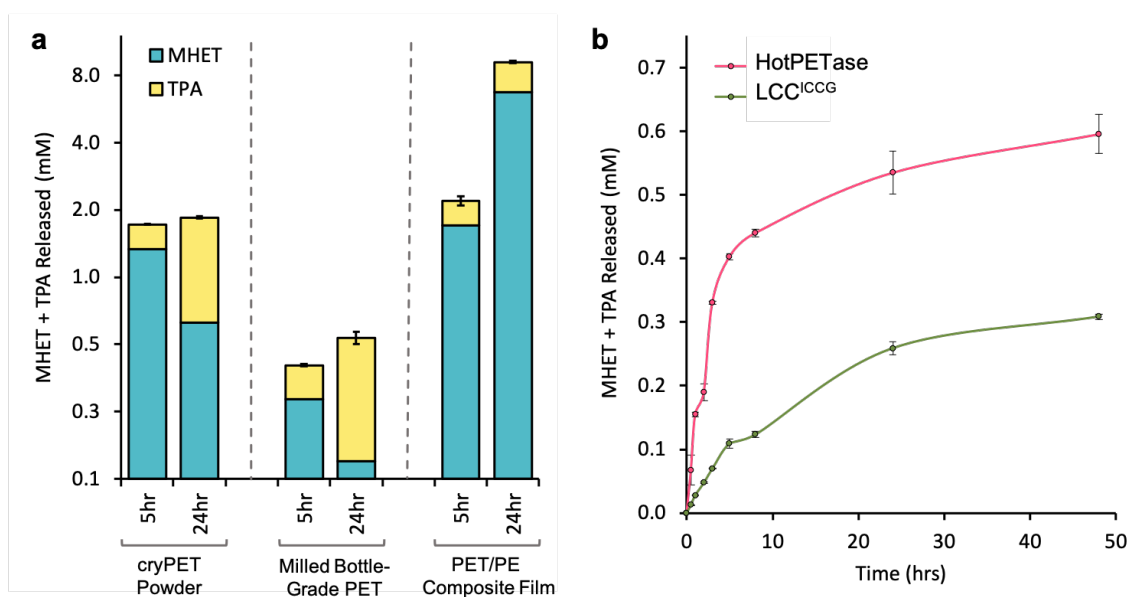


Figure 2. Biocatalytic deconstruction of a range of PET-based materials by HotPETase. (a) Bar chart showing soluble aromatic PET degradation products MHET (blue) and TPA (yellow) produced following reaction of HotPETase (0.04 μM) at 60°C over the course of 24 hrs with each PET substrate (4 mg mL^{-1}). HotPETase has activity on crystalline PET powder (cryPET), milled bottle grade PET powder (bgPET) and a PET/PE composite packaging film lid. Reactions were carried out in triplicate; error bars represent the s.d. of the total MHET and TPA produced in the replicates. The y-axis is on a logarithmic scale. (b) 48-hr time-course of a milled bottle-grade PET reaction (bgPET, 4 mg mL^{-1}), showing total released MHET and TPA with HotPETase (0.04 μM , pink) and LCC^{1CCG} (0.04 μM , green). Reactions were carried out at 60°C, with each enzyme in its reported optimal buffer. Reactions were carried out in triplicate; error bars represent the s.d. of the replicate measurements.

However, soluble monomer release can be improved by minimally milling the bottle-grade beads at ambient temperature, with only a small reduction in substrate crystallinity (bgPET, 41.9% crystallinity, 450-600 micron). Whilst the extent of monomer release is less than that produced from cryPET deconstruction, HotPETase demonstrates reasonable activity on bgPET, with 0.53 μ M of MHET and TPA released over the course of 24 hrs in a 60°C reaction (Fig. 2a), and is significantly better than the engineered cutinase LCC^{ICCG}, which releases 0.26 mM of soluble degradation products over the same time period under its own reported optimal buffer conditions (Fig. 2b). HotPETase is also significantly faster in the initial phase of the reaction, producing 0.16 mM of MHET and TPA after only one hour, as compared to the 0.03 mM of monomers released by LCC^{ICCG}. There was no additional benefit seen by running reactions at higher temperatures (Extended Data, Fig. 2). For both cryPET and bgPET there was no demonstrable change in the crystallinity or average molecular weight of the substrate material following enzymatic hydrolysis (Extended Data, Table 1, Fig. 3.). This may suggest that HotPETase is not substantially degrading the crystalline regions of the polymer, and may be acting in an exo- fashion on the ends of polymer chains, however, further analysis is needed.

We next explored the activity of HotPETase on a real-world packaging lid made from a PET/PE composite film (1.57% crystallinity, 6 mm disc, 325 micron PET/ 40 micron PE, avg. mw: 95.5 kDa). The enzyme is adept at deconstructing this material, releasing 9.2 mM of soluble monomers from the PET-portion of the composite over the course of 24 hrs (Fig. 2a). The origin of this impressive activity is likely due to the modest crystallinity and molecular weight of the PET used in this film as compared to cryPET and bgPET.

To examine the ability of HotPETase to depolymerise PET co-polymers, we also challenged the enzyme with a PETG powder, a PET derivative where a mixture of ethylene glycol and cyclohexane dimethanol units link terephthalate moieties. We demonstrate that HotPETase can use PETG as a substrate, producing three major aromatic products, MHET, TPA and mono-2-cyclohexylenedimethylene terephthalate (MCDT) (Fig. 3a). MHET is the major initial product of PET deconstruction; any conversion of MHET to TPA is a non-enzymatic process (Extended Data Fig. 4a). To explore the enzyme's behaviour further, we examined the ability of HotPETase to deconstruct the PETG subunits MCDT and bis(2-cyclohexylenedimethylene) terephthalate (BCDT), the PETG equivalent of bis(2-hydroxyethyl) terephthalate (BHET), a PET subunit which is a known substrate for

IsPETase.¹¹ BCDT is readily hydrolysed to MCDT by the enzyme, whilst MCDT does not appear to be a substrate, with its turnover to TPA being unaffected by the presence of HotPETase, consistent with the observed accumulation of MCDT product following reaction (Fig. 3b) (Extended Data Fig. 4b&c). PETG is a completely amorphous substrate (0% crystallinity), so it is interesting that the amount of MHET and TPA produced over the course of 24 hrs, a total of 1.11 mM of soluble products released, is less than that released from both the PET/PE film and cryPET. This is potentially due to the high avg. mw of PETG, or may suggest the enzyme prefers substrates with some degree of crystallinity (Supplementary Information, Table 1).

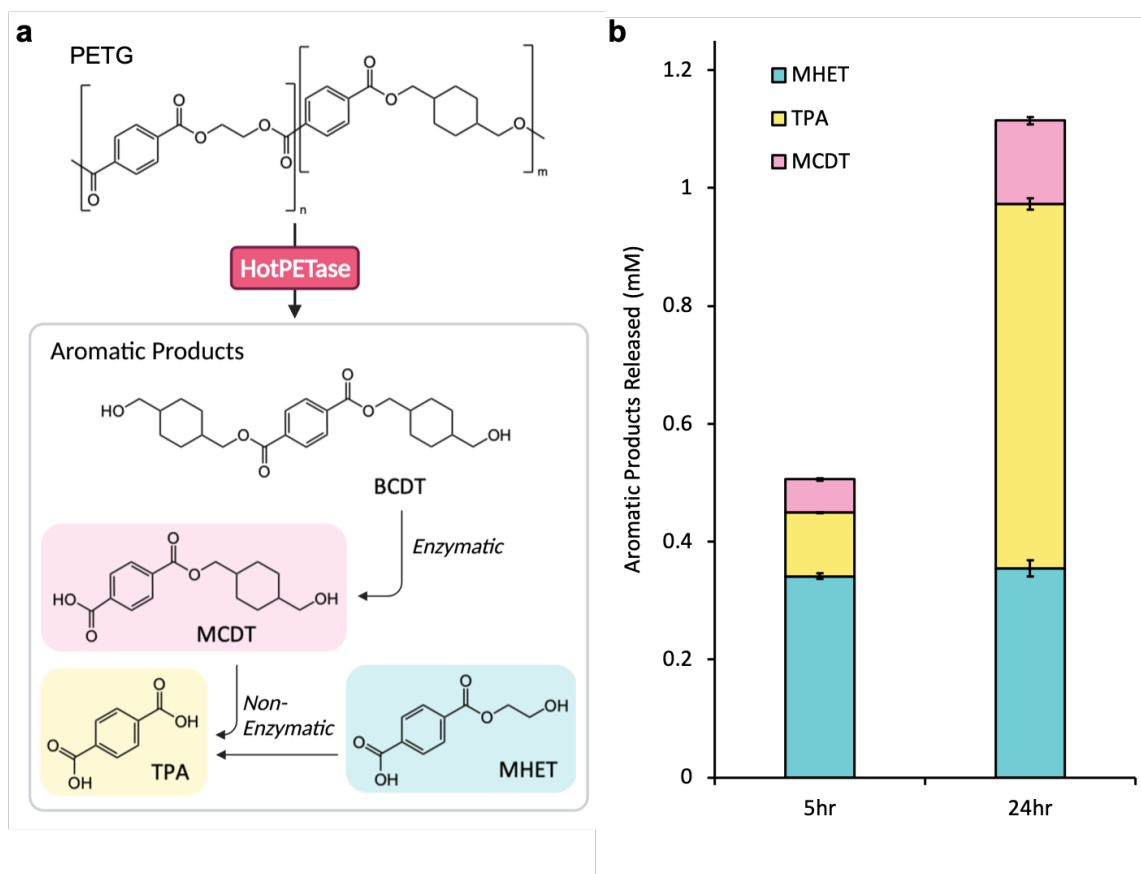


Figure 3. Biocatalytic deconstruction of PETG by HotPETase. (a) Monomeric and dimeric aromatic compounds produced by hydrolysis of PETG by HotPETase. BCDT is turned over quickly by HotPETase to MCDT, so is not seen as a major product by HPLC analysis. The slow turnover of MCDT is non-enzymatic. (b) Bar chart showing soluble aromatic PET degradation products MHET (blue), TPA (yellow) and MCDT (pink) produced following reaction of HotPETase (0.04 μM) at 60°C over the course of 24 hrs with milled PETG substrate (4 mg mL⁻¹). Reactions were carried out in triplicate; error bars represent the s.d. of total soluble aromatic compounds produced in the replicates.

Finally, we inspected the activity of HotPETase towards the purported successor to PET, the bio-derived PEF. HotPETase has the ability to depolymerise in-house synthesised PEF, consistent with previous reports for wild-type *IsPETase*.¹⁶ There appear to be two major UV-visible reaction products, 2,5-furandicarboxylic acid (FCA) and mono-2-hydroxyethyl furanoate (MHEF) (Fig. 4a), with the MHET-like MHEF being the major product and the TPA-like FCA, being the minor product (Fig. 4b). Further analysis revealed that in accordance with PET hydrolysis, the BHET equivalent, bis(2-hydroxyethyl) furanoate (BHEF), is a substrate for the enzyme, whilst, the MHET equivalent, MHEF, is not, correlating with the accumulation of MHEF in the reaction (Extended Data Fig. 5). As recently described with cryPET powder, raising the temperature of reaction from 40°C to 60°C, significantly increases the concentration of soluble products formed. An additional 2.04 mM of MHEF and 0.64 mM of FCA is produced over the course of 5 hrs at the higher temperature compared to at 40°C, highlighting the value of a thermostable PETase for new substrates as well as traditional ones.

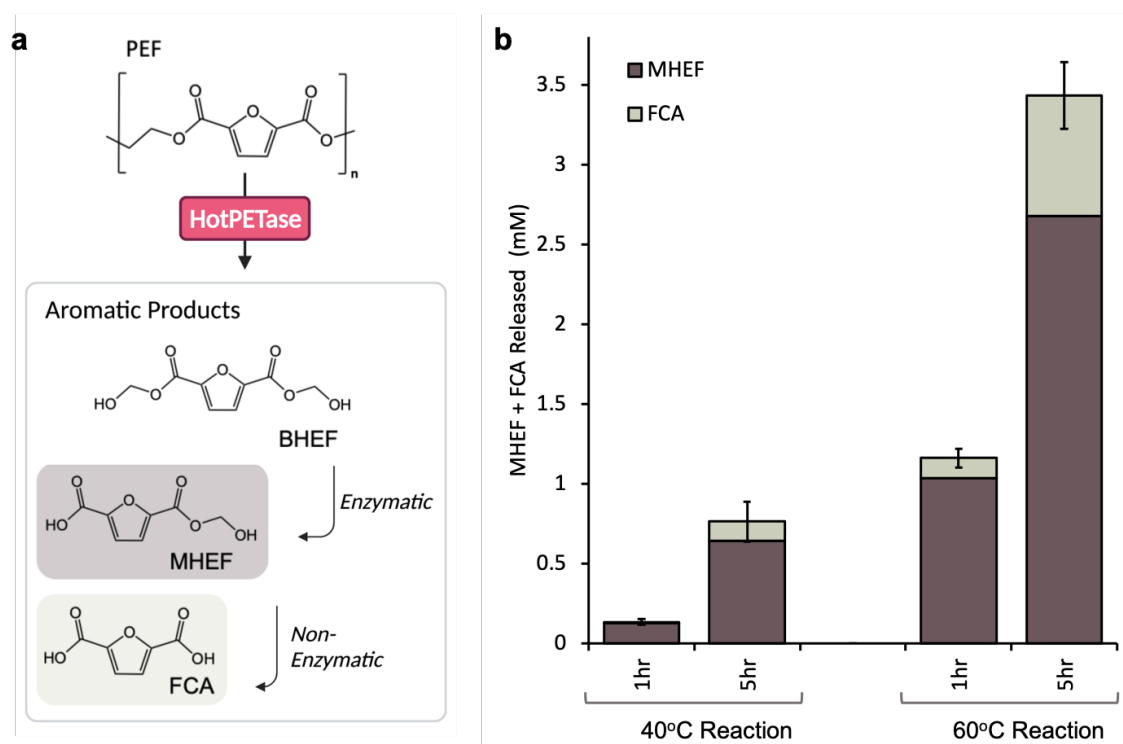


Figure 4. Biocatalytic deconstruction of PEF by HotPETase. (a) Monomeric and dimeric aromatic compounds produced by hydrolysis of PEF using HotPETase. BHEF is turned over quickly by HotPETase to MHEF, so is not seen as a major product by HPLC analysis. MHEF is turned over non-enzymatically to FCA. (b) Bar chart showing soluble aromatic PET degradation products MHEF (brown) and FCA (grey) produced following reaction of HotPETase (0.04 μM) at 60°C over the course of 5 hrs with PEF (4 mg mL^{-1}). Reactions were carried out in duplicate; error bars represent the s.d. of the total soluble aromatic compounds produced in the replicates.

5.6 Discussion

Plastic waste is an ever-evolving blend of polymers, moulded by consumer preferences and the necessary development of the next generation of materials. For even supposedly single-component waste streams, a complex mixture of plastic morphologies is usually present.⁵ The results presented here indicate that the engineering of *IsPETase* to produce the more active and thermostable *HotPETase*, using our in-house directed evolution platform, has delivered a biocatalyst with the scope to operate on a range of realistic PET-waste substrates. *HotPETase* has the ability to deconstruct a range of PET morphologies commonly found in packaging materials: it can depolymerise crystalline PET with a superior performance compared to the engineered cutinase, *LCC^{ICCG}*, and previous rationally engineered variants of *IsPETase*. *HotPETase* can also selectively deconstruct the PET portion of a PET/PE packaging lid, demonstrating the potential benefits of enzymatic recycling for composite materials. However, any long-term, sustainable recycling strategy must also be able to cope with inevitable perturbations of the plastic waste landscape.²³ We demonstrate that *HotPETase* can also degrade PETG, a polymer growing in popularity due to its use in 3D printing, and PEF, the suggested next-generation of bio-derived plastic material. This opens up the possibility of engineering new biocatalysts that can discriminate between PET-like polymers using *HotPETase* as a promiscuous starting template. By adapting the selection pressures during laboratory evolution, we will be able to tailor enzymes such as *HotPETase* to respond to future industrial demands.

5.7 References

1. MacLeod, M., Arp, H. P. H., Tekman, M. B. & Jahnke, A. The global threat from plastic pollution. *Science* **373**, (2021).
2. The Pew Charitable Trusts. *Breaking the Plastic Wave*. https://www.pewtrusts.org/-/media/assets/2020/10/breakingtheplasticwave_mainreport.pdf (2020).
3. Zimmermann, W. Biocatalytic recycling of polyethylene terephthalate plastic. *Philosophical Transactions of the Royal Society A: Mathematical, Physical and Engineering Sciences* **378**, 20190273 (2020).
4. Sadler, J. C. & Wallace, S. Microbial synthesis of vanillin from waste poly(ethylene terephthalate). *Green Chemistry* **23**, 4665–4672 (2021).
5. Korley, L., Epps, T., Helms, B. & Ryan, A. Toward polymer upcycling—adding value and tackling circularity. *Science* **373**, 66–69 (2021).
6. Herrero Acero, E. *et al.* Enzymatic Surface Hydrolysis of PET: Effect of Structural Diversity on Kinetic Properties of Cutinases from *Thermobifida*. *Macromolecules* **44**, 4632–4640 (2011).
7. Sulaiman, S. *et al.* Isolation of a novel cutinase homolog with polyethylene terephthalate-degrading activity from leaf-branch compost by using a metagenomic approach. *Applied and Environmental Microbiology* **78**, 1556–62 (2012).
8. Kawai, F. *et al.* A novel Ca²⁺-activated, thermostabilized polyesterase capable of hydrolyzing polyethylene terephthalate from *Saccharomonospora viridis* AHK190. *Applied Microbiology and Biotechnology* **98**, 10053–10064 (2014).
9. Ribitsch, D. *et al.* Hydrolysis of polyethylene terephthalate by *p*-nitrobenzylesterase from *Bacillus subtilis*. *Biotechnology Progress* **27**, 951–960 (2011).
10. Tournier, V. *et al.* An engineered PET depolymerase to break down and recycle plastic bottles. *Nature* **580**, 216–219 (2020).
11. Yoshida, S. *et al.* A bacterium that degrades and assimilates poly(ethylene terephthalate). *Science* **351**, 1196–9 (2016).
12. Erickson, E. *et al.* Comparative performance of PETase as a function of reaction conditions, substrate properties, and product accumulation. *ChemSusChem* **n/a**, (2021).
13. Cui, Y. *et al.* Computational Redesign of a PETase for Plastic Biodegradation under Ambient Condition by the GRAPE Strategy. *ACS Catalysis* **11**, 1340–1350 (2021).
14. Son, H. F. *et al.* Rational Protein Engineering of Thermo-Stable PETase from *Ideonella sakaiensis* for Highly Efficient PET Degradation. *ACS Catalysis* **9**, 3519–3526 (2019).
15. Son, H. F. *et al.* Structural bioinformatics-based protein engineering of thermo-stable PETase from *Ideonella sakaiensis*. *Enzyme and Microbial Technology* **141**, 109656 (2020).
16. Austin, H. P. *et al.* Characterization and engineering of a plastic-degrading aromatic polyesterase. *Proceedings of the National Academy of Sciences of the United States of America* **115**, E4350–E4357 (2018).
17. Knott, B. C. *et al.* Characterization and engineering of a two-enzyme system for plastics depolymerization. *Proceedings of the National Academy of Sciences* **117**, 25476 (2020).
18. Dai, L. *et al.* Enhancing PET hydrolytic enzyme activity by fusion of the cellulose-binding domain of cellobiohydrolase I from *Trichoderma reesei*. *Journal of Biotechnology* **334**, 47–50 (2021).
19. Ügdüler, S. *et al.* Towards closed-loop recycling of multilayer and coloured PET plastic waste by alkaline hydrolysis. *Green Chemistry* **22**, 5376–5394 (2020).

20. Chen, T., Zhang, J. & You, H. Photodegradation behaviour and mechanism of poly(ethylene glycol-co-1,4-cyclohexanedimethanol terephthalate) (PETG) random copolymers: correlation with copolymer composition. *RSC Advances* **6**, 102778–102790 (2016).
21. Hwang, K.-R., Jeon, W., Lee, S. Y., Kim, M.-S. & Park, Y.-K. Sustainable bioplastics: Recent progress in the production of bio-building blocks for the bio-based next-generation polymer PEF. *Chemical Engineering Journal* **390**, 124636 (2020).
22. Jiang, L. *et al.* PEF plastic synthesized from industrial carbon dioxide and biowaste. *Nature Sustainability* **3**, 761–767 (2020).
23. O'Dea, R. M., Willie, J. A. & Epps, T. H. 100th Anniversary of Macromolecular Science Viewpoint: Polymers from Lignocellulosic Biomass. Current Challenges and Future Opportunities. *ACS Macro Letters* **9**, 476–493 (2020).

CHAPTER 6

Introduction to Genetic Code Expansion

Elizabeth L Bell¹ & Anthony P Green¹

¹Manchester Institute of Biotechnology, 131 Princess Street, University of Manchester, Manchester, M1 7DN, UK.

6.1 Foreword

This chapter consists of an excerpt of a review published in Nature Reviews Methods Primers entitled “Biocatalysis”, on 24th June 2021, reviewing the state-of-the-art methodologies in the biocatalysis field. This excerpt entitled “Biocatalysts with non-canonical amino acids”, serves as an introduction and overview of the field of genetic code expansion and its recent applications.

6.2 Acknowledgements

The review article was a collaborative effort between the doctoral candidate and Anthony P. Green. The excerpt presented in this chapter was written and edited by the doctoral candidate and Anthony P. Green and the complete article was overseen by Sabine L. Flitsch.

6.3 Biocatalysts with Non-Canonical Amino Acids

The design and engineering of enzymes with an expanded amino acid alphabet is a nascent and rapidly developing area of biocatalysis. Enzymes are exceptionally powerful catalysts capable of promoting chemical transformations with efficiencies and selectivities that are difficult to achieve with small molecule systems. However, enzymes are typically biosynthesised from only twenty canonical amino acids that contain a limited number of functional groups, restricting the range of catalytic mechanisms that can be installed into designed active sites. Recent years have seen the emergence of powerful genetic code expansion methodologies that allow the site-specific installation of hundreds of structurally and functionally diverse non-canonical amino acids into proteins.^{1,2} Careful selection of a suitable non-natural amino acid and its positioning within the target protein scaffold is required to address the application of interest (Fig. 1). For instance, for mechanistic investigations of natural enzymes, we often replace a key active site residue with a non-canonical amino acid that is a close structural analogue to modulate catalytic function.³⁻⁷ Alternatively, to design enzymes with new functions, the selection of amino acid takes inspiration from structural motifs present in small molecule catalysts with positioning guided by computation.^{8,9}

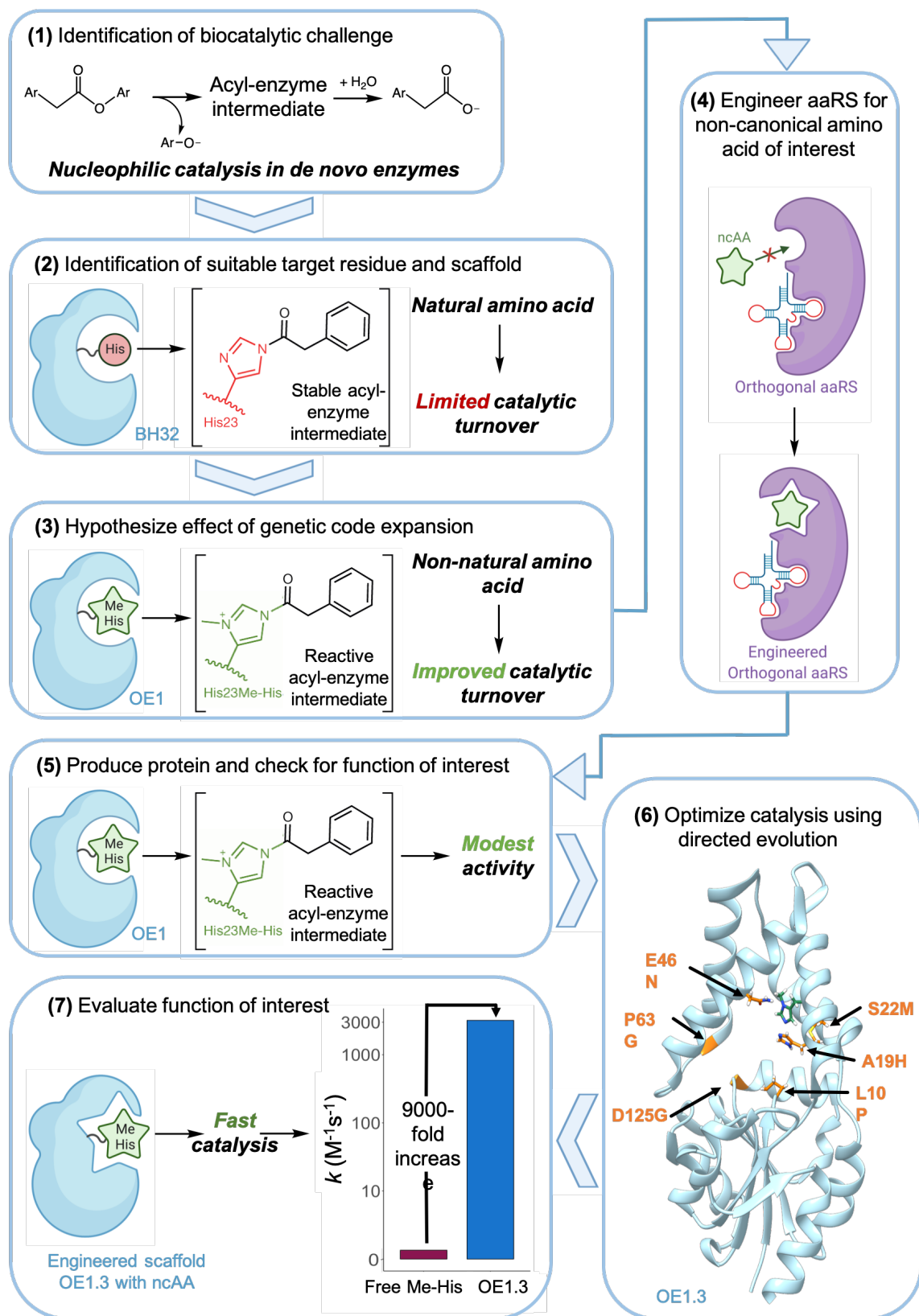


Figure 1. A representative workflow for the use of genetic code expansion to enhance biocatalytic function, using the design and engineering of a *de novo* enzyme with a non-natural catalytic nucleophile as an example.⁸

Figure 1. Continued. (1) The biocatalytic challenge to be addressed must be defined. (2) Identify a protein scaffold and a suitable target residue for modification. (3) If the challenge cannot be addressed through standard mutagenesis, identify a functional non-canonical amino acid (ncAA) to achieve the desired properties. For example, replacement of the His23 nucleophile of the *de novo* protein BH32 with N_δ-methylhistidine (Me-His) should increase the activity of acyl-enzyme intermediates. (4) Are translation components already available to incorporate the ncAA of interest? If not, an aminoacyl-tRNA synthetase (aaRS) can be evolved to accept the target ncAA using directed evolution.^{2,10} (5) Use engineered translation components to produce the catalytically modified protein, which is then evaluated for the activity of interest. (6) Catalytic function can be optimized using directed evolution workflows adapted for an expanded genetic code. The ribbon representation of the evolved OE1.3 enzyme structure (light blue) has a Me-His residue shown as a ball-and-stick representation (green) along with the sites of mutation revealed through directed evolution detailed in orange.⁸ (7) The optimized enzyme is characterized. In the case of OE1.3, ester hydrolysis was accelerated by >9000-fold compared with the free ncAA (Me-His) in solution.

The availability of an expanded set of amino acid building blocks offers exciting new opportunities in biocatalysis. Genetically encoded non-canonical amino acids have been used to improve both biocatalyst activity and stability¹² and provide new tools to understand how enzymes function at the molecular level.³⁻⁵ Key recent examples include the replacement of serine and cysteine catalytic nucleophiles with 2,3-diaminopropionic acid as a means of trapping acyl-enzyme intermediates for structural characterization⁶ and the use of non-canonical axial heme ligands to unravel the active site features that control the reactivities of high energy metal-oxo intermediates.⁷ The availability of an increased repertoire of covalently-embedded functional groups also provides exciting opportunities to design *de novo* enzymes with catalytic mechanisms inspired by small molecule catalysis. This approach was recently showcased through the design of an artificial hydrolase OE1,⁸ that employs N_δ-methyl histidine (Me-His) as a catalytic nucleophile, which operates with a similar mode of action to the widely employed small molecule catalyst dimethylaminopyridine (DMAP).¹³ Histidine methylation was integral to catalytic function and leads to the generation of reactive acyl-imidazolium intermediates which are readily hydrolysed to regenerate the catalytic nucleophile (Fig. 1). In contrast, the catalytic function of *de novo* hydrolases employing canonical histidine, serine or cysteine nucleophiles was compromised by the formation of unreactive acyl-enzyme intermediates.¹⁴⁻¹⁷ The modest initial hydrolysis activity of OE1 was subsequently enhanced via iterative rounds of directed evolution giving rise to variant OE1.3 containing six active site mutations.⁸ OE1.3 accelerates ester hydrolysis, being greater than 9000-fold and 2800-fold more efficient than free Me-

His and DMAP, respectively. Further rounds of evolution lead to the enantioselective hydrolase OE1.4. This study showcases how the interplay of genetic code expansion, computational design and directed evolution can provide a truly versatile platform for building *de novo* biocatalysts with new and improved catalytic functions.

6.3 References

1. Chin, J. W. Expanding and reprogramming the genetic code. *Nature* **550**, 53–60 (2017).
2. Liu, C. C. & Schultz, P. G. Adding New Chemistries to the Genetic Code. *Annual Review of Biochemistry* **79**, 413–444 (2010).
3. Seyedsayamdost, M. R., Xie, J., Chan, C. T. Y., Schultz, P. G. & Stubbe, J. Site-Specific Insertion of 3-Aminotyrosine into Subunit $\alpha 2$ of *E. coli* Ribonucleotide Reductase: Direct Evidence of Involvement of Y730 and Y731 in Radical Propagation. *Journal of the American Chemical Society* **129**, 15060–15071 (2007).
4. Faraldos, J. A. *et al.* Probing Eudesmane Cation– π Interactions in Catalysis by Aristolochene Synthase with Non-canonical Amino Acids. *Journal of the American Chemical Society* **133**, 13906–13909 (2011).
5. Wu, Y. & Boxer, S. G. A Critical Test of the Electrostatic Contribution to Catalysis with Noncanonical Amino Acids in Ketosteroid Isomerase. *Journal of the American Chemical Society* **138**, 11890–11895 (2016).
6. Huguenin-Dezot, N. *et al.* Trapping biosynthetic acyl-enzyme intermediates with encoded 2,3-diaminopropionic acid. *Nature* **565**, 112–117 (2019).
7. Ortmyer, M. *et al.* Rewiring the “Push-Pull” Catalytic Machinery of a Heme Enzyme Using an Expanded Genetic Code. *ACS Catalysis* **10**, 2735–2746 (2020).
8. Burke, A. J. *et al.* Design and evolution of an enzyme with a non-canonical organocatalytic mechanism. *Nature* **570**, 219–223 (2019).
9. Drienovská, I., Mayer, C., Dulson, C. & Roelfes, G. A designer enzyme for hydrazone and oxime formation featuring an unnatural catalytic aniline residue. *Nature Chemistry* **10**, 946–952 (2018).
10. Santoro, S. W., Wang, L., Herberich, B., King, D. S. & Schultz, P. G. An efficient system for the evolution of aminoacyl-tRNA synthetase specificity. *Nature Biotechnology* **20**, 1044–1048 (2002).
11. Pott, M. *et al.* A Noncanonical Proximal Heme Ligand Affords an Efficient Peroxidase in a Globin Fold. *Journal of the American Chemical Society* **140**, 1535–1543 (2018).
12. Li, J. C., Liu, T., Wang, Y., Mehta, A. P. & Schultz, P. G. Enhancing Protein Stability with Genetically Encoded Noncanonical Amino Acids. *Journal of the American Chemical Society* **140**, 15997–16000 (2018).
13. Wurz, R. P. Chiral Dialkylaminopyridine Catalysts in Asymmetric Synthesis. *Chemical Reviews* **107**, 5570–5595 (2007).
14. Bolon, D. N. & Mayo, S. L. Enzyme-like proteins by computational design. *Proceedings of the National Academy of Sciences of the United States of America* **98**, 14274–14279 (2001).
15. Richter, F. *et al.* Computational Design of Catalytic Dyads and Oxyanion Holes for Ester Hydrolysis. *Journal of the American Chemical Society* **134**, 16197–16206 (2012).
16. Moroz, Y. S. *et al.* New Tricks for Old Proteins: Single Mutations in a Nonenzymatic Protein Give Rise to Various Enzymatic Activities. *Journal of the American Chemical Society* **137**, 14905–14911 (2015).
17. Burton, A. J., Thomson, A. R., Dawson, W. M., Brady, R. L. & Woolfson, D. N. Installing hydrolytic activity into a completely *de novo* protein framework. *Nature Chemistry* **8**, 837 (2016).

CHAPTER 7

Capturing an *IsPETase* Acyl-Enzyme Intermediate Using Genetic Code Expansion

Elizabeth L. Bell¹, Chris Taylor¹, Maia Thompson¹, Ross Smithson¹ & Anthony P. Green^{1*}

¹Manchester Institute of Biotechnology, 131 Princess Street, University of Manchester, Manchester, M1 7DN, UK.

7.1 Foreword

This chapter consists of a research article describing the capture of a catalytic intermediate analogue of the *IsPETase*^{TS} enzyme by incorporating the non-canonical amino acid, DAP, in place of the catalytic serine.

7.2 Acknowledgements

The research presented in this chapter was a collaborative effort between the doctoral candidate and the following researchers: Chris Taylor, Maia Thompson, Ross Smithson and Anthony P. Green. The doctoral candidate carried out the molecular biology and data presentation. The doctoral candidate, Maia Thompson and Ross Smithson carried out the protein production, purification and assay development. Chris Taylor and Maia Thompson carried out all chemical syntheses. Reynard Spiess carried out protein mass spectrometry. The doctoral candidate and Anthony P. Green wrote the manuscript.

7.3 Abstract

IsPETase is a serine hydrolase that has evolved to depolymerise the abundant polyester plastic, poly(ethylene terephthalate) (PET). Despite enormous interest, our understanding of catalysis by *IsPETase* and key structural features important for polymer deconstruction remains incomplete. Here we use genetic code expansion to replace the catalytic serine of *IsPETase* with the close structural analogue 2,3-diaminopropionic acid (DAP). Reaction of DAP-modified *IsPETase* with the PET subunit, bis(2-hydroxyethyl) terephthalate (BHET), leads to the generation of a stable acyl-enzyme intermediate, via the formation of an amide linkage involving the active site DAP. This study provides the foundation for more detailed

exploration of the *IsPETase* catalytic mechanism and elucidation of the structural characteristics responsible for efficient plastic degradation.

7.4 Introduction

Biocatalysis is emerging as a promising technique for the efficient degradation of anthropogenic polymers to help circularise the plastics economy.¹ The feasibility of biocatalytic recycling strategies, has recently been bolstered by the identification of a naturally-evolved, cutinase-like enzyme, *IsPETase*, that can accelerate the hydrolysis of one of the most abundant polyester plastics, poly(ethylene terephthalate) (PET).² *IsPETase* has captured the attention of scientists, the public and the media alike, leading to a renewed interest in the engineering of plastic-deconstructing enzymes for industrial use and significant efforts to characterise these proteins fully.³⁻⁷

Crystallisation and computational analysis of *IsPETase* has enabled the elucidation of some of the important structural features that explain its PET-degrading activities (Fig. 1).⁵ For instance, *IsPETase* is a member of the serine α/β hydrolase superfamily of enzymes, containing a canonical catalytic triad consisting of Ser160, Asp206, and His237. Enzymes from this family operate through a conserved two-step hydrolytic mechanism, involving the production of a transient acyl-enzyme intermediate. Interestingly *IsPETase* contains an additional, active site adjacent, disulphide bridge (Cys203-Cys239) compared to homologous proteins, which is thought to both stabilise the active site and promote flexibility in other areas of the enzyme's architecture.⁸ In addition, the enzyme has a particularly broad active site as compared to its cutinase homologues, exhibiting an exposed, hydrophobic L-shaped cleft within which multiple PET moieties may sit.⁴ Of particular note is the presence of a conformationally flexible tryptophan, Trp185, unique amongst the *IsPETase*'s structural homologues; residue movement is enabled by Ser214 and Ile218, whose equivalents are strictly histidine and phenylalanine, respectively, in comparable enzymes.^{3,4} The "wobbling" of Trp185 is purported to facilitate the binding and release of long polymer chains, with the installation of this structural feature into homologous enzymes leading to a significant improvement in PET-degrading ability.⁹

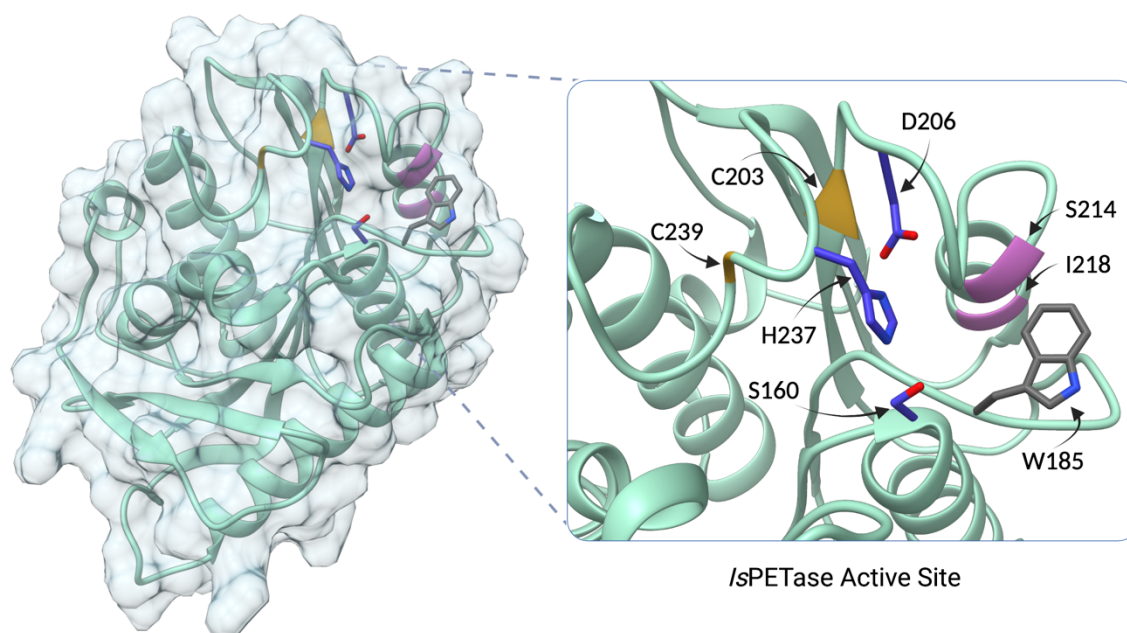


Figure 1. Crystal structure of *IsPETase*. The enzyme (turquoise ribbon) has a number of important features: a canonical catalytic triad (blue sticks); an active site adjacent disulphide bridge (highlighted yellow) and a “wobbling” tryptophan (grey stick), whose flexibility is aided by the presence of a serine and isoleucine residue pair (highlighted pink).

Despite substantial progress in understanding the behaviour of *IsPETase*, challenges associated with studying the catalytic deconstruction of heterogeneous, insoluble polymers, mean that many important questions about the mechanism of action of these types of enzymes remain unanswered.^{10,11} *In silico* docking of PET-surrogate molecules into the *IsPETase* active site have given some insight into how the enzyme may interact with its substrate,⁴ although the reliability of this type of computational modelling with regard to the stiff polymer chains has recently been called into doubt.¹² Furthermore, while crystal structures have been solved for small substrate analogues complexed with an *IsPETase* variant with the catalytic serine removed (S160A),^{3,4} to date there are no real structures of covalent complexes involving catalytically active Ser160, similar to those generated during the *IsPETase* catalytic cycle. There is therefore limited information about how *IsPETase* acts: whether the enzyme conducts depolymerisation in an exo- or endo- manner; if it operates in a processive or non-processive fashion; how the enzyme interacts with the solid polymer surface and how polymer composition affects biocatalytic activity.

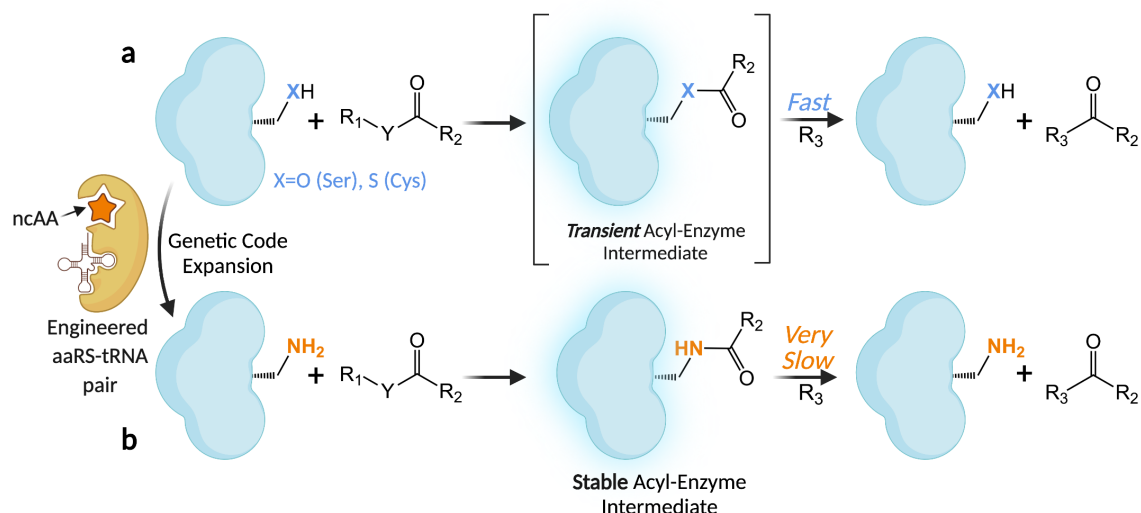


Figure 2. Capturing transient acyl-enzyme intermediates with DAP. (a) A catalytic serine or cysteine residue (X, blue) can react with a substrate carbonyl group, forming a tetrahedral intermediate (not shown), which then collapses to form a transient acyl-enzyme intermediate with the concurrent loss of R_1 -YH. This intermediate is then quickly resolved following nucleophilic attack by R_3 (usually a hydroxyl, amine or thiol) to regenerate the catalytic residue alongside the release of the previously bound substrate fragment. R_1 , R_2 and Y represent a range of chemical groups which can be found in suitable substrates. Genetic code expansion using an engineered aminoacyl tRNA synthetase (aaRS)-tRNA pair to install a non-natural amino acid (ncAA), could perturb the normal catalytic cycle. (b) Replacing the catalytic serine or cysteine with the ncAA, DAP (orange), may result in a first acyl-enzyme intermediate that is more resistant to attack due to the formation of an amide bond. The stable intermediate will be very slow to react further and so could subsequently be captured.

In recent years, genetic code expansion has emerged as a powerful mechanism for probing complex biological mechanisms.^{13,14} In contrast to standard, site-directed mutagenesis, where mutational freedom is restricted to the natural genetic code, genetic code expansion allows for the installation of precise modifications designed by biochemists to address particular challenges. In particular, the recent addition of 2,3-diaminopropionic acid (DAP) to the repertoire of available non-canonical amino acids (ncAAs) provides a potentially versatile mechanism for the trapping of near-native acyl-enzyme intermediates (Fig. 2).¹⁵ By replacing catalytic hydroxyls with amines, the half-lives of intermediates are extended by the formation of a stable amide bond. This process has been successfully used to characterise a cysteine protease and a thioesterase, with a catalytic serine.¹⁵ Intrigued we realised the potential of this technology to contribute to our understanding of catalytic polymer deconstruction by *IsPETase*. Here we report the successful engineering of *IsPETase* to incorporate DAP, and the trapping of acyl-enzyme intermediates, as confirmed by mass spectrometry. The preliminary data presented here will underpin future studies to

structurally characterise *IsPETase*, with the aim to resolve some of the unanswered questions regarding its mechanism of action.

7.5 Results

A three-point mutant, *IsPETase*^{TS} (*IsPETase*^{S121E/D186H/R280A}), was selected as the start point for this study, due to its enhanced, expression and stability as compared to *IsPETase*^{WT}.¹⁶ A photocaged version of DAP (p-DAP) was first incorporated into *IsPETase*^{TS}; the photoprotection of DAP is important for selective encoding of the nAA. To begin, the *IsPETase*^{TS} gene was genetically modified to encode the stop codon, TAG, in place of the catalytic serine, Ser160 to yield *IsPETase*^{TS}_S160TAG. The gene was fused to a C-term hexahistidine tag via ligation into an expression vector and the resulting construct was co-transformed into an *E. coli* expression strain, with a second vector containing the translation components (aminoacyl tRNA synthetase (aaRS) and tRNA pair) necessary for p-DAP incorporation.¹⁵ Protein expression was carried out in the presence of 1 mM p-DAP, synthesised as previously by Chin's lab,¹⁵ with subsequent purification yielding the full-length, C-term his-tagged, *IsPETase*^{TS}-p-DAP, which was confirmed by mass spectrometry (MS) (Fig. 3, all expected and observed MS data can be found in Extended Data Table 1). The expression of *IsPETase*^{TS}-p-DAP is compromised compared to *IsPETase*^{TS}, but sufficient protein was obtained for further experimentation. Protein expression of *IsPETase*^{TS}_S160TAG in the absence of p-DAP did not lead to a purifiable protein, verifying the specificity of p-DAP incorporation in *IsPETase*^{TS}_S160TAG. Photocage removal was then initiated by irradiating the protein at 365 nm, revealing the desired protein *IsPETase*^{TS}-DAP, again confirmed by MS, with an expected 297 Da reduction in mass (Fig. 4a).

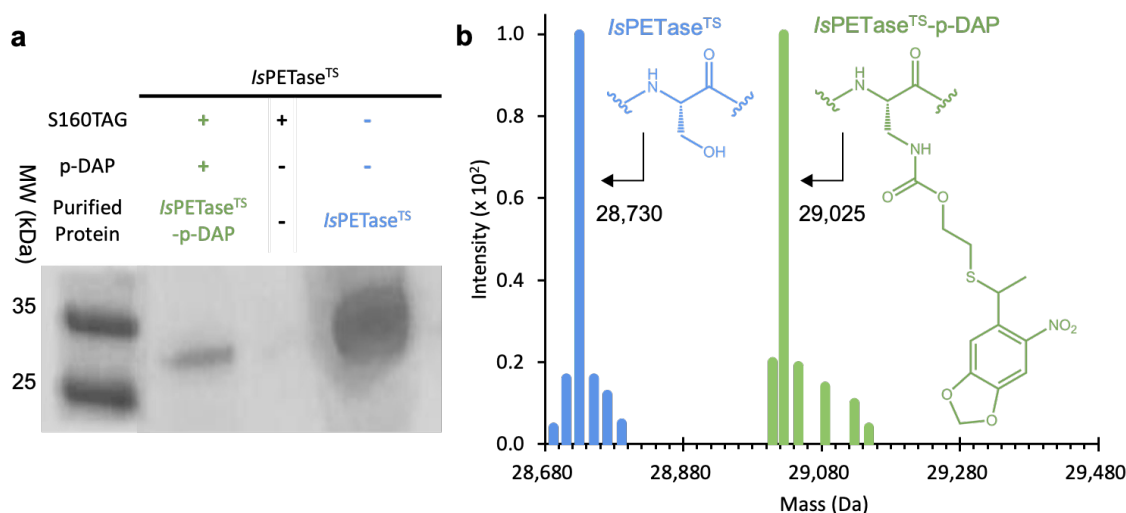


Figure 3. Incorporation of p-DAP into *IsPETase*^{TS}. (a) SDS-PAGE gel of purified cell lysates. Full length *IsPETase*^{TS}-p-DAP (green) is produced in the presence of the S160TAG genetic modification and p-DAP, but not in the absence of p-DAP. Protein expression of *IsPETase*^{TS}-p-DAP is less efficient than *IsPETase*^{TS} (blue). (b) Mass spectra of *IsPETase*^{TS} (blue) and *IsPETase*^{TS}-p-DAP (green). Only peaks with an intensity $>0.04 \times 10^2$ are shown (Extended Data, Fig. 1).

We next investigated whether the installed DAP was a competent nucleophile, using *IsPETase*^{TS} as a control. We presented both enzymes with the small, soluble plastic surrogate, bis(2-hydroxyethyl) terephthalate (BHET) (Fig. 4b). Following reaction, the mass of *IsPETase*^{TS} was unchanged, indicating that there was no off-pathway acylation of the protein, and confirming that serine complexed acyl-enzyme intermediates are not sufficiently long-lived to accumulate under our analysis conditions (Fig. 4c). In contrast, following BHET reaction, the mass of *IsPETase*^{TS}-DAP increased by 192 Da, consistent with the formation of an inert amide bond-tethered, MHET-protein complex. This demonstrates that DAP is a competent amine nucleophile. The use of the catalytically active *IsPETase*^{TS}-DAP will now underpin future studies to probe the enzyme's reaction mechanism.

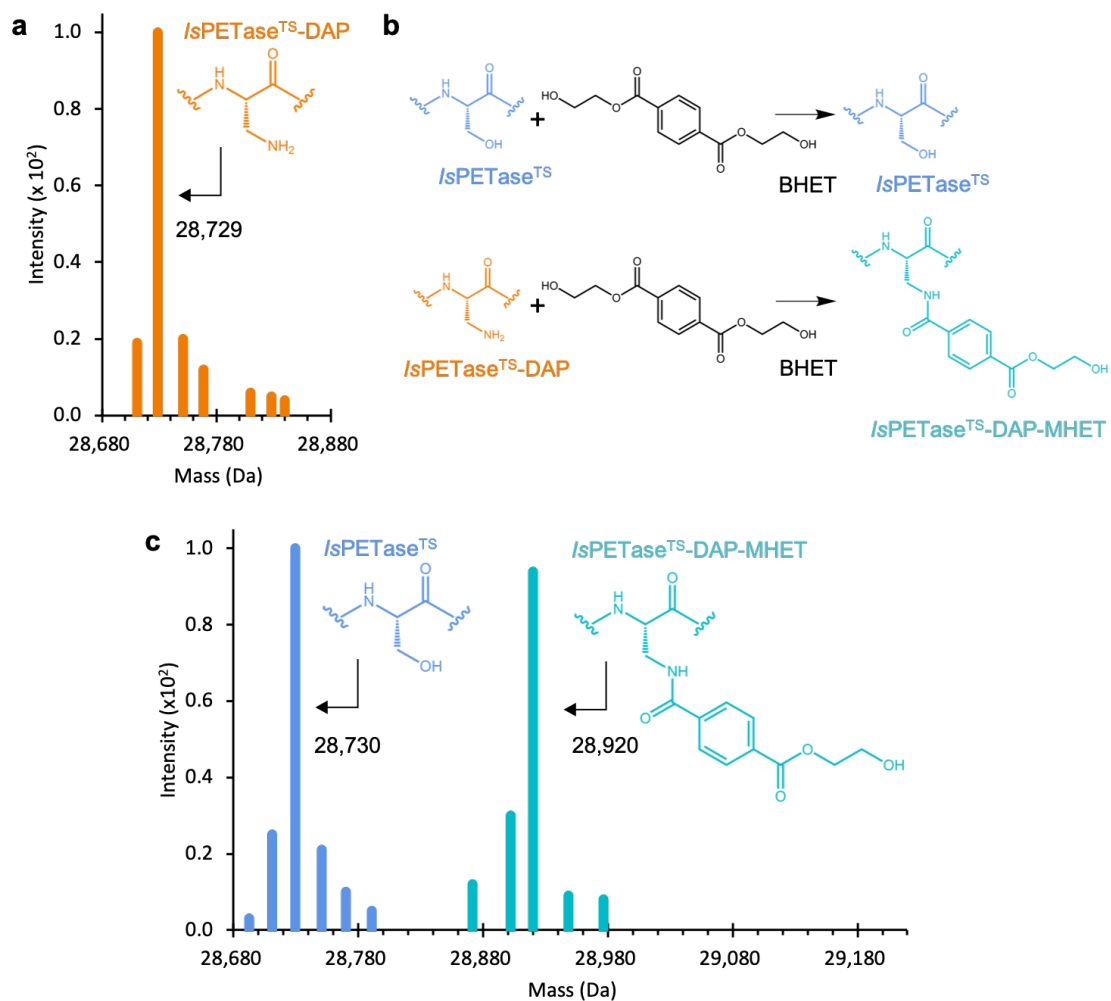


Figure 4. Production of *IsPETase*^{TS}-DAP and reaction with BHET. (a) Mass spectrum of photo-deprotected *IsPETase*^{TS}-DAP (orange). (b) Expected reaction scheme of unmodified and modified *IsPETase* proteins following reaction with BHET. (c) Mass spectra of *IsPETase*^{TS} and *IsPETase*^{TS}-DAP following reaction with BHET. The mass of *IsPETase*^{TS} is essentially unchanged (blue), whilst the mass of *IsPETase*^{TS}-DAP has increased to yield *IsPETase*^{TS}-DAP-MHET (turquoise). For mass spectra, only peaks with an intensity $>0.04 \times 10^2$ are shown (Extended Data, Fig. 1).

7.6 Discussion

The successful installation of a competent amine nucleophile in the *IsPETase* active site provides an exciting basis for future studies with this system. Structural characterisation of stable acyl-enzyme intermediates will shed light on catalytically important conformational changes of the protein along the reaction coordinate and advance our understanding of substrate positioning at a key stage of the catalytic cycle. Furthermore, the conversion of *IsPETase* into a single turnover catalyst that cleaves a single ester bond, should facilitate identification of the initial products of *IsPETase*-mediated polymer deconstruction, offering a new approach to study whether the enzyme preferentially cleaves PET in an exo- or endo-fashion. Finally, of particular interest for our own work, the approach described here can be readily extended to probe the catalytic mechanism of our recently evolved thermostable *IsPETase* variant, *HotPETase*, to further understand any structural and mechanistic changes that may have occurred during laboratory evolution. Any insights found will feed into additional directed evolution cycles to further improve the enzyme: for example, it could provide information to more finely tune substrate positioning to promote catalysis. Overall, we anticipate that non-canonical substitution of catalytic serines to DAP will provide an important tool in the study of PETase-mediated polymer deconstruction.

7.7 References

1. Kakadellis, S. & Rosetto, G. Achieving a circular bioeconomy for plastics. *Science* **373**, 49–50 (2021).
2. Yoshida, S. *et al.* A bacterium that degrades and assimilates poly(ethylene terephthalate). *Science* **351**, 1196–9 (2016).
3. Han, X. *et al.* Structural insight into catalytic mechanism of PET hydrolase. *Nature Communications* **8**, 2106 (2017).
4. Joo, S. *et al.* Structural insight into molecular mechanism of poly(ethylene terephthalate) degradation. *Nature Communications* **9**, 382 (2018).
5. Austin, H. P. *et al.* Characterization and engineering of a plastic-degrading aromatic polyesterase. *Proceedings of the National Academy of Sciences of the United States of America* **115**, E4350–E4357 (2018).
6. Cui, Y. *et al.* Computational Redesign of a PETase for Plastic Biodegradation under Ambient Condition by the GRAPE Strategy. *ACS Catalysis* **11**, 1340–1350 (2021).
7. Tournier, V. *et al.* An engineered PET depolymerase to break down and recycle plastic bottles. *Nature* **580**, 216–219 (2020).
8. Fecker, T. *et al.* Active Site Flexibility as a Hallmark for Efficient PET Degradation by *I. sakaiensis* PETase. *Biophysical Journal* **114**, 1302–1312 (2018).
9. Chen, C.-C. *et al.* General features to enhance enzymatic activity of poly(ethylene terephthalate) hydrolysis. *Nature Catalysis* **4**, 425–430 (2021).
10. Taniguchi, I. *et al.* Biodegradation of PET: Current Status and Application Aspects. *ACS Catalysis* **9**, 4089–4105 (2019).
11. Ellis, L. D. *et al.* Chemical and biological catalysis for plastics recycling and upcycling. *Nature Catalysis* **4**, 539–556 (2021).
12. Wei, R. *et al.* Conformational fitting of a flexible oligomeric substrate does not explain the enzymatic PET degradation. *Nature Communications* **10**, 3–6 (2019).
13. de la Torre, D. & Chin, J. W. Reprogramming the genetic code. *Nature Reviews Genetics* **22**, 169–184 (2021).
14. Zhao, J., Burke, A. J. & Green, A. P. Enzymes with noncanonical amino acids. *Current Opinion in Chemical Biology* **55**, 136–144 (2020).
15. Huguenin-Dezot, N. *et al.* Trapping biosynthetic acyl-enzyme intermediates with encoded 2,3-diaminopropionic acid. *Nature* **565**, 112–117 (2019).
16. Son, H. F. *et al.* Rational Protein Engineering of Thermo-Stable PETase from *Ideonella sakaiensis* for Highly Efficient PET Degradation. *ACS Catalysis* **9**, 3519–3526 (2019).

CHAPTER 8

Conclusions and Outlook

Plastics do not have to remain a problem for the modern world. If we can efficiently and effectively depolymerise them in a controlled, green, cost-effective manner, we can continue to reap their benefits without foregoing our duty to conserve the planet. Biocatalysis can assist in achieving this goal, aiding the development of a circular plastics economy, by using plastic waste as a low-cost feedstock for the production of monomers for repolymerisation or upcycling. Enzymes could offer an economical, environmentally friendly strategy for processing certain plastics, with the potential to reduce the costs associated with current polymer recycling methods. In order to realise this ambition, we need to develop enzymes with the necessary properties for commercially viable biocatalytic recycling strategies. These biocatalysts need to be able to deconstruct a range of polymer compositions and morphologies present in post-consumer waste, alongside being able to withstand industrial processing conditions.

Here, we present an automated, high-throughput, directed evolution platform for engineering plastic-deconstructing enzymes. We use the developed system to engineer *IsPETase*, the only known naturally evolved PET-depolymerising protein, focusing on improving its activity at elevated temperatures approaching the glass transition temperature of PET (60-70°C). Following evaluation of over 13,000 *IsPETase* variants, a HotPETase variant emerged that contains 21 mutations, with a melting temperature of 82.5°C, an improvement of 11.5°C above that of the previous most thermostable *IsPETase* derivative developed by Cui *et al.* (2021). HotPETase outperforms previously engineered PETases, including the engineered cutinase LCC^{ICCG}, with respect to the rate of depolymerisation. These improvements are most pronounced when deconstructing semi-crystalline PET material, a substrate more akin to that found in real post-consumer waste streams. Under optimised conditions, HotPETase can deconstruct 36% of 20 mg of semi-crystalline PET powder over 24 hrs. Structural characterisation reveals the formation of new bonding interactions in HotPETase which likely aid thermostability, alongside more nuanced changes to the electrostatic properties of the substrate binding cleft. Of particular note is the formation of a π -stacking interaction which restricts the conformational freedom of Trp185, hinting that flexibility of this residue is not necessarily required for *IsPETase*

catalysis. Overall, these properties make HotPETase an attractive candidate for practical applications. At its current stage of development, the enzyme is not without its limitations, exhibiting a deterioration in high-temperature catalysis over extended periods. However, we anticipate that through judicious adaptation of selection pressures, for example further increasing reaction times or temperatures, the directed evolution platform developed here can be used to increase biocatalyst longevity in the future.

It is important that engineered PETases are able to deal with the dynamic spectrum of post-consumer waste. Even single-plastic PET waste streams in actuality contain a plethora of different materials such as complex PET composites and copolymers, with the potential for waste streams to diversify even further with the emergence of bio-based plastics. In response to this challenge, we demonstrate that HotPETase can readily catalyse the deconstruction of a range of PET-based materials, from bottle-grade plastic to composite packaging lids, the common copolymer, PETG, and the bio-derived, PET-alternative, PEF. We also characterise the major soluble products released from the enzymatic depolymerisation of PETG and PEF. Moving forwards, these observations lay the foundations for future directed evolution efforts to mould HotPETase into a more effective PETGase or PEFase.

There are still several barriers to overcome before the adoption of biocatalysis for bulk polymer recycling. Efforts to develop industrially viable biocatalysts will be aided by a more complete understanding of the PETase catalytic mechanism. Here, we provide underpinning work to capture and study an important near-native catalytic cycle intermediate for *Is*PETase using genetic code expansion methodologies. As this enzyme engineering strategy converts the PETase into a protein capable of accelerating a single hydrolytic event, we anticipate that this approach will allow characterisation of initial products released during PET depolymerisation. This should thereby shed light on exo- versus endo- cleavage mechanisms operating in wildtype and engineered enzymes. Future work will scale up the production of the catalytically modified enzyme, alongside its structural and biochemical characterisation. Insights gained can then be used to guide future PETase engineering studies.

The research conducted here presents a versatile and powerful strategy for engineering plastic degrading enzymes. We envisage its use in a range of scenarios, for example to tailor broad-substrate scope enzymes for industrial application, or to pivot PETase activity

towards new substrates to enable more specific depolymerisations. Indeed, the platform developed here offers exciting opportunities to screen using different polymer substrates to create bespoke PETases with enhanced characteristics for target applications. We have successfully overcome past problems that hindered the development of directed evolution platforms for solid and interfacial reactions, and imagine that methods developed here may be of use to inform directed evolution studies concerning other insoluble substrates.

Beyond polyester deconstruction, we expect that in the future new families of enzymes will be discovered which can depolymerise alternative classes of plastic polymers. Directed evolution technologies will likely be required to engineer such biocatalysts for practical applications. We are hopeful that the work described in this thesis will contribute to development of a suite of plastic deconstructing enzymes in the future, to speed up progression towards a viable biocatalytic recycling strategy.

CHAPTER 9

Experimental

9.1 Foreword

This chapter contains the supporting information for the research presented in Chapters 4, 5 & 7. For all chapters, figures with cartoons were made using BioRender.com and protein crystal images were created using UCSF Chimera and ICM Browser.

9.2 Supporting Information for Chapter 4: Directed Evolution of an Efficient and Thermostable PETase

9.2.1 Methods

9.2.1.1 Materials

All chemical and biological materials were purchased from commercial suppliers. Kanamycin, ampicillin, tetracycline, DNase I, bis(2-hydroxyethyl) terephthalate (BHET) and terephthalic acid (TPA) were obtained from Sigma-Aldrich; LB agar, LB media, 2YT media, autoinduction (AIM) 2YT and arabinose from Formedium; BugBuster Protein Extraction Reagent from Merck; *Escherichia coli* (*E. coli*) Origami 2 (DE3) from Novagen; *E. coli* 5-alpha, *E. coli* BL21 (DE3), Q5 DNA polymerase, T4 DNA ligase, and restriction enzymes from New England BioLabs; 0.25 mm thickness amorphous PET film (amoPET) and 300 micron semi-crystalline PET powder (cryPET, 36.4% crystallinity) from Goodfellow, Cambridge; oligonucleotides were synthesized by Integrated DNA Technologies (IDT).

9.2.1.2 Gene Construction

The genes encoding *IsPETase*^{TS} (*IsPETase*^{S121E/D186H/R280A}, signal sequence removed as by Son *et al.* (2019)¹) and LCC^{ICCG} (LCC^{F243I/D238C/S283C/Y127G}), signal sequence removed as by Tournier *et al.* (2020)²) were commercially synthesised by Integrated DNA Technologies as gBlock fragments with codon optimisation for expression in *E. coli* cells. The *IsPETase*^{TS} gene was cloned into the NdeI (5' end) and XhoI (3' end) sites of a pBbE8K vector modified to contain a C-terminal hexa-histidine tag coding sequence following the XhoI restriction site,³ to form pBbE8K_*IsPETase*^{TS}. The HotPETase variant, HotPETase^{LR}, was created via overlap extension PCR with HotPETase as the template protein and primers designed to encode the wildtype residues at positions 212-215. Primer sequences are provided in Supplementary Information, Table 1. The resulting gene was cloned into the pBbE8K vector as described previously. The gene encoding LCC^{ICCG} was cloned into the NcoI (5' end) and XhoI (3' end) sites of pET-22b (Novagen) leading to fusion to a C-terminal hexa-histidine tag coding

sequence, to form pET-22b_LCC^{ICCG}. Plasmid maps, nucleotide sequences and expressed amino acid sequences of the genes used in this study are provided in Supplementary Information, Fig. 1, 2 and 3.

9.2.1.3 Library Construction

Rounds 1-6: Saturation mutagenesis. In each round 24-30 residues were selected and individually randomised using cassette mutagenesis. Positions were chosen for mutation based on a range of factors, detailed in Extended Data, Fig. 3. For residue identification via the Protein One Stop Repair Shop (PROSS) webserver,⁴ IsPETase^{WT} was used as the input protein (PDB: 6EQD), with all constraints fixed to the default settings; positions identified more than twice by the software were selected for mutation. For residue identification via the B-fitter software,⁵ IsPETase^{WT} was again used as the input protein (PDB: 6EQD); the 15 top positions ranked by highest B-factor were selected for mutation. DNA libraries at chosen residue positions were constructed via standard overlap extension PCR, using degenerate primer pairs (NNK codons) and pBbE8K_IsPETase^{TS} as the template for round 1, with the most active clone discovered at the end of each directed evolution cycle serving as the template for subsequent rounds. Primer sequences used for each round are provided in Supplementary Information, Table 2.

Shuffling by overlap extension PCR. After each round of evolution, beneficial diversity was combined by a process of DNA shuffling. Fragments were generated by overlap extension PCR using designed primers that encoded for either an identified beneficial mutation or the parental amino acid. Using these primers, up to six short fragments were created, DpnI digested, PCR-purified and mixed in appropriate combinations in overlap-extension PCRs. The resulting genes contained all possible combinations of mutations (from 2-5 mutations per gene) and were subsequently cloned into the pBbE8K vector as described previously.

9.2.1.4 Semi-Preparative Protein Production for Library Screening

For all protein expression and screening of libraries, transfer and aliquoting steps were performed using a Hamilton liquid-handling robot. pBbE8K_IsPETase libraries were expressed in chemically competent Origami 2 *E. coli* cells. Single colonies from a fresh transformation were used to inoculate 180 μ L LB media supplemented with 25 μ g mL⁻¹ kanamycin and 2.5 μ g mL⁻¹ tetracycline, in 96-deep-well plates. Each plate contained six positive controls consisting of clones of the parent template, and two negative controls consisting of clones containing pBbE8K_RFP (red fluorescent protein). Plates were incubated overnight at 30°C, 80% humidity in a shaking incubator (950 rpm). Expression cultures were then prepared by inoculating 460 μ L of 2YT media containing 25 μ g mL⁻¹ kanamycin and 2.5 μ g mL⁻¹ tetracycline with 40 μ L of overnight culture in deep-well blocks. The inoculated plates were incubated at 30°C, 80% humidity in a shaking incubator (950 rpm). When an optical density at 600 nm (OD₆₀₀) of 1 was reached, protein production was initiated by the addition of L-arabinose to a final concentration 10 mM and plates incubated for a further 20 hrs at 19°C, 80% humidity in a shaking incubator (950 rpm). Cells were harvested by centrifugation at 2,900 \times *g* for 10 minutes and the resulting pellets resuspended

in a lysis mix consisting of 50 μL of BugBuster Protein Extraction reagent containing 10 $\mu\text{g mL}^{-1}$ DNase I. Cell lysis was initiated by incubation for 30 minutes at 30°C, with 80% humidity in a shaking incubator (950 rpm), and the lysate produced diluted with 300 μL reaction buffer (50 mM glycine-OH, pH 9.2). Insoluble cell debris was removed via centrifugation for 10 minutes at 2,900 $\times g$, to produce a clear cell lysate.

9.2.1.5 Preparative Protein Production for Time-Course Assays

IsPETase and its derivatives were expressed in chemically competent Origami 2 *E. coli*. Single colonies of freshly transformed cells were cultured for 18 hrs at 30°C in 5 mL of LB medium supplemented with 25 $\mu\text{g mL}^{-1}$ kanamycin and 2.5 $\mu\text{g mL}^{-1}$ tetracycline. 1 mL of the resulting culture was used to inoculate 50 mL 2YT medium containing 25 $\mu\text{g mL}^{-1}$ kanamycin and 2.5 $\mu\text{g mL}^{-1}$ tetracycline. Cultures were grown at 35°C, 180 rpm to an OD_{600} of 1. Protein production was initiated by the addition of L-arabinose (final concentration of 10 mM) and cultures then grown at 19°C for 20 hrs. The *E. coli* cells were harvested by centrifugation at 3220 $\times g$ for 10 minutes and resuspended in lysis buffer (50 mM Tris-HCl, pH 7.5, 10 mM imidazole, 300 mM NaCl, 10 $\mu\text{g mL}^{-1}$ DNase I). Cells were disrupted by sonication and the resulting lysate clarified by centrifugation (13,500 $\times g$ for 15 minutes). The soluble fraction was subjected to affinity chromatography via application to Ni-NTA agarose (Qiagen). After washing off unbound proteins with the lysis buffer, bound proteins were eluted with elution buffer (50 mM Tris-HCl, pH 7.5, 300 mM imidazole, 300 mM NaCl). Proteins were desalted by application to IODG desalting columns (Bio-Rad) and eluted with storage buffer (50 mM Tris-HCl, pH 7.5, 150 mM NaCl). Protein purity was confirmed by sodium dodecyl sulphate-polyacrylamide gel electrophoresis (SDS-PAGE) and concentrations determined by measuring the absorbance at 280 nm, assuming an extinction coefficient of 39,670 $\text{M}^{-1} \text{cm}^{-1}$ for IsPETase^{TS}-IsPETase^{M2}, 41,160 $\text{M}^{-1} \text{cm}^{-1}$ for IsPETase^{M3}-IsPETase^{M7}, 41,285 $\text{M}^{-1} \text{cm}^{-1}$ IsPETase^{M8}-HotPETase.

For the cutinase, LCC^{ICCG}, the gene was expressed in chemically competent *E. coli* BL21 (DE3). Single colonies of freshly transformed cells were cultured for 18 hrs at 30°C in 5 mL of LB medium supplemented with 25 $\mu\text{g mL}^{-1}$ ampicillin. 1 mL of the resulting culture was used to inoculate 50 mL auto-inducible 2YT medium containing 25 $\mu\text{g mL}^{-1}$ ampicillin. Cultures were grown at 35°C, 180 rpm, to an OD_{600} of 1, upon which the incubator was cooled to 19°C, for expression cultivation for 20 hrs. Protein purification then proceeded as detailed for IsPETase, with protein concentrations determined using an extinction coefficient of 37,150 $\text{M}^{-1} \text{cm}^{-1}$.

9.2.1.6 Library Screening Using Amorphous PET Film (amoPET)

The clarified lysate was incubated for 30 mins - 1 hr at 55-80°C (pre-incubation step) and subjected to centrifugation at 2,900 $\times g$ for 10 minutes to remove any insoluble protein precipitate formed. To initiate the PET degradation reaction, 60-220 μL of clarified lysate was transferred to a 96-deep-well plate containing reaction buffer (50 mM glycine-OH, pH 9.2) and a single 6 mm amoPET film disc, to make a final reaction volume of 220-400 μL . Plates were then incubated for 3-7 hrs at 55-70°C, after which reactions were terminated by the addition of an equal volume of a cold methanol and 12.5 mM trifluoroacetic acid solution.

Following reaction quenching, plates were incubated for 30 mins at 30°C, 80% humidity in a shaking incubator, 950 rpm, and insoluble protein precipitate removed by centrifugation for 10 minutes at 2,900 x *g*. A UPLC analysis sample was then prepared by transferring 100 µL of the resulting reaction supernatant into a fresh 96-well microtiter plate. The most active clones of each round were then subjected to a second screening round, where each clone was represented in triplicate. All expression and screening protocols were as described above, apart from overnight culture preparation, where LB media was instead inoculated with 20 µL of a glycerol stock of the original overnight cultures. Details for the exact pre-incubation step temperature and length, the lysate volume added to the reaction, and the reaction incubation temperature and length for each round of directed evolution are provided in Extended Data, Fig. 3.

9.2.1.7 Time-Resolved PET Depolymerisation Assays Using Crystalline PET Powder

A 12 mL lidded glass vial containing 5 mL reaction buffer (50 mM glycine-OH, pH 9.2 with 4% BugBuster for *IsPETase*^{TS} and its derivatives or 100 mM potassium phosphate buffer, pH 8 for LCC^{ICCG}), with 20 mg crystalline PET powder (cryPET) was incubated for 1 hr at the reaction temperature (40-70°C) in order to equilibrate all reaction components to the reaction temperature (equilibration step). The reaction was initiated by adding 25 µL of an 8 µM solution of purified protein (*IsPETase*^{TS} and derivatives, or LCC^{ICCG}) coupled with incubation at the desired temperature under agitation at 180 rpm. Samples were taken at multiple time points, quenched and prepared for UPLC analysis as detailed previously. The percentage depolymerisation of plastic was calculated using the mass of TPA and MHET produced, determined from the concentrations of each compound as detected by UPLC.

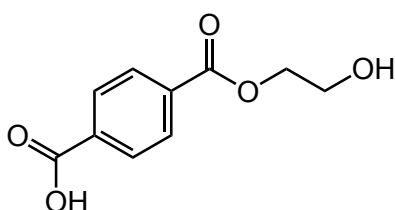
9.2.1.8 Chromatographic Analysis

UPLC analysis was performed on a 1290 Infinity II Agilent LC system including an autosampler with the UV detector set to 260 nm, using a Kinetex® XB-C18 100 Å, 5 µm, 50 x 2.1 mm, LC Column with a stepped, isocratic solvent ratio method. Mobile phase A was water containing 0.1% formic acid and mobile phase B was acetonitrile with a fixed flow rate of 1.1 mL min⁻¹. Either 1 µL or 4 µL of sample was injected for library screening reactions and time resolved assays, respectively. Following sample injection, the mobile phase was set to 13% buffer B for 52 seconds to separate TPA and MHET, stepped up to 95% buffer B for 33 seconds to separate larger reaction products and contaminants, and then stepped back down to 13% buffer B for column re-equilibration until a total run time of 1.8 minutes. Peaks were assigned by comparison to chemical standards prepared from commercial TPA and in-house synthesised MHET, and the peak areas integrated using Agilent OpenLab software. Using this method, TPA is eluted at ~0.4 minutes and MHET at ~0.6 minutes (Extended Data, Fig. 2). TPA and MHET concentrations were calculated by preparation of standard curves, reported in Extended Data, Fig. 16.

9.2.1.9 Melting Temperature Assessment

The melting temperatures (T_m) of *IsPETase*^{TS} and its variants were determined using differential scanning fluorimetry (DSF). 50 μ L samples of 5 μ M proteins were prepared in the reaction buffer (50 mM glycine-OH, pH 9.2) with a final concentration of 10X SYPRO Orange dye stock solution (Sigma-Aldrich) in optically clear lidded PCR tubes (Biorad). DSF melt-curve experiments were then carried out using a Biorad CFX Connect 96 Real-Time PCR system set on the FRET channel to use the 450/490 excitation and 560/580 emission filters. The temperature was increased from 25°C to 95°C with an increment of 0.3°C s⁻¹. The protein melting temperature was determined from the peak of the first derivatives of the melt-curve. Each T_m value corresponds to the average of three replicates.

9.2.1.10 Chemical Synthesis of Reaction Substrates and Standards



Preparation of Mono-2-hydroxyethyl Terephthalate (MHET). Commercial BHET (4 mM) was incubated at 40°C in buffer (glycine 0.1 M, pH 8.0) with *IsPETase*^{TS} (1 μ M). The reaction was acidified with 1 M HCl and extracted with ethyl acetate. The organic layer was dried with MgSO₄, filtered and the solvent was removed *in vacuo* to afford the crude product, which was purified by flash chromatography (cyclohexane: ethyl acetate, (1:1)). ¹H NMR (400 MHz, MeOD) δ 8.20 – 8.08 (m, 4H), 4.46 – 4.39 (m, 2H), 3.93 – 3.87 (m, 2H). ¹³C NMR (101 MHz, MeOD) δ 168.51, 167.04, 135.84, 134.99, 130.51, 130.41, 67.70, 60.85. NMR data is provided in Supplementary Information.

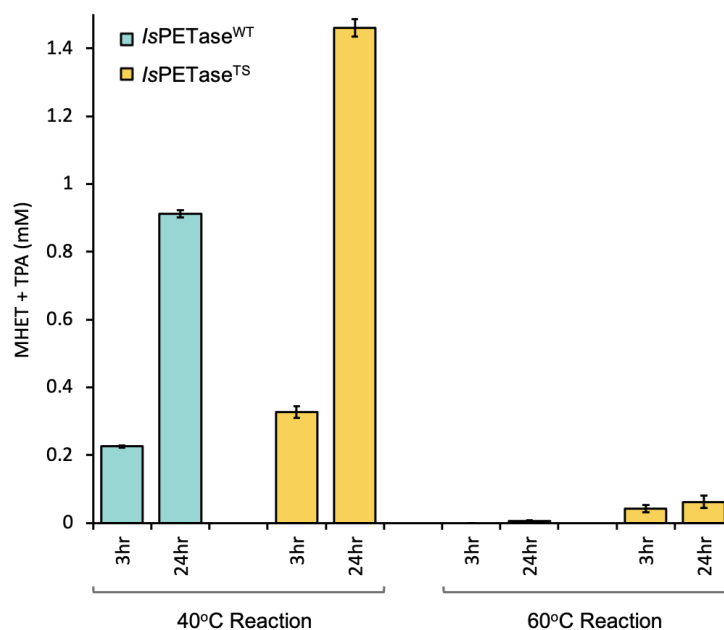
9.2.1.11 Structure Determination of HotPETase

Protein crystallisation of HotPETase was achieved by sitting drop vapour diffusion of 200 nL of 6 mg mL⁻¹ protein mixed with an equal volume of reservoir solution and incubated at 4°C. Crystals were observed after 72 hrs incubation with a reservoir solution comprised of 0.85 M sodium citrate tribasic dehydrate, 0.1 M Tris pH 8.0 and 0.1 M sodium chloride (LMB screen HT96 H7 Molecular Dimensions). Prior to data collection crystals were cryo-protected with the addition of 20% PEG 200 to the mother liquor and plunge cooled in liquid nitrogen. All data were collected at Diamond Light Source (Harwell, UK). Data reduction was performed with Dials and the structure solved by molecular replacement using a search model derived from *IsPETase* structure 5XJH. Model completion and refinement were performed in COOT and Phenix.refine respectively. Validation with MOLPROBITY and PDBREDO were incorporated into the iterative rebuild and refinement process. Data collection and refinement statistics are shown in Supplementary Information, Table 3.

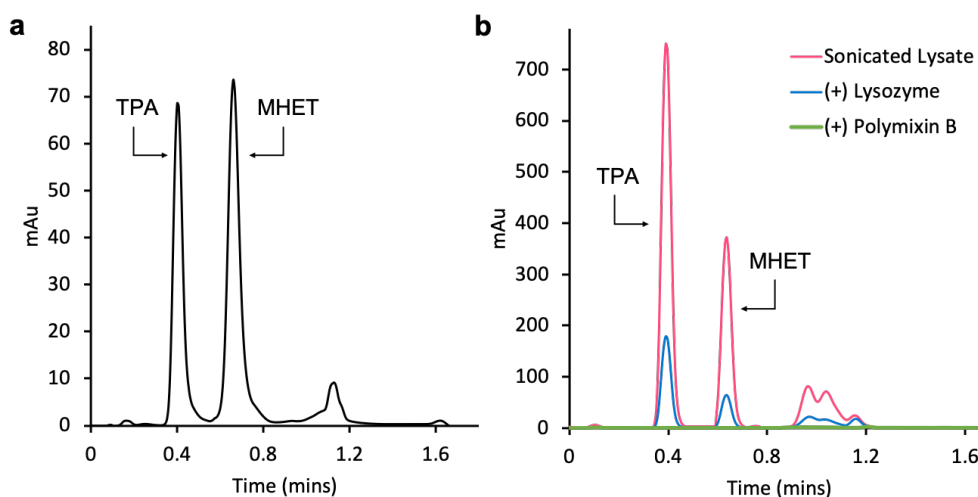
9.2.1.12 References

1. Son, H. F. *et al.* Rational Protein Engineering of Thermo-Stable PETase from *Ideonella sakaiensis* for Highly Efficient PET Degradation. *ACS Catalysis* **9**, 3519–3526 (2019).
2. Tournier, V. *et al.* An engineered PET depolymerase to break down and recycle plastic bottles. *Nature* **580**, 216–219 (2020).
3. Anderson, J. C. *et al.* BglBricks: A flexible standard for biological part assembly. *Journal of Biological Engineering* **4**, (2010).
4. Goldenzweig, A. *et al.* Automated Structure-and Sequence-Based Design of Proteins for High Bacterial Expression and Stability Molecular Cell Technology Automated Structure-and Sequence-Based Design of Proteins for High Bacterial Expression and Stability. *Molecular Cell* **63**, 337–346 (2016).
5. Reetz, M. T. & Carballera, J. D. Iterative saturation mutagenesis (ISM) for rapid directed evolution of functional enzymes. *Nature Protocols* **2**, 891–903 (2007).

9.2.2 Extended Data

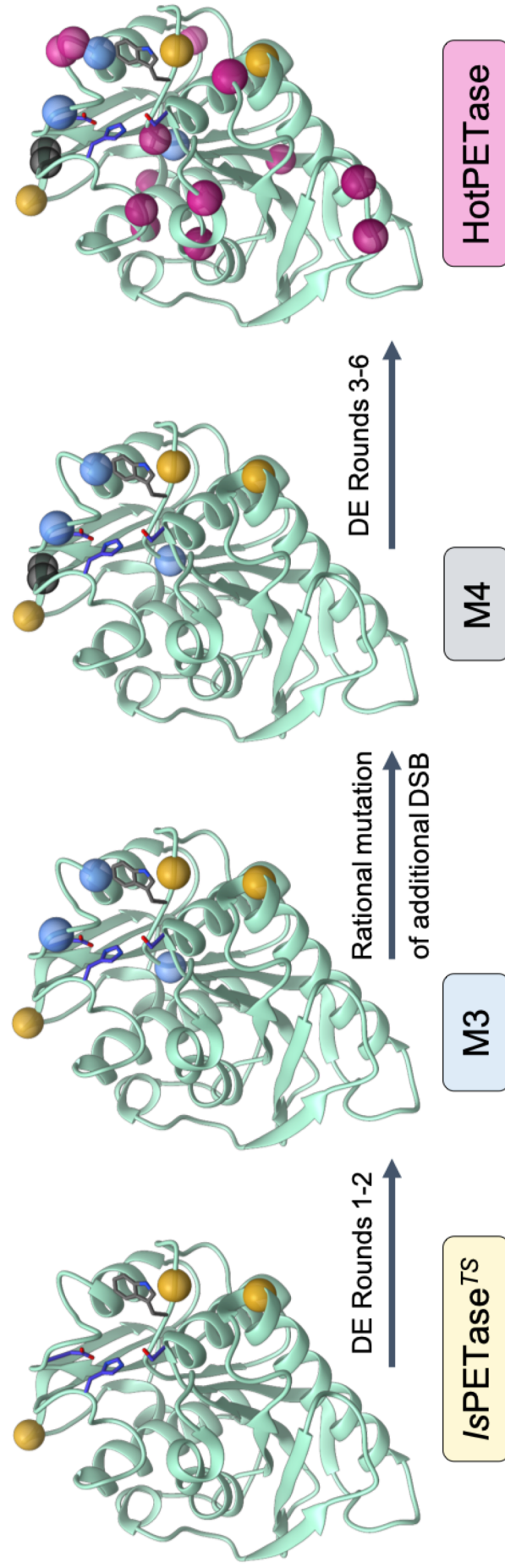


9.2.2.1 Extended Data, Figure 1. Comparison of *IsPETase*^{WT} with *IsPETase*^{TS} at 40°C and 60°C. Bar chart showing total MHET and TPA produced following reaction of *IsPETase*^{WT} (0.04 μM , gold) and *IsPETase*^{TS} (0.04 μM , turquoise) at either 40°C or 60°C over the course of 24 hrs with semi-crystalline PET powder substrate (4 mg mL⁻¹, cryPET). The amount of soluble PET degradation products released by *IsPETase*^{WT} after 3 hrs was too low to be detected by our analysis methods. Reactions were carried out in duplicate and error bars represent the s.d. of the replicates.



9.2.2.2 Extended Data, Figure 2. UPLC method for detection of MHET and TPA following PET deconstruction by pure protein and cell lysate. (a) Example UPLC trace for the deconstruction of cryPET (4 mg mL⁻¹) by purified *IsPETase*^{TS} protein (0.04 μM). (b) UPLC traces for deconstruction of amoPET using *IsPETase*^{TS} cell lysate. Addition of either 0.5 mg mL⁻¹ polymyxin B (blue) or 1 mg mL⁻¹ lysozyme (green) to lysate produced by sonication (pink) drastically reduces the amount of MHET and TPA produced in subsequent 220 μL reactions with an amoPET disc substrate at 40°C over the course of 5 hrs.

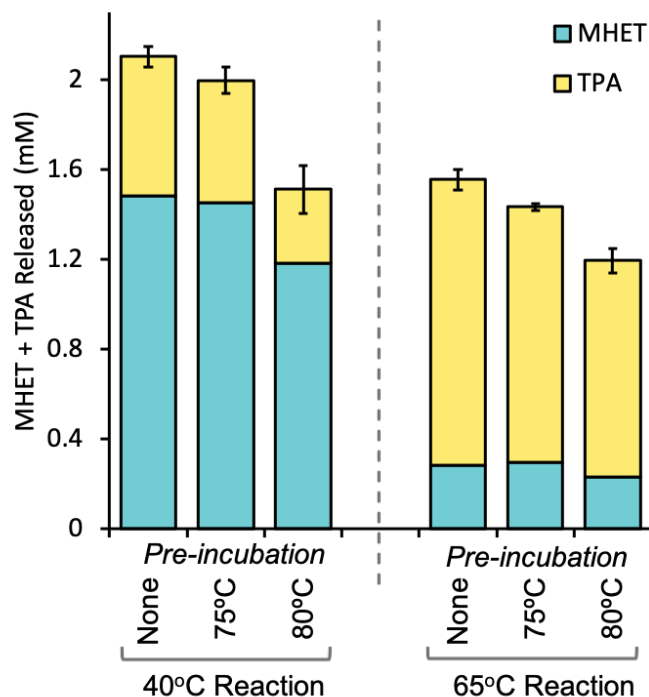
9.2.2.3 Extended Data, Figure 3. Overview of Directed Evolution strategy and outcomes. The crystal structures represent an overview of the evolution, with the *IsPETase*^{TS} protein represented as a turquoise ribbon, and mutations highlighted with spheres. The catalytic triad is represented as blue sticks. In the associated table (below), the residues mutated and the reasons for their selection for each directed evolution round are detailed; important reaction screening condition parameters that changed through the evolution rounds are highlighted in bold. The gene sequence used as the template for beneficial diversity shuffling (shuffling) is underlined. Any differences between the screening conditions used for the round of evolution and the conditions used to calculate the fold-change in activity for the best variant at each stage are identified in italics.



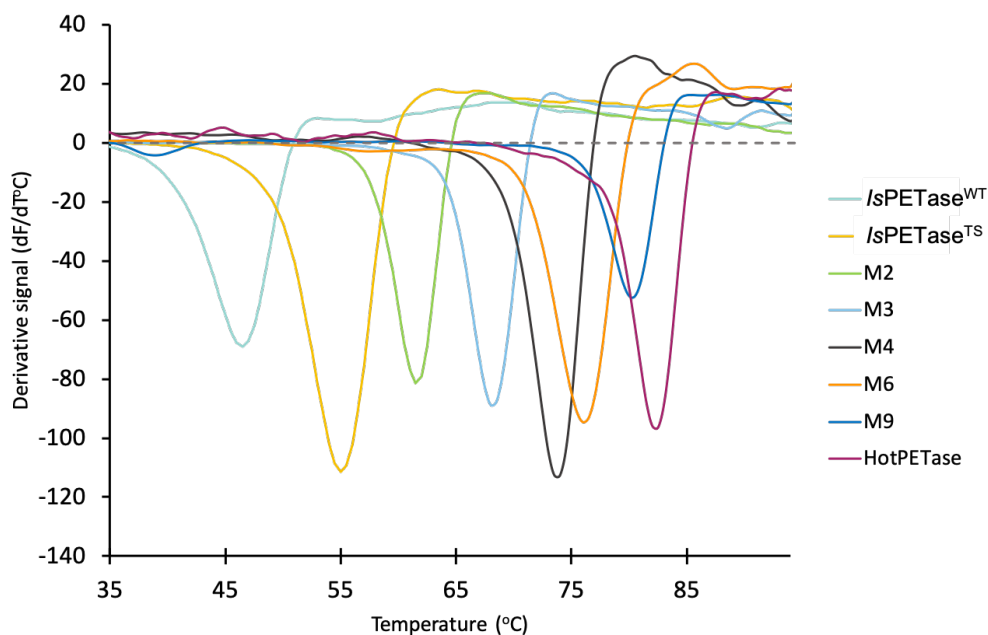
Round	Description	Screening Condition	Beneficial Mutations	Best Variant	Fold Change in Activity
1	<p>Saturation mutagenesis of positions potentially important for stability or catalysis identified by PROSS,¹ Han <i>et al.</i> (2017),² Ma <i>et al.</i> (2018),³ Austin <i>et al.</i> (2018),⁴ Joo <i>et al.</i> (2018)⁵ & Son <i>et al.</i> (2019)⁶: A47, T77, T88, R90, LI17, EI21, SI25, RI32, VI34, GI39, AI52, W159, II68, P181, W185, HI86, S207, I208, S238, A240, N241, M262, T270, A280.</p>	<p>Pre-incubate cell lysate for 1 hr at 55°C, then incubate amoPET disc in 96-well plate for 3 hrs at 55°C, with 220 µL cell lysate, 2300 clones screened.</p>	<p>EI21A, AI52V, P181V, HI86A, S207R.</p>	Best Variant from DE Round 1 (M1): <u>I</u> sPETase ^{TS} + S207R	2.96-fold increase in activity (Purified protein)
				Best Variant after shuffling (M2): <u>M</u> I + P181V	1.63-fold increase in activity (Purified protein)
2	<p>Saturation mutagenesis of positions identified as beneficial in DE Round 1 and positions identified computationally as potentially important for enzyme thermostability by Cui <i>et al.</i> (2019)⁷: T77, T88, K95, LI17, QII9, EI21, SI25, TI40, KI48, AI52, W159, GI65, SI66, II68, AI80, HI86, SI87, SI88, I208, N212, S214, S238, A248, A280.</p>	<p>Pre-incubate cell lysate for 1 hr at 60°C, then incubate amoPET disc in 96-well plate for 3 hrs at 60°C, with 220 µL cell lysate, 2300 clones screened.</p>	<p>K95A, K95S, K95N, QII9T, SI25V, SI25L, AI52G, GI65A, AI80C, N212A, S214C, S214Y, S214V.</p>	Best Variant from DE Round 2 (M3): <u>M</u> 2 + S214Y	2.89-fold increase in activity (Purified protein)

Rational insertion of additional disulphide bond (DSB)		3.14-fold increase in activity (Pure protein, 65°C)
	M4: <u>M3</u> + N233C + S282C	
3	<p>Saturation mutagenesis of positions identified as beneficial in DE Round 2, positions identified as part of the substrate binding pocket by Tournier <i>et al.</i> (2020)⁸ and positions that form part of loop connecting β7-α2: G86, Y87, T88, A89, S93, I94, K95, W70, K99, Q119, S125, A152, M161, G165, A183, W185, R207, I208, A209, P210, V211, N212, S213, S214.</p> <p>Pre-incubate cell lysate for 1 hr at 65°C, then incubate amoPET disc in 96-well plate for 3 hrs at 65°C, with 120 μL cell lysate + 100 μL buffer, 2300 clones screened.</p>	<p>Best Variant from DE Round 3 (M5): <u>M4</u> + S213E</p> <p>Best Variant after shuffling (M6): <u>M5</u> + Q119K</p> <p>Y87L, Q119K, S125E, S213E.</p> <p>1.96-fold increase in activity (Purified protein)</p> <p>2.35-fold increase in activity (Purified protein, 70°C)</p>
4	<p>Saturation mutagenesis of positions identified as beneficial in DE Round 3, positions identified as being important for protein flexibility (high B-factor values) by B-Fitter program,⁹ positions possibly involved in substrate binding identified by Sagong <i>et al.</i> (2020),¹⁰ residues adjacent to other positions fixed during previous DE Rounds: R34, R53, R59, Y87, T88, R90, P120, S125, A180, N205, A209, N212, R224, I232, G234, S279, S238, S242, N246, N277, T279, L291.</p> <p>Pre-incubate cell lysate for 1 hr at 75°C, then incubate amoPET disc in 96-well plate for 3 hrs at 70°C with 120 μL pre-incubated cell lysate + 200 μL buffer, 2100 clones screened.</p>	<p>Best Variant from DE Round 4 (M7): <u>M6</u> + R90T</p> <p>Best Variant after shuffling (M8): <u>M7</u> + N212K + R224L</p> <p>1.89-fold increase in activity (Purified protein)</p> <p>1.59-fold increase in activity (Purified protein)</p>

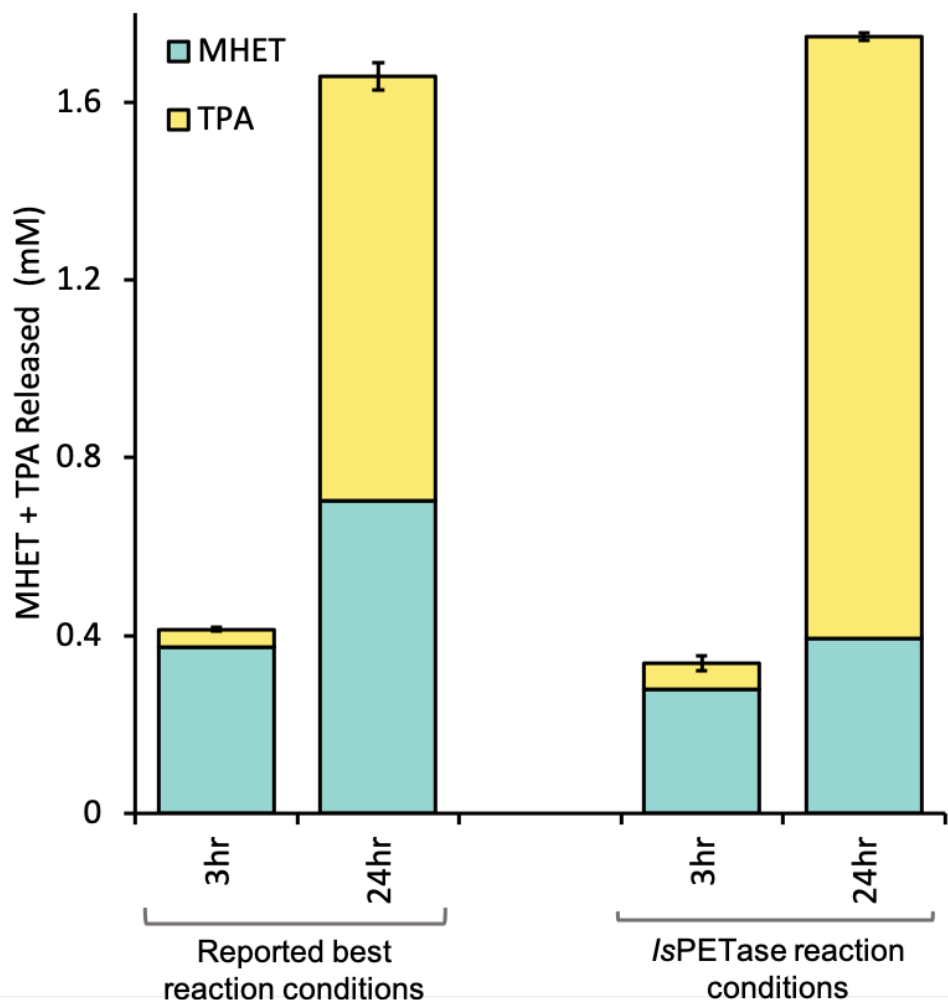
	<p>Saturation mutagenesis of positions identified as beneficial in previous DE Rounds, positions at the end of α-helices and β-sheets in the protein crystal structure: T39, A45, P49, S61, Y87, S93, K95, G98, S103, T113, S115, D118, P120, E121, G139, S143, V149, A152, M154, W159, G163, G165, N173, A178, Q182, A183, H186, S192, V194, S221, N246, D263.</p>	<p>Pre-incubate cell lysate for 1 hr at 80°C, then incubate amoPET disc in 96-well plate for 5 hrs at 70°C with 120 μL pre-incubated cell lysate + 280 μL buffer, 1930 clones screened.</p>	<p>Best Variant from DE Round 5 (M9): <u>M8</u> + Q182M</p> <p>Best Variant after shuffling (M10): <u>M9</u> + S61V + K95N</p>	<p>1.13-fold increase in activity (Purified protein, 5 mL reaction, cryPET powder substrate)</p> <p>1.19-fold increase in activity (as above)</p>
5				
	<p>Saturation mutagenesis of positions identified as beneficial in previous DE Rounds, positions adjacent to residue hits in previous DE Rounds, residues that form part of loop connecting β1-β2 as identified by da Costa <i>et al.</i> (2021),¹¹ previously mutationally unexplored regions of α-helix and β-sheet regions as identified on the protein's crystal structure: S58, R59, P60, S61, G62, Y63, G64, A65, I94, W96, Q127, RB2, V134, M154, W159, G163, S169, A180, M182, P184, W185, H186, V211, E213, Y214, A215, F229, N241, N244, K252, G254, T270.</p>	<p>Incubate amoPET disc in 96-well plate for 7 hrs at 70°C with 60 μL cell lysate + 340 μL buffer, 2300 clones screened.</p>	<p>Best Variant after 1st shuffling (M11): <u>M10</u> + N241C + K252M</p> <p>Best Variant after 2nd shuffling (M12): <u>M11</u> + S58A + M154G</p> <p>Best Variant after 3rd shuffling (HotPETase): <u>M12</u> + T270Q</p>	<p>1.4-fold increase in activity (Purified protein, 5 mL reaction, cryPET powder substrate, 24 hr reaction)</p> <p>1.16-fold increase in activity (as above)</p> <p>1.19-fold increase in activity (as above)</p>
6				



9.2.2.4 Extended Data, Figure 4. Reactions with HotPETase pre-incubated at elevated temperature prior to reaction. Bar chart showing accumulation of MHET (blue) and TPA (yellow) in 40°C and 60°C reactions with HotPETase (0.04 μM) that had been pre-incubated for 90 mins at the stated temperature prior to reaction, using cryPET (20 mg) as the reaction substrate. Reactions were carried out in duplicate and error bars represent the s.d. of the total MHET and TPA produced by the replicates.

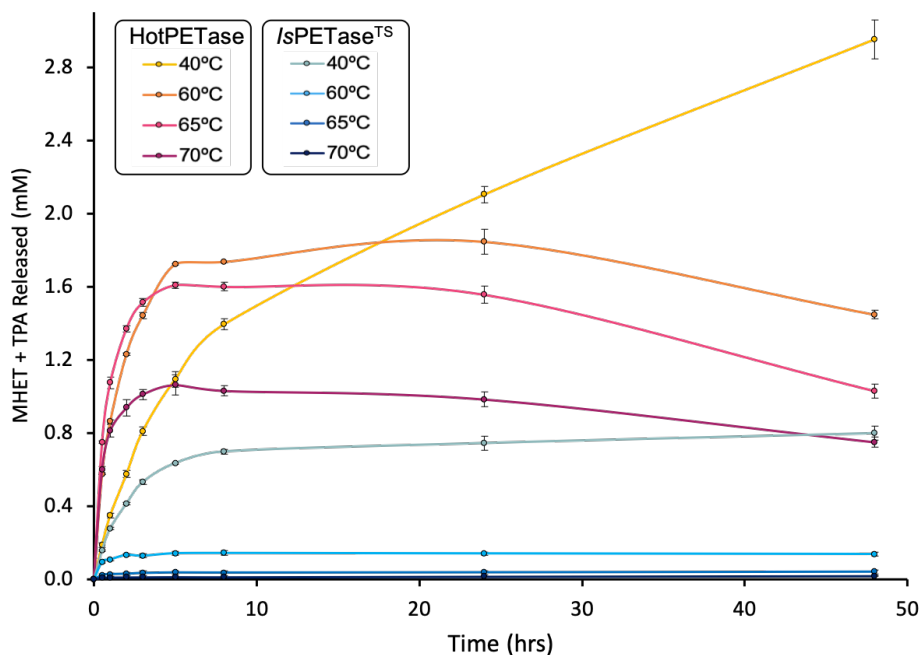


9.2.2.5 Extended Data, Figure 5. Melt curves for variants of *IsPETase* along the directed evolution trajectory. Melt curve readings were carried out in triplicate.

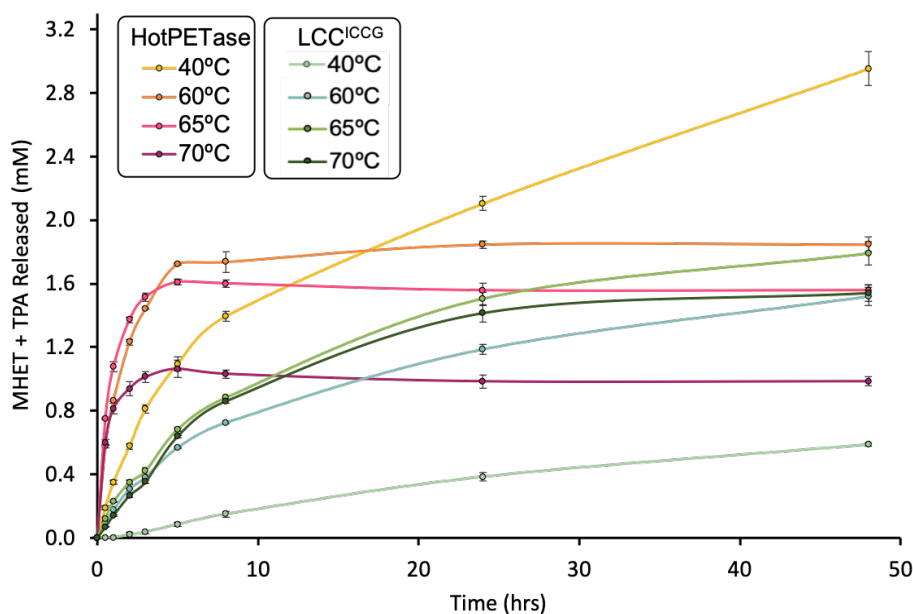


9.2.2.6 Extended Data, Figure 6. Reactions with LCC^{ICCG} under different buffer conditions.

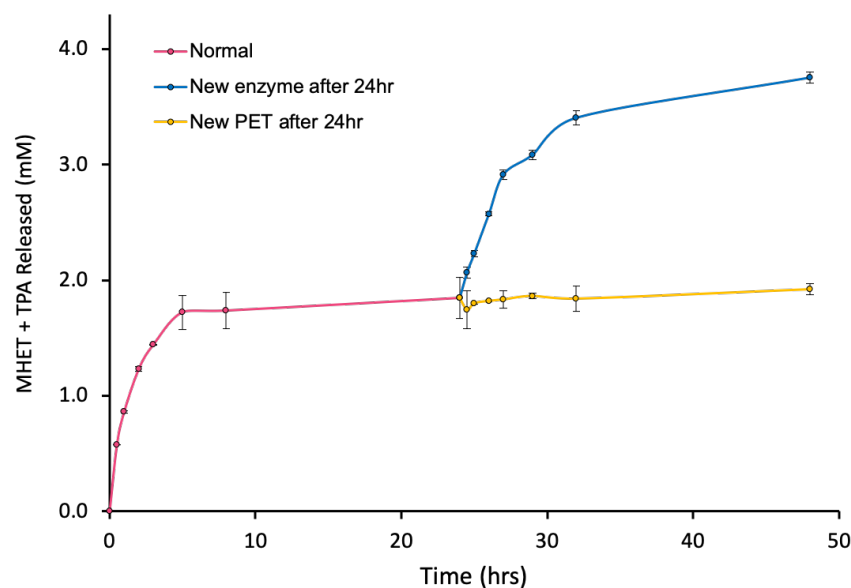
Bar chart showing the accumulation of MHET (blue) and TPA (yellow) over 24 hrs in 60°C reactions with LCC^{ICCG} (0.04 μM) using cryPET (4 mg mL⁻¹) as the reaction substrate. Reactions were carried out using either the reported best conditions for LCC^{ICCG} (100 mM potassium phosphate buffer, pH 8) or the best reaction conditions for IsPETase and its derivatives reported here (50 mM glycine-OH, 4% BugBuster, pH 9.2). Reactions were carried out in duplicate and error bars represent the s.d. of the total MHET and TPA produced by the replicates.



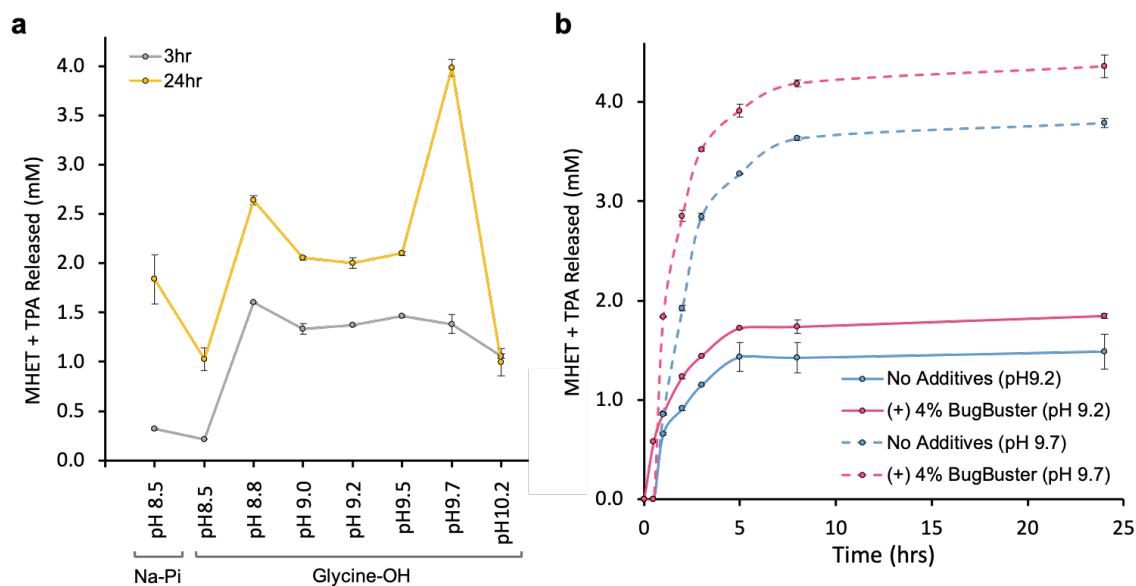
9.2.2.7 Extended Data, Figure 7. Comparison of reactions with *IsPETase*^{TS} and HotPETase over a range of temperatures. 48-hr time-courses of cryPET (4 mg mL⁻¹) reactions, showing total released MHET and TPA, with HotPETase (0.04 μM, yellow-pink) and *IsPETase*^{TS} (0.04 μM, blues) over time. Reactions were carried out in triplicate and error bars represent the s.d. of the replicate measurements.



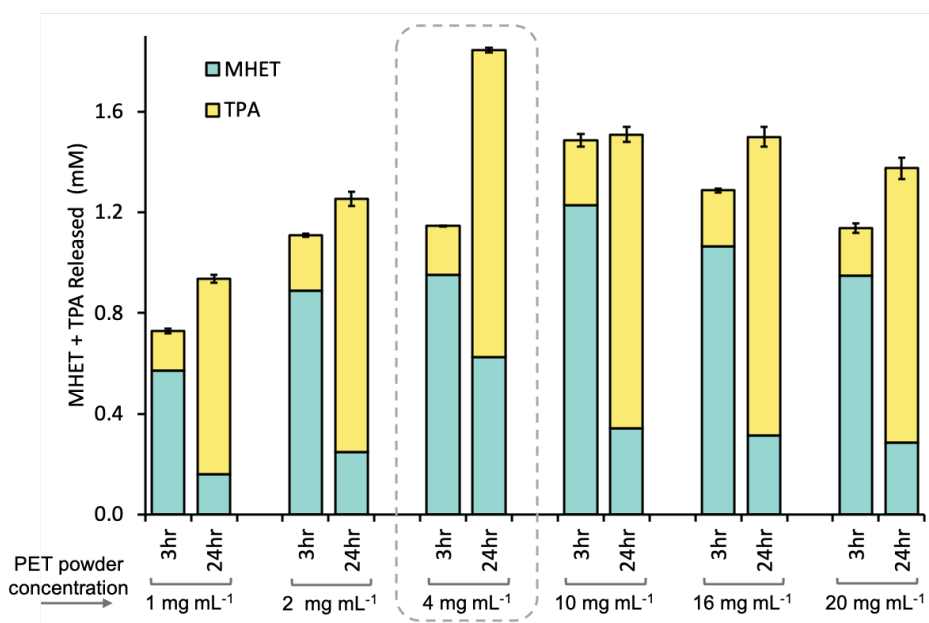
9.2.2.8 Extended Data, Figure 8. Comparison of reactions with HotPETase and LCC^{ICCG} over a range of temperatures. 48-hr time-courses of cryPET (4 mg mL⁻¹) reactions, showing total released MHET and TPA with HotPETase (0.04 μM, yellow-pinks) and LCC^{ICCG} (0.04 μM, greens) over time, at a range of temperatures. Enzymes were assayed at their optimal pHs, as reported in the Methods. Reactions were carried out in triplicate and error bars represent the s.d. of the replicate measurements.



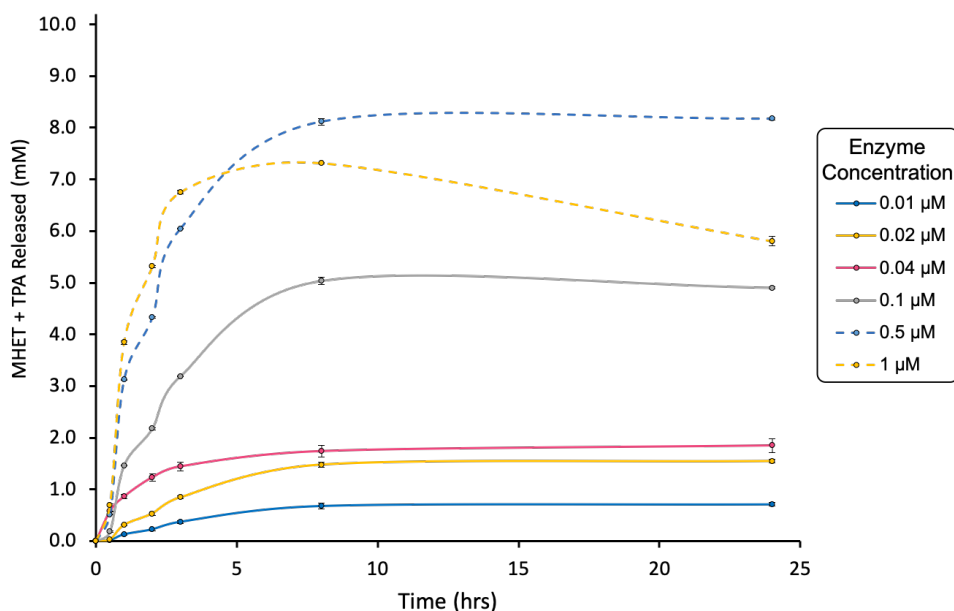
9.2.2.9 Extended Data, Figure 9. Comparison of reactions with additional enzyme or substrate added. 48-hr time-courses of cryPET (4 mg mL^{-1}) reactions, showing total released MHET and TPA, where following reaction with HotPETase ($0.04 \text{ } \mu\text{M}$) at 60°C for 24 hrs (pink), either $0.04 \text{ } \mu\text{M}$ fresh enzyme (blue) or 20 mg fresh cryPET substrate (yellow) was added.



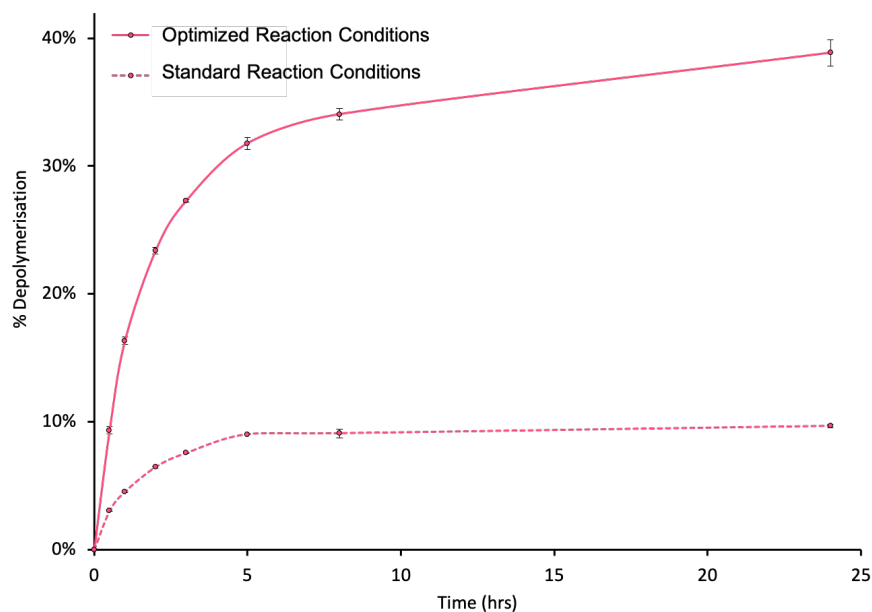
9.2.2.10 Extended Data, Figure 10. Comparison of HotPETase with different reactions buffer compositions. (a) Line graph showing total released MHET and TPA after either 3 hrs (grey) or 24 hrs (yellow) following reaction of HotPETase ($0.04 \text{ } \mu\text{M}$) at 60°C with cryPET (4 mg mL^{-1}) as the reaction substrate. Reactions were carried out in sodium phosphate buffer (100 mM) or glycine-OH buffer (50 mM) with 4% BugBuster, over a range of pHs. Reactions were carried out in duplicate; error bars represent the s.d. of the replicate measurements. (b) 24-hr time-courses of cryPET (4 mg mL^{-1}) reactions, showing total released MHET and TPA, in reactions with HotPETase ($0.04 \text{ } \mu\text{M}$) at 60°C . Reactions were carried out in 100 mM Glycine-OH, pH 9.2 (solid lines) or pH 9.7 (dashed lines) with (pink) or without (blue) 4% BugBuster. Reactions were carried out in duplicate and error bars represent the s.d. of the replicate measurements.



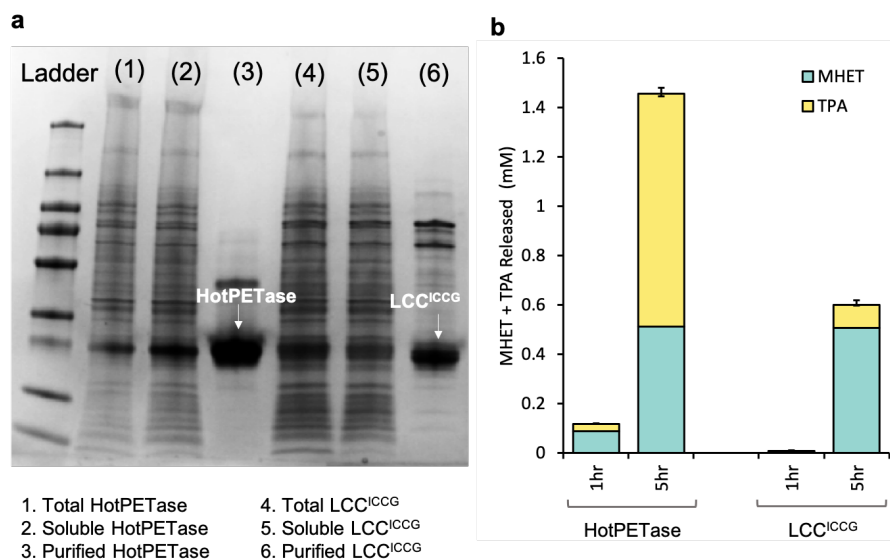
9.2.2.11 Extended Data, Figure 11. Comparison of HotPETase activity at different substrate concentrations. Bar chart showing accumulation of MHET (blue) and TPA (yellow) over 24 hrs in 60°C reactions with HotPETase (0.04 μM) using different concentrations of cryPET as the reaction substrate. The standard concentration of cryPET used in all reactions presented here was 4 mg mL⁻¹. Reactions were carried out in duplicate and error bars represent the s.d. of the total MHET and TPA produced by the replicates.



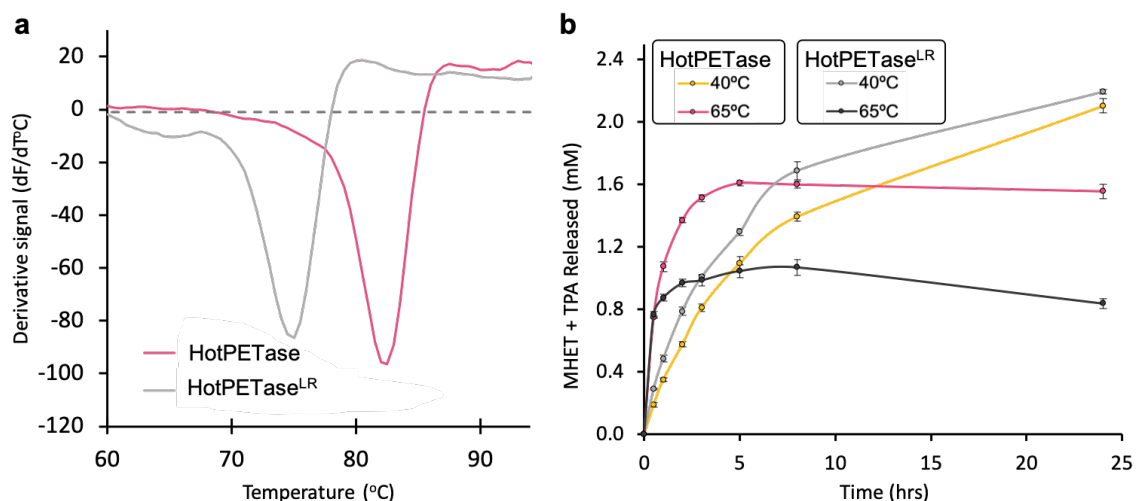
9.2.2.12 Extended Data, Figure 12. Comparison of HotPETase activity at different enzyme concentrations. 24-hr time-courses, showing total released MHET and TPA, in reactions at 60°C with cryPET (4 mg mL⁻¹) as the reaction substrate where the concentration of with HotPETase in the reaction was varied. Reactions were carried out in duplicate and error bars represent the s.d. of the replicate measurements.



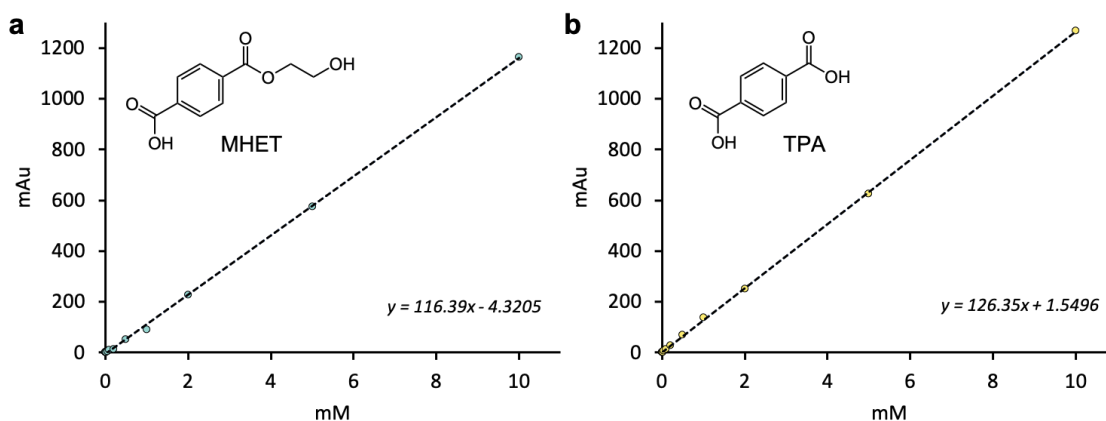
9.2.2.13 Extended Data, Figure 13. Comparison HotPETase activity under standard and optimised reaction conditions. 24-hr time-course of reactions conducted at 60°C, with HotPETase, showing percentage of 20 mg of cryPET (4 mg mL⁻¹) depolymerised, calculated using the concentration of MHET and TPA produced. Standard reaction conditions were 0.04 μM enzyme in 50 mM glycine-OH buffer, pH 9.2, with 4% BugBuster (dashed line). Optimised reaction conditions were 0.5 μM enzyme in 50 mM glycine-OH buffer, pH 9.7, with 4% BugBuster (solid line). Reactions were carried out in triplicate; error bars represent the s.d. of the replicate measurements.



9.2.2.14 Extended Data, Figure 14. Comparison of the expression of HotPETase and LCC^{ICCG} and their activities as cell lysates. (a) SDS-PAGE gel showing total, soluble and purified protein expression fractions from 50 mL expression cultures. (b) Bar chart showing accumulation of MHET (blue) and TPA (yellow) over 5 hrs in 60°C reactions with 5 mL of HotPETase or LCC^{ICCG} cell lysate, using cryPET (4 mg mL⁻¹) as the reaction substrate. Cell lysates were assayed in their optimal pHs, as reported in the Methods. Reactions were carried out in duplicate; error bars represent the s.d. of the replicate measurements.



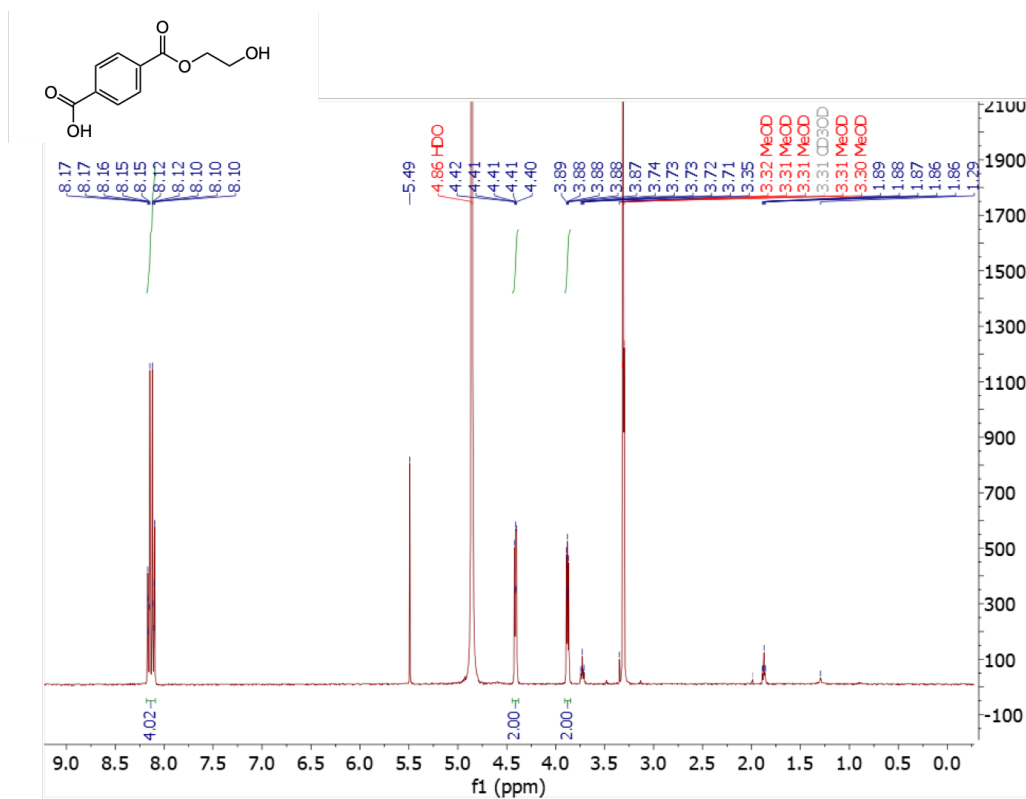
9.2.2.15 Extended Data, Figure 15. Comparison of HotPETase and HotPETase^{LR}. (a) Melt curves for HotPETase and HotPETase^{LR}. Melt curve readings were carried out in triplicate. (b) 24-hr time-courses, showing total released MHET and TPA, in reactions at either 40°C or 65°C with either HotPETase (0.04 μM) or HotPETase^{LR} (0.04 μM), with cryPET (4 mg mL⁻¹) as the reaction substrate. Reactions were carried out in triplicate; error bars represent the s.d. of the replicate measurements.



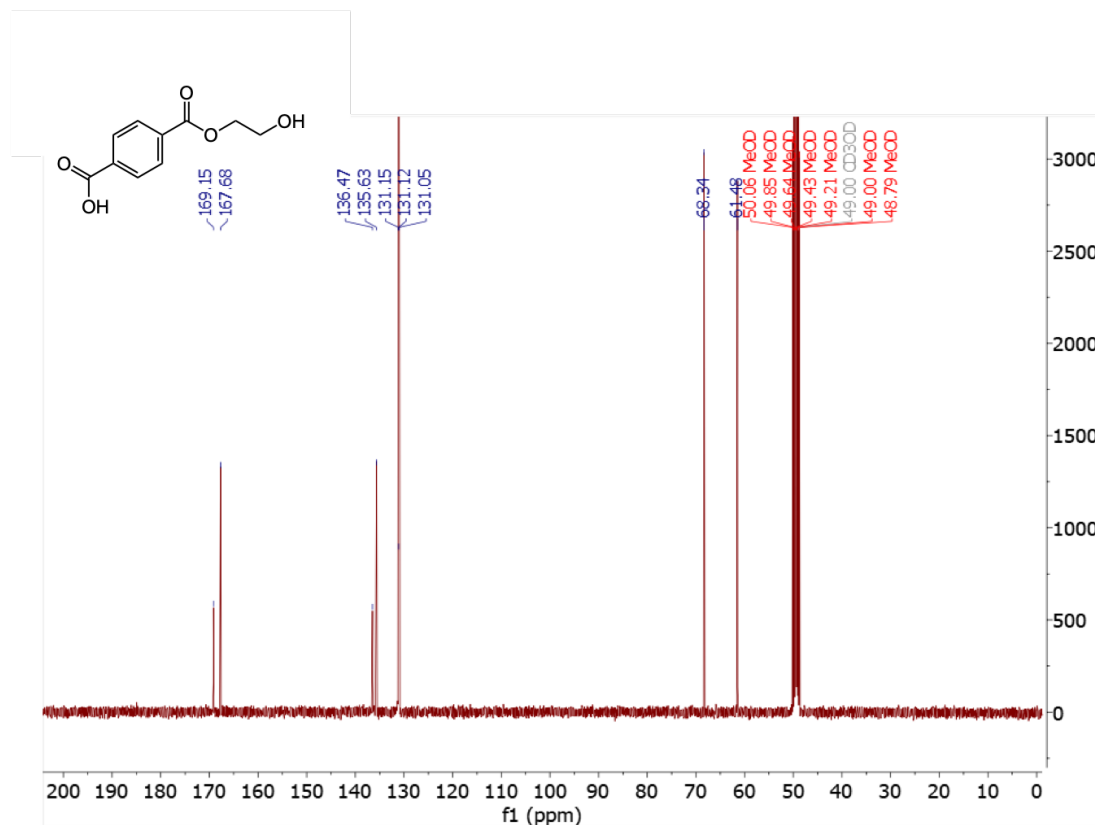
9.2.2.16 Extended Data, Figure 16. Calibration plots for MHET and TPA. (a) Calibration for in-house synthesised MHET. (b) Calibration curve for commercial TPA. For both calibration plots, points represent the mean of three triplicate readings. Error bars are too small to be visualised.

9.2.2.17 NMR Spectra.

Mono-2-hydroxyethyl Terephthalate (MHET). ^1H NMR (400 MHz, MeOD)



Mono-2-hydroxyethyl Terephthalate (MHET). ^{13}C NMR (101 MHz, MeOD)



9.2.2.18 References

1. Goldenzweig, A. *et al.* Automated Structure-and Sequence-Based Design of Proteins for High Bacterial Expression and Stability. *Molecular Cell Technology Automated Structure-and Sequence-Based Design of Proteins for High Bacterial Expression and Stability. Molecular Cell* **63**, 337–346 (2016).
2. Han, X. *et al.* Structural insight into catalytic mechanism of PET hydrolase. *Nature Communications* **8**, 2106 (2017).
3. Ma, Y. *et al.* Enhanced Poly(ethylene terephthalate) Hydrolase Activity by Protein Engineering. *Engineering* **4**, 888–893 (2018).
4. Son, H. F. *et al.* Rational Protein Engineering of Thermo-Stable PETase from *Ideonella sakaiensis* for Highly Efficient PET Degradation. *ACS Catalysis* **9**, 3519–3526 (2019).
5. Austin, H. P. *et al.* Characterization and engineering of a plastic-degrading aromatic polyesterase. *Proceedings of the National Academy of Sciences of the United States of America* **115**, E4350–E4357 (2018).
6. Joo, S. *et al.* Structural insight into molecular mechanism of poly(ethylene terephthalate) degradation. *Nature Communications* **9**, 382 (2018).
7. Cui, Y. *et al.* Computational redesign of PETase for plastic biodegradation by GRAPE strategy. *bioRxiv* (2019).
8. Tournier, V. *et al.* An engineered PET depolymerase to break down and recycle plastic bottles. *Nature* **580**, 216–219 (2020).
9. Reetz, M. T. & Carballera, J. D. Iterative saturation mutagenesis (ISM) for rapid directed evolution of functional enzymes. *Nature Protocols* **2**, 891–903 (2007).
10. Sagong, H.-Y. *et al.* Decomposition of the PET Film by MHETase Using Exo-PETase Function. *ACS Catalysis* 4805–4812 (2020).
11. da Costa, C. H. S. *et al.* Assessment of the PETase conformational changes induced by poly(ethylene terephthalate) binding. *Proteins: Structure, Function, and Bioinformatics* (2021).

9.2.3 Supplementary Information

9.2.3.1 Supplementary Information, Figure 1. Nucleotide and expressed amino sequence for production of *IsPETase*^{TS} and LCC^{ICCG}. For the expressed amino acid sequence of *IsPETase*^{TS}, mutated residues different from the wildtype protein are highlighted in bold and underlined. For HotPETase, the mutations introduced via directed evolution are in bold and underlined, the active site residues are coloured green, the mutated residues present in the starting protein are coloured red, and the rationally inserted cystines are coloured blue. For LCC^{ICCG}, the mutated residues different from the wildtype protein are highlighted in bold and underlined. All sequences were codon-optimized for expression in *E. coli* and were inserted between NdeI and XhoI restriction enzyme sites of the bacterial expression plasmids.

***IsPETase*^{TS} Nucleotide Sequence:**

```
ATGCAGACTAACCCCTATGCTCGCGGGCCGAATCCTACAGCGGCCTCGTTGGAAGCCAG
TGCAGGTCCTTCACCGTACGTTTCGTTTACTGTTTCCCGTCCATCTGGATATGGGGCTGG
CACCGTCTATTATCCGACTAACGCCGGTGGTACTGTGGGCGCAATCGCCATTGTCCCCG
GCTACACTGCACGCCAATCCTCGATTAAATGGTGGGGACCACGCTTGGCTAGCCACGGG
TTTGTGTTGATCACCATCGATACTAACAGTACGTTGGACCAGCCAGAGAGTCGCAGCTC
TCAGCAGATGGCGGCATTACGCCAGGTGGCGAGCTTAAATGGGACGAGTTCAAGTCCAA
TTTATGGCAAGGTCGATACCGCCCGTATGGGAGTAATGGGCTGGAGTATGGGTGGCGGC
GGATCTCTTATCTCGGCAGCGAATAATCCAAGCCTGAAGGCAGCAGCCCCGCAGGCACC
CTGGCATAGTAGTACGAACCTTTTCGTTCTGTTACGGTTCCTACGCTTATCTTTGCCTGTGA
GAATGATTCTATCGCACCAGTGAACCTCATCAGCCTTGCCAATTTACGACTCGATGTTCGG
CAACGCTAAACAGTTTCTTGAGATTAATGGGGGCTCTCACTCTTGTGCCAACAGTGGGA
ATTCCAATCAAGCCCTTATCGGAAAAAAGGGCGTTGCTTGGATGAAGCGCTTCATGGAC
AATGACACTCGTTATTCAACTTTTCGTTGCGAAAACCCAAACTCAACCGCCGTATCCGAT
TTTCGCACTGCTAACTGCAGC
```

***IsPETase*^{TS} Expressed Amino Acid Sequence (amino acid numbering starts at 27):**

```
M27QTNPYARGPNPTAASLEASAGPFTVRSFTVSRPSGYGAGTVYYPTNAGGTVGAIAIVPGY
TARQSSIKWWGPRLASHGFVVITIDTNSTLDQPESRSSQQMAALRQVASLNGTSSSPIYGKV
DTARMGVMGWSMGGGSLISAANNPSLKAAAPQAPWHSSTNFSSVTVPTLIFACENDSIAP
VNSSALPIYDSMSRNAKQFLEINGGSHSCANSNGNSNQALIGKKGVAWMKRFMDNDTRYST
FACENPNSTAVSDFRTANCS
```


HotPETase_Nucleotide Sequence:

ATGCAGACTAACCCCTATGCTCGCGGGCCGAATCCTACAGCGGCCTCGTTGGAAGCCAG
TGCAGGTCCTTCACCGTACGTTCTGTTACTGTTGCGCGTCCAGTGGGATATGGGGCTG
GCACCGTCTATTATCCGACTAACGCCGGTGGTACTGTGGGCGCAATCGCCATTGTCCCC
GGCTACACTGCAACTCAATCCTCGATTAATTGGTGGGGACCACGCTTGGCTAGCCACGG
GTTTGTGTGATCACCATCGATACTAACAGTACGTTGGACAAGCCAGAGAGTCGCAGCT
CTCAGCAGATGGCGGCATTACGCCAGGTGGCGAGCTTAAATGGGACGAGTTCAAGTCCA
ATTTATGGCAAGGTCGATACCGCCCGTGGTGGAGTAATGGGCTGGAGTATGGGTGGCGG
CGGATCTTTATCTCGGCAGCGAATAATCCAAGCCTGAAGGCAGCAGCCGTTATGGCAC
CCTGGCATAAGTAGTACGAACTTTTCGCTCTGTTACGGTTCCTACGCTTATCTTTGCCTGTG
AGAATGATAGGATCGCACCAGTGAAGGAGTACGCCTTGCCAATTTACGACTCGATGTGC
CTCAACGCTAAACAGTTTCTTGAGATTTGTGGGGGCTCTCACTCTTGTGCCTGTAGTGGG
AATTCCAATCAAGCCCTTATCGGAATGAAGGGCGTTGCTTGGATGAAGCGCTTCATGGA
CAATGACACTCGTTATTCACAGTTCGCTTGCGAAAACCCAACTCAACCGCCGTATGTG
ATTTTCGCACTGCTAACTGCAGC

HotPETase Expressed Amino Acid Sequence (amino acid numbering starts at 27):

M²⁷QTNPYARGPNPTAASLEASAGPFTVRSFTVARPVGYGAGTVYYPTNAGGTVGAIAIVPGY
TATQSSINWWGPRLASHGFVVITIDNSTLDKPESRSSQQMAALRQVASLNGTSSSPIYGKV
DTARGVVMGWSMGGGSLISAANNPSLKAAAVMAPWHSSTNFSSVTVPTLIFACENDRIA
PVKEYALPIYDSMSLNAKQFLEICGGSHSCASGNSNQALIGMKGVAVWMKRFMDNDTRY
QFACENPNSTAVCDFRTANCS

LCC^{ICCG} Nucleotide Sequence:

ATGAGCAACCCGTACCAGCGTGGCCCGAATCCGACCCGCAGCGCACTGACCGCAGATGG
CCCGTTTAGCGTGGCAACCTACACCGTCTCACGCCTGTCAGTCTCGGGTTTTGGCGGTG
GCGTGATTTATTACCCGACCGGCACGTCTCTGACGTTCCGGTGGCATCGCGATGAGTCCG
GGTTATACCGCAGATGCTAGCTCTCTGGCATGGCTGGGTCGTCGCCTGGCTTCCCATGG
CTTTGTGGTTCTGGTGATTAACACGAATTCACGTTTTGATGGCCCGGACAGCCGCGCCTC
TCAGCTGAGTGCCGCCCTGAACTACCTGCGTACCAGTTCCTCCGAGCGCCGTTTCGCGCAC
GTCTGGATGCAAATCGTCTGGCGGTTGCCGGTCATTCTATGGGTGGCGGTGGCACCCCTG
CGTATTGCAGAACAAAACCCGAGCCTGAAAGCGGCTGTCCCGCTGACCCCGTGGCACAC
CGATAAAACGTTTAATAACAGTGTCCCGGTGCTGATTGTTGGCGCAGAAGCTGACACCG
TGGCGCCGGTTTCGCAGCATGCCATCCCGTTTTATCAAACCTGCCGAGCACCACGCCG
AAAGTTTACGTCGAACTGTGCAACGCATCGCACATTGCTCCGAATAGCAACAATGCGGC
CATTTCCGTTTATACGATCTCATGGATGAACTGTGGGTCGATAATGACACCCGTTACCG
CCAGTTCCTGTGTAATGTGAACGACCCGGCTCTGTGCGACTTCCGCACCAATAATCGCC
ACTGCCAA

LCC^{ICCG} Expressed Amino Acid Sequence (amino acid numbering starts at 35):

M³⁵SNPYQRGPNPTRSALTADGPFVATYTVSRLSVSGFVGGVYYPTGTSFTFGGIAMSPGYT
ADASSLAWLGRRLASHGFVVLVINTNSRFDGPDSRASQLSALNYLRTSSPSAVRARLDANR
LAVAGHSMGGGGTLRIAEQNPSLKAAPLTPWHTDKTFNTSVPVLIVGAEADTVAPVSQH
AIPFYQNLPTTPKVYVELCNASHIAPNSNNAISVYTISWMKLWVDNDTRYRQFLCNVND
PALCDFRTNNRHCQ

9.2.3.2 Supplementary Information, Table 1. Primer sequences used to generate HotPETase^{LR}. Nucleotides which bind to the gene are in capitals, with overhangs in lower case.

Primer Name	Nucleotide Sequence
Nde_F	agaaggagatatacatATGCAGACTAACCCCT
Xho_R	ggtggtggtgCTCGAGGCTGCAGTTA
LR_F	TCGCACCAGTGAACATCATCTGCCTTGCCAATTTAC
LR_R	GTTCACCTGGTGCGATC

9.2.3.3 Supplementary Information, Table 2. Primer sequences used to generate DNA libraries. The forward (F) and reverse (R) library primers were paired with the opposite flanking primer to create two gene fragments, which when joined together formed the mutated gene. Bases which bind to the gene are in upper case, with overhangs in lowercase. Randomised codon positions are highlighted in red, where N = A, C, T, or G and K = T or G.

Flanking Primers	
Nde_F	agaaggagatatacatATGCAGACTAACCCCT
Xho_R	ggtggtggtgCTCGAGGCTGCAGTTA
Round 1	
A47_F	TCGTTGGAAGCCAGTNNKGGTCCCTTCACCGTA
A47_R	ACTGGCTTCCAACGA
T77_F	ACTAACGCCGGTGGTNNKGTGGGCGCAATCGCC
T77_R	ACCACCGGCGTTAGT
T88_F	ATTGTCCCCGGCTACNNKGCACGCCAATCCTC
T88_R	GTAGCCGGGGACAAT
R90_F	CCCGGCTACACTGCANNKCAATCCTCGATTAAATGGTGG
R90_R	TGCAGTGTAGCCGG
LII7_F	GATACTAACAGTACGNNKGACCAGCCAGAGAGT
LII7_R	CGTACTGTTAGTATCGATGG
SI21_F	ACGTTGGACCAGCCANNKAGTCGCAGCTCTCAG
SI21_R	TGGCTGGTCCAACG
SI25_F	CCAGAGAGTCGCAGCNNKCAGCAGATGGCGG
SI25_R	GCTGCCACTCTCTGG
RI32_F	CAGATGGCGGCATTANNKCAGGTGGCGAGCTTA
RI32_R	TAATGCCGCCATCTG
VI34_F	GCGGCATTACGCCAGNNKGCGAGCTTAAATGGGAC
VI34_R	CTGGCGTAATGCCG
GI39_F	GTGGCGAGCTTAAATNNKACGAGTTCAAGTCCAATTTATG
GI39_R	ATTTAAGCTCGCCACCT

Round 1**Continued.**

A152_F GGCAAGGTCGATACCNNKCGTATGGGAGTAATGGG
A152_R GGTATCGACCTTGCC
W159_F ATGGGAGTAATGGGCNNKAGTATGGGTGGCGG
W159_R GCCATTACTCCCATAC
I168_F GGCGGCGGATCTCTTNNKTCGGCAGCGAATAATC
I168_R AAGAGATCCGCCGC
P181_F CTGAAGGCAGCAGCCNNKCAGGCACCCTGG
P181_R GGCTGCTGCCTTC
W185_F GCCCCGCAGGCACCCNNKCATAGTAGTACGAACTTTTCGTC
W185_R GGGTGCCTGCG
D186_F CCGCAGGCACCCTGGNNKAGTAGTACGAACTTTTCGTC
D186_R CCAGGGTGCCTG
S207_F GCCTGTGAGAATGATNNKATCGCACCAGTGAAC
S207_R ATCATTCTCACAGGCAAAG
I208_F TGTGAGAATGATTCTNNKGCACCAGTGAACATC
I208_R AGAATCATTCTCACAGGCA
S238_F AATGGGGGCTCTCACNNKTGTGCCAACAGTGG
S238_R GTGAGAGCCCCATT
A240_F GGCTCTCACTCTTGTNNKAACAGTGGGAATTCCAATC
A240_R ACAAGAGTGAGAGCCC
N241_F TCTCACTCTTGTGCCNNKAGTGGGAATTCCAATCAAG
N241_R GGCACAAGAGTGAGAG
M262_F TGGATGAAGCGCTTCNNKGACAATGACACTCGTTATTCAA
M262_R GAAGCGCTTCATCCA
T270_F GACACTCGTTATTCANNNKTTCGCTTGCGAAAACC
T270_R TGAATAACGAGTGTCATTGTC
A280_F AACCCAAACTCAACCNNKGTATCCGATTTTCGCACTG
A280_R GGTTGAGTTTGGGTTTTTCG

Round 2

T77_R ACTAACGCCGGTGGTNNKGTGGGCGCAATCG
T77_F ACCACCGGCGTTAG
T88_F ATTGTCCTCCGGCTACNNKGCACGCCAATCCTC
T88_R GTAGCCGGGGACAAT
K95_F CGCCAATCCTCGATTNNKTGGTGGGGACCAC
K95_R AATCGAGGATTGGCGT
L117_F GATACTAACAGTACGNNKGACCAGCCAGAGAGT
L117_R CGTACTGTTAGTATCGATGG
Q119_F AACAGTACGTTGGACNNKCCAGAGAGTCGCAG
Q119_R GTCCAACGTACTGTTAGTATC
S121_F ACGTTGGACCAGCCANNKAGTCGCAGCTCTCAG
S121_R TGGCTGGTCCAACG
S125_F CCAGAGAGTCGCAGCNNKCAGCAGATGGCGG
S125_R GCTGCGACTCTCTGG
T140_F GCGAGCTTAAATGGGNNKAGTTCAAGTCCAATTTATGGC
T140_R CCCATTTAAGCTCGCC

Round 2**Continued.**

KI48_F AGTCCAATTTATGGC**NNK**GTCGATACCGCCC
KI48_R GCCATAAATTGGACTTGAAC
A152_F GGCAAGGTCGATACC**NNK**CGTATGGGAGTAATGGG
A152_R GGTATCGACCTTGCC
W159_F ATGGGAGTAATGGGC**NNK**AGTATGGGTGGCGG
W159_R GCCATTACTCCCATAC
G165_F AGTATGGGTGGCGGC**NNK**TCTCTTATCTCGGCAGC
G165_R GCCGCCACCCATA
S166_F ATGGGTGGCGGCGGA**NNK**CTTATCTCGGCAGCG
S166_R TCCGCCGCCA
I168_F GGCGGCGGATCTCTT**NNK**TCGGCAGCGAATAATC
I168_R AAGAGATCCGCCGC
A180_F AGCCTGAAGGCAGCA**NNK**GTTTCAGGCACCCTG
A180_R TGCTGCCTTCAGGC
D186_F_2 GTTCAGGCACCCTGG**NNK**AGTAGTACGAACTTTTCGTC
D186_R CCAGGGTGCCTG
S187_F CAGGCACCCTGGCAT**NNK**AGTACGAACTTTTCGTCTG
S187_R ATGCCAGGGTGCC
S188_F GCACCCTGGCATAGT**NNK**ACGAACTTTTCGTCTGTTAC
S188_R ACTATGCCAGGGTGC
I208_F TGTGAGAATGATAGG**NNK**GCACCAGTGAATCATC
I208_R CCTATCATTCTCACAGGC
N212_F AGGATCGCACCAGTG**NNK**TCATCAGCCTTGCCA
N212_R CACTGGTGCATCC
S214_F GCACCAGTGAATCA**NNK**GCCTTGCCAATTTACGA
S214_R TGAGTTCACTGGTGC
S238_F AATGGGGGCTCTCAC**NNK**TGTGCCAACAGTGG
S238_R GTGAGAGCCCCATT
A248_F GGGAATTCCAATCA**NNK**CTTATCGGAAAAAAGGGCG
A248_R TTGATTGGAATCCCCTG
S278_F TCGGAAAACCCAAAC**NNK**ACCGCCGTATCCG
S278_R GTTTGGGTTTTCGCAAG

Round 3

G86_F ATCGCCATTGTCCCC**NNK**TACACTGCACGCCA
G86_R GGGGACAATGGCGA
Y87_F GCCATTGTCCCCGGC**NNK**ACTGCACGCCAATC
Y87_R GCCGGGGACAATG
T88_F TTGTCCCCGGCTAC**NNK**GCACGCCAATCCTC
T88_R GTAGCCGGGGACA
A89_F GTCCCCGGCTACACT**NNK**CGCCAATCCTCGATTAAAT
A89_R AGTGTAGCCGGGG
S93_F ACTGCACGCCAATCC**NNK**ATTAAATGGTGGGGACCA
S93_R GGATTGGCGTGCAG
I94_F GCACGCCAATCCTCG**NNK**AAATGGTGGGGACCA
I94_R CGAGGATTGGCGTG

Round 3**Continued.**

K95_F CGCCAATCCTCGATTNNKTGGTGGGGACCAC
K95_R AATCGAGGATTGGCGT
W96_F CAATCCTCGATTAAAANNKTGGGGACCACGC
W96_R TTTAATCGAGGATTGGCG
Q119_F AACAGTACGTTGGACNNKCCAGAGAGTCGCAGC
Q119_R GTCCAACGTA CTGTTAGTATC
S125_F CCAGAGAGTCGCAGC NNK CAGCAGATGGCGG
S125_R GCTGCGACTCTCTGG
A152_F GGCAAGGTCGATACC NNK CGTATGGGAGTAATGGG
A152_R GGTATCGACCTTGCC
M161_F GTAATGGGCTGGAGT NNK GGTGGCGGCG
M161_R ACTCCAGCCCATTACT
G165_F AGTATGGGTGGCGGC NNK TCTCTTATCTCGGCAGC
G165_R GCCGCCACCCATA
A183_F GCAGCATGTGTTTCAG NNK CCCTGGCATAGTAGTACG
A183_R CTGAACACATGCTGCC
W185_F TGTGTTTCAGGCACCC NNK CATAGTAGTACGAACTTTTCGTC
W185_R GGGTGCCTGAACAC
R207_F GCCTGTGAGAATGAT NNK ATCGCACCAGTGAAC T
R207_R ATCATTCTCACAGGCAAAG
I208_F TGTGAGAATGATAGG NNK GCACCAGTGAAC TCATAC
I208_R CCTATCATTCTCACAGGC
A209_F AGAATGATAGGATC NNK CCAGTGAAC TCATACGC
A209_R GATCCTATCATTCTCACAGG
P210_F AATGATAGGATCGCA NNK GTGAAC TCATACGCCTTG
P210_R TCGGATCCTATCATTCTCA
V211_F GATAGGATCGCACCA NNK AACTCATA CGCCTTGC
V211_R TGGTGGGATCCTATCA
N212_F2 AGGATCGCACCAGTG NNK TCATACGCCTTGCCA
N212_R CACTGGTGGGATCC
S213_F TCGCACCAGTGAAC NNK TACGCCTTGCCAATTTAC
S213_R GTTCACTGGTGGGATC
S214_F GCACCAGTGAAC TCA NNK GCCTTGCCAATTTACGA
S214_R TGAGTTCACTGGTGC
A215_F CCAGTGAAC TCATAC NNK TTGCCAATTTACGACTCG
A215_R GTATGAGTTCACTGGTGC

Round 4

R34_F GAGATATACATATGCAGACTAACCCCTATGCT NNK GGGCCGAATCCTACA
R53_F GGTCCCTTCACCGTAN NNK TCGTTTACTGTTTCCCG
R53_R TACGGTGAAGGGACC
R59_F TCGTTTACTGTTTCC NNK CCATCTGGATATGGGG
R59_R GGAAACAGTAAACGAACGT
Y87_F GCCATTGTCCCCGGC NNK ACTGCACGCCAATC
Y87_R GCCGGGGACAATG
T88_F TTGTCCCCGGCTAC NNK GCACGCCAATCCTC

Round 4**Continued.**

T88_R GTAGCCGGGGACA
R90_F CCCGGCTACACTGCANNKCAATCCTCGATTAAATGGTGG
R90_R TGCAGTGTAGCCGG
P120_F AGTACGTTGGACAAGNNKGAGAGTCGCAGCTCT
P120_R CTTGTCCAACGTACTGTT
S125_F CCAGAGAGTCGCAGCNNKCAGCAGATGGCGG
S125_R GCTGCGACTCTCTG
A180_F AGCCTGAAGGCAGCANNKGTTTCAGGCACCCTG
A180_R TGCTGCCTTCAGGC
A180_R TGCTGCCTTCAGG
N205_F ATCTTTGCCTGTGAGNNKGATAGGATCGCACCAG
N205_R CTCACAGGCAAAGATAAGC
I208_F4 TGTGAGAATGATAGGNNKGCACCAGTGAACGAG
I208_R CCTATCATTCTCACAGGC
A209_F2 GAGAATGATAGGATCNNKCCAGTGAACGAGTACG
A209_R GATCCTATCATTCTCACAGG
N212_F3 AGGATCGCACCAGTGNKKGAGTACGCCTTGCC
N212_R CACTGGTGCGATCC
R224_F TACGACTCGATGTGCGNNKAACGCTAAACAGTTTCTTGAG
R224_R CGACATCGAGTCGTAAATT
I232_F AAACAGTTTCTTGAGNNKTGTGGGGGCTCTC
I232_R CTCAAGAAACTGTTTAGCGT
G234_F TTTCTTGAGATTTGTNNKGGCTCTCACTCTTGTG
G234_R ACAAATCTCAAGAAACTGTTTAGC
S236_F GAGATTTGTGGGGGCNNKCACTCTTGTGCCAACA
S236_R GCCCCACAAATCTC
S238_F TGTGGGGGCTCTCACNNKTGTGCCAACAGTGG
S238_R GTGAGAGCCCCCA
S242_F CACTCTTGTGCCAACNNKGGGAATTCCAATCAAGCC
S242_R GTTGGACAAGAGTGAG
N246_F AACAGTGGGAATTCCNNKCAAGCCCTTATCGGAAAAA
N246_R GGAATTCCCCTGTTGG
N277_F GCTTGCGAAAACCCANNKTCAACCGCCGTATGT
N277_R TGGGTTTTTCGCAAGC
T279_F GAAAACCCAACTCANNKGCCGTATGTGATTTTCG
T279_R TGAGTTTGGGTTTTTCGC
V281_R CGAGGCTGCAGTTAGCAGTGCGAAAATCACANNKGGCGGTTGAGTTTGG
D283_R CTCGAGGCTGCAGTTAGCAGTGCGAAAANNKACATACGGCGGTTGA
L291_R ggtggtggtgCTCNNKGCTGCAGTTAGCAGTG

Round 5

T39_F GCGGGCCGAATCCTNNKGC GGCCCTCGTTGG
T39_R AGGATTCGGCCCG
A45_F GCGGCCTCGTTGGAANNKAGTGCAGGTCCCTT
A45_R TTCCAACGAGGCCG
P49_F GAAGCCAGTGCAGGTNNKTTCACCGTACGTTCGT

Round 5**Continued.**

P49_R ACCTGCACTGGCTT
S61_F ACTGTTTCCCGTCCANNKGGATATGGGGCTGG
S61_R TGGACGGGAAACAGT
Y87_F GCCATTGTCCCCGGCANNKACTGCAACTCAATCCTC
Y87_R GCCGGGGACAATG
S93_F ACTGCAACTCAATCCANNKATTAATGGTGGGGACCA
S93_R GGATTGAGTTGCAGTGTAG
K95_F ACTCAATCCTCGATTNNKTGGTGGGGACCAC
K95_R AATCGAGGATTGAGTTGC
G98_F TCGATTAAATGGTGGNNKCCACGCTTGGCTAG
G98_R CCACCATTTAATCGAGGATT
S103_F GGACCACGCTTGGCTNNKCACGGGTTTGTGTGAT
S103_R AGCCAAGCGTGGT
T113_F GTGATCACCATCGATNNKAACAGTACGTTGGACAAG
T113_R ATCGATGGTGATCACAAC
S115_F ACCATCGATACTAACNNKACGTTGGACAAGCCA
S115_R GTTAGTATCGATGGTGATCAC
D118_F ACTAACAGTACGTTGNNKAAGCCAGAGAGTCGC
D118_R CAACGTA CTGTTAGTATCGATG
P120_F AGTACGTTGGACAAGNNKGAGAGTCGCAGCTCT
P120_R CTTGTCCAACGTA CTGTTAG
E121_F ACGTTGGACAAGCCANNKAGTCGCAGCTCTCA
E121_R TGGCTTGTCCAACGT
G139_F GTGGCGAGCTTAAATNNKACGAGTTCAAGTCCAATTTATG
G139_R ATTTAAGCTCGCCACC
S143_F AATGGGACGAGTTCAANNKCCAATTTATGGCAAGGTCG
S143_R TGA ACTCGTCCCATTTAAG
V149_F CCAATTTATGGCAAGNNKGATAACCGCCCGTATG
V149_R CTTGCCATAAATTGGACTTGA
A152_F GGCAAGGTCGATAACCNNKCGTATGGGAGTAATGGG
A152_R GGTATCGACCTTGCC
M154_F GTCGATAACCGCCGTNNKGGAGTAATGGGCTGGA
M154_R ACGGGCGGTATCG
W159_F ATGGGAGTAATGGGCNNKAGTATGGGTGGCGG
W159_R GCCATTACTCCCATAC
G163_F GGCTGGAGTATGGGTNNKGGCGGATCTCTTATCTC
G163_R ACCCATACTCCAGCC
G165_F AGTATGGGTGGCGGCNNKTCTCTTATCTCGGCAGC
G165_R GCCGCCACCATA
NI73_F ATCTCGGCAGCGAATNNKCCAAGCCTGAAGGC
NI73_R ATTCGCTGCCGAGAT
A178_F AATCCAAGCCTGAAGNNKGCAGCCGTTTCAGG
A178_R CTTTCAGGCTTGGATTATTCG
Q182_F AAGGCAGCAGCCGTTNNKGCACCCTGGCATAGT
Q182_R AACGGCTGCTGC
A183_F GCAGCAGCCGTTTCAGNNKCCCTGGCATAGTAGTACG

Round 5**Continued.**

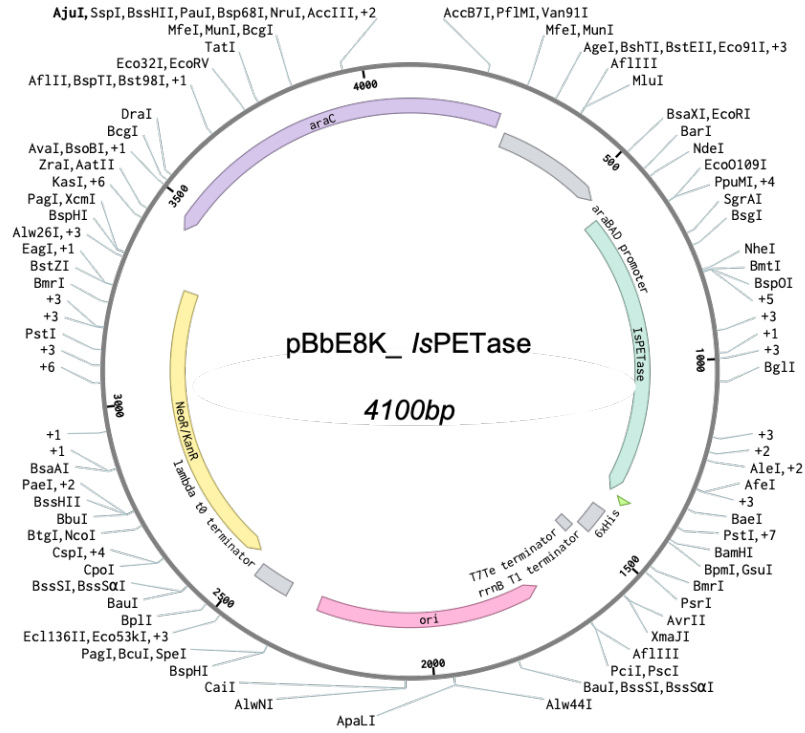
A183_R CTGAACGGCTGCTG
 H186_F GTTCAGGCACCCTGGNNKAGTAGTACGAACTTTTCGTCT
 H186_R CCAGGGTGCCTGA
 S192_F AGTAGTACGAACTTTNNKTCTGTTACGGTTCCTACG
 S192_R AAAGTTCGTACTACTATGCCA
 V194_F ACGAACTTTTCGTCTNNKACGGTTCCTACGCTT
 V194_R AGACGAAAAGTTCGTACTACT
 S221_F TTGCCAATTTACGACNNKATGTTCGATGAACGCTAAAC
 S221_R GTCGTAAATTGGCAAGG
 N246_F AACAGTGGGAATTCCNNKCAAGCCCTTATCGGAAAA
 N246_R GGAATTCCCCTGTTGG
 D263_F ATGAAGCGCTTCATGNNKAATGACACTCGTTATTCAACTT
 D263_R CATGAAGCGCTTCATCC
 N264_F AAGCGCTTCATGGACNNKGACACTCGTTATTCAACTTTTCG
 N264_R GTCCATGAAGCGCTTC
 D265_F CGCTTCATGGACAATNNKACTCGTTATTCAACTTTTCGC
 D265_R ATTGTCATGAAGCGC
 R267_F ATGGACAATGACACTNNKTATTCAACTTTTCGCTTGCG
 R267_R AGTGTCATTGTCCATGAAG
 E274_F TCAACTTTTCGCTTGCNNKAACCCAACTCAACCG
 E274_R GCAAGCGAAAGTTGAATAAC

Round 6

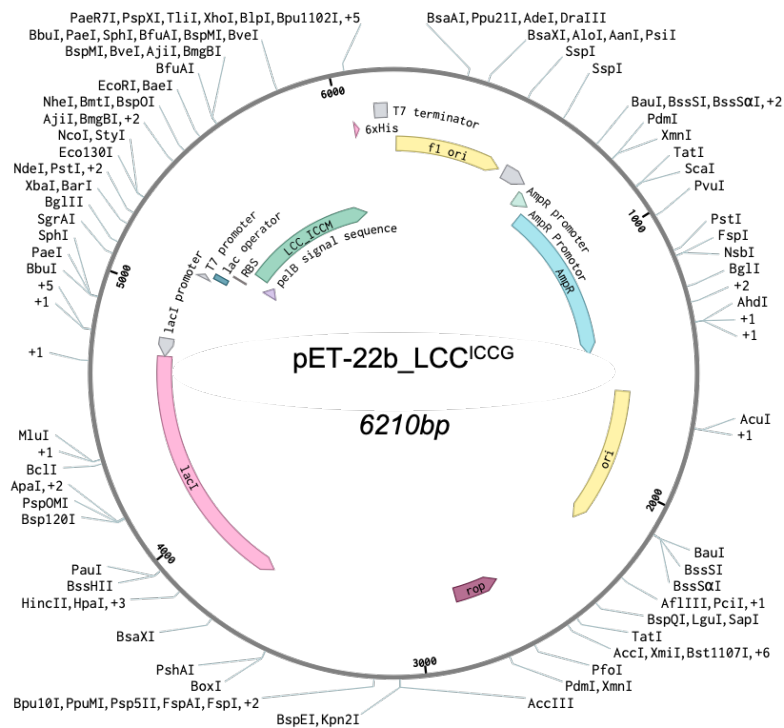
S58_F ACCGTACGTTCGTTTACTGTTNNKCGTCCAGTGGGATATG
 S58_R AACAGTAAACGAACGTACG
 R59_F TCGTTTACTGTTTCCNNKCCAGTGGGATATGGG
 R59_R GGAAACAGTAAACGAACGT
 P60_F TTTACTGTTTCCCGTNNKGTGGGATATGGGGCT
 P60_R ACGGGAAACAGTAAACG
 S61_F ACTGTTTCCCGTCCANNKGGATATGGGGCTGG
 S61_R TGGACGGGAAACAGT
 G62_F GTTTCCCGTCCAGTNNKTATGGGGCTGGCA
 G62_R CACTGGACGGGAAAC
 Y63_F TCCCGTCCAGTGGGANNNKGGGGCTGGCAC
 Y63_R TCCCCTGGACGG
 G64_F CGTCCAGTGGGATATNNKGCTGGCACCCTC
 G64_R ATATCCCCTGGACGG
 A65_F CCAGTGGGATATGGGANNNKGGCACCCTCTATTATCC
 A65_R CCCATATCCCCTGGGA
 I94_F GCAACTCAATCCTCGNNKAATTGGTGGGGACCA
 I94_R CGAGGATTGAGTTGCAG
 W96_F CAATCCTCGATTAATNNKTGGGGACCACGC
 W96_R ATTAATCGAGGATTGAGTTGC
 Q127_F AGTCGCAGCTCTCAGNNKATGGCGGCATTACG
 Q127_R CTGAGAGCTGCGAC
 R132_F CAGATGGCGGCATTANNKCAGGTGGCGAGC

Round 6**Continued.**

RI32_R TAATGCCGCCATCTG
VI34_F GCGGCATTACGCCAGNNKGCGAGCTTAAATGGGAC
VI34_R CTGGCGTAATGCCG
MI54_F GTCGATACGCCCGTNNKGGAGTAATGGGCTGGA
MI54_R ACGGGCGGTATCG
W159_F ATGGGAGTAATGGGCNNKAGTATGGGTGGCGG
W159_R GCCCATTACTCCCATAC
GI63_F GGCTGGAGTATGGGTNNKGGCGGATCTCTTATCTC
GI63_R ACCCATACTCCAGCC
SI69_F GGCGGATCTCTTATCANNKGCAGCGAATAATCCAAGC
SI69_R GATAAGAGATCCGCCG
A180_F AGCCTGAAGGCAGCANNNKGTTATGGCACCCCTGG
A180_R TGCTGCCTTCAGGC
M182_F AAGGCAGCAGCCGTTNNKGCACCCTGGCATAG
M182_R AACGGCTGCTGC
PI84_F GCAGCCGTTATGGCANNNKTGGCATAGTAGTACGAACTT
PI84_R TGCCATAACGGCTG
W185_F GCCGTTATGGCACCCNNKCATAGTAGTACGAACTTTTCGTCT
W185_R GGGTGCCATAACGG
HI86_F GTTATGGCACCCCTGGNNKAGTAGTACGAACTTTTCGTCT
HI86_R CCAGGGTGCCATAAC
V211_F GATAGGATCGCACCANNNKAAGGAGTACGCCTTG
V211_R TGGTGCGATCCTATCA
E213_F ATCGCACCAAGTGAAGNNKTACGCCTTGCCAATTTAC
E213_R CTTCACTGGTGCGATC
Y214_F GCACCAGTGAAGGAGNNKGCCTTGCCAATTTACG
Y214_R CTCCTTCACTGGTGC
A215_F CCAGTGAAGGAGTACNNKTTGCCAATTTACGACTCG
A215_R GTACTCCTTCACTGGTG
F229_F CTCAACGCTAAACAGNNKCTTGAGATTTGTGGGGG
F229_R CTGTTTAGCGTTGAGCG
N241_F TCTCACTCTTGTGCCNNKAGTGGGAATTCCAATCAAG
N241_R GGCACAAGAGTGAGAG
N244_F TGTGCCAACAGTGGGNNKTCCAATCAAGCCCTTATC
N244_R CCCACTGTTGGCAC
K252_F CAAGCCCTTATCGGANNNKAAGGGCGTTGCTTG
K252_R TCCGATAAGGGCTTGATT
G254_F CTTATCGGAAAAAAGNNKGTTGCTTGGATGAAGCG
G254_R CTTTTTCCGATAAGGGCTT
T270_F GACACTCGTTATTCANNNKTTTCGCTTGCGAAAACC
T270_R TGAATAACGAGTGTCAATTGTC



9.2.3.4 Supplementary Information, Figure 2. Plasmid map of pBbE8K_ /sPETase and variants of /sPETase (including HotPETase).



9.2.3.5 Supplementary Information, Figure 3. Plasmid map of pET-22b_LCC^{ICCG}.

9.2.3.6 Supplementary Information, Table 3. Data collection and refinement statistics for structure determination of HotPETase.

	HotPETase
Wavelength	0.9795
Resolution range	72.63 - 2.1 (2.175 - 2.1)
Space group	P 1 21 1
Unit cell	81.7002 74.8551 82.7012 90 118.574 90
Total reflections	357426 (35870)
Unique reflections	51246 (5059)
Multiplicity	7.0 (7.1)
Completeness (%)	99.74 (98.48)
Mean I/sigma(I)	4.34 (0.45)
Wilson B-factor	37.14
R-merge	0.2469 (1.7)
R-meas	0.2668 (1.836)
R-pim	0.1004 (0.6874)
CC1/2	0.987 (0.573)
CC*	0.997 (0.854)
Reflections used in refinement	51131 (5000)
Reflections used for R-free	2398 (305)
R-work	0.2122 (0.3590)
R-free	0.2519 (0.3479)
CC (work)	0.946 (0.764)
CC (free)	0.916 (0.789)
Number of non-hydrogen atoms	6207
macromolecules	6003
ligands	0
solvent	204
Protein residues	810
RMS (bonds)	0.009
RMS (angles)	1.13
Ramachandran favoured (%)	95.89
Ramachandran allowed (%)	4.11
Ramachandran outliers (%)	0
Rotamer outliers (%)	0
Clashscore	3.66
Average B-factor	40.5
macromolecules	40.52
solvent	39.78

9.3 Supporting Information for Chapter 5: Deconstruction of PET-Based Materials and a Bio-Derived Plastic by a Thermostable PETase

9.3.1 Methods

9.3.1.1 Materials

All chemical and biological materials were purchased from commercial suppliers. Kanamycin, ampicillin, tetracycline, DNase I, bis(2-hydroxyethyl) terephthalate (BHET), terephthalic acid (TPA) and 2,5-furandicarboxylic acid (FCA) were obtained from Sigma-Aldrich; LB agar, LB media, 2YT media, AIM 2YT media and arabinose from Formedium; BugBuster Protein Extraction Reagent from Merck; *E. coli* Origami 2 (DE3) from Novagen; *E. coli* BL21 (DE3) from New England BioLabs. pBbE8K_HotPETase and pET-22b_LCC^{ICCG} were obtained from previous work. Semi-crystalline PET powder (cryPET), was sourced from Goodfellow, UK, PET/PE composite film lids from iPac, PETG pellets from Push Plastic, USA and Bottle-grade PET pellets (Ramapet NI) from Indorama Ventures.

9.3.1.2 Preparation of PET Materials for Assays

Semi-crystalline PET powder (cryPET), 300 micron, was used as supplied. Amorphous PET film, (amoPET) and 325 micron PET/ 40 micron PE composite packaging lids, 0.25 mm thickness, were cut into 6 mm discs. Bottle-grade PET pellets (RamaPET NI) were used as provided or were milled prior to use. Bottle-grade PET pellets were micronized using a RETSCH PM100 Planetary Ball Mill at 500 rpm for 30 mins to form a powder, bgPET. PETG pellets were milled prior to use. Pellets were mixed with an equivalent mass of dry ice, before being micronized in an identical fashion. After sieving, only the 450-600 micron fraction of the resulting powders was used. Substrate characteristics are detailed in Supplementary Information, Table. 1. In-house synthesised PEF, was used as produced.

9.3.1.3 Protein Production

pBbE8K_HotPETase was expressed in chemically competent Origami 2 *E. coli*. Single colonies of freshly transformed cells were cultured for 18 hrs at 30°C in 5 mL of LB medium supplemented with 25 µg mL⁻¹ kanamycin and 2.5 µg mL⁻¹ tetracycline. 1 mL of the resulting culture was used to inoculate 50 mL 2YT medium containing 25 µg mL⁻¹ kanamycin and 2.5 µg mL⁻¹ tetracycline. Cultures were grown at 35°C, 180 rpm to an OD₆₀₀ of 1. Protein production was initiated by the addition of L-arabinose (final concentration of 10 mM) and cultures then grown at 19°C for 20 hrs. The *E. coli* cells were harvested by centrifugation at 3220 x *g* for 10 minutes and resuspended in lysis buffer (50 mM Tris-HCl, pH 7.5, 10 mM imidazole, 300 mM NaCl, 10 µg mL⁻¹ DNase I). Cells were disrupted by sonication and the resulting lysate clarified by centrifugation (13,500 x *g* for 15 minutes). The soluble fraction was subjected to affinity chromatography via application to Ni-NTA agarose (Qiagen). After

washing off unbound proteins with the lysis buffer, bound proteins were eluted with elution buffer (50 mM Tris-HCl, pH 7.5, 300 mM imidazole, 300 mM NaCl). Proteins were desalted by application to 10DG desalting columns (Bio-Rad) and eluted with storage buffer (50 mM Tris-HCl, pH 7.5, 150 mM NaCl). Protein purity was confirmed by SDS-PAGE and concentrations determined by measuring the absorbance at 280 nm, assuming an extinction coefficient of 41,285 M⁻¹cm⁻¹.

For the cutinase, LCC^{ICCG}, the gene was expressed in chemically competent *E. coli* BL21 (DE3). Single colonies of freshly transformed cells were cultured for 18 hrs at 30°C in 5 mL of LB medium supplemented with 25 µg mL⁻¹ ampicillin. 1 mL of the resulting culture was used to inoculate 50 mL auto-inducible 2YT medium containing 25 µg mL⁻¹ ampicillin. Cultures were grown at 35°C, 180 rpm, to an OD₆₀₀ of 1, upon which the incubator was cooled to 19°C, for expression cultivation for 20 hrs. Protein purification then proceeded as detailed for IsPETase, with protein concentrations determined using an extinction coefficient of 37,150 M⁻¹cm⁻¹.

9.3.1.4 Solid Substrate Depolymerisation Assays

A 12 mL lidded glass vial containing 5 mL reaction buffer, 50 mM glycine-OH, 4% BugBuster, pH 9.2, for HotPETase, or 100 mM potassium phosphate buffer, pH 8 for LCC^{ICCG} and 20 mg of the desired PET material or PEF was incubated for 1 hr at the reaction temperature (40-70°C) in order to equilibrate all reaction components to the reaction temperature (equilibration step). The reaction was initiated by adding 25 µL of an 8 µM solution of purified protein (HotPETase or LCC^{ICCG}) coupled with incubation at the desired temperature under agitation at 180 rpm. Samples were taken at multiple times points, with the reaction terminated by the addition of an equal volume of a cold methanol and 12.5 mM trifluoroacetic acid solution. Following reaction quenching, samples were incubated for 30 mins at 30°C in a shaking incubator, 300 rpm, and insoluble protein precipitate removed by centrifugation for 10 minutes at 2,900 x *g*. A UPLC analysis sample was then prepared by transferring 100 µL of the resulting reaction supernatant into a fresh 96-well microtiter plate.

9.3.1.5 PETG and PEF Subunit Hydrolysis Assays

Soluble PETG and PEF subunit assays, were carried out in 2 mL of reaction buffer 50 mM glycine-OH, pH 9.2. The monomer or dimer subunit was dissolved in DMSO and added to the reaction mix at a final concentration of 2 mM for MHET, BCDT, MCDT, 1 mM for BHEF and 0.4 mM for MHEF, with no more than 1% DMSO added to the reaction. Reactions were initiated by the addition of 0.02 µM HotPETase, and incubated at 60°C. For control assays, no enzyme was added. Samples were taken at multiple times points, quenched and prepared for UPLC analysis as detailed previously.

9.3.1.6 Chromatographic PET Depolymerisation Analysis

For assays containing amoPET, cryPET, bgPET (pellets and milled powder) and PET/PE laminate film, UPLC analysis was performed on a 1290 Infinity II Agilent LC system

including an autosampler with the UV detector set to 260 nm, using a Kinetex® XB-C18 100 Å, 5 µm, 50 x 2.1 mm, LC Column with a stepped, isocratic solvent ratio method. Mobile phase A was water containing 0.1% formic acid and mobile phase B was acetonitrile with a fixed flow rate of 1.1 mL min⁻¹ and 4 µL of sample injected. Following sample injection, the mobile phase was set to 13% buffer B for 52 seconds to separate TPA and MHET, stepped up to 95% buffer B for 33 seconds to separate larger reaction products and contaminants, and then stepped back down to 13% buffer B for column re-equilibration until a total run time of 1.8 minutes. Using this method, TPA is eluted at ~0.4 minutes and MHET at ~0.6 minutes. TPA and MHET were measured according to standard curves, prepared from commercial TPA and in-house synthesised MHET.

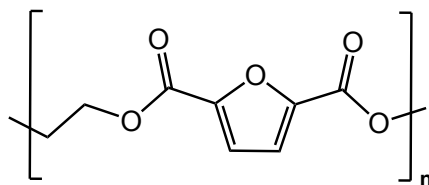
9.3.1.7 Chromatographic PETG and PETG Subunit Hydrolysis Analysis

For assays containing PETG, UPLC analysis was performed on a 1290 Infinity II Agilent LC system including an autosampler with the UV detector set to 260 nm, using an InfinityLab Poroshell 120 EC-C18, 4 µm, 4.6 x 200 mm, LC Column. MHET, TPA and MCDT were eluted over 5 minutes using a gradient of 5-95% acetonitrile in water supplemented with 0.1% TFA at a fixed flow rate of 1.5 mL min⁻¹ using an injection volume of 4 µL. Peaks were assigned by comparison to chemical standards prepared from commercial TPA and in-house synthesised MHET and MCDT, and the peak areas integrated using Agilent OpenLab software. Using this method, TPA is eluted at ~2.1 minutes, MHET at ~2.3 minutes and MCDT at ~3.6 minutes (Supplementary Information, Fig. 1a). TPA, MHET and MCDT concentrations were calculated by preparation of standard curves. For assays for the hydrolysis of the PETG subunits BCDT and MCDT, the same HPLC methodology and analysis was used, with peaks assigned by comparison to in-house synthesised standards. The standard curves for MCDT is reported in Supplementary Information, Fig. 2. For analysis, the extinction coefficient for BCDT was assumed to be the same as that for MCDT.

9.3.1.8 Chromatographic PEF and PEF Subunit Hydrolysis Analysis

For assays containing PEF, UPLC analysis was performed on a 1290 Infinity II Agilent LC system including an autosampler with the UV detector set to 260 nm, using an InfinityLab Poroshell 120 EC-C18, 4 µm, 4.6 x 200 mm, LC Column. FCA and MHEF were eluted over 13.5 minutes using a gradient of 5-95% acetonitrile in water supplemented with 0.1% TFA at a fixed flow rate of 1.5 mL min⁻¹ using an injection volume of 5 µL. Peaks were assigned by comparison to commercial FCA and in-house synthesized MHEF, and the peak areas integrated using Agilent OpenLab software. Using this method, FCA is eluted at ~1.7 minutes and MHEF at ~2.1 minutes (Supplementary Information, Fig. 1b). FCA and MHEF concentrations were calculated by preparation of standard curves, reported in Supplementary Information, Fig. 2. For assays for the hydrolysis of the PEF subunits BHEF and MHEF, the same HPLC methodology and analysis was used, with peaks assigned by comparison to in-house synthesised standards. The standard curves for MHEF and FCA are reported in Supplementary Information, Fig. 2. For analysis, the extinction coefficient for BHEF was assumed to be the same as that for MHEF.

9.3.1.9 Chemical Synthesis of Reaction Substrates



Preparation of Poly(ethylene Furanoate) (PEF). Dimethylfuran-2,5-dicarboxylate (DMDC) and 1,2-ethylene glycol (EG) were added in a 1:3 (DMDC:EG) molar ratio with titanium butoxide in 450 ppm (with respect to the mass of DMDC). The mixture was sequentially heated and stirred at 160°C for 2 hrs, 170°C for 2 hrs and 190°C for 2 hrs, then placed under vacuum and heated to 220°C for 2 hrs, 235°C for 2 hrs and 250°C for 2.5 hrs. The reaction was allowed to cool to r.t. and the crude mixture dissolved in minimal concentrated TFA, and then poured into water. The solid was recovered by vacuum filtration and washed with 5 x 50 mL of water followed by extensive washes with ethyl acetate, yielding a brown brittle powder.

9.3.1.10 Characterisation of PET-based Substrates

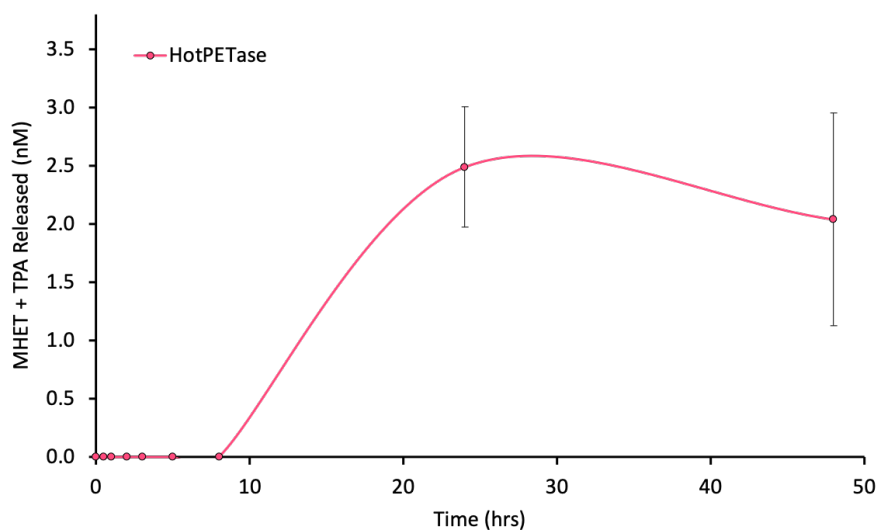
Polymer crystallinity was determined using differential scanning calorimetry (DSC), using 4 mg of material. DSC data was obtained from using a TA DSC instrument system. DSC heating and cooling curves were run in triplicate in series between -150 and 300 °C under a nitrogen atmosphere at a heating rate of ± 10 °C min⁻¹ in a 40 μ L aluminium crucible.

The average molecular weights (avg. mw.) of polymer chains were determined by gel permeation chromatography (GPC). Samples (4 mg) were dissolved in hexafluoro-2-propanol (120 μ L) at room temperature. Once dissolved, HPLC-grade chloroform (1880 μ L) was added to form a uniform, colourless solution. Samples were then filtered through 0.24 μ m polytetrafluoroethylene (PTFE) filter. GPC analysis was performed on a system composed of an Agilent 1260 Infinity II LC system equipped with an Agilent guard column (PLGel 5 μ M, 50 x 7.5 mm) and two Agilent Mixed-C columns (PLGel 5 μ M, 300 x 7.5 mm). The mobile phase used was HPLC grade CHCl₃ at 35°C at a flow rate of 1.0 mL min⁻¹. SEC samples were calibrated against linear polystyrene standards (162 – 2.4 x 10⁵ g mol⁻¹).

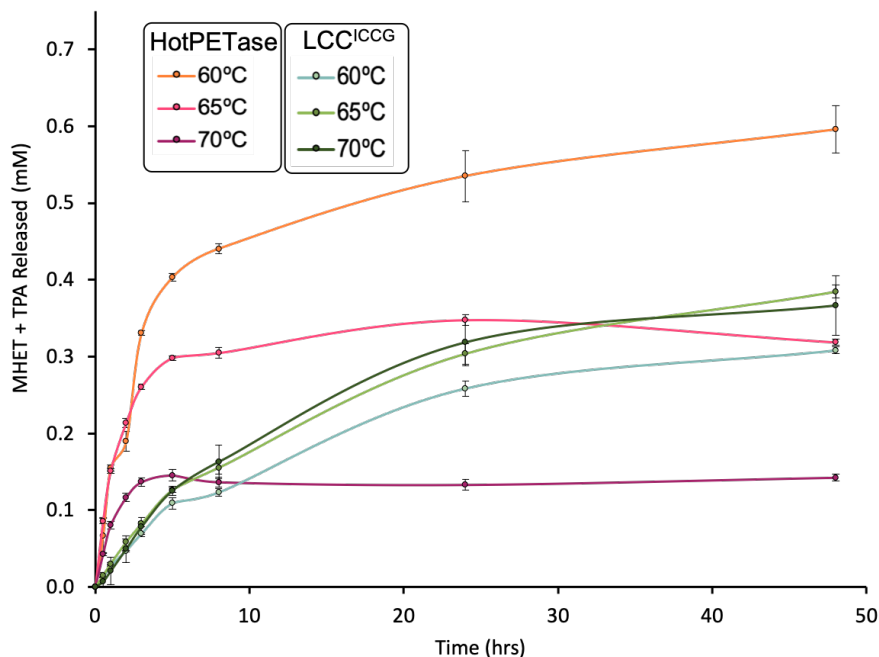
9.3.1.11 Chemical Synthesis of PETG and PEF subunits

The synthesis of chemical standards, PETG and PEF subunits was carried out by Ross Smithson independently from the PhD candidate, so is not detailed here.

9.3.2 Extended Data



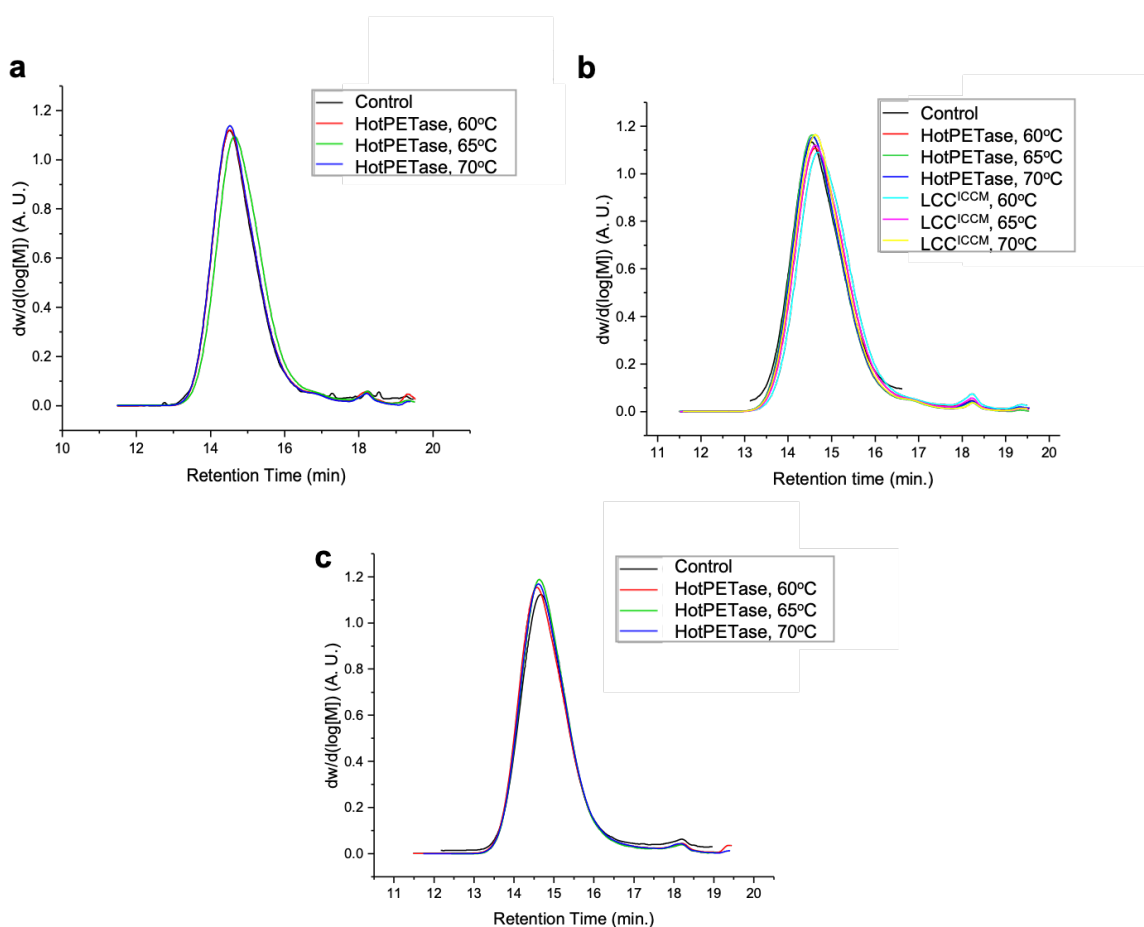
9.3.2.1 Extended Data, Figure 1. Reaction of HotPETase with bgPET pellets. 48-hr time-course of bottle-grade PET pellet reactions (10 pellets), showing total released MHET and TPA following reaction with HotPETase ($0.04 \mu\text{M}$) at 60°C . Reactions were carried out in triplicate; error bars represent the s.d. of the replicate measurements. Note that the x-axis is in nM, product release prior to the 24-hr reaction time point was too small to detect using our HPLC analysis method.



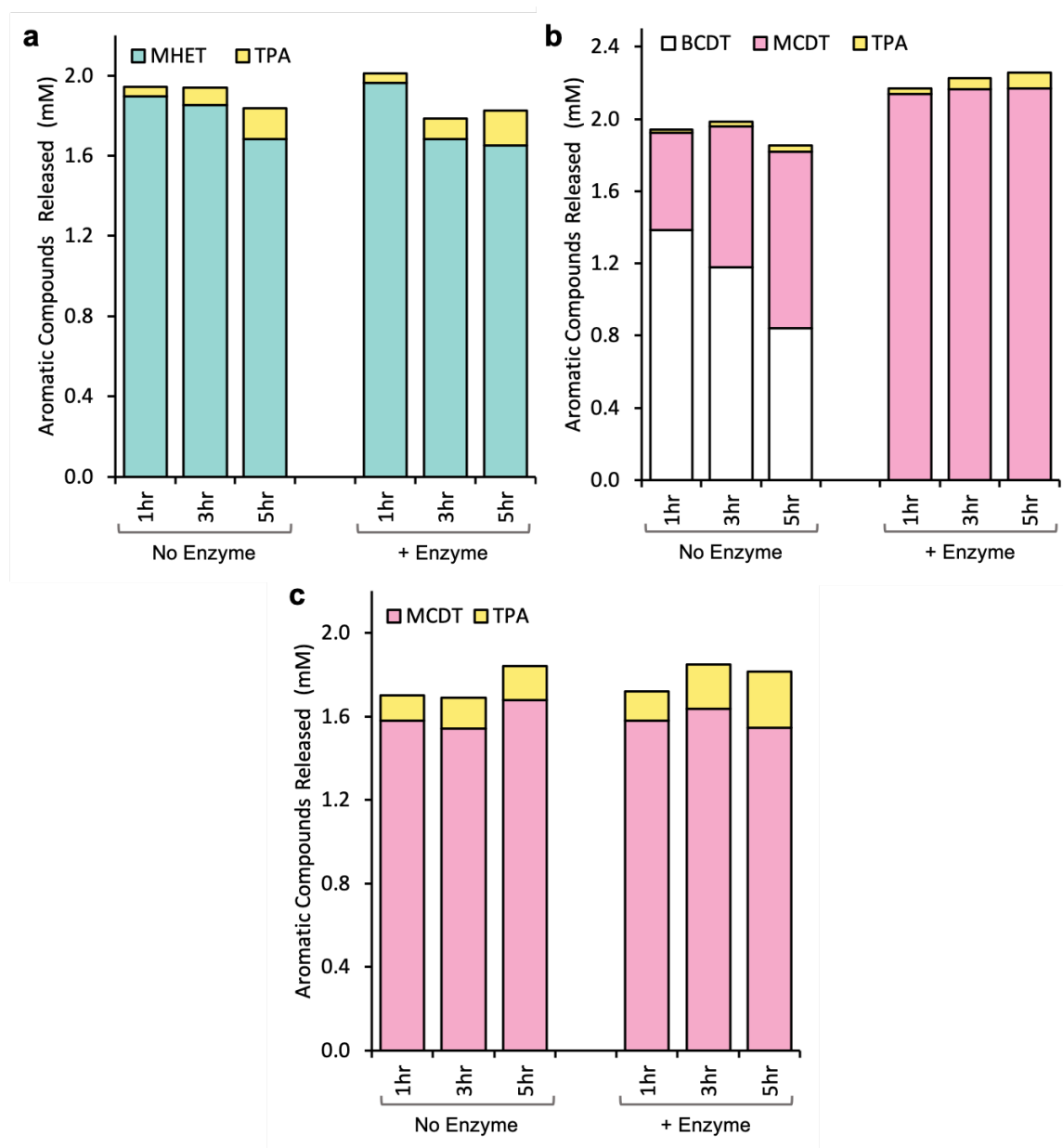
9.3.2.2 Extended Data, Figure 2. Comparison of reaction of HotPETase and LCC^{ICCG} with bgPET at different temperatures. 48-hr time-courses of milled bottle-grade PET reactions (4 mg mL^{-1}), showing total released MHET and TPA with HotPETase ($0.04 \mu\text{M}$, pinks) and LCC^{ICCG} ($0.04 \mu\text{M}$, greens) over time. Reactions were carried out at 60°C , 65°C and 70°C , with each enzyme in its reported optimal buffer, as reported in the Methods. Reactions were carried out in triplicate; error bars represent the s.d. of the replicate measurements.

9.3.2.3 Extended Data, Table 1. PET substrate crystallinity after enzyme reaction. Post reaction crystallinity was assessed after a 48-hr reaction of the substrate (4 mg mL^{-1}) with HotPETase ($0.04 \text{ }\mu\text{M}$) at 60°C .

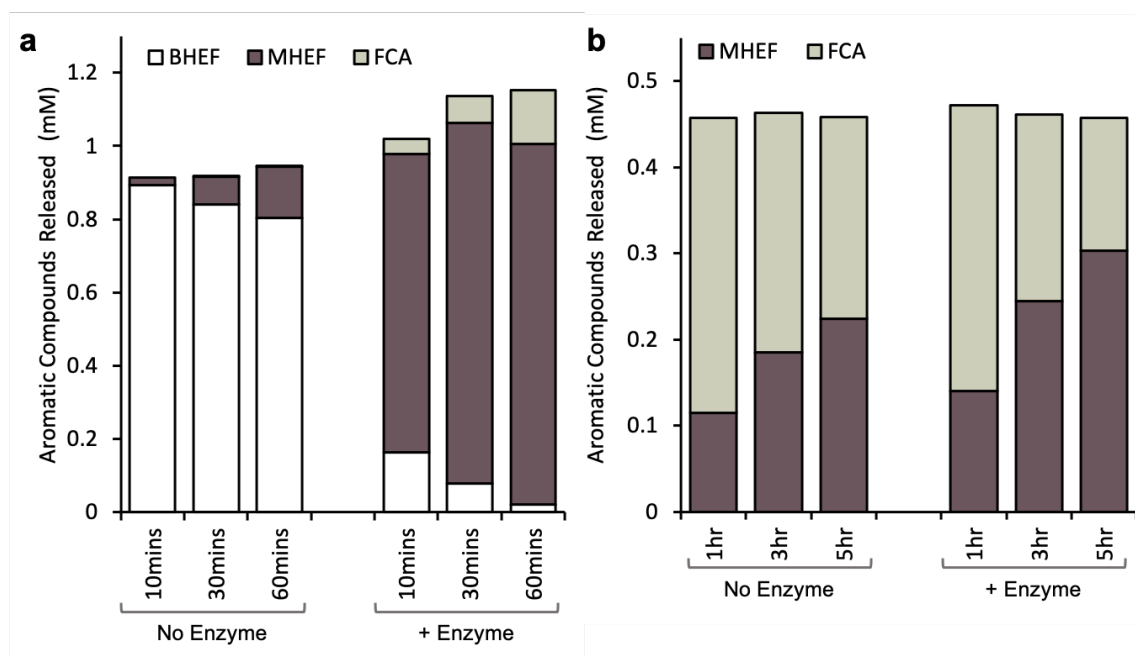
Substrate	Crystallinity (pre-reaction)	Crystallinity (post-reaction)
Semi-crystalline PET powder (cryPET)	36.4%	38.2%
Milled bottle-grade PET pellets (bgPET)	41.9%	42.3%



9.3.2.4 Extended Data, Figure 3. PET substrate average molecular weight after enzyme reactions. The average molecular weight (avg. mw.) was assessed following reaction with the stated enzyme ($0.04 \text{ }\mu\text{M}$) at the stated temperature for 48 hrs, with (a) crystalline PET powder (cryPET, 4 mg mL^{-1}), (b) milled bottle-grade PET (bgPET, 4 mg mL^{-1}) and (c) milled PETG (4 mg mL^{-1}). The control reaction with no enzyme for each substrate is represented in black.



9.3.2.5 Extended Data, Figure 4. Examination of substrate preference of HotPETase towards PETG subunits. (a) Bar chart showing results of non-enzymatic and enzymatic hydrolysis of MHET (2 mM, blue) to TPA (pink) over the course of 5 hrs. Conversion of MHET to TPA is not accelerated in the presence of HotPETase (0.02 μ M). (b) Bar chart showing results of non-enzymatic and enzymatic hydrolysis of BCDT (2 mM, white) to MCDT (pink) over the course of 5 hrs. Conversion of BCDT to MCDT is accelerated in the presence of HotPETase (0.02 μ M). (c) Bar chart showing results of non-enzymatic and enzymatic hydrolysis of MCDT (2 mM, pink) to TPA (yellow) over the course of 5 hrs. Conversion of MCDT to TPA is not accelerated in the presence of HotPETase (0.02 μ M).

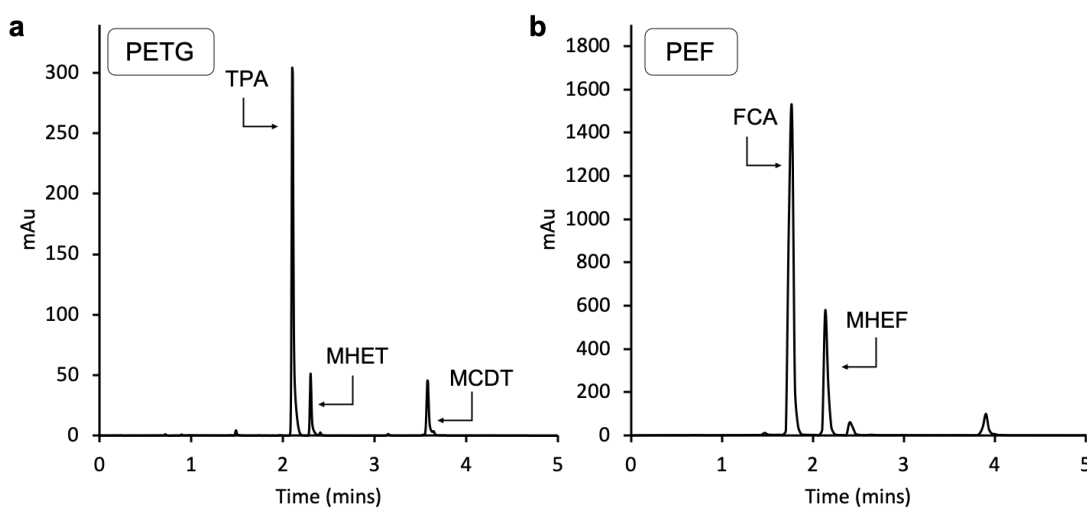


9.3.2.6 Extended Data, Figure 5. Examination of substrate preference of HotPETase towards PEF subunits. (a) Bar chart showing results of non-enzymatic and enzymatic hydrolysis of BHEF (1 mM, white) to MHEF (brown) and FCA (grey) over the course of 1 hr. Conversion of BHEF to MHEF is accelerated in the presence of HotPETase (0.02 μ M). (b) Bar chart showing results of non-enzymatic and enzymatic hydrolysis of MHEF (1 mM, brown) to FCA (grey) over the course of 5 hrs. Conversion of MHEF to FCA is not affected by the presence of HotPETase (0.02 μ M).

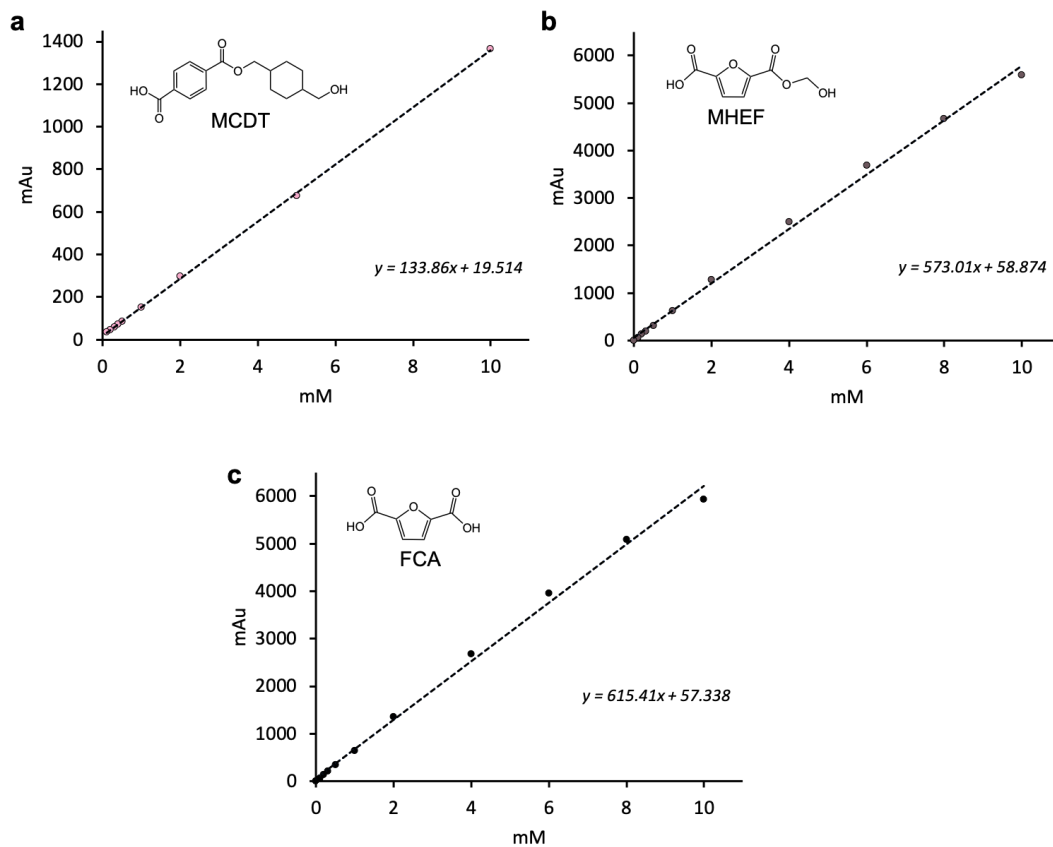
9.3.3 Supplementary Information

9.3.3.1 Supplementary Information, Table 1. Characterisation of PET-based substrates used in enzyme assays. Substrate crystallinity and average molecular weight (avg. mw.) was characterised after incubation in reaction buffer for 48 hrs at 60°C.

Substrate	Form	Crystallinity	Avg. mw. (kDa)
Semi-crystalline PET powder (cryPET)	<300 micron powder	36.4%	156
Bottle-grade PET pellets	~5 mm diameter solid pellet	61.0%	147
Milled bottle-grade PET pellets (bgPET)	250-450 micron powder	41.9%	147
PET/PE composite packaging lid	~6 mm diameter film disc, 325 micron PET/40 micron PE	1.57%	95.5
Milled PETG pellets	250-450 micron powder	0%	282



9.3.3.2 Supplementary Information, Figure 1. Example HPLC traces for the enzymatic degradation of PETG and PEF. (a) An example HPLC trace showing the major hydrolysis products of TPA, MHET and MCDT following degradation of PETG by HotPETase. (b) An example HPLC trace showing the major hydrolysis products of FCA and MHEF following degradation of PEF by HotPETase.



9.3.3.3 Supplementary Information, Figure 2. Calibration Curves for HPLC analysis.

(a) MCDT, (b) MHEF, (c) FCA. Measurements were carried out in triplicate; error bars are too small to be visualised.

9.4 Supporting Information for Chapter 7: Capturing an *IsPETase* Acyl-Enzyme Intermediate Using Genetic Code Expansion

9.4.1 Methods

9.4.1.1 Materials

All chemical and biological materials were purchased from commercial suppliers. Kanamycin, chloramphenicol, tetracycline, DNase I and bis(2-hydroxyethyl) terephthalate (BHET) were obtained from Sigma-Aldrich; LB agar, LB media, 2YT media and arabinose from Formedium; *Escherichia coli* Origami 2 (DE3) from Novagen; *E. coli* 5-alpha, Q5 DNA polymerase, T4 DNA ligase, and restriction enzymes from New England BioLabs; pBbE8K_ *IsPETase*^{TS} was obtained from previous work, oligonucleotides were synthesized by Integrated DNA Technologies (IDT).

9.4.1.2 Gene Construction

The gene encoding *IsPETase*^{TS} (*IsPETase*^{S121E/D186H/R280A}, signal sequence removed as by Son *et al.* 2019¹) was commercially synthesised by Integrated DNA Technologies as a gBlock fragment with codon optimisation for expression in *E. coli* cells. An amber stop codon (TAG) was introduced in place of S160 by site-directed mutagenesis, and the resulting gene cloned into the NdeI (5' end) and XhoI (3' end) sites of a pBbE8K vector modified to contain a C-terminal hexa-histidine tag coding sequence following the XhoI restriction site,² to form pBbE8K_ *IsPETase*^{TS}_S160TAG. Primers used are detailed in Supplementary Information, Table 1. The *E. coli* optimised *Methanosarcina barkeri* PylRS gene (*Mb* Y271C/N311Q/Y349F/V366C)³ was synthesised by IDT. Two copies of the gene were cloned into a pEVOL vector,⁴ which also contained the *MbtRNA*_{CUA},⁵ using BglII/SalI and NdeI/PstI restriction sites, to form pEVOL_ *MbPylRS*_{DAP}/tRNA_{CUA}. Nucleotide sequences, expressed amino acid sequences and plasmid maps of the DNA constructs used in this study are provided in Supplementary Information, Fig. 1 and 2.

9.4.1.3 Protein Production

To produce *IsPETase*^{TS} protein, pBbE8K_ *IsPETase*^{TS} was expressed in chemically competent Origami 2 *E. coli*. Single colonies of freshly transformed cells were cultured for 18 hrs at 30°C in 5 mL of LB medium supplemented with 25 µg mL⁻¹ kanamycin and 2.5 µg mL⁻¹ tetracycline. 1 mL of the resulting culture was used to inoculate 50 mL 2YT medium containing 25 µg mL⁻¹ kanamycin and 2.5 µg mL⁻¹ tetracycline. Cultures were grown at 35°C, 180 rpm to an OD₆₀₀ of 1. Protein production was initiated by the addition of L-arabinose (final concentration of 10 mM) and cultures then grown at 19°C for 20 hrs. The *E. coli* cells were harvested by centrifugation at 3220 x *g* for 10 minutes and resuspended in lysis buffer (50 mM Tris-HCl, pH 7.5, 10 mM imidazole, 300 mM NaCl, 10 µg mL⁻¹ DNase I). Cells were disrupted by sonication and the resulting lysate clarified by centrifugation (13,500 x *g* for

15 minutes). The soluble fraction was subjected to affinity chromatography via application to Ni-NTA agarose (Qiagen). After washing off unbound proteins with the lysis buffer, bound proteins were eluted with elution buffer (50 mM Tris-HCl, pH 7.5, 300 mM imidazole, 300 mM NaCl). Proteins were desalted by application to 10DG desalting columns (Bio-Rad) and eluted with storage buffer (50 mM Tris-HCl, pH 7.5, 150 mM NaCl). Protein purity was confirmed by SDS-PAGE.

To produce *IsPETase*^{TS}-p-DAP protein, Origami 2 *E. coli* cells were co-transformed with pBbE8K_*IsPETase*^{TS}_SI60TAG and pEVOL_*MbPylRS*_{DAP}/tRNA_{CUA}. Single colonies of freshly transformed cells were cultured for 18 hrs at 30°C in 5 mL of LB medium supplemented with 25 µg mL⁻¹ kanamycin, 25 µg mL⁻¹ chloramphenicol and 2.5 µg mL⁻¹ tetracycline. 1 mL of the resulting culture was used to inoculate 50 mL 2YT medium containing 25 µg mL⁻¹ kanamycin, 25 µg mL⁻¹ chloramphenicol and 2.5 µg mL⁻¹ tetracycline. Cultures were grown at 30°C, 180 rpm to an OD₆₀₀ of 1. Photocaged-DAP (p-DAP) was then added, to a final concentration of 1 mM, and protein production was initiated by the addition of L-arabinose (final concentration of 10 mM). Cultures were grown at 19°C for 20 hrs. The *E. coli* cells were harvested by centrifugation at 3220 x *g* for 10 minutes and purified as detailed above for *IsPETase*^{TS}. The purified *IsPETase*^{TS}-p-DAP protein was irradiated with UV light (365 nm, 35 mW cm⁻², 4°C) for 30 mins, and subsequently purified by application to a PD10 desalting column (Cytiva) and eluted with reaction buffer (50 mM glycine-OH, pH 9.2), to afford *IsPETase*^{TS}-DAP.

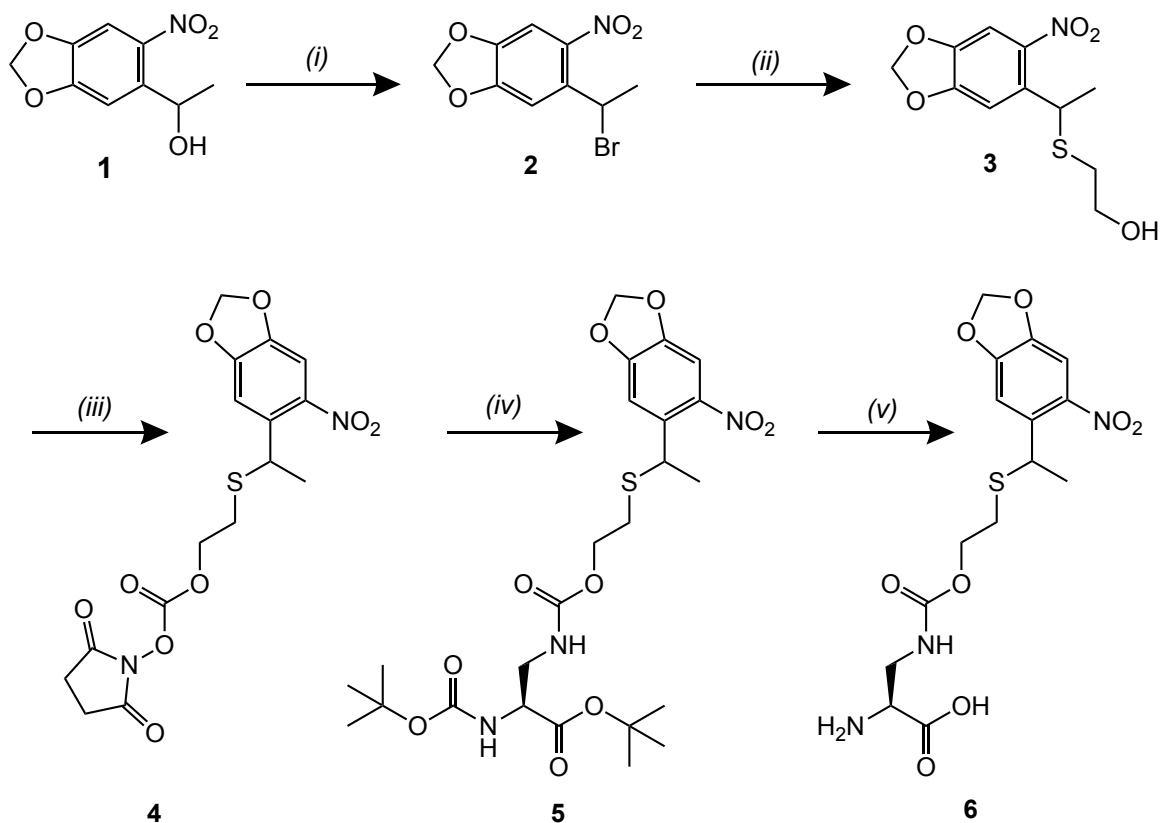
9.4.1.4 Acyl-Enzyme Intermediate Capture Assays

A reaction was set up containing *IsPETase*^{TS}-DAP (5.5 µM, final concentration) and BHET (160 µM, final concentration) in 200 µL of reaction buffer (50 mM glycine-OH, pH 9.2) in a 96-well microtiter plate. The plate was foil-sealed and incubated at 37°C for 20 hrs. The reaction solution was then analysed by mass spectrometry. Reactions were carried out in triplicate.

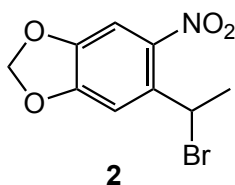
9.4.1.5 Mass Spectrometry

Protein analysis was carried out by mass spectrometry, performed using a 1200 series Agilent LC with 5 µL injection into 5% acetonitrile (with 0.1% formic acid) and desalted inline for 1 min. Protein was eluted over 1 min using 95% acetonitrile with 5% water. The resulting multiply charged spectrum was analysed using an Agilent QTOF 6510 and deconvoluted using Agilent MassHunter Software.

9.4.1.6 Chemical Synthesis of Photocaged 2,3-Diaminopropionic Acid (p-DAP)

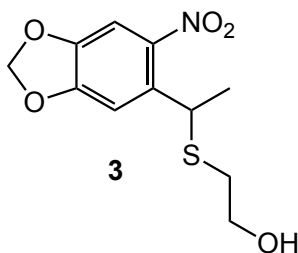


Scheme 1. Synthesis of photocaged 2,3-diaminopropionic acid (p-DAP). Reagents and conditions: (i) **1** (3.64 mmol), PBr_3 (0.4 eq., dropwise addition), dry CH_2Cl_2 , 0°C , then dry pyridine (cat.), 0°C , 15 min, then r.t., 1.5 hrs, 54 %, (**2**); (ii) **2** (2.12 mmol), 2-mercaptoethanol (1.05 eq.), 1,4-dioxane, aq. NaOH (1.0 eq.), r.t., 14 hrs, dark, nitrogen atm., 86%, (**3**); (iii) **3** (1.11 mmol), Su_2O (1.4 eq.), DIPEA (3.0 eq.), CH_3CN , r.t., dark, 14 hrs, quant. conv., (**4**); (iv) **4** (1.11 mmol), Boc-L-Dap-O^tBu.HCl (2 eq.), r.t., 14 hrs, dark, nitrogen atm., 65%, (**5**); (v) **5** (0.72 mmol), HCl (4M in 1,4-dioxane) (22.2 eq.), r.t., 14 hrs, dark, 77%, (**6**). NMR data is presented in Supplementary Information.



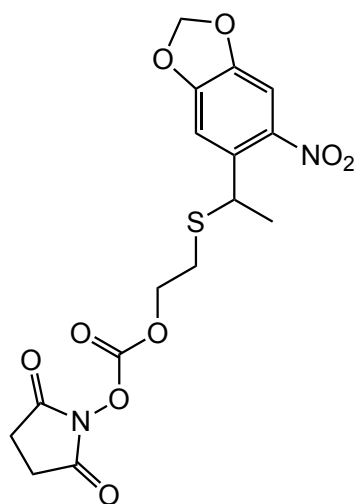
Preparation of (R,S)-1-bromo-1-[4',5'-(methylenedioxy)-2'-nitrophenyl]ethanol (2).

In a dry, 3-necked round-bottomed flask, (R,S)-1-[4',5'-(methylenedioxy)-2'-nitrophenyl]ethanol (1 g, 3.64 mmol, 1 eq.) was dissolved in dichloromethane (24 mL). The flask was cooled to 0°C under a nitrogen atmosphere and wrapped in aluminium foil to exclude light. After 20 min, PBr₃ (0.14 mL, 1.45 mmol, 0.4 eq.) was added dropwise. The reaction mixture was stirred at 0°C for 15 min, then brought to r.t. and stirred continuously for 1.5 hrs. The reaction was monitored by TLC analysis (SiO₂, eluent: 100% dichloromethane). The product was extracted with dichloromethane and washed with NH₄Cl. The organic layer was dried with MgSO₄, filtered and the solvent removed *in vacuo* to obtain a yellow oil. The crude product was purified by flash column chromatography (hexane: dichloromethane (2:1)) to obtain (R,S)-1-bromo-1-[4',5'-(methylenedioxy)-2'-nitrophenyl]ethanol (2) as a yellow solid (697 mg, 54 %). Spectral data is consistent with literature values. ¹H NMR (400 MHz, CDCl₃) δ ppm 2.06 (d, *J* = 6.72 Hz, 3 H) 5.92 (m, 1 H) 6.15 (s, 2 H) 7.29 (s, 1 H) 7.37 (s, 1 H). ¹³C NMR (101 MHz, CDCl₃) δ ppm 27.5, 42.7, 103.2, 105.0, 108.7.



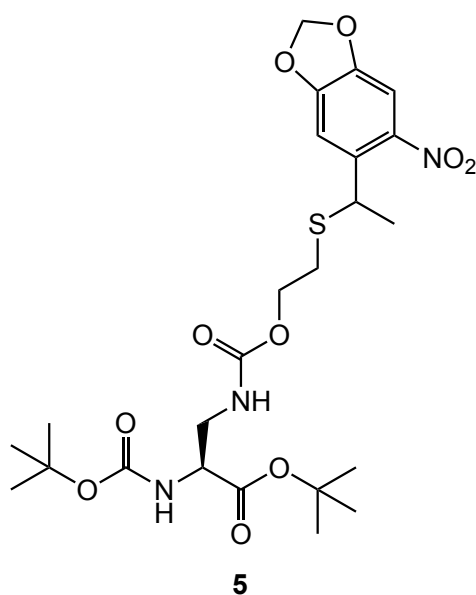
Preparation of 2-[[1-(6-nitrobenzo[d][1,3]dioxol-5-yl)ethyl]thio]ethan-1-ol (3).

(R,S)-1-bromo-1-[4',5'-(methylenedioxy)-2'-nitrophenyl]ethanol (1) (582 mg, 2.12 mmol, 1 eq.) was dissolved in 1,4-dioxane (1.8 mL). The resulting solution was added dropwise to a flask containing a solution of NaOH (0.5 M, 3.65 mL) with 2-mercaptoethanol (25 μL, 2.23 mmol, 1.05 eq.), followed by an additional 5.4 mL 1,4-dioxane. The flask was covered in aluminium foil to exclude light, and left to stir overnight at r.t. under a nitrogen atmosphere. The reaction was monitored by TLC analysis (SiO₂, eluent: EtOAc: cyclohexane (3:7)). The solvent was removed *in vacuo*, then the reaction extracted with EtOAc and washed with NH₄Cl solution then brine. The organic layer was dried with MgSO₄, filtered and the solvent removed *in vacuo* to obtain a yellow oil. The crude product was purified by flash column chromatography (EtOAc: cyclohexane (3:7)) to obtain 2-[[1-(6-nitrobenzo[d][1,3]dioxol-5-yl)ethyl]thio]ethan-1-ol (3), as a sticky, yellow oil (495 mg, 86 %). Spectral data is consistent with literature values. ¹H NMR (400 MHz, CDCl₃) δ ppm 1.57 (d, *J* = 1.00 Hz, 3 H) 1.90 (t, *J* = 6.05 Hz, 1 H) 2.49 - 2.64 (m, 2 H) 3.59 - 3.70 (m, 2 H) 4.79 (m, 1 H) 6.10 (m, 2 H) 7.27 (s, 1 H) 7.29 (s, 1 H). ¹³C NMR (101 MHz, CDCl₃) δ ppm 23.1, 34.8, 38.2, 60.8, 102.9, 104.7, 107.9.

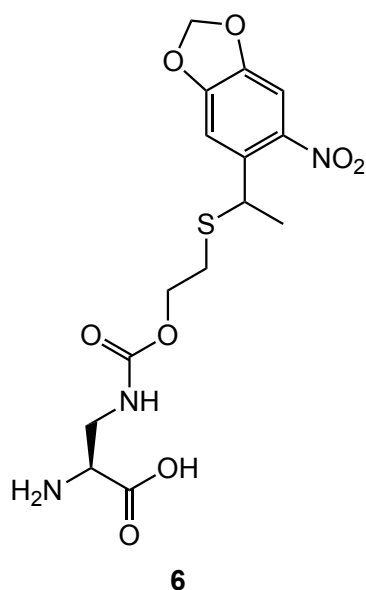


4

Preparation of 2,5-Dioxopyrrolidin-1-yl-(2-([1-(6-nitrobenzo[d][1,3]dioxol-5-yl)ethyl]thio)ethyl) Carbonate (4). 2-([1-(6-nitrobenzo[d][1,3]dioxol-5-yl)ethyl]thio)ethan-1-ol (**3**) (301 mg, 1.11 mmol, 1 eq.) was dissolved in CH₃CN (5.6 mL). DIPEA (0.59 mL, 3.33 mmol, 3 eq.) was added to the solution followed by *N,N*-disuccinimidyl carbonate (419 mg, 1.55 mmol, 1.4 eq.). The flask was covered in aluminium foil to exclude light, and the reaction mixture was stirred overnight at r.t., to afford 2,5-dioxopyrrolidin-1-yl-(2-([1-(6-nitrobenzo[d][1,3]dioxol-5-yl)ethyl]thio)ethyl) carbonate (**4**). The reaction was monitored by TLC analysis (SiO₂, eluent: EtOAc: cyclohexane (1:1)). Intermediate **4** was immediately carried forward to the next step without purification.



Preparation of tert-Butyl (2S)-2-[(tert-Butoxycarbonyl)amino]-3-[[2-[[1-(6-nitrobenzo[d][1,3]dioxol-5-yl)ethyl]thio]ethoxy]carbonyl]amino]propanoate (5). Boc-L-Dap-O^tBu.HCl (578 mg, 2.22 mmol, 2 eq.) was added to the solution 4, prepared as above. The flask was covered in aluminium foil to exclude light, and the reaction mixture stirred overnight at r.t. under a nitrogen atmosphere. The reaction mixture was washed with aqueous NH₄Cl, followed by 1M NaHCO₃. The organic layer was dried with MgSO₄, filtered and the solvent removed *in vacuo*. The crude product was purified by flash column chromatography (EtOAc: cyclohexane (1:4)) to obtain *tert*-butyl (2S)-2-[(*tert*-butoxycarbonyl)amino]-3-[[2-[[1-(6-nitrobenzo[d][1,3]dioxol-5-yl)ethyl]thio]ethoxy]carbonyl]amino]propanoate (4), as a yellow gum (401.9 mg, 65 %). Spectral data is consistent with literature values.¹ ¹H NMR (400 MHz, CDCl₃) δ ppm 1.44 (s, 9 H) 1.47 (s, 9 H) 1.52 - 1.56 (d, *J* = 6.9, 3 H) 2.50 (m, 2 H) 3.56 (m, 2 H) 4.05 - 4.19 (m, 2 H) 4.25 (br s, 1 H) 4.80 - 4.89 (m, 1 H) 5.08 - 5.19 (br s, 1 H) 5.35 - 5.46 (br s, 1 H) 6.09 - 6.13 (d, 2 H) 7.28 (s, 1 H) 7.29 (s, 1 H).



Preparation of (2S)-2-Amino-3-[[[2-[[1-(6-nitrobenzo[d][1,3]dioxol-5-yl)ethyl]thio]ethoxy]carbonyl]amino]propanoic acid (6). *Tert*-butyl(2*S*)-2-[(*tert*-butoxycarbonyl)amino]-3-[[2-[[1-(6-nitrobenzo[d][1,3]dioxol-5-yl)ethyl]thio]ethoxy]carbonyl]amino]propanoate (**5**) (401.9 mg, 0.72 mmol, 1 eq.) was dissolved in 4N HCl in dioxane (4 mL, 16 mmol, 22.2 eq.) and stirred overnight at r.t. The solvent was removed *in vacuo*, to obtain (2*S*)-2-amino-3-[[2-[[1-(6-nitrobenzo[d][1,3]dioxol-5-yl)ethyl]thio]ethoxy]carbonyl]amino]propanoic acid (photocaged-DAP, p-DAP), (**6**), as a yellow-brown gum needing no further purification (309 mg, 77%). Spectral data is consistent with literature values.¹ ¹H NMR (400 MHz, CD₃OD) δ ppm 1.52 - 1.57 (d, J = 7.0 Hz, 3 H) 2.48 - 2.68 (m, 2 H) 3.55 - 3.61 (dd, 1 H) 3.67 - 3.77 (ddd, 1 H) 4.00 - 4.16 (m, 3 H) 4.75 (q, J = 6.97 Hz, 1 H) 6.12 - 6.15 (m, 2 H) 7.29 (s, 1 H) 7.33 (s, 1 H).

9.4.1.7 References

1. Son, H. F. *et al.* Rational Protein Engineering of Thermo-Stable PETase from *Ideonella sakaiensis* for Highly Efficient PET Degradation. *ACS Catalysis* **9**, 3519–3526 (2019).
2. Anderson, J. C. *et al.* BglBricks: A flexible standard for biological part assembly. *Journal of Biological Engineering* **4**, (2010).
3. Huguenin-Dezot, N. *et al.* Trapping biosynthetic acyl-enzyme intermediates with encoded 2,3-diaminopropionic acid. *Nature* **565**, 112–117 (2019).
4. Young, T. S., Ahmad, I., Yin, J. A. & Schultz, P. G. An Enhanced System for Unnatural Amino Acid Mutagenesis in *E. coli*. *Journal of Molecular Biology* **395**, 361–374 (2010).
5. Neumann, H., Peak-Chew, S. Y. & Chin, J. W. Genetically encoding N^{ϵ} -acetyllysine in recombinant proteins. *Nature Chemical Biology* **4**, 232–234 (2008).

9.4.2 Extended Data

9.4.2.1 Extended Data, Table 1. Calculated and observed masses of proteins. Mass spectrometry data for *IsPETase*^{TS}, *IsPETase*^{TS}-DAP production and for enzymes after reaction with BHET.

Protein	Expected Mass (Da)	Observed Mass (Da)
<i>IsPETase</i> ^{TS}	28,733.9	28,729.6
<i>IsPETase</i> ^{TS} -p-DAP	29,025.9	29,025.2
<i>IsPETase</i> ^{TS} -DAP	28,728.6	28,728.5
<i>IsPETase</i> ^{TS} post BHET reaction	28,729.6	28,729.4
<i>IsPETase</i> ^{TS} -DAP post BHET reaction (<i>IsPETase</i> ^{TS} -DAP-MHET)	28,921.5	28,920.1

9.4.3 Supplementary Information

9.4.3.1 Supplementary Information, Table 1. Primer sequences for construction of *IsPETase^{TS}_S160TAG*. Nucleotides which bind to the gene are in capitals, with overhangs in lower case.

Primer Name	Nucleotide Sequence
Nde_F	agaaggagatatacatATGCAGACTAACCCCT
Xho_R	ggtggtggtgCTCGAGGCTGCAGTTA
S160_TAG_F	GGAGTAATGGGCTGGTAGATGGGTGGCGGC
S160_R	CCAGCCCATTACTCCCA

9.4.3.2 Supplementary Information, Figure 1. Nucleotide and expressed amino sequence for production of *IsPETase^{TS}* and *IsPETase^{TS}-DAP*. The DNA codons and amino acid residues modified in *IsPETase^{TS}-DAP* are highlighted in orange, with the original *IsPETase^{TS}* codons and residues highlighted in blue. Genes were codon optimised for expression in *E. coli*, and were inserted between NdeI and XhoI restriction sites of the bacterial expression plasmid.

***IsPETase^{TS}-DAP* Nucleotide Sequence:**

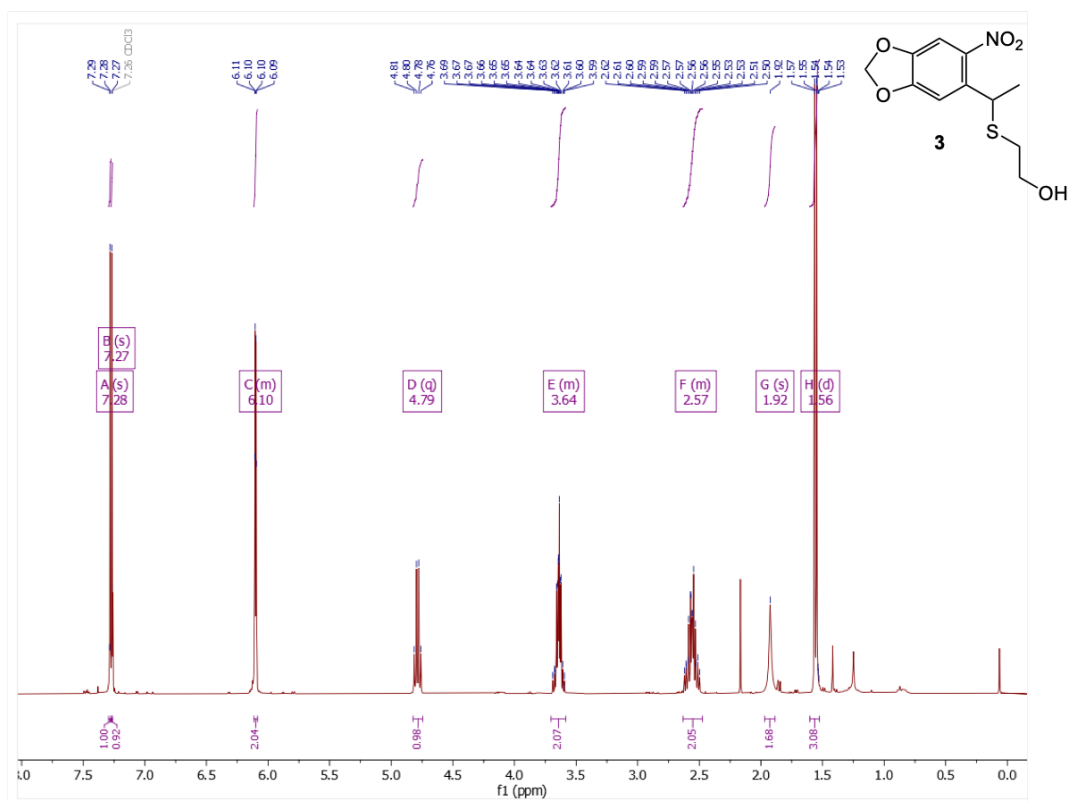
ATGCAGACTAACCCCTATGCTCGCGGGCCGAATCCTACAGCGGCCTCGTTGGAAGCCAG
TGCAGGTCCTTCACCGTACGTTTCGTTTACTGTTTCCCCTCCATCTGGATATGGGGCTGG
CACCGTCTATTATCCGACTAACGCCGGTGGTACTGTGGGCGCAATCGCCATTGTCCCCG
GCTACACTGCACGCCAATCCTCGATTAATGGTGGGGACCACGCTTGGCTAGCCACGGG
TTTGTGTTGATCACCATCGATACTAACAGTACGTTGGACCAGCCAGAGAGTTCGCAGCTC
TCAGCAGATGGCGGCATTACGCCAGGTGGCGAGCTTAAATGGGACGAGTTCAAGTCCAA
TTTATGGCAAGGTCGATACCGCCCGTATGGGAGTAATGGGCTGGAGT(ATAG)ATGGGTG
GCGGCGGATCTCTTATCTCGGCAGCGAATAATCCAAGCCTGAAGGCAGCAGCCCCGCAG
GCACCCTGGCATAAGTAGTACGAACTTTTTCGTTCTGTTACGGTTCCTACGCTTATCTTTGCC
TGTGAGAATGATTCTATCGCACCAGTGAACCTCATCAGCCTTGCCAATTTACGACTCGATG
TCGCGCAACGCTAAACAGTTTCTTGAGATTAATGGGGGCTCTCACTCTTGTGCCAACAGT
GGGAATCCAATCAAGCCCTTATCGGAAAAAAGGGCGTTGCTTGGATGAAGCGCTTCAT
GGACAATGACACTCGTTATTCAACTTTCGCTTGCGAAAACCCAACTCAACCGCCGTATC
CGATTTTCGCACTGCTAACTGCAGC

***IsPETase^{TS}-DAP* Expressed Amino Acid Sequence**

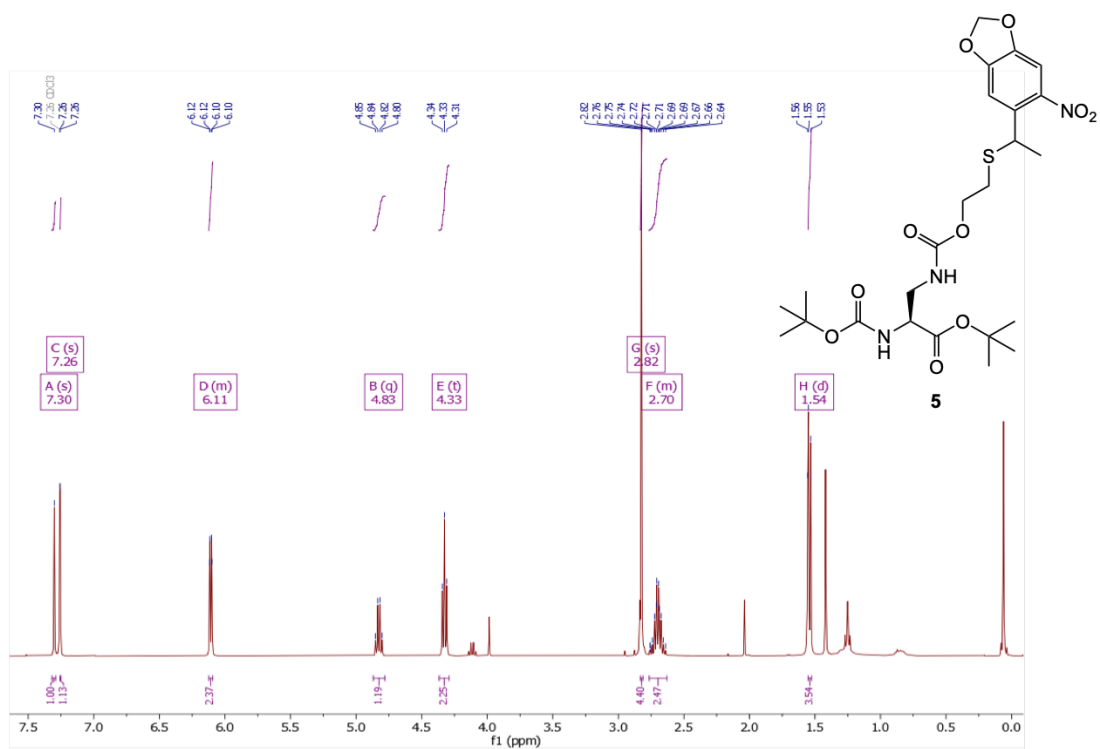
(amino acid numbering starts at 27):

M²⁷QTNPYARGPNPTAASLEASAGPFTVRSFTVSRPSGYGAGTVYYPTNAGGTVGAIAIVPGY
TARQSSIKWWGPRLASHGFVVITIDTNSTLDQPESRSSQQMAALRQVASLNGTSSSPIYGKV
DTARMGVMGWS(DAP)MGGGSLISAANNPSLKAAAPQAPWHSSTNFSVTVPTLIFACEN
DSIAPVNSSALPIYDSMSRNAKQFLEINGGSHSCANSNSNQUALIGKKGVAWMKRFMDND
TRYSTFACENPNSTAVSDFRTANCS

3. ^1H NMR (400 MHz, CDCl_3)



5. ^1H NMR (400 MHz, CDCl_3)



6. ^1H NMR (400 MHz, CD_3OD)

